

1965

Ultimate shear tests of full-sized prestressed concrete beams

Howard E. Brecht
Lehigh University

Follow this and additional works at: <https://preserve.lehigh.edu/etd>



Part of the [Civil and Environmental Engineering Commons](#)

Recommended Citation

Brecht, Howard E., "Ultimate shear tests of full-sized prestressed concrete beams" (1965). *Theses and Dissertations*. 3291.
<https://preserve.lehigh.edu/etd/3291>

This Thesis is brought to you for free and open access by Lehigh Preserve. It has been accepted for inclusion in Theses and Dissertations by an authorized administrator of Lehigh Preserve. For more information, please contact preserve@lehigh.edu.

ULTIMATE SHEAR TESTS
OF
FULL-SIZED PRESTRESSED CONCRETE BEAMS

by

Howard E. Brecht

A THESIS

Presented to the Graduate Faculty

of Lehigh University

in Candidacy for the Degree of

Master of Science

Lehigh University

1965

CERTIFICATE OF APPROVAL

This thesis is accepted and approved in partial fulfillment of the requirements for the degree of Master of Science.

May 20, 1965

(Date)

C. L. Hulst

Professor in Charge

C. L. Hulst for

Professor W. J. Eney, Head
Department of Civil Engineering

A C K N O W L E D G E M E N T S

The work described in this thesis was conducted in Fritz Engineering Laboratory of the Department of Civil Engineering, Lehigh University, Bethlehem, Pennsylvania. Professor W. J. Eney is Head of the Department of Civil Engineering and Dr. L. S. Beedle is the Director of the Fritz Engineering Laboratory. This work constituted part of a research investigation sponsored by: Commonwealth of Pennsylvania, Department of Highways; U. S. Department of Commerce, Bureau of Public Roads; and the Reinforced Concrete Research Council.

The author wishes to acknowledge his gratitude to Dr. John M. Hanson, thesis supervisor, for his continued advice, suggestions and assistance, and to Dr. C. L. Hulsbos, professor in charge of this thesis, for his guidance and encouragement.

The cooperation and capable help of the personnel of Schuylkill Products, Inc. during fabrication is gratefully appreciated. Completion of the testing of the specimens was facilitated by the capable help of the Fritz Engineering Laboratory staff and technicians. Mr. Joseph Nagle's cooperation in the fabrication and shipping of the test specimens is especially appreciated. The assistance extended by the author's associates, especially Messrs. R. G. Adams, J. C. Badoux and A. A. Guilford, is gratefully appreciated. Miss Valerie Austin typed the manuscript and her patience and cooperation are appreciated.

T A B L E O F C O N T E N T S

	Page
ABSTRACT	1
1. INTRODUCTION	3
1.1 Background and Previous Investigations at Lehigh University	3
1.2 Object and Scope	6
2. TEST SPECIMENS	8
2.1 Description	8
2.2 Materials	10
2.2.1 Concrete	10
2.2.2 Prestressing Steel	13
2.2.3 Reinforcing Bars	14
2.2.4 Void Forms	14
2.3 Fabrication	15
2.3.1 Stressing	16
2.3.2 Placement of Non-Prestressed Steel	17
2.3.3 Placement of Instrumentation and Miscellaneous Items	18
2.3.4 Forming	19
2.3.5 Casting	20
2.3.6 Initial and Intermediate Curing	21
2.3.7 Releasing	22

	Page
2.3.8 Final Curing	23
2.4 Instrumentation	24
2.4.1 Strand Dynamometers	24
2.4.2 Internal Strain Bars	24
2.4.3 Whittemore Strain Targets	26
2.4.4 Ames Dial Gages	26
2.4.5 SR-4 Electrical Strain Gages	27
2.4.6 Miscellaneous	27
2.5 Prestress Force	27
2.6 Storage and Handling	30
2.7 Dimensional Tolerances	31
3. METHOD OF TESTING	34
3.1 Test Setup	34
3.2 Test Procedure	35
3.3 Test Schedule	37
4. "I" BEAM TESTS	39
4.1 Test Results	39
4.2 Behavior and Mode of Failure of Beam G-2	40
4.2.1 First Test	40
4.2.2 Second Test	43
4.3 Behavior and Mode of Failure of Beam G-4	45
4.3.1 First Test	45
4.3.2 Second Test	46
4.3.3 Third Test	48

	Page
5. "BOX" BEAM TESTS	50
5.1 Test Results	50
5.2 Behavior and Mode of Failure of Beam G-1	51
5.2.1 First Test	51
5.2.2 Second Test	53
5.3 Behavior and Mode of Failure of Beam G-3	56
5.3.1 First Test	56
5.3.2 Second Test	58
6. STRENGTH OF TEST BEAMS	59
6.1 General	59
6.2 Flexural Cracking Strength	61
6.3 Inclined Cracking Strength	64
6.3.1 Types of Inclined Cracking	64
6.3.2 Web Stresses	66
6.3.3 Inclined Cracking Shear	68
6.4 Ultimate Flexural Strength	76
6.5 Ultimate Shear Strength	85
7. SUMMARY AND CONCLUSIONS	96
8. NOTATION	100
9. TABLES	105
10. FIGURES	116

	Page
11. APPENDIX A - Crack Patterns	147
12. APPENDIX B - Strain Distributions	155
13. REFERENCES	162
14. VITA	165

LIST OF TABLES

<u>Table No.</u>		<u>Page</u>
1	Properties of the G Series Beams	106
2	Properties of the Concrete	107
3	Schedule of Operations	108
4	Prestress Data	108
5	I-Beam Test Results	109
6	Box Beam Test Results	110
7	Slip Measurements	111
8	Crack Widths	112
9	Flexural Cracking Strength	113
10.	Ultimate Flexural Strength	113
11	Inclined Cracking Stress Conditions	114
12	Test to Predicted Shear Strength Ratios	115

LIST OF FIGURES

<u>Figure No.</u>		<u>Page</u>
1	Details of Full-Sized, G Series Beams	117
2	Section Views of Full-Sized, G Series Beams	118
3	Gradation of Fine and Coarse Aggregate	119
4	Cylinder Tests for Beam G-1	119
5	Load-Strain curve for Prestressing Strand	120
6	Load-Strain Curve for Non-Prestressed Steel	120
7	Stressing of Individual Strands	121
8 (a,b)	Reinforcing Steel for Box Beams	121
9	Location of Internal Strain Bars	122
10	Strain Bar Assembly	123
11	Strain-Temperature Curve for Strain Bar Gages	123
12	Location of Whittemore Targets and Electrical Strain Gages	124
13 (a,b)	Beams Arriving at Fritz Engineering Laboratory	125
14 (a-c)	Cross Section of Box Beam G-3	126
15	Testing Arrangement	127
16 (a-d)	Test Setup	128
17 (a,b)	Load-Deflection Curves	129
18 (a-c)	First Test on Short I-Beam, G-2	130
19 (a,b)	Diagonal Tension Inclined Crack Width Growth	131
20 (a-c)	Second Test on Short I-Beam, G-2	132
21 (a,b)	Inclined Crack Width Growth	133

<u>Figure No.</u>		<u>Page</u>
22 (a,b)	First Test on Long I-Beam, G-4	134
23	First Test on Long I-Beam, G-4 Strain Distribution at Mid-Span	135
24 (a-c)	Second Test on Long I-Beam, G-4	136
25 (a,b)	Third Test on Long I-Beam, G-4	137
26 (a,b)	First Test on Short Box Beam, G-1	138
27 (a-e)	Second Test on Short Box Beam, G-1	139
28 (a,b)	First Test on Long Box Beam, G-3	141
29 (a,b)	First Test on Long Box Beam, G-3	142
30 (a,b)	Second Test on Long Box Beam, G-3	143
31	Types of Inclined Cracking Observed During Testing	144
32	Internal Torsional Effects of Box Beams which Sustained Inclined Cracks in One Web Only	145
33	Assumed Strain and Stress Distribution at Flexural Failure	146

A B S T R A C T

Four full-sized prestressed concrete bridge girders were subjected to static shear strength tests in order to compare the behavior and strength of these girders with the behavior and strength of smaller beams tested in previous investigations at Lehigh University. The girders were selected from standard cross sections in use by the Pennsylvania Department of Highways.

A 36-in. square hollow box-shaped cross section and a 36-in. deep I-shaped cross section with a top flange width of 12-in. and a bottom flange width of 18-in. were selected for this series of tests. One beam of each cross section had a total length of 47-ft. and the other had a total length of 29-ft. Prestress was applied with 7/16-in. diameter 270 ksi strand initially tensioned to 21.7 kips.

Hot rolled deformed No. 2 and No. 3 bars were used for the vertical web reinforcement in the shear spans of the girders. The amount of web reinforcement used was based on the results of previous research at Fritz Engineering Laboratory and in most of the beams was a little less than the amount which was expected to be needed to develop the flexural capacity of the section. Spacing of the stirrups ranged from 12-in. to 22½-in.

Information was obtained on the compressive strength, splitting tensile strength, and modulus of elasticity of concrete cast in waxed

cardboard, steel, and cast iron molds. Some of the cylinders cast in each type of mold were rodded and the others were vibrated. The concrete strength varied between 6660 psi and 7930 psi, and the average concrete strength at the time of test was 7520 psi.

The beams were cast in a commercial prestressing plant and a complete description of the fabrication of the specimens is included. Each of the beams was subjected to a symmetrical two point loading arrangement for the first test. Shear failures were obtained in three beams. The fourth beam failed in the exact center due to flexure. The remaining sections of the first three beams and each end of the fourth beam were then subjected to another test using a single point load applied at mid-span. One of these tests was invalidated by damage sustained during the first test. Eight valid tests were obtained from this series of beams.

Diagonal tension, flexure shear and torsional inclined cracking were observed in the tests. Inclined crack widths are reported. Four types of failures occurred: three beams failed in shear, two failed in shear but were influenced by torsion, one failed in flexure, and two failed in flexure but were influenced by shear. Comparisons of the test results with current design requirements for shear were made for all of the shear failures. Similar comparisons were made with a proposed design method which was developed from previous research at Lehigh University and elsewhere.

1. I N T R O D U C T I O N

1.1 B A C K G R O U N D A N D P R E V I O U S I N V E S T I G A T I O N S A T L E H I G H U N I V E R S I T Y

The field of prestressed concrete has expanded rapidly in the United States since construction of the 160-ft main span Walnut Lane Bridge in Philadelphia was started in April, 1949. This bridge, composed of I-shaped beams, was the first large prestressed concrete structure to be built in this country and was completed in early 1951.⁽¹⁾ Prestressed concrete bridge members in use today are of two basic types: I-beams and hollow box beams.

In 1951 the first full-sized prestressed concrete beam research commenced at Lehigh University.^(2,3) Pretensioned and post-tensioned concrete members were subjected to a minimum of 1,000,000 cycles of dynamic loading without any apparent damage, thus showing that prestressed concrete beams were durable. The loading arrangement used for these beams simulated H20-S16 loading with a 30 percent impact factor. The study was continued with field tests of multi-beam bridges to determine primarily the lateral load distribution.^(4,5) Bond in pretensioned members, and fatigue characteristics of prestressed beams were investigated^(6,7) before the problem of shear strength was undertaken in 1957. A static test was conducted on a 70-ft prestressed concrete rectangular box beam to determine the feasibility of this type of beam for long span bridges.⁽⁸⁾ This test was followed by the testing of a 55-ft

prestressed concrete rectangular box beam with repeated loading. (9)

The beam sustained 3,000,000 load cycles without damage, and was subsequently subjected to an ultimate static test. A comparison was made between this test and the previous static test on the 70-ft member. The mode of failure of the first full-sized beams tested in 1951 and these beams was essentially the same, and was characterized by crushing of the concrete within the compression flange. All of these investigations, except for the field tests of multi-beam bridges, had one objective in common - to determine the ultimate strength of prestressed concrete beams as affected by the various phenomena studied.

Walther formulated a theoretical analysis to explain the shear carrying characteristics of a pretensioned prestressed concrete beam. (10)

Walther and Warner then tested 20 beams without web reinforcement and showed that the mode of failure could be changed from shear to flexure by increasing the prestress force. (11) They also demonstrated that prestressing with different size strands had little effect on the ultimate strength of the beams. Further investigations into the shear strength of prestressed beams without web reinforcement were continued by McClarnon, Wakabayashi and Ekberg. (12) Their beams were used to determine the effect on the ultimate strength due to length of overhang at the reaction, existing inclined cracks, and height of the load point.

Hanson and Hulsbos extended the Lehigh research to prestressed beams with web reinforcement. (13) Sixteen beams, designated as the E series, were tested statically and used to evaluate the overload behavior of the specimens. Two additional tests conducted with repeated

loading showed that a prestressed beam, which had been subjected to an overload such that diagonal tension inclined cracking had occurred, may be more critical in fatigue of the web reinforcement than in fatigue of the prestressing strand. This study was continued and 38 tests were conducted on 23 beams, designated as the F series, to determine the static ultimate shear strength of prestressed I-beams with vertical stirrups. (14,15) The effects of the amount of web reinforcement and the length of the shear span were investigated. All of the test beams had a depth of 18-in., a flange width of 9-in., and a web width of 3-in. The length of shear span to effective depth ratio varied from 2.12 to 7.76. Three different modes of failure were observed due to inclined cracking which remained entirely within the shear span. These were associated with failure by crushing of the concrete in the web, by shear compression, and by fracture of the web reinforcement. An additional mode of failure was associated with inclined cracks crossing under the load point into the constant moment region.

Based on the tests at Lehigh University and elsewhere, a method was proposed for design of web reinforcement in prestressed concrete beams. (15) The method assumes that the shear in the concrete is equal to the shear causing significant inclined cracking, and that the shear in the web reinforcement crossed by an idealized crack is equal to the product of the area of the web reinforcement and the yield point of the stirrup. Ultimate shear capacity is assumed equal to the sum of the two contributions. The prediction of shear causing significant diagonal tension inclined cracking is based on a maximum principal tensile stress in

the web of the beam at the center of gravity. The prediction of shear causing significant flexure shear cracking is based on a maximum tensile stress in the bottom fibers of the beam.

1.2 OBJECT AND SCOPE

The objective of this investigation was to compare the behavior and strength of full-sized prestressed concrete beams with the behavior and strength of the smaller F series beams. In this manner, it was hoped to demonstrate the adequacy of the proposed method to predict the ultimate shear strength of full-sized prestressed concrete bridge members. The girders were selected from standard cross sections in use by the Pennsylvania Department of Highways and were designated as the G series beams.

Four full-sized beams were included in the series: two had an I-shaped cross section and the other two had a hollow box-shaped cross section. One beam of each cross section had a total length of 47-ft, and the other had a total length of 29-ft; all specimens had a depth of 36-in. The prestress force and eccentricity were selected so that allowable stresses in the top and bottom fibers at transfer were not exceeded, ⁽¹⁶⁾ and so that the neutral axis at failure, if the beam should fail in flexure, would be located in the compression flange. The selection of the amount of web reinforcement to be used was based on the results of the previously tested F series beams. ⁽¹⁵⁾ In most of the tests a little less web reinforcement was used than that which was expected to be required to develop the flexural capacity of the section.

The analysis of the test results proceeded virtually the same for both cross sections tested. The load causing flexural cracking, and the load causing inclined cracking was determined because each represents a change in the behavior of the specimen. The ultimate flexural capacity was computed since it represents an upper bound on the ultimate shear strength. Determination of the ultimate shear strength of the beam is the primary objective of this series of tests.

Internal and external dimensions were to be obtained for all specimens in the series. Information was desired on the crack widths of the inclined cracks and also on the growth of these cracks after formation. A study of concrete cylinder strengths was to be undertaken to determine the influence due to type of mold and type of compaction on the ultimate compressive strength and the splitting tensile strength of the cylinders.

2. TEST SPECIMENS

2.1 DESCRIPTION

The G series test beams were comprised of two 47-ft and two 29-ft pretensioned, prestressed concrete bridge members. One beam of each length was a 36-in. square, hollow box-shaped cross-section, and the other was a 36-in. deep, I-shaped cross-section. These beams were fabricated in accordance with standard Pennsylvania Department of Highways specifications⁽¹⁶⁾ except for the amount of vertical web reinforcement, which was less than is currently required. Dimensions of the beams are presented in Figs. 1 and 2.

The total length of each beam consisted of the test span and two reinforced regions of one foot length at each end. The test span was divided into three equal regions, designated A, B, or C, in which different amounts of vertical web reinforcement were provided. Size and spacing of web reinforcement in the test beams are also presented in Fig. 1. The amount of vertical web reinforcement in the different beams can be compared by the ratio $rf_y/100$. The properties of the cross-section are tabulated in Table 1. Nominal properties are based on the nominal dimensions, whereas all other properties are based on dimensions measured at a minimum of seven sections along the length of the I-beams and at nineteen sections along the length of the box beams. The values presented in Table 1 are the averages of the cross-sectional

properties which were determined at each section.

Stirrups used for the I-beams were inverted U-shaped bars. Stirrups used for the box beams were comprised of two pieces; one was a lower stirrup, the other an upper stirrup as seen in Fig. 2. These two pieces were lapped in the lower level of the web on each side to form a box shape.

Beams similar to the ones tested are used in present bridge construction as composite members with a $7\frac{1}{2}$ -in. deck slab placed on top. Members of a committee composed of representatives of the sponsoring agencies decided that the beams should be tested without the composite slab. It was felt that this would facilitate the correlation of the results obtained from the full-sized beams with the earlier F series beams. (15)

If the beam did have the composite deck slab, the neutral axis at failure, if the beam would fail in flexure, would be located in the compression flange. In order to have the conditions at failure in the test beams without a composite slab similar to the actual bridge members with the composite slab, it was decided that the location of the neutral axis at failure should also be in the compression flange. Consequently, the prestressing force was selected so that the allowable stresses in the top and bottom fibers at transfer⁽¹⁶⁾ were not exceeded and so that the location of the neutral axis, if the beam would fail in flexure, would be in the compression flange. This modification resulted in a smaller prestress force with a greater eccentricity, and a stress at transfer

equal to the maximum allowable in the top fibers of 540 psi. The stress at transfer in the bottom fibers was less than the allowable: the box beam bottom fiber stress was 2130 psi, and the I-beam bottom fiber stress was 1780 psi. If the member would fail in flexure, the strain in the prestressing strand would be greater than 1 percent.

The prestressing force was provided by straight prestressing elements of 7/16-in. diameter high tensile strength strands used in all of the beams. Sixteen strands were used for the I-beams; twenty-six were used for the box beams; thus resulting in a longitudinal reinforcement ratio of 0.46 percent and 0.52 percent respectively. Each strand was pretensioned to a nominal initial force of 21.7 kips, providing a total initial design prestress force of 347.2 kips for the I-beams and 564.2 kips for the box beams.

2.2 MATERIALS

2.2.1 Concrete

The concrete used for the test beams was an approved Pennsylvania Department of Highways mix and was supplied by Schuylkill Products, Inc., Cressona, Pennsylvania. The mix contained 8.5 bags per cu yd of high early cement manufactured by Lone Star Cement Corporation. Proportions by weight of the cement to sand to coarse aggregate were 1 to 1.15 to 2.4. The sand was obtained by the supplier from the Refractory Sand Company, Andreas, Pennsylvania, and the coarse aggregate, which was crushed limestone, from Berks' Products, Reading, Pennsylvania. Coarse aggregate was obtained from two stockpiles of material; one was classi-

fied by the Pennsylvania Department of Highways as aggregate 1-B, the other as aggregate 2-B. Aggregate 1-B was graded to $\frac{1}{2}$ -in. maximum size, and aggregate 2-B was graded to $\frac{3}{4}$ -in. maximum size. These two aggregates were combined in the ratio 1 to 1.5 respectively. Gradation curves of the sand, both coarse aggregates, and the combined material are shown in Fig. 3. The fineness modulus of the sand was 2.8, and the uniformity coefficient was 4.8. Ready mix trucks delivered the dry concrete mix to the end of the prestressing building. Here the materials were dry mixed before the water was added. Slump for all of the mixes varied between one-and-one-eighth inches to two inches. Plastiment was added to delay the setting of the concrete for a maximum period of 1 hr. The percentage of entrained air in the mix ranged from 4.5 to 7.2 percent.

Forty two 6- by 12-in. standard cylinders were prepared from the concrete used to produce each beam, resulting in a total of 168 standard cylinders. Two basic types of molds were used to form the cylinders: waxed cardboard molds with light metal bottoms, and metal molds. Metal molds were either steel cylinders with a steel base or cast iron cylinders with a cast iron base. The cardboard molds were obtained from the Philadelphia Container Company and were constructed with $\frac{5}{64}$ -in. waxed cardboard walls and 33 gage metal bottoms. Three cylinders of each type mold from each beam were rodded, and all of the others were internally vibrated with a small, 12,000 vpm, $\frac{7}{8}$ -in. diameter shaft, hand vibrator.

The ultimate compressive strength of the concrete, f'_c , was determined from each type of cylinder just prior to releasing of the prestress force and also at the time of the first test. Strains were mea-

sured on randomly selected cylinders with a compressometer to determine the shape of the stress-strain curve for the concrete and the modulus of elasticity at the time of releasing and at test. Splitting tensile tests were conducted to determine the splitting tensile strength of the concrete, f'_{sp} , at test. Standard 6- by 12-in. cylinders were used for splitting tensile test specimens. Strips of 1/8-in. plywood, 1-in. wide and 12-in. long were placed on the diametrical upper and lower bearing lines of the cylinder to ensure uniform bearing in the splitting test.

All cylinders except those tested as splitting tensile test specimens were capped with carbo-vitrobond material. The results of all cylinder tests are tabulated in Table 2. The average ultimate compressive strength of the concrete, f'_c , in the test beam ranged from 5910 psi to 6820 psi at transfer and from 6660 psi to 7920 psi at test, as determined from the vibrated cylinders cast in metal molds.

An analysis of the cylinder tests indicated that:

1. Values of f'_c at transfer and at test averaged 5.1 percent and 5.2 percent lower, respectively, for vibrated cylinders cast in waxed cardboard molds rather than metal molds.
2. Values of f'_c at test averaged 6.0 percent lower for rodded cylinders cast in waxed cardboard molds rather than metal molds.
3. Values of f'_c at test for cylinders cast in metal molds averaged 1.2 percent higher for vibrated rather than rodded cylinders.
4. Values of f'_c at test for cylinders cast in waxed cardboard molds averaged 2.1 percent higher for vibrated rather than rodded cylinders.

5. Values of f'_c at test averaged 2.2 percent lower for vibrated^{SP} cylinders cast in waxed cardboard molds rather than metal molds.

In general, concrete strength was found to be affected more by the type of mold than by the type of compaction. These results, although determined from higher strength concrete, agree with the work conducted by Cusens.⁽¹⁷⁾ The wall thickness of the cardboard molds was the same as that used by Burmeister in his work on steel vs. cardboard Type B cylinder molds.⁽¹⁸⁾ His results indicated much higher differences but the concrete strength was considerably weaker.

The stress-strain curves for the concrete were typical to those shown in Fig. 4 for the concrete representative of beam G-1. Values of the modulus of elasticity for the concrete, E_c , determined from the stress-strain curves are listed in Table 2. The results indicate that the modulus of elasticity at test was 2.5 percent higher than at transfer, and the value obtained from the cylinders cast in metal molds was 1.6 percent higher than the value obtained from the tests on the cylinders cast in waxed cardboard molds.

2.2.2 Prestressing Steel

Uncoated stress relieved 270 ksi 7/16-in. diameter strand, meeting the requirements of ASTM A416-59 specifications, was used for the pretensioning elements. The strand was manufactured by John A. Roebling's Sons Division of The Colorado Fuel and Iron Corporation. The load-strain curve shown in Fig. 5 is the plot of the average values obtained from 3 strand tests conducted in the laboratory. Special Supreme Products Corporation No. 350 chucks were used during the testing of the

strand; however, all 3 specimens failed in the grips at an average load of 31.9 kips and strain of 4.48 percent. Specifications provided by the manufacturer stated that the strand had an area of 0.1167-sq. in., and a minimum tension test breaking load of 31.0 kips. All of the strand used in the 4 beams were cut from the same roll of strand, the surface of which was free from rust and dirt.

2.2.3 Reinforcing Bars

Hot rolled deformed reinforcing bars of intermediate grade steel were used for non-prestressed reinforcement within the beams. The bars were clean and free from rust or mill scale. Nos. 4, 5, and 6 bars were used as tensile reinforcement in the top flange and as end reinforcement in the beams. The web reinforcement within the center, C, region of each beam was made from deformed No. 5 bars. Web reinforcing within the tested shear spans was made from No. 2 or No. 3 deformed bars. A minimum of 4 specimens of each size bar were tested in the laboratory, and the results of one typical test on each size bar are shown in Fig. 6. The values listed in the table are the average values of at least 4 tests. The deformed No. 2 bars were taken from the stock used for previous research at the laboratory.⁽¹⁵⁾ All other reinforcing bars were taken from the stock at the prestressing plant, which was obtained by the fabricator from Bethlehem Steel Company, Inc.

2.2.4 Void Forms

Waxed cardboard void forms for the box beams were supplied by the fabricator. The interior of the voids were constructed with a

criss-cross interlocking arrangement of cardboard. Lengths of the voids were within +1-in. of the specified length.

2.3 FABRICATION

The beams were commercially fabricated by Schuylkill Products Inc., Cressona, Pennsylvania. This plant has produced many beams similar to the test specimens for the Pennsylvania Department of Highways. Standard fabrication procedures were followed as closely as possible and were interrupted only to install instrumentation or to obtain readings from various control devices. Approximately 10 hrs. were required to instrument and cast each beam. The dates of fabrication are presented in Table 3.

The major steps in the casting of the I-beams and box beams were similar except for one step. The first operation was the cutting and stressing of the prestressing strand. This was followed by the placement of the mild steel reinforcement and the internal strain bars. All of this material was installed for the I-beams prior to placing the concrete. Only the bottom flange material was installed for the box beams since the concrete for the bottom flange had to be placed before the voids and the remainder of the mild steel reinforcement could be installed. Then the remainder of the concrete for the box beams was placed. In the following sections a detailed description of the fabrication is presented.

2.3.1 Stressing

A 76-ft, column-type bed was employed for all of the beams. The prestressing strand was strung between the bulk-heads of the bed, and load cells were placed on 12 strands at one end of the bed. Each strand was individually stressed with a hydraulic jacking system at the opposite end of the bed. Figure 7 shows a general view of the stressing operation. The load was measured during jacking by means of a Chatillon strand dynamometer (0-50,000 lb range) connected in the linkage between the strand and the hydraulic jack. This dynamometer was calibrated approximately 3 days prior to the fabrication of the first beam, and found to be within ± 1 percent accuracy in the range to be used during the stressing operation. The load on the strand had to be raised to approximately 24 kips, if after locking the chucks and releasing the jacking force, the design load of 21.7 kips was to be applied. This loss of about 2.3 kips was partially due to slippage in the chucks at each end and some elastic deformations in the bed itself. After all 16 or 26 strands had been stressed, the load on the 12 instrumented strands was checked by means of the load cells at the opposite end of the bed. An adjustment was made on the strands which were considerably below the design load, as determined by the 12 instrumented strands. The total prestress force in any of the beams, as measured by the 12 strand dynamometers, was within ± 1 percent of the design force. The force in any strand was within ± 5 percent of the design force except for strands which sustained single wire failures as discussed in the next paragraph.

Five single wire failures occurred during the stressing of the beams. These failures occurred during the adjustment procedure used to increase the load on strands which had considerably less than the design load. Two single wire failures occurred in the chucks during the stressing of each of the shorter beams, G-1 and G-2, but these strands were not replaced. Three of these occurred at the jacking end and one at the opposite end of the bed. Failures in the chucks were probably caused by biting of the chuck into the strand causing a reduction in area, since in each case an outside wire failed and not the center wire of the strand. The force recorded by the dynamometers indicated that the strands lost approximately 10 percent of the design force at the time of a single wire failure.

Another single wire failure occurred in one strand in the center region of the bed during the stressing of beam G-1. This failure was probably at the location of a weldment, and was replaced since the failure would have been encased in concrete.

2.3.2 Placement of Non-Prestressed Steel

The web reinforcement and top longitudinal steel was made up into a cage at an auxiliary work area. Some of the stirrups were tack welded to the longitudinal steel, while others were tied with No. 16 gage wire ties. The cages were checked for accuracy of stirrup spacing prior to installation.

I-beam fabrication and box beam fabrication varied at this point; since, the box beam fabrication had to allow for the installation

of the cardboard voids, whereas the I-beam fabrication did not. For the I-beams, the cage of reinforcement was transferred to the bed and lowered into position where it was tied with No. 16 gage wire ties as used at other locations. This completed the installation of non-prestressed reinforcement for the I-beams. The lower web reinforcement members of the box beams were tied individually to the prestressing strands at the required locations. The end block reinforcement was then installed.

The second stage of the box beam fabrication commenced as soon as the bottom flange concrete was placed and checked for thickness, as discussed in Section 2.3.5. Previously assembled waxed cardboard voids were placed in the proper location on top of the bottom flange. The cage of web reinforcement was transferred to the bed and placed over the cardboard voids. Small grout blocks (sand and cement) were used to elevate the longitudinal tensile steel to the proper location above the top of the void. The reinforcement was checked for alignment and location, and the voids were centered between the forms before completing the inner system by tightening the straps which held the above placed items during the remainder of the pouring operation.

2.3.3 Placement of Instrumentation and Miscellaneous Items

Internal strain bars, to be discussed in greater detail in the next section, were then installed. These devices had been previously fabricated, assembled and tested at Fritz Laboratory. Wire ties were used to hold the strain bars in location and the electrical wires routed out of the beam through the top. The wires were taped to the

vertical reinforcement in the center region of the beam, thus not affecting the shear span reinforcement.

Lifting wire inserts made from scrap prestressing steel were installed in each end of the beams. The hooks were bent and interwoven with the end block reinforcing steel. Water drains of 3/4-in. diameter plastic tubing and air vents of 1/2-in. diameter copper tubing were installed in the center of the box beams so that one drain and one vent would be provided for each void.

Straps of 5/8-in. wide No. 25 gage steel, were placed under the strands in the bottom of the box beams approximately every 5 feet along the length of the beam, and were draped out and over the top of the forms, as can be seen in Fig. 8. These straps were subsequently used to hold the cardboard void in place.

2.3.4 Forming

Wood end plates, cut to the appropriate cross section from 3/4-in. plywood stock, were installed at the longitudinal limits of the beam. Openings were cut in order to allow the strand to pass through the end plates.

Oiled 3/4-in. thick plywood base pallets were used to form the base of the beam. Triangular wedge-shaped strips were nailed to the sides in order to form the chamfer in the bottom of the finished beam.

Steel forms made from 3/16-in. thick plates were placed in position to cast the beam. I-beam forms bent to the shape of the beam are standard equipment at the plant; box beam forms are straight sided,

and are also standard equipment at the plant. The forms were cleaned and waxed prior to their positioning. The forms were horizontally braced at the base and through spreaders, braced horizontally together at the top. Figures 8a and 8b are of beam G-1 just prior to pouring.

2.3.5 Casting

The concrete was handled with 1 and 3/4 cu yd buckets which were suspended from overhead cranes. Buckets were lowered to within 1-ft of the top of the forms before discharging the concrete. The I-beams were cast in two lifts, each extending the full length of the beam. The first lift was up to the level of the junction of the bottom flange and web, and the second to the top of the beam. Box beam casting entered the first stage which was the placing of the concrete composing the bottom flange of the beam. The concrete was vibrated with two 12,000 vpm, 1 and 3/8-in. diameter shaft, internal vibrators, as the concrete was placed.

The thickness of the bottom flange of the box beam was checked at closely spaced, randomly located places along the length of the beam before the voids and the remainder of the mild steel was installed. Delay required for this intermediate work never amounted to more than 1/2 hr, and the concrete pouring was immediately resumed. One final lift was required to pour the web and top flange of the beams. This lift included the two end blocks and two diaphragms along the length of the beam.

Samples of concrete for slump tests, entrained air tests, and cylinder tests were taken from every bucket poured. Care was taken

when placing the concrete and vibrating around the location of the internal strain bars, so as not to damage any of the internal gages. None were damaged in the fabrication of all of the beams. The top of the beams was some distance below the top of the forms in each case. The top was screeded with a bar attachment secured on a vibrator, such that it vibrated transversely as the vibrator was moved longitudinally along the beam. Final trowel finishing was accomplished after the concrete developed a set. The cylinders were prepared during the pouring of the beams.

2.3.6 Initial and Intermediate Curing

A double thickness of saturated burlap was placed over the top of the forms. After the cylinders had developed an initial set they were gently positioned on top of the forms. The cylinders, beam and forms were draped with another covering of saturated burlap which extended down to the floor of the bed. Steel cables were supported approximately 2-ft above the top of the forms and 2-ft horizontally away from the beam by poles, over which tarp was suspended. The tarp extended to the floor and formed a completely enclosed steam circulating region around the beam into which steam jets were placed so that they did not strike the forms or concrete surfaces. Initial curing began with the beam thus covered and lasted for a minimum period of 2 hrs. A continuous temperature recording instrument was connected by placing the recording bulb within the beam enclosure. The instrument provided a continuous record of the average curing temperature conditions.

Intermediate curing began with the application of steam into the region under the tarp around the beam. The steam supplied was of 100 percent relative humidity and the temperature in the enclosure maintained at 140 degrees \pm 10 degrees F. Steam curing was continued for a minimum of 36 hours.

Six cylinder specimens were removed from the curing process during the final period of the intermediate curing phase. These cylinders were stripped of their molds, capped with carbo-vitrobond material and allowed to cool for 2 hrs. before being tested in a Forney model QC 225 compression testing machine at the fabricating plant. The ultimate compressive strength of all cylinders tested at transfer surpassed the 4500 psi requirement and therefore the beam was prepared for transferring the prestress force to the concrete.

Steam was discontinued at the time of removal of the 6 test cylinders. Some limited uncovering of the beam was necessary to loosen the forms at the bottom and remove the spreaders at the top, but the beam was covered up again as soon as this was accomplished. The electrical wires for the internal strain bars were connected and recordings taken of the initial value of the gages. The remaining cylinders were removed from the top of the beam and stripped of their molds. Final readings of the 12 strand dynamometers were obtained.

2.3.7 Releasing

The strands were released by torch cutting individual strands at both ends simultaneously. Cuts were made about 10-ft from the end

of the beam. The strand was heated with the torch to obtain as much yielding of the strand as possible in order to obtain a slow transfer. The entire process of cutting the strand was completed in about 15 mins. The forms were removed from the bed and the beam lifted slightly by the overhead cranes, one end at a time, to free it of the pallets. It was set on wood blocks at the future location of the supports. Strain bar readings were taken to determine the initial loss at transfer. The coverings on the beam were removed and the beam was visually inspected along its length for cracks due to transfer in the end regions or to high tensile stresses in the top fibers. No cracks were found in any of the beams.

Lifting the beam by the lifting inserts, the overhead cranes transported the beam to another location within the prestressing building for temporary storage. Again the beams were set on wood blocks at the support locations and the cylinder specimens placed adjacent to the beams. Whittemore target positions, referred to in the next section, were layed out on the beam and their installation accomplished within 1 hr. The strands were cut off approximately 3-in. from the ends of the beam. The prestressing bed was cleaned and prepared for the casting of another beam.

2.3.8 Final Curing

Final curing was carried out with the beam in the supported position within the plant. Conditions were extremely moist for the final phase of curing which ended after approximately 72 hrs., when the temperatures throughout the beam were nearly atmospheric.

2.4 INSTRUMENTATION

Instrumentation consisted of strand dynamometers, internal strain bars, Whittemore strain targets, Ames dial gages, strip scales, SR-4 electrical resistance gages, and miscellaneous items. Photographs were taken of all beams during and after testing in order to study the crack patterns, and to help ascertain the failure mode of the beam.

2.4.1 Strand Dynamometers

Twelve strand dynamometers were used as discussed in the previous section, during the stressing of the prestressing steel and to determine the prestress force prior to release. A detailed description of the dynamometers used at the laboratory can be found in a previous report.⁽¹⁹⁾ Calibration tests were conducted at Fritz Laboratory, both before and after the fabrication of the test beams.

2.4.2 Internal Strain Bars

The normal procedure to determine initial prestress loss used at the laboratory is to remove the forms and attach Whittemore targets along the cgs of the beam before releasing. Steam curing of the beams prohibited removing the forms completely and allowing the beams to cool before the prestress force was released since shrinkage cracks would develop. An alternate method using internal strain bars was adopted to determine the initial losses in the specimen.

Internal strain bars have been used in previous pavement studies.^(20,21) Eight strain bar sets consisting of a 36-in. length

of No. 4 deformed reinforcing bar with an SR-4 gage attached to the center and a small separate temperature-compensating gage were installed in each beam at the locations shown in Fig. 9. The strain bars shown in Fig. 10 were fabricated at the laboratory. A hand grinder was employed to obtain a 1-in. smooth surface at approximately the center of the reinforcing bar. A resistance wire strain gage, type AB-7, was attached at this location with a resin compound. This procedure was repeated for the temperature-compensating elements which were identical to the active strain gages except that the length of bar was approximately 1-in. The gages were wired and waterproofed prior to assembling into the strain bar set. The temperature-compensating gage had to be subjected to all of the conditions of the active gage except load. Felt padding was wrapped around the small 1-in. length of bar, and a rubber finger cot held closed against the lead wires with a rubber band, completed the compensating gage. Electrical tape was used to secure the compensating gage to the center of the strain bar in such a way that the compensating gage protected the active gage.

Temperature-resistance tests were conducted on 3 of the completely wired and waterproofed gages. The results of a typical 5 min. immersion test are shown in Fig. 11, and appear to approximate a linear relationship. A change in the resistance readings of the compensating gage was thus related to a temperature change at the location of the gage. Assuming that the active gage experienced the same temperature change as the compensating gage the true strain in the concrete could thus be found by subtracting the strain due to temperature change from

the total strain recorded by the active gage. Waterproofing appeared to be sufficient since a 20 hr. immersion test resulted in a similar relationship, as seen in Fig. 11.

2.4.3 Whittemore Strain Targets

Deformations were measured by the use of a 5-in. and a 10-in. Whittemore Strain Gage, and also a 0.001-in. calibration extensometer made at the laboratory. Brass plugs, 7/32-in. in diameter and 3/32-in. in thickness were drilled with a No. 1 center drill and used for gage points on the beam. The targets were cemented to the beams with Armstrong Adhesive A-6 epoxy resin. Figure 12 shows the location of all of the targets placed on the beams. Targets represented by a solid circle were installed on both sides of the beam at the prestressing plant after release; targets represented by an open circle were installed on one side of the beam at the laboratory prior to the first test. Targets on rows B and C were used exclusively for crack width measurements. Targets on row D are at the level of the cgs.

The Whittemore strain indicators give the relative movement of two gage points, which can be converted into strain by dividing the readings by the gage length.

2.4.4 Deflection Gages

Deflection measurements were obtained by the use of 0.001-in. Ames dial gages placed under the beam along the longitudinal centerline. Deflection and support settlements were obtained by the use of 0.01-in. strip scales which were read by levels.

2.4.5 SR-4 Electrical Strain Gages

Type A-9, electrical resistance strain gages were attached to the beam at the laboratory prior to the first test. Most of these were located in the compression region of the beam. A Budd Datran Digital Strain Indicator was used in obtaining the strain readings from the 19 gages used on the I-beams and the 38 gages used on the box beams. Figure 12 gives the location of all external electrical gages placed on the beams. These gages had a gage length of 6-in.

2.4.6 Miscellaneous

In every beam the strands projected about 3-in. outside of the end faces of the beam. Plastic tape was wrapped around each strand prior to testing. Measurements were taken of the distance from a reference point on the tape to the end of the beam both at the start of testing and after the failure.

2.5 PRESTRESS FORCE

A deviation in the normal laboratory procedure of obtaining the prestress force was caused by the steam curing of the test beams. Whittemore targets are normally attached to the laboratory size beams after the beam has been uncovered and the forms have been removed but prior to releasing of the prestress force.⁽¹⁵⁾ Shrinkage cracks due to rapid cooling would occur in steam-cured beams if the same procedure were followed. To prevent shrinkage cracks from forming, the forms would have to be pulled back from the beam and the Whittemore targets attached to the surface while the beam remained enclosed within the tarp

canopy. These conditions would not be conducive to locating and attaching the targets to the beam, and therefore, another method had to be employed.

Load dynamometers were placed on 12 strands in each beam to determine the force during stressing and immediately prior to release. Internal strain bars were relied upon to determine the initial elastic strains, and Whittemore targets were placed on the beams as soon as possible after releasing in order to check the results obtained by the strain bars. The strain in the concrete at the level of the cgs is assumed equal to the strain in the prestressing steel for each of the devices used. Furthermore in the case of the strain bars, the strain in the strain bar is assumed equal to the strain in the concrete at the same level in the beam, and in the case of the Whittemore targets, the strain at the surface of the concrete is assumed equal to any interior point at the same level.

Pertinent prestress force information is tabulated in Table 4. The value of F_i was determined from the 12 strand dynamometers used for each beam, and the percent loss at test was determined from considering both the internal strain bar data and the Whittemore readings. A value of F was thus computed by multiplying F_i by the factor 100 percent minus the percent loss at test and dividing the result by 100. The total percent loss is very low however, in these particular test beams it is not out of the possible range. An estimate of the expected elastic initial losses can be obtained by a regression procedure, since an exact value of the prestress force immediately after transfer is not known. Thus:

$$F_{e_{m+1}} = F_i - 3280 \left(\frac{\frac{F_{e_m}}{A} + \frac{(F_{e_m} e - M_d)e}{I}}{E_c} \right) p_t \quad (1)$$

where F_i = prestress force before transfer
 F_{e_m} = prestress force immediately after transfer and m is the number of the trial value for F_e
 p_t = total number of prestressed strands

The terms within the large bracket determine the strain at the level of the cgs in in./in. immediately after transfer and the coefficient is the slope of the load-strain curve for the prestressing strand in the elastic range as discussed in Section 6.5.

The dead load moment at mid-span, including the effect of the 1-ft overhang at each end is:

$$M_d = w \left(\frac{L^2}{8} - \frac{1}{2} \right) \quad (2)$$

A first trial value for F_{e_1} was taken as F_i , and resulted in a calculated value for F_{e_2} . The second trial value for F_{e_2} was taken as the calculated value from the preceding step. This procedure was repeated until F_{e_m} was equal to $F_{e_{m+1}}$. The calculated percent initial elastic loss was determined by dividing $F_{e_{m+1}}$ by F_i and multiplying by 100. All of the values of computed initial elastic loss are presented in Table 4, and the average value of 4.37 is approximately 0.6 times the measured values of the total loss.

Typical prestressed beams of the cross sections tested in use in Pennsylvania today have some important differences from the test

beams. Values of the percent prestress steel are listed in Table 4. An average percentage of only 0.51 percent prestressed steel was used in the box beams, whereas typical values for current designs range from 0.75 to 0.90 percent. (16) I-beams had an average of 0.45 percent prestressed steel, whereas typical values range from 0.70 to 0.85 percent. (16) Thus, the total prestress force for each cross section was considerably less than most typical current designs.

The allowable compressive stress in the concrete at the time of release, f_c^b , is 0.6 times the ultimate compressive strength of the concrete at release, f'_{ci} , according to present specifications. (16) Values of the stress in the bottom fibers at release are presented in Table 4. The average maximum compressive stress for the 4 beams at the time of release was 1740 psi, or only 0.27 times f'_{ci} . This relatively low stress in the concrete was the major factor which reduced the losses to the values obtained.

2.6 HANDLING AND STORAGE

The beams were stored indoors for approximately 3 weeks after fabrication in order to facilitate the various data readings which had to be taken. They were subsequently stored outdoors where the weather conditions were very similar to the conditions indoors except for the moisture content of the atmosphere. All of the cylinders representative of the concrete in each beam were transported with the beams. Beams G-1 and G-2, the two short beams were shipped by truck to Lehigh together as shown in Fig. 13a. Cylinders were packed in straw alongside

the beams. Beams G-3 and G-4 were shipped separately by truck as needed at the laboratory. Figure 13b shows beam G-4 arriving at the laboratory. Beam G-1 was the last beam tested, and arrived on the first shipment with beam G-2. It was stored in a simply supported position on the laboratory floor until it was tested.

2.7 DIMENSIONAL TOLERANCES

Each beam was carefully examined and measured prior to the first test. Beam dimensions were taken at important sections along the length of the I-beams, and at 3-ft spacings along the length of the box beams. The box beam dimensions were particularly valuable since the location of the cardboard void could critically affect the test results. Figure 1 shows the design values of all dimensions. In general the fabrication tolerances were within allowable limits as set by the state specifications. ⁽¹⁶⁾ The length of all of the beams was within $\pm\frac{1}{4}$ -in. Strand location was determined at each end of the beam.

I-beam dimensions were in every case conservative. The web width, top flange width, bottom flange width, and depth were consistently $+\frac{1}{8}$ to $+\frac{1}{4}$ -in. All of the strands were located approximately $\frac{1}{8}$ to $\frac{3}{16}$ -in. high in the beam cross section. Few shrinkage cracks were found, and no cracking was observed in the top fibers of the beams. A horizontal crack in both ends of beam G-4 was observed at the level of the junction of the web and bottom flange. These cracks had not developed at transfer but were easily found when the beam arrived at the laboratory for testing. The crack extended into the beam approximately

2-in. to the location of the first stirrup, but did not affect the behavior of the beam during test.

The box beam dimensions were not always conservative; however, they were usually within the state specifications.⁽¹⁶⁾ Spreader angles used to support the top of the box beam forms were incorrectly measured and resulted in top widths consistently $\frac{1}{4}$ -in. less than the design value of 36-in. The bottom width was within $+1/8$ -in. of the design value and the height was measured to be 36 to $36\frac{1}{2}$ -in. All of the strands were located approximately $\frac{1}{4}$ -in. high and $\frac{1}{4}$ -in. laterally eccentric in the beam cross section. Examination of beam G-1 before testing revealed tension cracks approximately 10-in. apart in the top fibers of the end region of the beam. The cracks near the end of the beam extended downward approximately 10-in. into the beam. These cracks closed as the load was applied and did not affect the behavior of the beam during the test. Tension cracking occurred in the top fibers of beam G-3 approximately 2-ft from each end of the beam at the location of the junction of the hollow box section and the solid end block. The cracks were approximately 5-in. deep at the sides of the beam and did not influence the behavior of the beam during the test.

After the testing was completed, the box beams were broken apart and the cardboard void removed so that inside dimensions could be taken at the same section which was measured on the exterior. Web thickness was found to vary as much as $7/8$ -in. from the design dimensions of 5-in., whereas the maximum tolerance set by the specifications

was $\pm 3/4$ -in. If one side of the web was found to be smaller than the design dimension, the other side was found to be greater; therefore the total web thickness at any section was approximately 10-in. Figure 14a shows the remainder of beam G-3 after the B shear span was removed at the failure region. The right web is 5 and $3/4$ -in. thick at the top near the compression flange; the left web is only 4 and $1/8$ -in. thick at the top. The interior walls and ceiling of the hollow box were smooth since the concrete was vibrated against the in-place void. Figure 14a also illustrates the extremely rough bottom of the hollow box since the bottom flange was placed and vibrated before the void was placed. The top flange of beam G-1 was as thin as $2\frac{1}{2}$ -in. at some locations; beam G-3 had a minimum top flange thickness of 2 and $11/16$ -in. at the section shown in Fig. 14b. Internal diaphragms and end blocks were found bulged out approximately 2-in. The waxed cardboard voids were saturated and the vents and drains were found to have been clogged. Figure 14c shows the wet discolored interior walls of the beam, and one exposed strap used to hold the cardboard void in place during casting of the beam.

3. METHOD OF TESTING

3.1 TEST SETUP

All of the tests were static ultimate load tests, and were conducted in the 5 million pound Baldwin universal testing machine. Using the arrangement of loadings shown in Fig. 15, it was anticipated that a second test could be conducted on the A shear span after the B shear span failed in the first test.

Throughout this report reference will be made to the two sides of the beams by establishing that if one stands at the B end of the beam and looks toward the A end, the side to the right will be denoted as the right side and correspondingly, the side to the left will be denoted as the left side.

Two steel loading beams were required to transmit the load from the testing machine head to the two load points of the first test on all of the test beams except the short I-beam. Loading beam 1 was a 23-in. deep, welded box section and loading beam 2 was a length of a rolled 14W320 section, which is currently unavailable. The end reactions were transmitted through rigid pedestals to the flexure slab floor of the laboratory. Support settlements under full load of up to 1/16-in. were observed during testing. The second test setup was simplified considerably by eliminating the steel loading beam arrangement required in the first test.

The two steel loading beams were carefully aligned and centered before placing under the head of the testing machine. Considerable care was taken to ensure that the test beam was exactly under the center of the testing machine head, and that the loading arrangement introduced no eccentric loading into the test beam. Hydro-stone grout manufactured by U. S. Gypsum Co., was used between the 2-in. steel plates and the beams. The plates located at the load points were checked with a builder's level after the grout was placed.

Figures 16a and b are views of beams G-4 and G-3 respectively prior to the first test. The stub columns placed under the center region of the beam were only safety precautions and did not constitute any support during testing. Wire rope slings were used to catch the loading beams in case of sudden failure; rope slings were used to catch the heavy rollers. Figure 16c is of beam G-1 during the second test. Figure 16d is of beam G-4 during the third test on the A shear span. External steel reinforcement composed of 1-in. diameter rods and steel plates was required to hold the one end together so that the test could be conducted on the other, uncracked end of the beam. Heavy tarp was wrapped around this external reinforcement in some tests in order to confine the steel rods and nuts in case of a failure of the threads on the rods.

3.2 TEST PROCEDURE

First tests commenced by a series of initial readings on all of the instrumentation. Load was then applied statically in increments

of approximately 5 percent of the predicted failure load. These increments were decreased as the load approached the expected flexural cracking, inclined cracking, or failure load. Deflection readings, internal strain bar readings, and external SR-4 gage readings were taken after the application of each load increment. Whittemore readings were taken at selected load levels to determine the strain in the beam, and also to record a history of the width of cracks which developed. Felt tipped pens were used to mark the development of the crack patterns after the application of each load increment. Numbers written on the side of the beam indicate the shear in kips which caused the cracking. Flexural cracking and inclined cracking loads were carefully determined and recorded, along with the ultimate load and various observations made during the test. Photographs were taken before, during, and after the completion of the test.

If an inclined crack suddenly developed in the beam during loading, the loading valve was closed in order to maintain the displacement until the beam stabilized at a lower load. Then the load was increased by increments to the cracking load before taking readings.

Due to the formation and growth of cracks, a long delay in the loading near ultimate was required after reaching a particular load. The loading valve on the testing machine had to be left partially open in order to maintain the load near ultimate. All readings were taken after the deflection stabilized at a given load.

After the completion of the first test the beam was separated at the failure region by means of jacks, wedges, sledge hammers and an

acetylene torch. The remaining part of the beam was examined and reset under the testing machine for the second test. Flexure and shear cracks closed and noticeable camber remained in the beams at the start of the second test. Second tests were conducted on all beams; however, the effects of the first test failure on the long box beam, G-3, were so severe that the second test results were influenced by the damage incurred during the first test.

Crack patterns developing during the second test were again marked with the felt tipped pens; however, dashed lines were used for these patterns. Less instrumentation was employed during this test; however, photographs were taken of all important sequences of the test.

3.3 TEST SCHEDULE

Approximately 2 days were required to complete preparations for the first test. Cylinder tests were conducted immediately after completion of the first test, requiring approximately a total of 10 to 12 hrs. to complete the first test. Separation and preparation required for the second test was completed in approximately $\frac{1}{2}$ day, and the second test was completed within 3 to 4 hrs. Table 3 gives the exact testing schedule followed.

The beams were fabricated and tested in the same order. I-beams were tested in previous research projects,^(13,15) and therefore the small I-beam was first to be tested. The long I-beam was tested next, followed by the long box-beam, and finally the short box-beam.

Preliminary reinforcing bar tests, a strand dynamometer calibration test and 12 load cell calibration tests were completed before the actual test beams were fabricated. A series of 23 reinforcing bar tests, and a series of 5 prestressing strand specimen tests were conducted after the completion of the testing of the test beams. The 12 load cells were recalibrated to ensure the accuracy of the data obtained during fabrication. A gradation analysis was completed on the 3 distinct aggregates used in the concrete.

4. I - B E A M T E S T S

4.1 TEST RESULTS

A summary of the 5 tests conducted on the I-beam specimens is presented in Table 5. Values of shear at flexural cracking, V_{cr} , at inclined cracking, V_{ic} , and at failure, V_u , were obtained from dividing the load indicated on the testing machine, P , by 2.

The short I-beam, G-2, failed in the weaker B shear span in the first test as was anticipated. A sudden but non-catastrophic shear failure occurred. The descriptive title "non-catastrophic", as pertaining to a failure in this series of tests, is indicative of a failure in which, although it occurs suddenly, the beam does not collapse but continues to carry appreciable load after failure. A "catastrophic" failure is indicative of a complete collapse whereby the beam can carry little or no load after failure. A second test on the A shear span resulted in a slow failure due to crushing of the concrete in the compression flange adjacent to the load point. This failure occurred above the top of an inclined crack.

A sudden catastrophic flexural failure was obtained from the first test on the long I-beam, G-4. Two additional tests were then conducted on the undamaged A and B shear spans of this beam. A sudden non-catastrophic shear failure was obtained from the test on the B shear span which was very similar to the failure obtained from the first test on the shorter I-beam, G-2. A slow crushing failure of the compression

flange occurred in the test on the A shear span, which was also very similar to the failure obtained from the second test on the shorter I-beam.

Strand slip during testing was not recorded. Instrumentation on strand slip was limited due to time and the objectives of the tests. Some slip was recorded after completion of the tests, and the results are compiled in Table 7. The mid-span deflection is plotted against the applied load shear for the first tests in Fig. 17a, and for the second and third tests in Fig. 17b. Table 8 contains the crack width data for the I-beams. All of the crack widths were determined from the Whittemore targets located on Rows B and C in Fig. 12. The cracks have been classified as will be discussed in Section 6.3 and are denoted as torsional inclined cracks (T.C.), diagonal tension inclined cracks (D.T.), and flexure shear inclined cracks (F.S.).

4.2 BEHAVIOR AND MODE OF FAILURE OF BEAM G-2

4.2.1 First Test

Beam G-2 was loaded to 144 kips before flexural cracks were observed, first on the right side of the beam, and then progressing across the bottom of the beam to the left side. Diagonal tension inclined cracking occurred suddenly in the heavier reinforced, A end, while the load was being held constant at 208 kips, which was 94 percent of the load causing failure. The load shown on the testing machine dropped off when the inclined cracking occurred and, with the loading valve closed to maintain the displacement, stabilized at 199 kips.

Figure 18a shows the resulting cracks in the A shear span, which had a maximum width at formation of 0.05-in. The load was increased again to 208 kips and held constant while the readings were taken. Diagonal tension inclined cracking occurred suddenly in the lesser reinforced, B end, of the beam after holding this load for approximately 15 minutes. With the displacement maintained, the load on the beam stabilized at 196 kips. Figure 18b shows the resulting cracks in the B shear span, which are very similar to those in the A shear span, except that the maximum width at formation was 0.15-in.

The load was increased to 220 kips, when a sudden but non-catastrophic shear failure occurred in the B end. First indications of failure were spalling of the compression fibers in the B shear span adjacent to the load point, followed seconds later by an inclined crack suddenly shearing through the compression flange, intersecting the location of the spalling, shown in Fig. 18c. There was some relative displacement along the inclined cracking; however, no stirrups were broken during the failure.

Appendix A contains sketches of the crack patterns in the web of the test beams. Two patterns are presented for beam G-2, one for each shear span at the inclined cracking load. These sketches will be discussed in full in Section 6.3.1.

Appendix B contains graphs of the strain distribution in the compression fibers of the beams as obtained from electrical resistance SR-4 gages used in the first tests only. The location of the SR-4 gages

is shown in Fig. 12. Five gages were placed at the sections one-half times d from the load points; whereas, only 3 were placed at the centerline. The extra 2 gages were positioned 4-in. below the top of the beam and thus the strain is less at this level as seen in the graphs.

Beam G-2 exhibited somewhat greater strains on the left side than on the right side of the beam. The longitudinal strain distribution indicates constantly increasing strain along the axis of the beam from the gages nearest the support toward those near the load point until a shear of 104 kips is reached. This is the shear causing diagonal tension inclined cracking in first the A shear span of the beam and later in the B shear span. The strain distribution in each end indicates that the strain at a distance of one-half of d from the load point continued to increase past the cracking load; however, all of the other gages further back from the load point decreased their strain value. A decrease in the strain is due to the change in the direction of the resultant compressive force which must point down toward the reaction in order to maintain the equilibrium requirements within the cracked member. The loss of compressive strain on the A end is much less than on the B end during the formation of the inclined cracks. The gages nearest the support indicate that tensile strains were occurring in these regions. After inclined cracking the A end strains remained constant indicating that the resultant compressive force did not change its direction further; however, the B end strains recorded additional tensile strain indicating further rotation of the resultant compressive force downward toward the support.

After failure it was noted that inclined cracking in the B end had progressed to within a few inches of the end of the beam as seen in Fig. 18b. This cracking was at the level of the top strand, indicating that the beam may have been close to a failure by separation of the tension flange from the remainder of the beam. No slip was recorded at the A end of the beam on any of the strands, but all 4 of the strands at the B end of the top level recorded a slip of approximately 3/32-in.

Towards the end of the test the inclined cracks in the B shear span had opened up approximately 0.06-in. from after formation, while those in the A shear span had only opened up an additional 0.013-in. A 0.21-in. maximum crack width was the last measured value, and was obtained while the load was 98.2 percent of the load causing failure. Figure 19a shows a linear relationship for the opening of each crack as the load was increased beyond the cracking load.

4.2.2 Second Test

After separating the specimen at the location of the failure in the first test it was reset under the testing machine. Complete recovery was apparent since there was practically no change in the strain at the level of the cgs from the start of the first test to the start of the second test. Tension cracks developed in the top fibers of the A shear span during the failure of the first test as can be seen in Fig. 20a. The diagonal tension inclined cracks closed approximately 0.027-in. after the first test. Flexural cracks which had developed during the first test reopened noticeably in the region below the load point at a load of 120 kips which was 51 percent of the load causing failure in the

second test. This was another indication that there was no loss of prestress force in the first test. At a load of 200 kips, inclined cracks developed across existing flexural cracks in the C shear span. No significant new inclined cracking occurred in the A shear span during this test.

A slow failure occurred at a load of 236 kips due to crushing of the concrete in the compression flange adjacent to the load point, as seen in Fig. 20b. This beam failed in flexure, but was certainly influenced to some extent by the existence of the inclined cracking, since the failure occurred in the weaker shear span above the top of an inclined crack. Approximately 15 minutes elapsed while the beam held the load of 236 kips before it failed. Tension cracks parallel to the direction of the compressive stress were observed in the region in which crushing occurred, at a load of 232 kips. A detail of the failure region is seen in Fig. 20c.

Figure 20b shows the same inclined cracking extending back toward the end of the beam as was seen in the first test; however, no slip was recorded on any of the strands at the A end. No measurements of slip could be made on the other end at the separation location. The last measured maximum value of the width of the diagonal tension inclined crack was 0.106-in., obtained while the load was 98.4 percent of the load causing failure. This width was approximately $\frac{1}{2}$ that measured for the cracks in the B shear span. Figure 21a contains a plot of the reopening of the diagonal tension inclined crack in the A shear span during reloading in the second test. A residual opening of 0.038-in. remained after completion of the first test.

4.3 BEHAVIOR AND MODE OF FAILURE OF BEAM G-4

4.3.1 First Test

Beam G-4 was loaded to 68 kips before flexural cracks were observed, first on the right side of the beam, and then progressing across the bottom to the left side at a load of 76 kips. Figure 22a shows the beam carrying a load of 124 kips, which was 94 percent of the ultimate load. The deflection was approximately $4\frac{1}{2}$ -in. at the time this picture was taken. The beam failed in flexure, suddenly and catastrophically, after it had held a load of 132 kips for several minutes.

Inclined flexure shear cracking had developed as a continuation of flexural cracks in both shear spans prior to failure. At failure these flexure shear cracks had formed a distance of approximately $1\frac{1}{2}$ times the effective depth of the beam from the load point into each shear span, as seen in the crack patterns in Appendix A. At no time did it appear that these cracks would cause failure, and additional cracking would probably have had to form further from the load point before shear would have been critical.

Failure occurred in the exact center of the beam. Figure 22b shows the detail of the failure region. Note the crushing of the concrete and the buckling of the two No. 6 bars used as tensile reinforcement in the top of the beam. Warning of the failure was given by spalling and by tension cracking parallel to the direction of the compressive stress just below the top fibers of the beam.

Figure 23 shows the strain distribution history at the centerline of the beam. The change in strain from before transfer to after

transfer is an elastic strain, and the additional change in strain to before the first test is an inelastic strain due to creep of the concrete and relaxation of the prestressed steel. All elastic changes in strain which occurred during testing were therefore plotted from the after transfer strain plot. The last strain reading which was recorded prior to failure was 0.23 percent strain in the top fibers at the centerline of the beam and at the center of the cross section. The values of strain on either side of the beam at the same location were 0.215 percent strain. These values of strain were obtained at the failure load, approximately 2 minutes prior to failure.

Appendix B contains graphs of the strain distribution during the first test. Beam G-4 exhibited uniform strain distribution at the three locations instrumented. The longitudinal strain distribution indicates constantly increasing strain along the axis of the beam from the gages nearest the support toward the gages near the load point.

No appreciable slip of any of the strands was recorded at either end of the beam. Maximum flexure shear inclined crack widths of 0.032-in. and 0.027-in. were obtained for the A and B shear spans respectively, while the load was maintained at 97 percent of the load causing failure. These measurements were obtained from the targets, on Row C in Fig. 12.

4.3.2 Second Test - B Shear Span

The second test on the B shear span was conducted with a 15-ft span since the center, C region, of the beam was destroyed in

the first test. External reinforcement was used to strengthen that part of region B which was cracked during the first test. The first flexural crack appeared on the right side of the beam under the load point, at a load of 152 kips. This crack did not progress across the bottom of the beam to appear on the left side until the load had reached 200 kips.

Diagonal tension inclined cracking first occurred in the reinforced shear span at a load of 223 kips, which was 98 percent of the load causing failure. With the deflection maintained at what it was when the inclined cracking occurred, the load indicated on the testing machine dropped to 202 kips. During reloading, diagonal tension inclined cracking occurred in the test region when the load was increased to 221 kips, and the load subsequently dropped to 209 kips. Figure 24a shows the resulting crack in the test region which is also shown in the crack pattern sketch in Appendix A. A maximum crack width of 0.079-in. was obtained at the formation of this crack.

The beam was reloaded to 228 kips and held the load for approximately 10 minutes when a sudden but noncatastrophic shear failure occurred due to shearing of the compression flange adjacent to the load point in the test region, as seen in Fig. 24b. The failure occurred at 85 percent of the moment causing failure in the first test. Figure 24c shows a close view of the failure crack shearing through the compression flange. This failure was similar to the failure of the B shear span on beam G-2.

No stirrups were broken in the failure. The inclined crack again extended back toward the end of the beam as can be seen in Fig. 24b. This crack had not developed when the inclined crack formed since it does not appear in Fig. 24a. No slip was recorded on any of the strands at this end of the beam. A maximum diagonal tension inclined crack width of 0.131-in. was obtained while the beam was sustaining the failure load, but prior to failure. Figure 19b shows a linear relationship for the opening of the diagonal tension inclined crack in the test region as the load was increased beyond the cracking load.

4.3.3 Third Test - A Shear Span

The second test on the A shear span was also conducted on a 15-ft span. External reinforcement was used to strengthen that part of Region A which was cracked during the first test. The first flexural crack appeared on the right side of the beam under the load point, again at a load of 152 kips as it did in the preceding test on the B shear span. This crack, like the preceding one in the B shear span, did not progress across the bottom of the beam to appear on the left side until the load had reached 208 kips.

Diagonal tension inclined cracking occurred in the reinforced region at a load of 232 kips. With the loading valve closed to maintain the displacement that caused the cracking, the load dropped to 225 kips. Subsequent increase in the load caused additional inclined cracks to form in the reinforced region. Diagonal tension inclined cracking occurred in the test region at a load of 238 kips, as seen in the crack pattern sketch in Appendix A. This diagonal tension inclined crack appeared at

a slightly higher load than those in the second test on the B shear span. A maximum crack width of 0.033-in. was obtained at the formation of this inclined crack.

Failure was preceded by the formation of tension cracks parallel to the direction of the compressive stress and adjacent to the load point in the test region. At a load of 272 kips the beam failed due to crushing of the concrete in the compression flange at the location of the tension cracking, as seen in Fig. 25a. Figure 25b shows the crushing of the concrete in the compression flange, and a view of the external reinforcement used for the cracked region. The failure occurred at 102 percent of the moment causing failure in the first test. A flexural failure was obtained, but again, as in the second test on beam G-2, was influenced by the inclined cracking which existed in the region of failure.

None of the stirrups were broken during the failure. A slip of $3/32$ -in. was recorded on 3, non-adjacent strands in the strand pattern. A maximum diagonal tension inclined crack width of 0.098-in. was obtained while the beam sustained 98.5 percent of the load causing failure. Figure 19b shows a linear relationship for the opening of the inclined crack as the load was increased beyond the cracking load.

5. BOX BEAM TESTS

5.1 TEST RESULTS

A summary of the 4 tests conducted on the box beam specimens is presented in Table 6, and the values listed were obtained in the same manner as those in Table 5 which were discussed in Section 4.1.

The short box beam developed inclined cracking in the two shear spans at different applied loads, and furthermore, the left and right webs of the beam in each shear span developed inclined cracking at different applied loads as indicated in Table 6. Inclined cracks were observed which formed back toward the support and were very high in the beam. These cracks appeared to be torsional cracks. The beam failed suddenly and catastrophically in the stronger A shear span due to crushing and shearing of the concrete at the head of an inclined crack.

A second test was conducted on the B shear span of Beam G-1, but again the action of the beam was modified due to the cracked web on the right side. Torsional cracking developed in the left web and top of the beam, and failure followed shortly thereafter. A flexural crack developing a distance approximately $1\frac{1}{2}$ times d from the load point, triggered the failure.

An extremely violent and catastrophic failure occurred in the B shear span of the long box beam, G-3. No torsional effects were observed since the predominate cracking was flexure shear inclined crack-

ing which was symmetrical. Stirrup fractures triggered the failure in the B shear span. The damage from the first test was not limited to the immediate failure region at the B load point, but extended into the A shear span.

A second test was conducted on the A shear span, but the resulting, arch-type cracking patterns on both sides indicated that the damage due to the first test had altered the action of the beam for the second test. The test data was retained and studied for a plausible explanation of the failure.

Strand slip, previously discussed in Section 4.1 in connection with the I-beam tests, is included in Table 7. The mid-span deflection is plotted against the applied load shear for the first tests in Fig. 17a, and for the second tests in Fig. 17b.

5.2 BEHAVIOR AND MODE OF FAILURE OF BEAM G-1

5.2.1 First Test

Beam G-1 was loaded to 240 kips before flexural cracks were observed. Diagonal tension inclined cracking occurred on the right side of the B shear span at a load of 272 kips, which was 68 percent of the load causing failure. This crack appeared very early in the loading of the beam, and followed the expected path of most diagonal tension cracks, extending from the reaction up toward the load point, but contained within the web of the beam. Appendix A contains a sketch of this shear span immediately after the crack formed. The load indicated on the testing machine dropped to 261 kips. When the load was subsequently increased,

inclined cracking occurred on the left side of the A shear span at a load of 304 kips, which was 77 percent of the load causing failure, causing the load to drop to 300 kips. A maximum initial crack width at the cg in the left web was measured as 0.035-in. The crack formed well back from the load point and extended up to and partially through the top flange. It can be seen in the sketch contained in Appendix A. Cracking of this type results from torsional stresses in the beam.

Diagonal tension inclined cracking next occurred on the right side of the A end at a load of 384 kips, which was 97 percent of the load causing failure, causing the load to drop to 370 kips. This crack is also sketched in Appendix A. Each diagonal tension crack formed after the beam had sustained the cracking load for several minutes.

The beam failed in shear suddenly and catastrophically in the A end at a load of 397 kips. The failure started at the head of the inclined crack on the right side of the beam shown in Fig. 26a. Failure was due to crushing and shearing of the concrete in the compression flange at the head of the inclined crack. Figure 26b shows the effect of the failure on the left side where the lower crack formed as a result of the failure starting on the opposite side of the beam.

The strain distribution for Beam G-1, as seen in Appendix B, indicates that the strain was approximately uniform near the B load point until a shear of 136 kips was reached. The effects of the diagonal tension inclined crack which occurred at this load can be clearly seen from the distribution. Very little increase in strain took place

at the head of the inclined crack. The strain at the left side near the A load point does not correspond to this pattern because the crack was a torsional crack and formed well back toward the support; however, on the right side, the effects of the diagonal tension inclined cracking can be clearly seen to reduce the compressive strain at the head of the crack by approximately one-half. Longitudinal strain distributions for the short box beam, G-1, indicate that there is a reduction in the incremental strain as the load is increased beyond the inclined cracking load for each side of each shear span. The left side of the B shear span did not develop any inclined crack during the first test.

No stirrups were broken during the failure; however, some of the stirrups on the right side, Fig. 26a, pulled out at the splice which was crossed by the inclined crack. Stirrups on the left side shown in Fig. 26b were deformed considerably by the crushing of the concrete, but were not broken. Slip readings of 1/16-in. were recorded on 3 strands, but most of the strands did not record any slip at the A end of the beam. The maximum crack width of the torsional crack in the left side of the A shear span was measured as 0.05-in. at 89 percent of the load causing failure.

5.2.2 Second Test

The B shear span was prepared for testing after the separation was performed at the failure region near the A load point. Figure 27a shows the condition of the right side of the B shear span at the start of the second test. Crack widths were measured with a microscope at the 3 locations circled on the beam and numbered 1 to 3. Crack width data

was not obtained from these inclined cracks during the first test. The maximum inclined crack width at the start of the second test on the right side, B end was 0.06-in. at location number 2. A width of 0.05-in. and 0.04-in. was measured at locations numbered 1 and 3 respectively. Figure 27b shows the condition of the left side of the B shear span which had not developed any inclined cracks during the first test. Tension cracks in the compression flange of the B shear span formed during the sudden failure in the first test. Full recovery of the prestress force was evident since the strain along the cgs was the same at the start of the second test as it had been at the start of the first test.

Flexural cracks beneath the load point, which had formed during the first test in the C region, opened noticeably at a load of 208 kips, which was 48 percent of the load causing failure. Inclined cracks formed in the C region across the existing flexural cracks at a load of 208 kips. These cracks formed back toward the reaction; however, they did not extend into the top flange and did not cause suspicion of torsion. Inclined cracking occurred on the left side of the B end at a load of 413 kips, which was 96 percent of the load causing failure, causing the load to drop to 402 kips. This crack, shown in Fig. 27c and sketched in Appendix A, was the one which is high in the web and farthest back from the load point. It developed suddenly and ran through into the top compression flange, where it ran parallel to the direction of the compressive stress and terminated at the load point, creating a critical region at the head of the crack.

A sudden shear failure occurred at a load of 431 kips, due to crushing and shearing of the compression flange adjacent to the load point in the B shear span. The small dotted flexural crack at the bottom of the beam shown in Fig. 27c, formed at a section approximately 2 times the effective depth of the beam, d , from the load point. It precipitated the inclined crack which ran up to the load point. This region was already critical due to the crack in the top flange of the beam, and when the inclined crack formed, the beam failed. Figure 27d is a close view of the failure region in the top of the beam. Extensive crushing of the concrete occurred in the failure region adjacent to the load point. Figure 27e shows the resulting cracks on the right side of the beam. These cracks were extremely far back from the load point and caused strands adjacent to this side to pull out.

Slip measurements of 3/8-in. were recorded on some strands, and almost all of the strands had some appreciable slip. The 2 strands adjacent to the right side slipped so far that the tape on the strand was in contact with the end of the beam, thus destroying any measurement at all. None of the stirrups were broken during the test. Maximum inclined crack widths on the right side, B end, were measured as 0.06-in., 0.17-in., and 0.08-in. at locations 1, 2, and 3 respectively at a load of 97 percent of the load causing failure. Figure 21a contains a plot of the reopening during the second test of the diagonal tension inclined crack which had formed during the first test on the right side of the B shear span. This data was obtained from a micro-

scope reading of a 0.01-in. scale, and thus is not as fine a measurement as could be obtained from Whittemore targets.

5.3 BEHAVIOR AND MODE OF FAILURE OF BEAM G-3

5.3.1 First Test

Beam G-3 was the largest and heaviest beam in the series. Flexural cracks developed simultaneously on both sides of the beam at a load of 136 kips. Inclined flexure shear cracking developed in both shear spans and extended to both sides of the beam. At a load of 192 kips, flexural cracks had developed a distance of approximately 2 times the effective depth of the beam into the shear span from the load point. The action in all 4 web locations was quite similar, unlike the first test on the smaller box beam. Figure 28a shows the beam carrying a load of 232 kips which was 91 percent of the ultimate load, and the deflection was $5\frac{1}{2}$ -in. at the time this picture was taken.

The beam failed in shear adjacent to the load point in the B shear span as seen in Fig. 28b. The failure occurred suddenly and very catastrophically at a load of 255.3 kips. Two stirrups were fractured on each side at a flexure shear crack which had begun as a flexural crack at a distance from the load point approximately equal to twice the effective depth of the beam. As soon as the stirrups failed, the beam collapsed, impinging the center region on the stub columns which were about 6-in. lower than the beam. The momentum of the beam after impinging on the stub column caused it to rotate about the stub column. The A end, which weighed approximately $6\frac{1}{2}$ tons, was lifted upward off

of the support, and the 2-in. thick plate placed on top of the roller fell to the floor before the beam came back down on the support. Safety cables were partially fractured as they received the sudden load of the 2 steel loading beams. Tension cracks developed all along the top of the beam in the center region, almost causing a separation to occur at the center of the beam as seen in Fig. 29c.

Figure 29a shows the complete ruin of the right side of the beam at the B load point. Figure 29b shows the equally demolished left side of the beam at the same location, and the compression flange adjacent to the B load point. This was the most dynamic failure observed in the series. Flexure shear cracks in the A shear span reached a maximum width of 0.05-in. at 97.2 percent of the load causing failure. Those in the B shear span reached a maximum width of 0.132-in. at the same load. These crack widths were measured at the level of the cg of the section, and are plotted against the applied load in Fig. 21b.

The strain distribution for Beam G-3, which is presented in Appendix B, appears to be very uniform at the centerline of the beam. Some small decrease in strain is seen on the right side near the load point, prior to the shear failure. The longitudinal strain distributions for the long box beam, indicate a similar pattern to the uncracked shear span of the shorter box beam. Only a slight reduction occurred in the compressive strain at the head of the flexure shear cracks on the right side near the B load point prior to failure.

No slip was recorded in any of the strands at either end of the beam, despite the sudden impact load on the strand as the beam

impinged on the stub column. After separation and internal examination it was discovered that the strand had been pushed upward at the location of the impinging such that all of the concrete cover in the bottom flange was broken loose, exposing the strand. It was impossible to determine if any wire failures occurred in the strand at this location. Extensive flexure shear cracking had occurred in the A shear span during the first test, as can be seen in the crack patterns presented in Appendix A.

5.3.2. Second Test

Since the center region was almost split in half, the second test was conducted with a 15-ft span consisting of the portion of the beam which had been the A shear span. External bracing was used to reinforce the region nearest the load point in the first test.

Cracking developed in a very unorthodox manner, and the beam failed in shear in the unreinforced region at approximately 80 percent of the expected capacity. Figures 30a and b show the arching type cracks which developed on each side of the beam. The behavior of the beam indicated that the test was definitely affected by the violent failure in the first test.

Strand slip of approximately 1/16-in. was observed in approximately half of the strands at the A end of the beam. A maximum crack width of 0.126-in. was measured on the left side at the cg in the test shear span at a load of 87.5 percent of the load causing failure.

6. STRENGTH OF TEST BEAMS

6.1 GENERAL

The analysis of the strength of the test beams followed closely the analysis of the smaller F series beams.⁽¹⁵⁾ I-beams only were considered in the F series beams; however, this series included 2 box and 2 I-beams. The analysis proceeded virtually the same for both cross sections tested. The load causing flexural cracking was determined because it marks the beginning of the transition range from uncracked beam action to cracked beam action. It is also important in determining the inclined cracking strength of members with long shear spans. The load causing inclined cracking in these tests marks the most important change in the loading of the beam. This load is used in every current design procedure and the method of calculating this load is the basic difference behind the various methods which have been proposed. The ultimate flexural capacity of a beam can be thought of as an upper limit on the amount of web reinforcement to be supplied in a shear span, since increasing the ultimate shear strength beyond the ultimate flexural capacity is theoretically not feasible. Determination of the ultimate shear strength of the beam is the primary objective of this series of tests.

In the following sections of this chapter each of these four capacities is determined. None of the previous research projects at Lehigh University have tested a prestressed concrete box beam in order

to investigate the shear capacity. Analysis of the box beams and I-beams differed in the determination of the inclined cracking strength of the beams. By virtue of the 2 web walls being separated by the width of the cardboard void, the action in one web is not necessarily the same as in the other web. Torsional cracks resulted in the unsymmetrical inclined cracking of the short box beam tests.

Response to loading was linear prior to the detection of any flexural cracking, which occurred at the marked shears on the load-deflection curves for the first tests in Fig. 17a. A relatively sharp change in slope is noted after the formation of flexural cracking in the center of the beams. This sharp change in slope marks the beginning of the transition range from the uncracked to cracked loading range. Response to loading again approaches a linear relationship as the load is increased beyond the transition range for beams G-3 and G-4. Beams G-1 and G-2, both having a span of 27-ft, failed essentially at the end of the transition region of the curve. Beams G-3 and G-4, both having a span of 45-ft, failed after sustaining a relatively long quasi-linear response region of the load-deflection curve. Shears at which diagonal tension inclined cracking occurred have been marked on the load-deflection curves of G-1 and G-2.

Load-deflection curves for the second tests are shown in Fig. 17b. Although flexural cracks existed at the start of the second test on beam G-1, the response to load was again essentially linear. The second test results for G-3 and both tests on G-4, show a linear response to load for a beam which had developed flexural cracking prior

to loading. A very short region of the load deflection curve for the second test on G-2 can be considered linear. This particular beam developed diagonal tension inclined cracking during the first test, thus practically eliminating any linear response to load during the second test. An extremely short transition range is exhibited for both tests on beam G-4, probably because the span was only 15-ft.

The presence of web reinforcement increased the ultimate capacity of the beams and also permitted greater deflection prior to failure. A prestressed beam without web reinforcement can be expected to fail at loads close to the load causing significant inclined cracking. The quasi-linear portion of the load-deflection curve is attributable to the web reinforcement and thus provides the extremely important greater ductility of prestressed beams with web reinforcement.

A majority of the analysis conducted on these beams was simplified and aided by the use of the Lehigh University, GE-225 digital computer. In the following analyses, it would appear to be too laborious to include all of the refinements which have been included; however, through the use of the computer, the solution becomes almost trivial once the basic theoretical analysis is completed. There were, however, some cases in which the amount of savings in time resulting from a computer solution would be small, and in such cases conventional calculation procedures were preferred.

6.2 FLEXURAL CRACKING STRENGTH

The value of applied shear causing flexural cracking, V_{cr} ,

was the first significant change in the action of the beam during testing. Values of the maximum applied load moment causing flexural cracking are related to V_{cr} by:

$$M_{cr} = V_{cr} a \quad (3)$$

Values of both V_{cr} and M_{cr} for the first tests are listed in Table 9.

The flexural cracking moment, M_{fc} , can be calculated from the equation:

$$M_{fc} = M_{cr} + M_d = Z^b \left(f'_t + \frac{F}{A} + \frac{Fe}{Z^b} \right) \quad (4)$$

which when solved for f'_t becomes:

$$f'_t = \frac{V_{cr} a + M_d}{Z^b} - F \left(\frac{1}{A} + \frac{e}{Z^b} \right) \quad (5)$$

The dead load moment at mid-span including the effect of the 1-ft overhang at each end, was computed by Eq. 2 from Section 2.5 and is listed in Table 9.

Equation 5 was used to compute values of the flexural tensile strength of the concrete using the actual dimensions and the transformed properties of the section. The average value of the computed tensile stress in the bottom fibers at flexural cracking was 498 psi, and all of the values of f'_t are listed in Table 9.

The average value of f'_t obtained from the F series beams was 770 psi. Hanson and Hulsbos tried to relate f'_t to $\sqrt{f'_c}$ and f'_{sp} ; however, their data did not reveal any definite trend. (15) Most of their

data was for values of f'_c between 6000 and 7000 psi. Except for beam G-2, where f'_c was equal to 6660 psi, the other 3 beams had values of f'_c ranging from 7580 to 7920 psi. The value of f'_t and the value of the ratios f'_t to $\sqrt{f'_c}$ and f'_t to f'_{sp} for beam G-2 fit the F series data relatively well. Values for the other 3 beams are below the average values of the F series beams, but it is impossible to compare them directly because of the higher strength concrete. The high cement factor used in the mix and the steam curing of the concrete both tend to increase the occurrence of shrinkage cracks which might have caused lower values of f'_t .

Equation 5 was rearranged and solved for V_{cr} . The value of the flexural tensile strength was assumed equal to $9.5\sqrt{f'_c}$, the average value obtained from the F series beams, ⁽¹⁵⁾ resulting in the equation:

$$V_{cr} = \frac{z^b (9.5\sqrt{f'_c} + \frac{F}{A} + \frac{Fe}{Zb}) - M_d}{a} \quad (6)$$

Values of the calculated flexural cracking shear and the ratio of test to the thus calculated shear are given in Table 9. The average ratio is 0.87.

The flexural cracks developed at spacings ranging from 12-in. to 24-in. in the C region of the beams. The initial development extended up to the level of the cgs; however, the cracks extended rapidly up to the mid-height of the web with increasing load. Additional flexural cracks developed half-way between the spacings of the initial cracks and extended likewise up to the mid-height. Considerable "Y" branching of individual flexural cracks was noted after they attained a height

somewhere near the mid-height of the web, as can be seen in Fig. 29c, which is of the first test on the long box beam. Flexural cracks developing near vertical stirrups tended to be very close to the stirrup locations; however, other flexural cracks which developed mid-way between stirrups did not appear to be pulled over toward the stirrup locations.

All of the beams exhibited a slight lateral eccentricity of the prestress force ranging up to $\frac{1}{4}$ -in. eccentric toward the left side of the beam. Flexural cracking developed simultaneously on both sides of the box beams; however, flexural cracks appeared first on the right side of each I-beam and did not progress across the beam until the load was increased by one or two increments. Since all of the beams exhibited the lateral eccentricity, it could probably be traced to some characteristic of the prestressing bed.

6.3 INCLINED CRACKING STRENGTH

6.3.1 Types of Inclined Cracking

Three distinctly different types of inclined cracks were observed in the test beams. Diagonal tension inclined cracking and flexure shear inclined cracking occurred on both I-beams and box beams; torsional cracking occurred only on the box beams. The important characteristics of these types of cracking are illustrated in Fig. 31, and are discussed below.

Diagonal tension inclined cracking started from an interior point in the web of the beam, and on the particular shear spans tested,

always occurred at a higher load than that which caused flexural cracking. Each side of the same shear span of the box beam had a different shear causing diagonal tension inclined cracking.

Flexure shear inclined cracking was always associated with the formation of a flexural crack some distance from the load point toward the support. If the distance was short, the flexural crack would turn toward the load point and if the distance was relatively long, it would precipitate the formation of inclined cracking in the web above it. In general both sides of the shear span of the box beams had the same load causing flexure shear inclined cracking, since the controlling stress occurs in the bottom fibers of the beam which are physically connected by the concrete in the bottom flange, whereas the diagonal tension cracking is a phenomena associated with a stress in an interior portion of the web which is not physically connected to the opposite side of the beam at that height.

Torsional inclined cracks developed in only the box beams in which diagonal tension inclined cracking had already occurred at a lower load at some location in the beam. These cracks formed well back toward the support and although they appeared to start in the web, progressed rapidly up into the top compression flange of the beam. The cracks ran longitudinally along the compression flange toward the load point, in one case reaching the load point and in another case being restrained before reaching the load point.

A discussion and analysis of the inclined cracking will follow the derivation of the web stresses and description of the sketches pre-

sented in Appendix A.

6.3.2 Web Stresses and Crack Patterns

Appendix A contains sketches of the crack patterns in the webs of the test beams as reconstructed from photographs taken during testing. Elevation views are presented for crack patterns which developed at the inclined cracking load, and sometimes also at the failure load. All cracking which had developed in the first test of the beams prior to the applied load indicated at the load point is shown by heavy solid lines. All cracking which developed in the second test is shown by a dashed line. One sketch for each end of each I-beam was sufficient to present the cracks which had developed; however, box beam crack patterns had to be presented in two sketches for each end, one for each side, since the crack patterns in the separate webs were not the same in most cases. The value of shear in the shear span corresponding to the load at which the flexural cracks were first observed is written below the crack in the sketches. Cracks which were extension of shear cracks and extended downward from the web to the bottom fibers have no value of shear written beneath them, since they are not flexural cracks. Vertical web reinforcement locations are shown in the conventional manner. Values of shear which caused individual cracks to form can be obtained from the photographs presented for the discussion of the specific tests referred to in Chapters 4 and 5.

Web stresses were computed at various locations in the beam. The vertical normal stress was assumed to be zero, and thus the state of stress in the web was defined by a horizontal normal stress and a

shearing stress. The normal stress was calculated from:

$$f = F \left(\frac{ey}{I} - \frac{1}{A} \right) - \frac{y}{I} (V_{ic} x + M_d) \quad (7)$$

The origin of the coordinate system is taken at the intersection of the grid line through the support reaction and the cg of the transformed section, x being positive when measured along the cg of the transformed section in the direction toward the centerline of the beam, and y being positive upwards. The shearing stress was calculated from:

$$v = \frac{Q (V_{ic} + V_d)}{Ib} \quad (8)$$

where the dead load shear and moment were calculated from:

$$V_d = w \left(\frac{L}{2} - x \right) \quad (9)$$

$$M_d = \frac{w}{2} (Lx - x^2 - 1) \quad (10)$$

The dead load moment equation includes the effect of the 1-ft overhang at the support and is valid for x and L expressed in feet. The principal tensile stress was determined from the relationship derived from Mohr's circle which can be written as:

$$f_{pt} = \frac{f}{2} + \sqrt{\left(\frac{f}{2}\right)^2 + v^2} \quad (11)$$

The slope of the compressive stress trajectory was calculated from:

$$\theta = \frac{1}{2} \tan^{-1} \left(\frac{2v}{f} \right) \quad (12)$$

The compressive stress trajectory was drawn as a light dashed line through the intersection of a grid line with the horizontal plane passing through the cg of the box beam or mid-height of the web of the I-beam. The slope of the compressive stress trajectory was known at this intersection and the slope at either upper or lower limit of the web could be approximated very closely by interpolating between values of θ calculated at the intersection of the top or bottom of the web and the grid lines. Values of the principal tensile stress are written at the intersections of the grid lines and the horizontal plane.

By substituting $-\bar{y}$ for y in Eq. 7, the flexural stresses at the intersection of the grid lines and the bottom fibers were calculated. These stresses are based on an uncracked section and thus are not exact; however, they do give an indication of the value of stress.

6.3.3 Inclined Cracking Shear

Because of the interplay of the three different types of inclined cracking discussed in Section 6.3.1, and also because of the few test results obtained, it seems wise to discuss the inclined cracking behavior for each beam separately. Reference to the sketches in Appendix A will be helpful in visualizing the subsequent discussion. The magnitudes of crack widths measured during testing are presented in Table 8.

The average principal tensile stress existing at the cg of the cross section in the webs of the smaller F series beams at the inclined cracking load was found to be expressed by: ⁽¹⁵⁾

$$f_{pt} = (8 - 0.78 \frac{a}{d}) \sqrt{f'_c} \quad (13)$$

Table 11 includes the predicted values of f_{pt}^{cg} at inclined cracking for the G series beams. The value of the ultimate compressive strength of the concrete, f'_c , was taken as the average of the vibrated cylinders cast in waxed cardboard molds as given in Table 2, since the above equation was obtained from data based on similar type cylinders. The values of f_{pt} as observed in the G series beams are listed and compared to the predicted values. The method developed from the F series beams⁽¹⁵⁾ recommends that the value of f_{pt} be calculated at the junction of the web and bottom flange, if the cg is located in the bottom flange. After studying the crack patterns for the I-beams, it was apparent that the maximum principal tensile stress along the inclined cracks for these members occurred nearer the mid-height of the web. Hence, the stress, f_{pt} , is taken at the cg for the box beams, but at the mid-height of the web for the I-beams. The following information in this section is a discussion of the selected values of the inclined cracking shears for each beam.

Beam G-2

Perhaps the simplest inclined cracking occurred on the short I-beam, G-2. Although both shear spans had identical inclined cracking loads, and although the crack patterns are somewhat similar, the cracking phenomena were caused by different actions within the beam.

The A shear span of the beam was the first to develop an inclined crack. A flexural crack formed at a distance d from the load

point, indicated by the \surd mark on the sketch. This flexural crack influenced the stress condition in the web above it, and precipitated the inclined cracking which first formed close to the load point and then progressed back toward the support. The path of these cracks, although generally parallel to the principal stress trajectory at the mid-height of the web, does not bend at the top and bottom of the web. The cracks are almost straight lines. Stresses in the web calculated from the uncracked assumptions indicate that a maximum stress of 316 psi was reached, which is only 63 percent of the predicted value from the F series results. This cracking is classified as flexure shear inclined cracking and the flexural crack formed at a stress of 640 psi in the bottom fibers of the beam.

The B shear span developed an inclined crack at the same load, but due to diagonal tension inclined cracking. No flexural crack was found beyond the one marked at approximately 12-in. from the load point which occurred at a shear of 104 kips. Stresses in the bottom fibers of the beam indicate that a flexural crack could have been expected to form; however, the flexural crack which formed at 104 kips caused a reduction in the stress for some distance along the bottom fibers. The maximum stress in the web at this load was 376 psi, which is 88 percent of the predicted value and is high enough to have caused diagonal tension inclined cracking. The cracking started back near the support and then in progression, forward toward the load point. Some slight curvature can be detected as the cracks turn at the extremities of the web in order to follow the path of the principal stress trajectory.

Beam G-4

The long I-beam, G-4, produced the only pure flexural failure in this series of tests. The shear span crack patterns indicate that only flexure shear cracking had formed prior to failure. Stresses generally below 200 psi were produced at the mid-height of the web, and stresses of this magnitude are below the values normally associated with diagonal tension inclined cracking. Flexural cracks had developed a distance of approximately one and one-half times d from the load point, and additional flexural cracking further back from the load point would probably have had to form before flexure shear inclined cracking could have lead to failure.

Both second tests were conducted on uncracked shear spans. Flexural cracks had just appeared under the load point when diagonal tension inclined cracking occurred in each test. A shear of 110.5 kips caused the diagonal tension cracks to form in the B shear span test at a corresponding principal tensile stress of 360 psi at the mid-height of the web, or 72 percent of the predicted value. A shear of 119.2 kips caused the same type of cracking to form in the A shear span test. The corresponding maximum principal tensile stress was 403 psi or 81 percent of the predicted value. These cracks followed the path of the principal stress trajectory extremely well.

Beam G-1

Considerable complicating developments occurred during the testing of the short box beam G-1. A diagonal tension inclined crack first formed on the right side of the B shear span at a shear of 136

kips and a corresponding principal tensile stress of only 294 psi. This stress was only 62 percent of the predicted value. No flexural cracks had developed in the shear span at the formation of this crack. The crack extended deep down into the bottom flange and back toward the support.

The cracked web of the right side of the beam caused an important change in the internal forces within the specimen. Figure 16b is a view of the test setup for the long box beam, G-3. The same setup was used for beam G-1, and an elevation view is shown in Fig. 32. A spherical head was placed under the head of the testing machine so that it could not be moved horizontally as denoted in Fig. 32. If the beam does not move in the horizontal plane, and the spherical head does not move in the horizontal plane, then the spherical head cannot rotate after the test has commenced. Thus the plane A-A at the level of the top of the beam must remain parallel to the head of the testing machine which is level.

A diagonal tension crack on one side of the beam only, has two important effects. First, it causes the shear center, s.c., to move toward the opposite side of the beam at the instant this crack forms; however, the shear center returns to its original position, at the centerline of the cross section, as soon as the stirrups which are crossed by the inclined crack yield and carry the shear in the cracked web. It is possible that it does not come all the way back to the centerline, but it is relatively close since the shear strength of the cracked web has not been exhausted. The second important change is the relative stiff-

ness of the sides of the beam. A web sustaining an inclined crack has a reduced stiffness and will tend to deflect more. Since plane A-A must remain horizontal, the resultant load on the beam must shift toward the uncracked web. The resultant can move anywhere within the envelope shown in the elevation. An approximate maximum movement of 8-in. could result; however, any shifting outside of the envelope would cause the loading beam arrangement to become unstable.

A change in the internal forces occurs when the resultant of the load shifts. A torsional moment, M_t , is produced which causes additional shearing stresses in the uncracked web and reduces the shearing stresses in the cracked web.

As discussed in Section 5.2, the next crack to form was a torsional inclined crack in the left side of the A shear span. This crack formed at a shear of 152 kips and a corresponding maximum principal tensile stress based on shear stress only of 354 psi at the cg in the web, but it formed well back from the load point and extended up into the compression flange of the beam. Between grid lines ④ and ⑤ on the sketch, the crack disappeared from the side of the beam, but traveled inward approximately 6-in. before running longitudinally toward the load point. It was restrained near grid line ⑥. This crack was due to the internal twisting moment, M_t .

Another diagonal tension inclined crack developed in the right side of the A shear span at a shear of 192 kips and a corresponding maximum principal tensile stress at the cg in the web of 491 psi. This stress was 104 percent of the predicted value. This crack extended

from the load point downward to the extreme bottom fibers of the beam, following the path of the principal stress trajectory in the region of the web. Some flexure shear cracking had occurred in this shear span prior to the development of this inclined crack, thus the stress in the web may have been somewhat lower than that given. The diagonal tension inclined crack was instrumental in causing the shear failure.

A second test was conducted on the B shear span after the beam failed in the A shear span during the first test. The cracks marked by solid lines in the sketch were produced during the first test. Relatively minor flexure shear cracking had occurred and 2 tension cracks occurred in the top fibers during the failure of the first test. The right shear span had sustained the diagonal tension inclined crack previously discussed during the first test; however, the left side was free from any such cracks. At a shear of 206.5 kips, and a corresponding stress of 545 psi, a torsional crack developed well back from the load point and quite high in the beam. This was 115 percent of the predicted value. This crack crossed into the top compression flange between grid lines ③ and ④ and then at a distance of approximately 10-in. from the edge of the beam, ran forward toward the load point, stopping only inches short of the plate at the load point. This crack, although not in the web of the beam, was instrumental in producing the failure.

Beam G-3

The test of the long box beam, G-3, was not complicated by any torsional cracks occurring as was the short box beam test. Flexural cracks and flexure shear cracks developed practically the same on each

side of each shear span. The flexural crack which subsequently lead to the critical inclined shear crack, developed on each side of the B shear span at a shear of 116 kips, and at a distance of approximately 1.8 times d on the left side and 1.7 times d on the right side from the load point. A \checkmark mark is placed under these cracks in the sketches. Corresponding bottom fiber stresses were 655 psi and 744 psi for each side. The principal tensile stress in the web at the cg above the initiating flexural crack was 245 psi for each web.

The A shear span had developed flexural cracks at a distance of approximately 2.1 times d from the load point on the left side at incipient failure. A lack of photographs for the right side makes it impossible to determine the last flexural crack which formed. A stress of approximately 630 psi caused the flexural crack to form on the left side. If the B shear span had been sufficiently reinforced to prevent a shear failure, then this flexural crack would probably have been the one to cause the critical inclined crack in the A shear span.

Values of the principal tensile stress in the webs of the G series beams averaged 15 percent lower than the predicted values based on results from the F series beams. Torsional cracking values fall within the range of values for diagonal tension and flexure shear inclined cracking. Higher concrete strength and the use of a rich mix could be the cause of the lower values, because of the additional shrinkage cracks.

An average value of the tensile stress in the bottom fibers of the beams causing flexure shear inclined cracking was 680 psi.

This is 20 percent lower than the value obtained from the F series beams.

6.4 ULTIMATE FLEXURAL STRENGTH

The beams were designed to be critical in shear; however, it was desirable to design for a failure which was close to the flexural capacity of the cross section, in order that a reasonable amount of web reinforcement would be required. Consequently the amount of web reinforcement provided in the shear spans of most beams was equal to or slightly less than the minimum amount required to get a flexural failure.

Beam G-4, the long I-beam, failed in flexure. A strain of 0.0023-in. per in. was recorded in the extreme fiber in compression at the failure load. The beam sustained the failure load for approximately 3 minutes after the strain reading was obtained. It is reasonable to expect that this strain increased during this period of time, and that it probably approached a value of 0.0025 to 0.003 at failure. Strains of this magnitude were experienced in the E series tests. (13)

The calculation of the ultimate flexural strength of the test beams was based on the assumed strain and stress distribution shown in Fig. 33. A linear concrete strain distribution through the depth of the section has been shown to be a reasonable assumption by previous investigators. (13) From the equilibrium of internal forces:

$$C = T$$

(14)

$$T = \sum_{i=1}^n T_i = \sum_{i=1}^n A_s f_{s_i} P_i \quad (15)$$

- where
- C = resultant compressive force
 - T = resultant tensile force in the prestressed steel
 - T_i = resultant tensile force in the prestressed steel at a particular level, i
 - A_s = cross sectional area of prestressing strand
 - f_{s_i} = stress in prestress strand at a particular level, i
 - P_i = number of prestressed strand at a particular level, i
 - n = number of levels of prestressed strand

Equations 14 and 15 are valid for all cases. The total compressive force can be separated into two parts; one part due to the force in the concrete, C', and another part due to the force in the non-prestressed steel, C''. Therefore:

$$C = C' + C'' \quad (16)$$

$$C'' = \sum_{i=1}^{n'} C''_i = \sum_{i=1}^{n'} A'_s (f'_{s_i} - k_3 f'_c) P'_i \quad (17)$$

If the lower limit of the rectangular stress block is within the top flange:

$$k_1 c \leq t_{tf} \quad (18a)$$

and for a box or an I-beam:

$$C' = (k_3 f'_c) (b_t k_1 c) \quad (18b)$$

$$k_2 = \frac{1}{2} \quad (18c)$$

If the lower limit of the rectangular stress block is within the chamfer region beneath the top flange:

$$t_{tf} + \lambda u > k_1 c > t_{tf} \quad (19a)$$

and for a box beam:

$$C' = (k_3 f'_c) (b_t t_{tf} + h (b + 2u - \frac{2h}{\lambda}) + \frac{h^2}{\lambda}) \quad (19b)$$

$$k_2 = \frac{(b_t t_{tf}) (\frac{t_{tf}}{2}) + h (b + 2u - \frac{2h}{\lambda}) (t_{tf} + \frac{h}{2}) + \frac{h^2}{\lambda} (t_{tf} + \frac{h}{3})}{(b_t t_{tf} + h (b + 2u - \frac{2h}{\lambda}) + \frac{h^2}{\lambda}) c} \quad (19c)$$

and for an I-beam:

$$C' = (k_3 f'_c) (b_t t_{tf} + h (b_t - \frac{2h}{\lambda}) + \frac{h^2}{\lambda}) \quad (19d)$$

$$k_2 = \frac{(b_t t_{tf}) (\frac{t_{tf}}{2}) + h (b_t - \frac{2h}{\lambda}) (t_{tf} + \frac{h}{2}) + (\frac{h^2}{\lambda}) (t_{tf} + \frac{h}{3})}{(b_t t_{tf} + h (b_t - \frac{2h}{\lambda}) + \frac{h^2}{\lambda}) c} \quad (19e)$$

If the lower limit of the rectangular stress block is within the web:

$$t_{tf} + \lambda u + d_w \geq k_1 c \geq t_{tf} + \lambda u \quad (20a)$$

and for a box beam or an I-beam:

$$C' = (k_3 f'_c) (b_t t_{tf} + bh + \lambda u^2) \quad (20b)$$

$$k_2 = \frac{(b_t t_{tf}) \left(\frac{t_{tf}}{2}\right) + (bh) \left(t_{tf} + \frac{h}{2}\right) + \lambda u^2 \left(t_{tf} + \frac{\lambda u}{3}\right)}{(b_t t_{tf} + bh + \lambda u^2) c} \quad (20c)$$

- where
- C' = resultant compressive force in the concrete
 - C'' = resultant compressive force in the non-prestressed reinforcing steel
 - C''_i = resultant compressive force in the non-prestressed reinforcing steel at a particular level, i
 - k_1 = ratio of maximum compressive stress to average compressive stress
 - k_3 = ratio of maximum compressive stress to strength of concrete, f'_c , determined from standard cylinder tests
 - c = distance from extreme fibers in compression to neutral axis
 - A'_s = cross sectional area of a non-prestressed reinforcing bar
 - f'_{s_i} = stress in the non-prestressed reinforcing steel at a particular level, i
 - P'_i = number of non-prestressed reinforcing bars at a particular level, i
 - n' = number of levels of non-prestressed reinforcing bars
 - t_{tf} = thickness of the top flange without the chamfered portion
 - b_t = width of the top flange of the beam
 - u = width of the chamfer
 - λu = depth of chamfer
 - λ = ratio of depth of chamfer to width of chamfer
 - h = $k_1 c - t_{tf}$ = depth to lower limit of rectangular stress block measured from bottom of the top flange

- d_w = depth of web
- b = total web width
- k_2 = ratio of distance from extreme fiber in compression to the resultant of the compressive force in the concrete to c

From equilibrium of internal and external moments:

$$M_{fu} = T d_c - C' k_2 c - C'' d'_c \quad (21)$$

where

$$d_c = \frac{\sum_{i=1}^n A_s f_{s_i} p_i d_i}{\sum_{i=1}^n A_s f_{s_i} p_i} = \text{distance from extreme fiber in compression to resultant horizontal tensile force in the prestressed steel} \quad (22)$$

$$d'_c = \frac{\sum_{i=1}^{n'} A'_s (f'_{s_i} - k_3 f'_c) p'_i d'_i}{\sum_{i=1}^{n'} A'_s (f'_{s_i} - k_3 f'_c) p'_i} = \text{distance from extreme fiber in compression to resultant horizontal compressive force in the non-prestressed steel} \quad (23)$$

d_i = distance from extreme fiber in compression to a particular level, i , of non-prestressed steel

Assuming a linear concrete strain distribution through the depth of the section:

$$\epsilon_{cu_i} = \left(\frac{d_i - c}{c} \right) \epsilon_u \quad (24)$$

and

$$f'_{s_i} = E \epsilon'_i = \left[\left(\frac{c - d'_i}{c} \right) \epsilon_u + \epsilon_{s1} \right] E \quad (25a)$$

but

$$f'_{s_i} \leq f_y \quad (25b)$$

where

- ϵ_{cu_i} = tensile concrete strain at a particular level, i
- ϵ'_i = compressive concrete strain at a particular level, i
- ϵ_u = ultimate concrete compressive strain
- ϵ_{sl_i} = compressive strain in non-prestressed steel due to inelastic losses in the concrete between time of transfer and time of test at a particular level, i

Values of ϵ_{sl_i} are listed in Table 10, and were obtained from experimental Whittemore readings taken at the time of transfer and at the time of test. The values are less than 10 percent of the strain at yielding for the bars, and were not used in the calculation since Eq. 25b limited f'_{s_i} to a value equal to f_y in every case. The strain at the i -th level of prestressed steel is expressed as:

$$\epsilon_{su_i} = \epsilon_{se} + \epsilon_{ce_i} + \epsilon_{cu_i} \quad (26)$$

$$\epsilon_{ce_i} = \left(\frac{F}{A} + \frac{Fe}{I} y_i \right) \left(\frac{1}{E_c} \right) \quad (27)$$

The strain in the prestressed steel at the effective prestress force, ϵ_{se} , can be determined from an experimental load-strain curve. This procedure is discussed later in this section; however, since the effective prestress force is less than the force required to reach the elastic limit of the material, a form of Eq. 31a could be used.

$$\epsilon_{se} = \frac{F}{32.8 p} \quad (28)$$

- where
- ϵ_{su_i} = total strain in prestressed steel at a particular level, i
 - ϵ_{se} = strain in prestressed steel at the effective prestress force
 - ϵ_{ce_i} = compressive strain in the concrete
 - F = prestress force at the time of test
 - y_i = vertical distance from the cg to a particular level, i , positive upwards
 - E_c = modulus of elasticity of the concrete
 - p = number of prestressed strands

Values for the constants k_1 and k_3 which determine the magnitude of the resultant compressive force in the concrete, as recommended by Mattock, Kriz, and Hognestad,⁽²²⁾ were used as follows:

$$\left. \begin{aligned} k_1 &= 0.85 && \text{for } f'_c \leq 4000 \text{ psi} \\ k_1 &= 0.85 - 0.00005 (f'_c - 4000) && \text{for } f'_c \geq 4000 \text{ psi} \end{aligned} \right\} (29)$$

$$k_3 = 0.85 \quad (30)$$

Assuming a value of ϵ_u equal to 0.3 percent, and the values for the constants expressed in Eqs. 29 and 30, it is possible to make a trial and error solution to determine the location of the neutral axis at failure. The compressive strain in the concrete, ϵ_{ce_i} , can be determined from Eq. 27, for each level of the strand, since it is a function of the initial conditions in the beam, and not the ultimate conditions. Likewise, ϵ_{se} can be determined from Eq. 28. A "c"

distance is then assumed; therefore, ϵ_{su_i} can be determined from Eqs. 24 and 26 for each level of prestressed strand. The load, $A_s f_{s_i}$, can be graphically determined from the load-strain characteristic curve for the strand, Fig. 5. The resultant force due to the prestressed steel can be determined from Eq. 15. Equations 25a or 25b and 17 may be used to determine the resultant compressive force in the non-prestressed reinforcing steel in the top flange of the beam. Depending on the location of the lower limit of the rectangular stress block and the cross section, C' can be determined from Eq. 18b, 19b, 19d, or 20b. The one applicable equation from the preceding four is solved in terms of c . The total resultant compressive force can be determined in terms of c from Eq. 16. A calculated value of c is obtained from Eq. 14. This value is then compared to the assumed value of c and if not equal, a new value of c must be assumed and the procedure repeated until agreement is obtained. When a satisfactory agreement is obtained, the value of k_2 can be determined from Eq. 18c, 19c, 19e, or 20c, depending again on the location of the lower limit of the rectangular stress block and the cross section of the beam. The ultimate flexural strength, M_{fu} , can be determined from Eqs. 22, 23 and 21.

A least squares polynomial curve fitting procedure was followed in order to obtain an equation to represent the load-strain curve of Fig. 5. It was possible to divide the curve into 3 regions; the straight line elastic region, the approximately straight line strain hardening region, and a transition region between these 2 regions. The equations expressing the prestress force in kips, and the strain, ϵ_{su_i} , in per-

cent, obtained are as follows:

$$A_s f_{s_i} = 32.8 \epsilon_{su_i} \quad \text{for } 0 < \epsilon_{su_i} \leq 0.70\% \quad (31a)$$

$$A_s f_{s_i} = -39.5 + 171.8 \epsilon_{su_i} - 157.9 \epsilon_{su_i}^2 + 63.6 \epsilon_{su_i}^3 - 9.4 \epsilon_{su_i}^4 \quad \text{for } 0.70\% < \epsilon_{su_i} \leq 2.0\% \quad (31b)$$

$$A_s f_{s_i} = 29.3 + 0.599 \epsilon_{su_i} \quad \text{for } 2.0\% < \epsilon_{su_i} \quad (31c)$$

Using these equations in place of the graphical determination of the value for $A_s f_{s_i}$, the entire calculation is one which is quite suitable for a computer solution. Consequently, all of the foregoing equations were programmed such that once an initial c was given, along with the various required physical parameters of the cross section, the computer was able to make all of the decisions as to which equations to use, and it subsequently made several trials before being satisfied only when the calculated value of c was within 0.001-in. of the assumed value.

The computed ultimate flexural strengths of the test beams are tabulated in Table 10. Dead load moment at mid-span was computed by Eq. 2. The neutral axis at the computed ultimate flexural capacity was approximately 6.2-in. from the extreme fiber in compression for the I-beam, and 3.25-in. from the extreme fiber in compression for the box beam. Ratios of M_u to the calculated values of $(M_{fu} - M_d)$ are given in the table. The calculated ultimate flexural capacity for the long I-beam,

G-4, failing in flexure was 2.2 percent greater than the test value obtained. This one test correlated very well; however, it was the only true flexural failure in the series.

In the calculation of the flexural strength of the test beams, the actual average dimensions were used, thus accounting for the slight discrepancy between the two box beam results, or between the two I-beam results. These calculations were repeated for values of ϵ_u ranging from 0.25 to 0.3 percent, but the ultimate flexural capacity was extremely insensitive to changes in ϵ_u . The average ultimate concrete strain was 0.27 percent for several flexural failures in the E series tests; however, using this value in the computation changed M_{fu} by only 0.13 percent.

6.5 ULTIMATE SHEAR STRENGTH

A total of 9 ultimate failure tests were conducted on the 4 test beam specimens. One test result was invalid due to a damaged specimen, and of the remaining 8 tests, 3 failed in shear, 2 failed in shear but were influenced by torsion, one failed in flexure, and 2 failed in flexure but were influenced by shear. Tables 5 and 6 present a summary of the test results. None of the test failures appeared to have been influenced by slip of the prestressing strand, and the slip which did occur was a result, rather than a cause of the failure.

Four different modes of shear failures were obtained from the laboratory size F series beams: (15) shearing of the compression flange, fracture of the web reinforcement, crushing of the web, and a

shear compression type failure. All except the last type were due to inclined cracks which remained entirely within the shear span. The fourth type of failure was associated with inclined cracks which crossed under the load point into the constant moment region.

Five beams in the F series failed by shearing of the compression flange;⁽¹⁵⁾ all of these were on second tests. This type of failure was characterized by a sudden, but non-catastrophic shearing of the compression flange as a continuation of an inclined crack. Two I-beams in the G series tests failed in this mode of failure. Beam G-2 failed in this manner at the B end during the first test, as seen in Fig. 18c, and beam G-4 failed in the same manner at the B end during the second test as seen in Fig. 24c. No crushing of the concrete in the failure region was observed during the failure, and both failures occurred on the shear spans with the least amount of web reinforcement.

A somewhat similar failure occurred in two other tests on I-beams. Figures 20c and d are of the second test on beam G-2 and the failure occurred in the A shear span. Figures 25a and b are of the second test on beam G-4 and the failure occurred in the A shear span again. This type of failure was classified as a flexural failure, although influenced to some extent by shear. Beam G-2 failed at 97.5 percent of the computed flexural capacity and is seen to have caused bursting action in the compression flange. Beam G-4 failed at 92.1 percent of the computed flexural capacity and is seen to be less characterized by bursting as it is by crushing and possibly some shearing. This test might be classified as a shearing of the compression

flange type of failure; however, the ultimate moment was 94.5 percent of the moment causing failure in the first test and thus the failure was probably primarily due to flexure. No clear distinction can be drawn between flexural failures and shear failures as shown in this test result. The failures were characterized by a slow crushing of the concrete in the compression flange. The presence of the inclined crack influenced the failure to some degree, since the crushing occurred at the head of the inclined crack, whereas if there was no influence, the crushing might have occurred on either side of the load point. High compressive strains were reached at the location of the incipient failure, since cracking parallel to the direction of the compressive stress trajectory was observed and some "popping" of the concrete occurred in the top fibers of the beam adjacent to the load point. The amount of web reinforcement in these beams was sufficient to carry the additional shear in order to reach the flexural capacity of the members, whereas the amount provided in the opposite ends of the beams was not sufficient and shear failures were obtained.

Ten beams in the F series failed during the first test and 4 additional ones failed during the second test due to fracture of the web reinforcement.⁽¹⁵⁾ These failures were sudden and usually catastrophic, occurring when one or more stirrups, which were crossed by an inclined crack, fractured. A stirrup fracture failure occurred on the long box beam, G-3. This failure was very sudden and catastrophic, as can be seen in Figs. 28b and 29a and b. The failure indicates that the full shear capacity was developed, and occurred when 2 stirrups on each side of the beam fractured.

Eight beams in the F series failed during the first test and 6 additional ones failed during the second test due to crushing of the concrete in the web.⁽¹⁵⁾ A localized region in the webs of the members was crushed and the beams continued to deflect as the load was maintained nearly constant during the slow failure. None of the beams in the G series tests failed in this mode.

Two beams in the F series failed during the first test due to shear compression type failures.⁽¹⁵⁾ Inclined cracks which developed in the critical shear span, undercut the load point and crossed over into the constant moment region where a crushing failure occurred at the head of the cracks in the compression flange. None of the beams in the G series tests failed in this mode either.

Shear failures which were influenced by torsion occurred on the short box beams in the G series tests, whereas, no box beams and no torsional effects were encountered in the F series beams. Other prestressed concrete box beam tests conducted at Lehigh were tests on long members,^(2,8,9) and flexure shear cracking predominated, hence there were no torsional effects. The test results of the short box beam were extremely complicated by the addition of torsional cracking to the other types of cracking in the beam. Both failures involved a shear rather than a flexural mode of failure. Two independent actions existed between the separate webs of the beam. The B end formed a diagonal tension inclined crack on the right side. This crack certainly affected the conditions in the A shear span and caused the torsional inclined crack to form in the left side of the A end. The torsional crack

ran forward toward the load point and thus tended to rip the compression flange longitudinally. The shear in the A shear span had to be carried by the web reinforcement on the left side crossing the crack, the concrete in the compression flange and also the concrete in the uncracked right side of the beam. The shear in the B shear span likewise had to be carried by the web reinforcement on the right side crossing the crack, the concrete in the compression flange, and the concrete in the uncracked left side of the beam. Herein lies the difference of the two ends of the beam. The torsional crack running longitudinally along the compression flange of the A shear span reduces the amount of shear carried in the compression flange on the left side of the beam. Thus greater shear is carried on the right side of the beam in the A shear span than is carried on the left side of the beam in the B shear span. The diagonal tension inclined crack in the A shear span resulted from this shear distribution. A shear failure occurred when the crack suddenly ran through the compression flange to the load point, and, being that the other side of the beam was not able to carry the additional load because of the presence of the torsional crack, the beam failed. Some crushing of the concrete adjacent to the load point at the head of the inclined crack was observed. No cracking parallel to the direction of the principal stress trajectory was noted prior to failure. Comparing Fig. 26a which shows the inclined crack after failure with Fig. 29b which shows the failure of the long box beam, it is evident that this type of breaking up is associated with shear failures and not flexural failures. Although the crushing of the concrete in the longer box beam failure was much more extensive, both failures

indicate crushing along a shear plane, and relatively large pieces of concrete remain.

During the second test on the short box beam, G-1, torsional cracking again effected the failure. Figure 27c shows the torsional crack which formed due to the existence of the diagonal tension inclined crack on the right side of the beam. (The torsional crack is the one closest to the sign.) This crack extended up into the compression flange, ran forward parallel to the compressive stress direction, and stopped only inches short of the load point. A small flexural crack (shown dotted on the photograph) then formed, altering the stress condition above it, and precipitating the inclined crack in the web. This inclined crack ran up toward the load point and was not restrained as it might have been had the region not been at a critical condition due to the torsional crack, and thus caused the shear failure.

Both of the failures on the short box beam were caused by shear; however, due to the presence of the torsional cracks, the beams failed at probably lower values of shear than would otherwise be expected to cause failure.

A significant difference was observed between the shear failures which occurred in the F series beams and those which occurred in the G series beams. Twenty eight out of 35 shear failures in the smaller beams occurred in the webs of the members. Fourteen of these 28 were due to crushing of the concrete in the web, and the others were due to fractures of the web reinforcement. Only 5 of the tests resulted in a shearing failure of the compression flange. All of the shear failures in

the G series beams except for the one fracture of the web reinforcement on the long box beam, occurred in the compression flange. The G series beams were weakest in the compression flange region of the beam; the F series beams were weakest in the web region of the beams. The compression flange of the F series specimens was the same size as the tension flange and amounted to approximately 38 percent of the cross sectional area of concrete. The web comprised 24 percent of the cross sectional area. The compression flange of the G series specimens was much smaller than the tension flange and amounted to 25 and 22 percent of the cross sectional area for the box and I-beams respectively. The webs comprised 38 and 18 percent for the box and I-beams respectively.

Information from the F series beams was used to support a proposed method for designing web reinforcement in prestressed concrete bridge members.⁽¹⁵⁾ The method is basically one of predicting the inclined cracking strength of the beam and adding to this inclined cracking shear, some quantity of shear based on the amount of web reinforcement used in the design. The dependable ultimate shear strength of prestressed concrete beams without web reinforcement has been determined from previous research at Lehigh University to be the load which caused significant inclined cracking.⁽¹⁵⁾ The increase in shear strength beyond the load causing significant inclined cracking was found to be approximately equal to the force in the stirrups which are crossed by an idealized inclined crack. Equation 32 is the proposed ultimate shear equation which, for design purposes, could be solved for A_v or s .

$$V_u = V_c + A_v f_y \frac{d_s}{s} \quad (32)$$

- where
- V_u = ultimate shear strength
 - V_c = shear carried by the concrete, assumed equal to the shear causing significant inclined cracking
 - A_v = area of web reinforcement placed perpendicular to the longitudinal axis of the member
 - f_y = yield point of the web reinforcement, but not larger than 60,000 psi
 - d_s = distance from the extreme fiber in compression (in composite sections from the top of the girder alone) to the lowest level at which the stirrups are effective
 - s = spacing of web reinforcement

Limits are placed on the web reinforcement term of this equation, but the problem resolves itself to one of predicting the shear causing significant inclined cracking. Equations 33 and 34 are the limiting quantities of web reinforcement, but they were waived for the G series beams.

$$A_v \geq \frac{\lambda V_u s}{f_y d_s} \quad (33)$$

$$A_v \leq \frac{7 bs\sqrt{f'_c}}{f_y} \quad (34)$$

- where
- b = total width of web at the section under consideration
 - λ = 0.15 for beams with single webs and 0.20 for beams with double webs

A limiting stress condition is applied against the two types of inclined cracking observed in the smaller beams. The smaller of the shears V_{cd} or V_{cf} is taken as the inclined cracking shear. V_{cd} is the shear causing a principal tensile stress of f_{pt} at the cg of the section, if the cg is within the web, or at the junction of the web and bottom flange if the cg is in the bottom flange, and can be expressed by:

$$V_{cd} = \frac{B_2 + \sqrt{B_2^2 - 4 B_1 B_3}}{2 B_1} \quad (35)$$

and

$$B_1 = \frac{Q_y^2}{I^2 b^2} \quad (36a)$$

$$B_2 = - \frac{x y f_{pt}}{I} \quad (36b)$$

$$B_3 = f_{pt} \left(f_{pt} + \frac{F}{A} - \frac{F e y}{I} + \frac{M_d y}{I} \right) \quad (36c)$$

where

$$f_{pt} = (6 - 0.6 \frac{x}{d}) \sqrt{f'_c} \quad (37a)$$

$$f_{pt} \geq 2\sqrt{f'_c} \quad (37b)$$

The dead load moment, M_d , can be computed by using Eq. 10 from section 6.3.2. Equation 35 is a second degree equation in V_{cd} because a general case has been solved where the stress is taken at any point in the web. A value of f_{pt} is computed at the intersection of the web and the bottom flange for the I-beams because the center of gravity is not located in the web. If "y" is set equal to zero, as would be the case if the center

of gravity did fall in the web, Eq. 35 would reduce to Eq. 38 and the same limiting stress conditions as expressed in Eqs. 37 would be true. The box beams in this series had the center of gravity in the web.

$$V_{cd} = \frac{I b}{Q} \sqrt{f_{pt}^2 + f_{pt} \frac{F}{A}} \quad (38)$$

Flexure shear inclined cracking is initiated by a flexural crack in the bottom fibers of the beam. V_{cf} is the shear causing a tensile stress of f_t^b at a section located a distance d from the section under consideration in the direction of decreasing moment, and is expressed by:

$$V_{cf} = \frac{z^b \left(\frac{F}{A} + \frac{F e}{z^b} + f_t^b \right)}{x - d} \quad (39)$$

where

$$f_t^b = 8\sqrt{f'_c} \quad (40)$$

The ultimate shear strength of the G series beams was predicted by the proposed method. Test to predicted ratios were calculated and the results assembled in Table 12. Beams failing in shear but influenced by torsion are included in the table for completeness; however, they were not included in the computation of the average value of 1.05 for the proposed method. Values of the ratio for beams failing in flexure but influenced by shear are in line with the results for beams failing in shear alone. Likewise, values of the ratio for beams failing in shear but influenced by torsion are in line with the same values. The proposed method adequately predicted all of the failures which are listed in table 12. This composes all valid failures in the series of tests

except for the single flexural failure.

The ultimate shear strength was also predicted by the American Concrete Institute (ACI) Code, ⁽²³⁾ and by the American Association of State Highway Officials (AASHO) Specification. ⁽²⁴⁾ The corresponding values of the ratios are included in Table 12. The average test to predicted ratios for the AASHO and ACI codes were 2.45 and 1.09, respectively.

7. SUMMARY AND CONCLUSIONS

The objective of this investigation was to compare the behavior and strength of full-sized prestressed concrete beams with the behavior and strength of smaller F series beams tested at Lehigh University. Eight valid tests were obtained from these G series beams. Four full-sized beams were included in the series; two had an I-shaped cross section and the other two had a hollow box-shaped cross section. One beam of each cross section had a total length of 47-ft., and the other had a total length of 29-ft; all specimens had a depth of 36-in.

The beams were chosen from standard sections used for prestressed concrete bridges in Pennsylvania. Prestress was applied with 7/16-in. diameter 270 ksi strand. Each strand was initially tensioned to 21.7 kips. Hot rolled deformed No. 2 and No. 3 bars were used for vertical web reinforcement in the shear spans of the girders. Spacing of the stirrups ranged from 12-in. to 22½-in. The concrete strength varied from 6660 psi to 7930 psi, and the average concrete strength at the time of test was 7520 psi.

Diagonal tension, flexure shear, and torsional inclined cracking were observed in the tests. Diagonal tension inclined cracking was due to high principal tensile stresses in the webs of the members. Flexure shear inclined cracking was due to flexural cracks that either turned and became inclined in the direction of increasing moment, or precipitated inclined cracking in the web above the flexural crack. Both of these

types of inclined cracking were observed in the smaller F series beams. Torsional inclined cracking in the box beams developed as a result of diagonal tension inclined cracking developing in one web independent of the web on the other side of the beam. The F series included only I-beams and no torsional inclined cracking developed. The shear causing significant inclined cracking was chosen as the shear causing the formation of an inclined crack which later became associated with the failures. Principal tensile stresses in the webs of the members at inclined cracking was approximately 20 percent lower than the average stress conditions in the smaller F series beams.

Four types of failures were observed: three beams failed in shear, two failed in shear but were influenced by torsion, one failed in flexure, and two failed in flexure but were influenced by shear. The shear failures which were influenced by torsion occurred on the box beam where diagonal tension inclined cracking was important. Only one of the shear failures was in the web of the members, and that failure was due to fracture of the web reinforcement. All other shear failures occurred in the compression flange of the beams. Very few shear failures from the F series tests occurred in the compression flange. The majority of failures on these smaller I-beams were in the webs of the members. Thus, the larger G series beams were weakest in the compression flange region and the smaller F series beams were weakest in the web region of the beams.

Conclusions which were determined from these tests are:

1. The proposed method was found to be applicable to these full-sized prestressed beams, despite the fact that the majority of the failures occurred in a different region of the beam. The average test to predicted ratio for the proposed method of designing web reinforcement was 1.05 which was less than the ratio for the AASHO specification or the ACI Code.
2. Box beam members in which diagonal tension inclined cracking may occur are susceptible to premature failure.
3. Cardboard cylinder molds were found to reduce the strength of cylinders from the values obtained with cast iron or steel molds by about 6 percent.
4. Vibrating the cylinders tended to increase their strength by about 1 to 3 percent from the values obtained by rodding.
5. The effects of these variables on the splitting tensile test strength was less than on the ultimate compressive test strength, for which the preceding figures were given.
6. Internal dimensions were found to be maintained within the tolerances provided by the specifications, except in

some limited instances where web walls of the box beams were found to be slightly less than the minimum allowed.

7. Crack width measurements were obtained and the maximum inclined crack width prior to failure was 0.21-in.

8. NOTATION

a	Length of shear span
a_A, a_B, a_C	Length of shear span in first or second test
A	Cross sectional area of beam
A_s	Cross sectional area of prestressing strand
A'_s	Cross sectional area of tensile reinforcing bar
A_v	Cross sectional area of one stirrup
b	Total web width of box or I-beam
b_t	Width of top flange of beam
c	Distance from extreme fibers in compression to neutral axis
cg	Center of gravity of beam cross section
cgs	Center of gravity of prestressing strand
C	Resultant compressive force
C'	Resultant compressive force in the concrete
C''	Resultant compressive force in the non-prestressed reinforcing steel
C''_i	Resultant compressive force in the non-prestressed reinforcing steel at a particular level, i
d	Distance from extreme fibers in compression to cgs , or effective depth
d_c	Distance from extreme fibers in compression to resultant horizontal tensile force in prestressed steel
d'_c	Distance from extreme fibers in compression to resultant horizontal compressive force in non-prestressed steel

d_i	Distance from extreme fibers in compression to a particular level, i , of prestressed steel
d'_i	Distance from extreme fibers in compression to a particular level, i , of non-prestressed steel
d_w	Depth of web
e	Eccentricity, distance from cg to cgs
E	Modulus of elasticity of non-prestressed reinforcing bars
E_c	Modulus of elasticity of concrete
f	Normal stress
f_b^t	Tensile normal stress in bottom fibers
f_c^b	Allowable compressive stress in concrete at release
f'_c	Ultimate compressive strength of concrete
f'_{ci}	Ultimate compressive strength of concrete at release
f_{pt}	Principal tensile stress
f_{pt}^{cg}	Principal tensile stress at cg
f_{s_i}	Stress in the prestressed steel at a particular level, i
f'_{s_i}	Stress in the non-prestressed steel at a particular level, i
f'_{sp}	Splitting tensile strength of concrete
f'_t	Flexural tensile strength of concrete
f_v	Stress in stirrup
f_y	Yield stress of non-prestressed steel
F	Prestress force at time of test
F_{e_m}	Prestress force immediately after release and m is the number of the trial value for F_e
F_i	Prestress force before transfer

i	Particular level of steel
I	Moment of inertia
k_1	Ratio of maximum compressive stress to average compressive stress
k_2	Ratio of distance from extreme fibers in compression to resultant compressive force in the concrete to c
k_3	Ratio of maximum compressive stress to strength of concrete, f'_c , determined from standard cylinder tests
L	Span length
M	Moment
M_{cr}	Applied load moment causing flexural cracking
M_d	Dead load moment
M_{fc}	Moment causing flexural cracking
M_{fu}	Moment causing flexural failure
M_t	Torsional moment
M_u	Ultimate applied load moment
n	Number of levels of prestressed strand
n'	Number of levels of non-prestressed steel
Q	Moment, about the cg, of the area of the cross section on one side of the horizontal section on which the shearing stress is desired
Q^{bf}	Q for a section taken at the junction of the web and bottom flange
Q^{cg}	Q for a section taken at the cg
Q^{tf}	Q for a section taken at the junction of the web and top flange
Q_y	Q at any level, y
P_i	Number of prestressed strands at a particular level, i

P_i'	Number of non-prestressed bars at a particular level, i
P_t	Number of prestressed strands
P	Applied load as indicated on testing machine
r	Vertical web reinforcement ratio in percent, equal to $100 A_v/bs$
s	Spacing of vertical stirrups
$s.c.$	Shear center
t_{tf}	Thickness of the top flange not including the chamfer
T	Resultant tensile force in prestressed steel
T_i	Resultant tensile force at a particular level, i
u	Width of chamfer
v	Shear stress
vpm	Vibrations per minute
V	Shear
V_{cd}	Shear causing diagonal tension inclined cracking
V_{cf}	Shear causing flexure shear inclined cracking
V_{cr}	Applied load shear causing flexural cracking
V_d	Dead load shear
V_{ic}	Applied load shear causing significant inclined cracking
V_l, V_r	Internal shear in the left or right web of the box beam, respectively
V_u	Ultimate applied load shear
w	Uniform dead load
x	Horizontal location of general point measured from the reaction
y	Vertical location of general point measured from the cg, positive upwards

\bar{y}	Vertical distance from bottom fibers to the centroid of the section
y_i	Vertical distance from the cg to a particular level, i , positive upwards
y_w	Distance from the cg to the intersection of the web and top flange
Z^b	Section modulus with respect to stress in the bottom fibers
Z^t	Section modulus with respect to stress in the top fibers
ϵ	Strain
ϵ_{ce_i}	Compressive strain in the concrete at a particular level, i
ϵ_{cu_i}	Tensile concrete strain at a particular level, i
ϵ'_i	Compressive concrete strain at a particular level, i
ϵ_{se}	Strain in prestressed steel at the effective prestress force
ϵ_{sl}	Strain in non-prestressed steel due to inelastic losses in the concrete between time of transfer and time of test
ϵ_{su_i}	Total strain in prestressed steel at a particular level, i
ϵ_u	Ultimate concrete compressive strain
θ	Angle, with respect to the horizontal, of the compressive stress trajectory
λ	Ratio of depth of chamfer to width of chamfer
λ_u	Depth of chamfer

9. T A B L E S

Table 1 Properties of the G Series Beams

36" x 36" Box Beams						
Properties	Units	Nominal	Beam G-1		Beam G-3	
			Concrete	Transformed	Concrete	Transformed
A	in. ²	585.44	562.1	579.2	588.4	606.2
\bar{y}	in.	15.59	15.46	15.31	15.58	15.43
e	in.	12.17	11.78	11.63	11.80	11.65
I	in. ⁴	88,593	86,140	89,320	90,010	93,310
z ^t	in. ³	4,341	4,167	4,289	4,352	4,479
z ^b	in. ³	5,682	5,572	5,834	5,777	6,048
Q ^{tf}	in. ³	2,667	2,551	2,643	2,681	2,776
Q ^{cg}	in. ³	3,469	3,353	3,463	3,497	3,611
Q ^{bf}	in. ³	3,317	3,206	3,319	3,357	3,475

18" x 36" I-Beams						
Properties	Units	Nominal	Beam G-2		Beam G-4	
			Concrete	Transformed	Concrete	Transformed
A	in. ²	398.44	403.4	416.5	404.6	418.0
\bar{y}	in.	15.21	15.29	15.27	15.34	15.31
e	in.	10.21	10.13	10.11	10.10	10.07
I	in. ⁴	48,742	49,770	52,070	50,150	52,510
z ^t	in. ³	2,344	2,390	2,498	2,407	2,517
z ^b	in. ³	3,205	3,254	3,411	3,270	3,429
Q ^{tf}	in. ³	1,488	1,523	1,603	1,536	1,619
Q ^{cg}	in. ³	1,979	2,014	2,096	2,025	2,110
Q ^{bf}	in. ³	1,977	2,012	2,095	2,024	2,108

Table 2 Properties of the Concrete

BEAM	AT TRANSFER				AT TEST							
	METAL MOLD		CARDBOARD MOLD		METAL MOLD				CARDBOARD MOLD			
	VIBRATED		VIBRATED		VIBRATED			RODDED	VIBRATED			RODDED
	f' _c	E _c	f' _c	E _c	f' _c	E _c	f' _{sp}	f' _c	f' _c	E _c	f' _{sp}	f' _c
	psi	ksi x10 ⁻³	psi	ksi x10 ⁻³	psi	ksi x10 ⁻³	psi	psi	psi	ksi x10 ⁻³	psi	psi
G-1 3 Days** 46 Days	6370		6190		8240*		505		7830*		540	
	6900*		6610*		7760*		660*		7250*		670*	
	6790*		5870*		7600*		690*		7800*	5.3*	615*	
	6740	5.0	6210	4.7	7520*		585*	7690*	7300*	5.0*	520*	6840*
	7340*	5.0*	6980*	4.7*	8710*	5.2*	580*	7850*	7290*	4.9*	540*	7410*
	6760*	5.0*	6690*	4.9*	7660*	5.3*	580*	7680*	8260*	5.1*	610*	7210*
	AVE.	6820	5.0	6430	4.8	7920	5.3	600	7740	7620	5.1	585
G-2 3 Days 32 Days	5660		5480		6910		620		6430			
	5550*		5380*		6720*		605		6190*		570	
	5480*		5730*				555*		6310*		540	
	6210	4.9	5850		6530	4.6	575*	6790*	6540*		600*	
	6440*	4.9*	5620*		6300*	5.0*	600*	6880*	7160	5.1	615*	6570*
	6140*	4.8*	6200*		6840*	5.0*	560*	6880*	6280*	4.8*	580*	6420*
	AVE.	5910	4.9	5710		6660	4.8	585	6880	6520	4.9	570
G-3 2 Days 42 Days	5770		5910		7650		695		7270		665	
	7000*		5800*		8180*		670*		6990*		545*	
	6120*		5220		8360*		580*		6210		650*	
	6130	5.0	6000	4.6	7560	5.0	705*	7460*	7360	4.7	675*	6800*
	7290*	5.0*	6810*	4.7*	7790*	5.5*	580*	7600*	7530*	4.8*	535*	7070*
	7090*	4.6*	5180	5.4	8020*	5.2*	660	7410*	7000*	4.9*	590*	6860*
	AVE.	6570	4.9	5820	4.9	7930	5.2	650	7490	7060	4.8	610
G-4 2 Days 36 Days	6150		6150		7500*		645		7550*		680	
	6120*		5770*		8180*		645		7760*		605	
	6260*		6010*		7890*		565*		7370*		675*	
	6250	4.8	6420	4.5	7620	4.7	580*	7850	7620	4.5	610*	7160
	5990*	4.6*	6660*	5.0*	6810	4.9	730*	7820	7360	4.8	540*	7640
	6440*	4.8*	6460*	4.9*	7480*	4.8*	570*	7600*	7790*	5.1*	635*	7320*
	AVE.	6200	4.7	6250	4.8	7580	4.8	625	7760	7580	4.8	640

* Strength of cylinders representative of concrete in the web and compression flange of the test beams.

** Age of cylinders at transfer and at test

Table 3 Schedule of Operations

Beam	Date					Age At 1st Test (days)
	Cast	Transfer	1st Test	2nd Test	3rd Test	
G-1	4/24/64	4/27/64	6/ 9/64	6/10/64	-	46
G-2	4/17/64	4/20/64	5/19/64	5/20/64	-	32
G-3	4/22/64	4/24/64	6/ 3/64	6/ 5/64	-	42
G-4	4/20/64	4/22/64	5/26/64	5/27/64	5/29/64	36

Table 4 Prestress Data

Beam	F_i (kips)	Percent Loss at Test	F (kips)	Calc. Initial Elas. Loss (percent)	Percent Prestress Steel	f_c^b (psi)	$\frac{f_c^b}{f_{ci}^b}$
G-1	563.8	8	518.7	5.00	0.524	1918	0.281
G-2	345.6	6	324.9	4.20	0.448	1808	0.306
G-3	558.6	8	513.9	4.44	0.501	1678	0.256
G-4	344.8	6	324.1	3.85	0.447	1558	0.252
Ave.				4.37		1741	0.274

Table 5 I-Beam Test Results

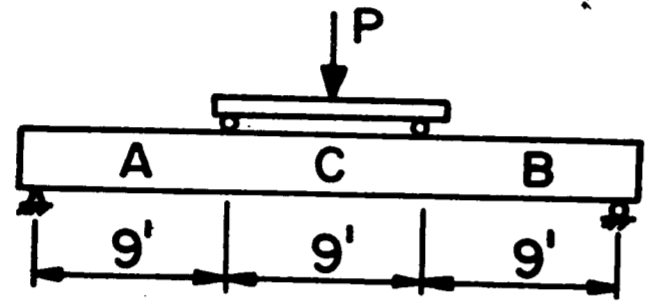
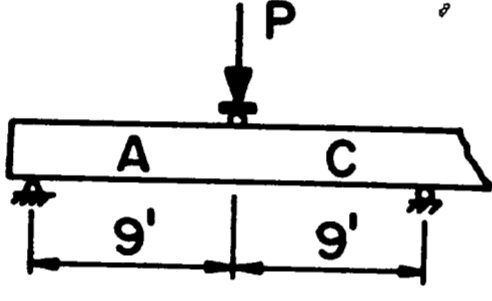
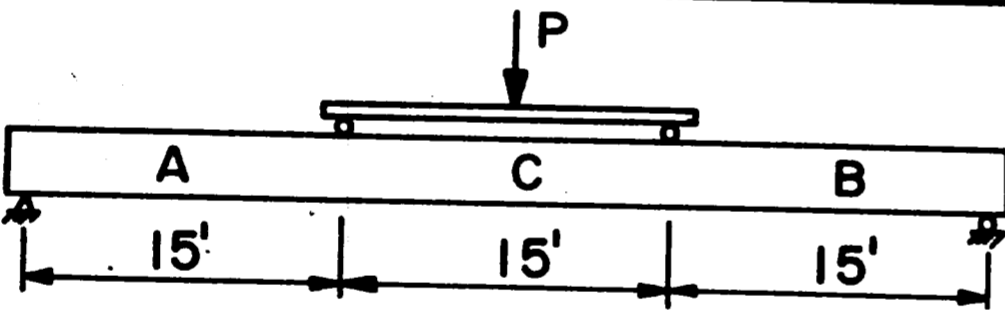
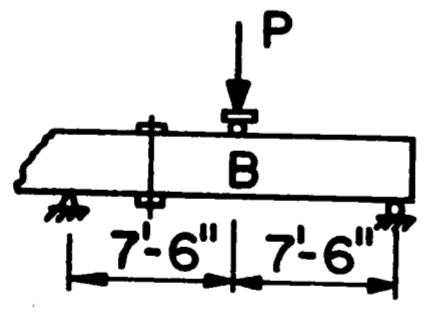
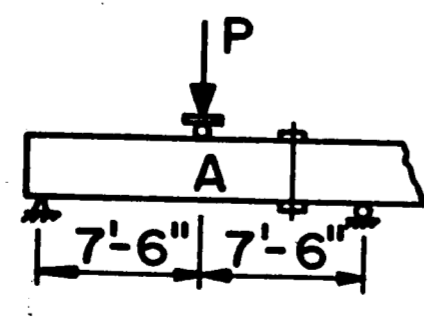
Beam	Test	Test Setup	L (ft)	$\frac{a}{d}$	V_{cr} (kips)	V_{ic} (kips)	V_u (kips)	Failure	Comments
G-2	1		27	3.49	72	A End 104 B End 104	110	B End Shear	Shearing of the Compression Flange
	2		18	3.49	—	C End 100	118	A End Flexure	Influenced by Shear
G-4	1		45	5.84	34	—	66	C Region Flexure	At Exact Center of Span
	2		15	2.92	76	110.5	114	B End Shear	Shearing of the Compression Flange
	3		15	2.92	76	119	136	A End Flexure	Influenced by Shear

Table 6 Box Beam Test Results

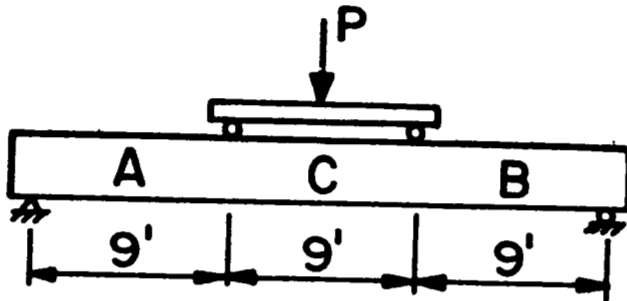
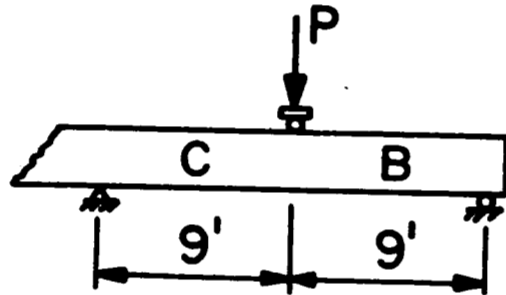
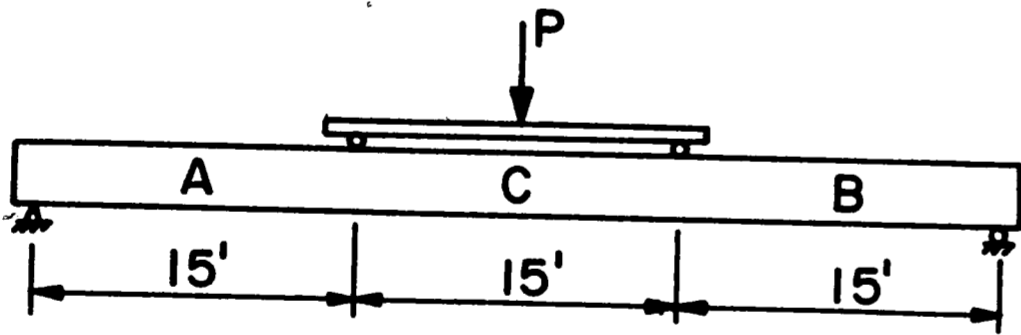
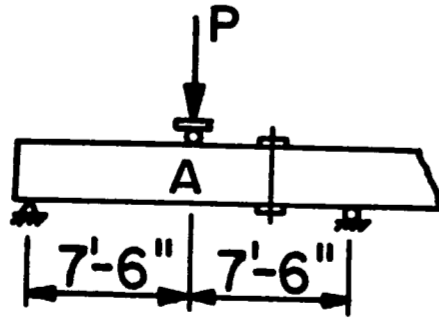
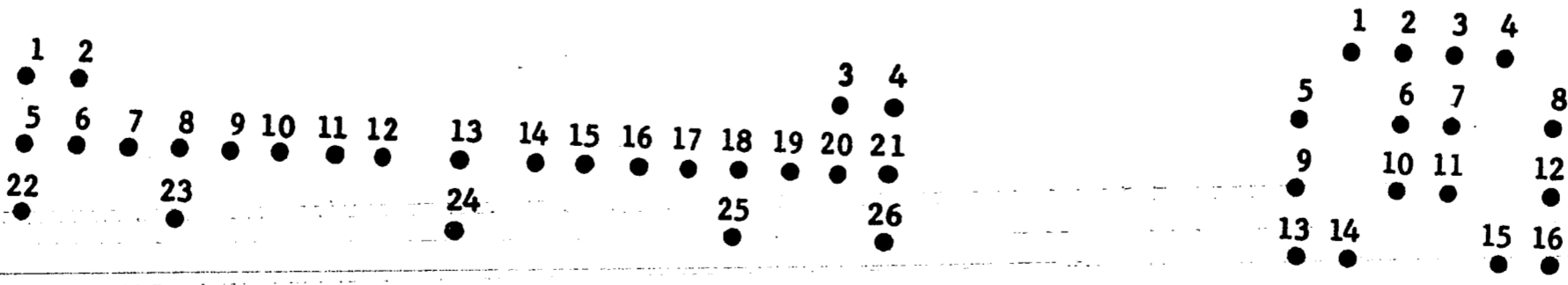
Beam	Test	Test Setup	L (ft)	$\frac{a}{d}$	V_{cr} (kips)	V_{ic} (kips)	V_u (kips)	Failure	Comments
G-1	1		27	3.34	120	(A West) 192 (B West) 136 (A East) 152 (B East) —	198.5	A End Shear	Influenced by Torsion
	2		18	3.34	—	B (East) 206.5	215.5	B End Shear	Influenced by Torsion
G-3	1		45	5.56	68	A End 96 B End 96	127.6	B End Shear	Fracture of Web Reinforcement
	2		15	2.78	—	—	192	A End —	Influenced by Cracking Sustained in the First Test

Table 7 Slip Measurements

STRAND	G - 1			G - 2			G - 3			G - 4			
	FIRST TEST		SECOND TEST	FIRST TEST		SECOND TEST	FIRST TEST		SECOND TEST	FIRST TEST		SECOND TEST	THIRD TEST
	A end	B end	B end	A end	B end	A end	A end	B end	A end	A end	B end	B end	A end
1	-2	0	-1	0	-6	-1	0	0	-4	0	+2	-1	-2
2	0	0	0	+3	-7	-1	+1	0	-3	+1	0	-6	-2
3	0	0	-22	0	-6	0	-2	-1	+1	-2	0	0	-3
4	-1	0	-	+3	-7	-2	-1	+1	0	0	+1	-1	-3
5	0	-5	0	+1	-2	+1	-1	0	-4	+1	+1	-2	-3
6	-4	-1	-3	0	-5	-3	-1	+1	-3	+1	-1	0	-4
7	-2	0	-4	-2	-4	+1	-1	+1	-3	+3	0	-2	-4
8	-3	-4	-4	0	-3	+1	-2	+1	-4	+4	-2	-5	-3
9	-4	+1	-5	0	-3	0	-2	-1	+1	+1	0	-2	0
10	-3	+1	-13	+6	-2	-1	-2	+1	-1	+2	-1	-1	0
11	-2	0	-17	-1	-2	-1	+1	-1	-4	+2	+1	-5	-3
12	-3	0	-13	+1	-4	-2	0	-2	-2	+2	-1	-1	-1
13	-4	+1	-14	0	-1	0	-1	+1	-2	-1	-1	-1	0
14	-3	-1	-14	-2	-3	+1	0	+1	-4	+2	0	-1	0
15	-1	+1	-18	0	-2	-2	-2	-2	-2	-1	0	-1	-4
16	0	0	-19	+1	-3	+1	-1	-1	-3	0	-1	-1	0
17	0	0	-19	-	-	-	0	-2	-6	-	-	-	-
18	-2	0	-20	-	-	-	+1	-5	-7	-	-	-	-
19	-1	0	-20	-	-	-	0	-1	-6	-	-	-	-
20	+1	0	-25	-	-	-	+1	-1	-3	-	-	-	-
21	0	+1	-	-	-	-	+2	-1	-2	-	-	-	-
22	-2	0	-1	-	-	-	-1	+1	0	-	-	-	-
23	0	0	-6	-	-	-	-1	-2	-1	-	-	-	-
24	-1	0	-3	-	-	-	-1	0	0	-	-	-	-
25	0	+1	-10	-	-	-	-2	0	0	-	-	-	-
26	0	0	-	-	-	-	+1	-1	0	-	-	-	-



Box-Beams

I-Beams

Location of Strands

Table 8 Crack Widths

Beam	Test	End	Type of Crack	$\frac{rf_y}{100}$ (psi)	At Cracking		Last Reading	
					Crack Width (in.)	Percent of Ult. Load	Crack Width (in.)	Percent of Ult. Load
G-1	1	A	T.C.	105	0.035	77	0.05	88.6
G-1	2	B	D.T.	59	-	68	0.17	97
G-2	1	A	D.T.	114	0.052	94.5	0.065	98.2
G-2	1	B	D.T.	55	0.154	94.5	0.213	98.2
G-2	2	A	D.T.	114	-	-	0.106	98.4
G-3	1	A	F.S.	70	-	-	0.05	97.2
G-3	1	B	F.S.	56	-	-	0.132	97.2
G-4	1	A	F.S.	91	-	-	0.032	97
G-4	1	B	F.S.	44	-	-	0.027	97
G-4	2	B	D.T.	44	0.079	97	0.131	100
G-4	3	A	D.T.	91	0.033	87.5	0.098	98.5

Table 9 Flexural Cracking Strength

Beam	V_{cr} (kips)	M_{cr} (kip-ft)	M_d (kip-ft)	f'_t (psi)	$\frac{f'_t}{\sqrt{f'_c}}$	$\frac{f'_t}{f'_{sp}}$	Calc. V_{cr} (kips)	$\frac{V_{cr}(\text{Test})}{V_{cr}(\text{Calc})}$
G-1	120	1080	52.9	401	4.54	0.67	144.0	0.83
G-2	72	648	38.0	670	8.21	1.14	75.3	0.96
G-3	68	1020	154.2	492	5.52	0.76	79.9	0.85
G-4	34	510	106.3	430	4.94	0.69	41.6	0.82
Ave.				498	5.79	0.81		0.87

Table 10 Ultimate Flexural Strength

Beam Test	L (ft)	ϵ_{s1i} $\frac{\epsilon_{s1i}}{i}$ (%)	V_u (kips)	M_u (kip-ft)	M_d (kip-ft)	Calc. M_{fu-M_d} (kip-ft)	$\frac{M_u}{M_{fu-M_d}}$ (%)		
G-1	1	27	1	0.0076	198.5	1786.5	52.9	2002	89.2
	2	18	2	0.0082	215.5	1939.5	23.3	2032	95.4
G-2	1	27	1	0.0095	110	990	38.0	1068	92.7
	2	18	1		118	1062	16.8	1089	97.5
G-3	1	45	1	0.0125	127.6	1914.4	154.2	1899	100.8
	2	15	2	0.0129	192	1440	16.9	2036	70.7
G-4	1	45			66	990	106.3	1012	97.8
	2	15	1	0.0165	114	855	11.6	1107	77.2
	3	15			136	1020	11.6	1107	92.1

Table 11 Inclined Cracking Stress Conditions

Beam	End	a/d	f'_c (psi)	Type of Crack	f_{pt}^{cg} (psi)	f_{pt} (psi)	$\frac{f_{pt}}{f_{pt}^{cg}}$	f_t^b (psi)
G-1	A	3.34	7620	D.T.	472	right 491	1.04	-
				T.C.		left 354	0.75	-
	B	D.T.		right 294		0.62	-	
		T.C.		left 545		1.15	-	
G-2	A	3.49	6520	F.S.	428	269	-	640
	B			D.T.		376	0.88	-
G-3	B	5.56	7060	F.S.	308	right 245	-	744
				F.S.		left 245	-	655
G-4	A	2.92	7580	D.T.	498	403	0.81	-
	B			D.T.		360	0.72	-
Ave.							0.85	680

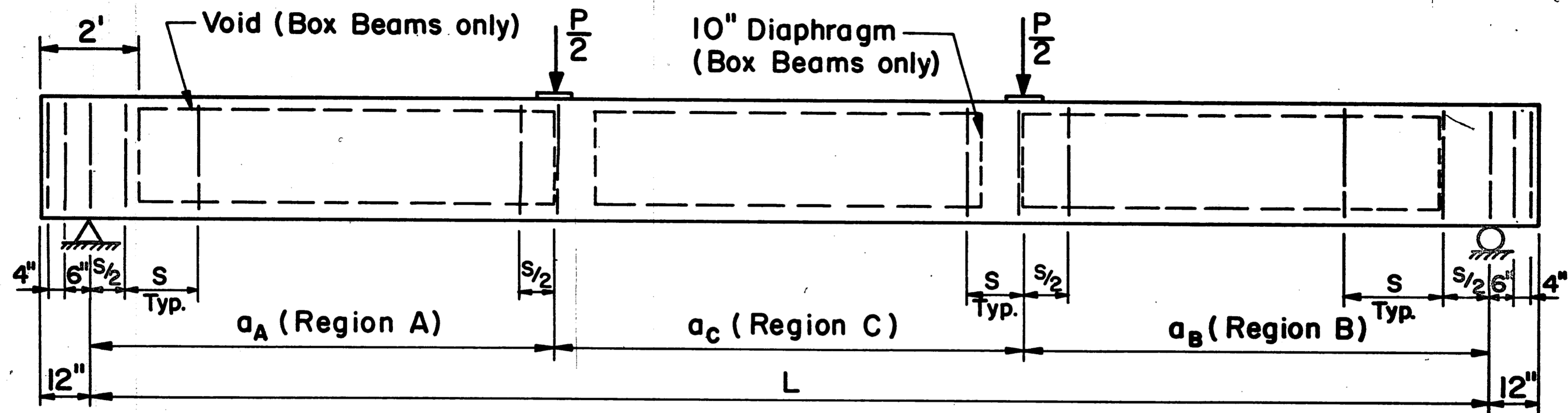
Table 12 Test to Predicted Shear Strength Ratios

Beam	Test	Shear Span	V_u Test/ V_u Pred.		
			Proposed Specification	AASHO Code	ACI Code 318-63
G-1	1**	A	0.96	1.90	0.98
	2**	B	1.14	2.79	1.14
G-2	1	B	1.04	2.53	1.13
	2*	A	1.02	1.87	1.06
G-3	1	B	1.08	1.81	1.13
G-4	2	B	1.03	3.21	1.07
	3*	A	1.13	2.63	1.17
Ave.			1.05	2.45	1.09

* Flexural Failures

** Influenced by Torsion

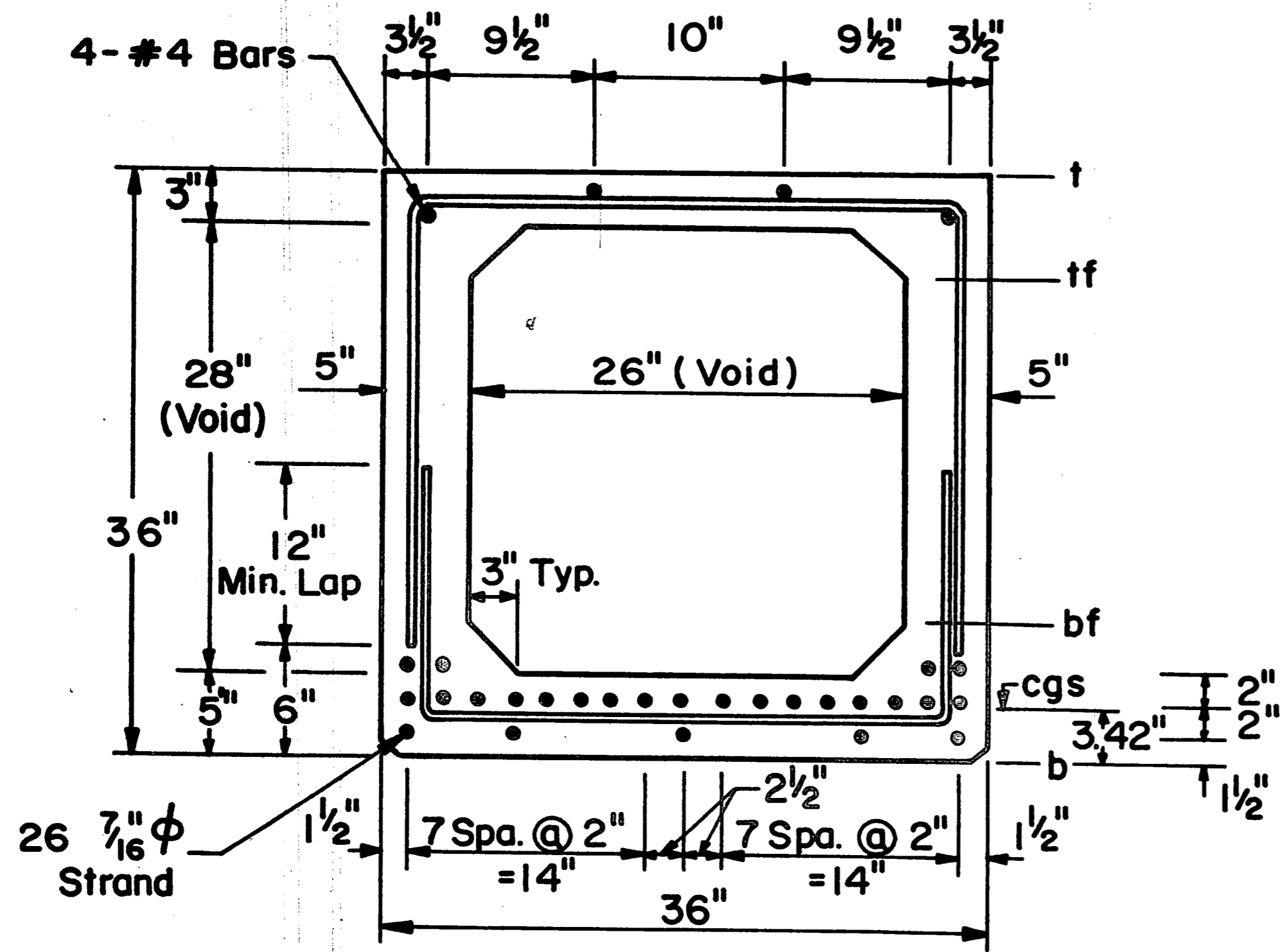
10. FIGURES



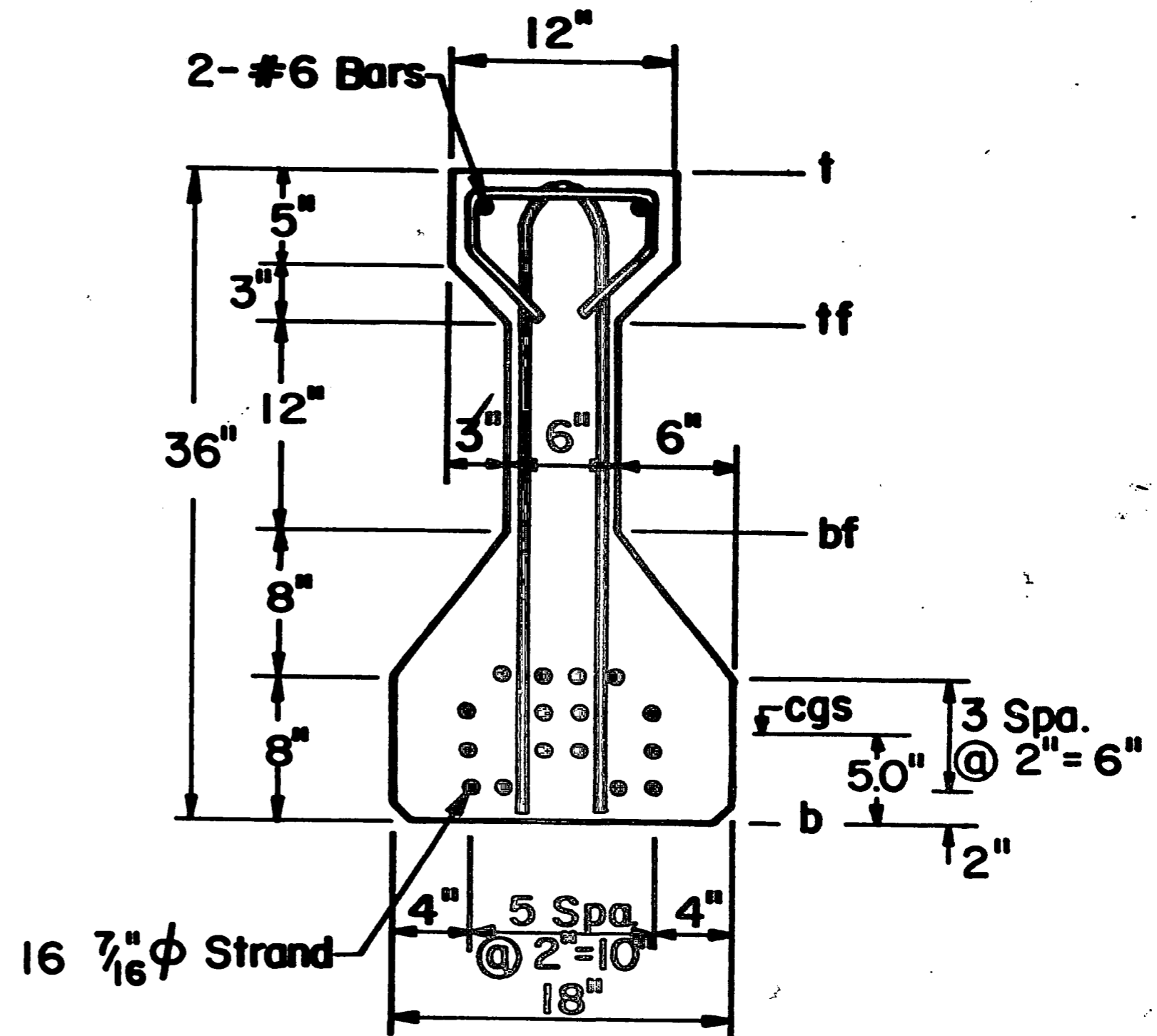
Elevation of Test Beams

Beam	Dimensions			Web Reinforcement								
				Region A			Region C			Region B		
	$a_A = a_B$ (ft)	a_C (ft)	L (ft)	Size (No.)	S (in.)	$r_{fy}/100$ (psi)	Size (No.)	S (in.)	$r_{fy}/100$ (psi)	Size (No.)	S (in.)	$r_{fy}/100$ (psi)
G-1	9	9	27	3	12	105	5	12	247	3	21.6	59
G-2	9	9	27	3	18	114	5	12	412	2	18	55
G-3	15	15	45	3	18	70	5	12	247	3	22.5	56
G-4	15	15	45	3	22.5	91	5	12	412	2	22.5	44

Fig. 1 Details of Full-Sized, G Series Beams



Box Beams G-1 and G-3



I Beams G-2 and G-4

Note: Dimensions and details not shown conform to standards in Reference I.

Fig. 2 Sectional Views of Full-Sized, G Series Beams

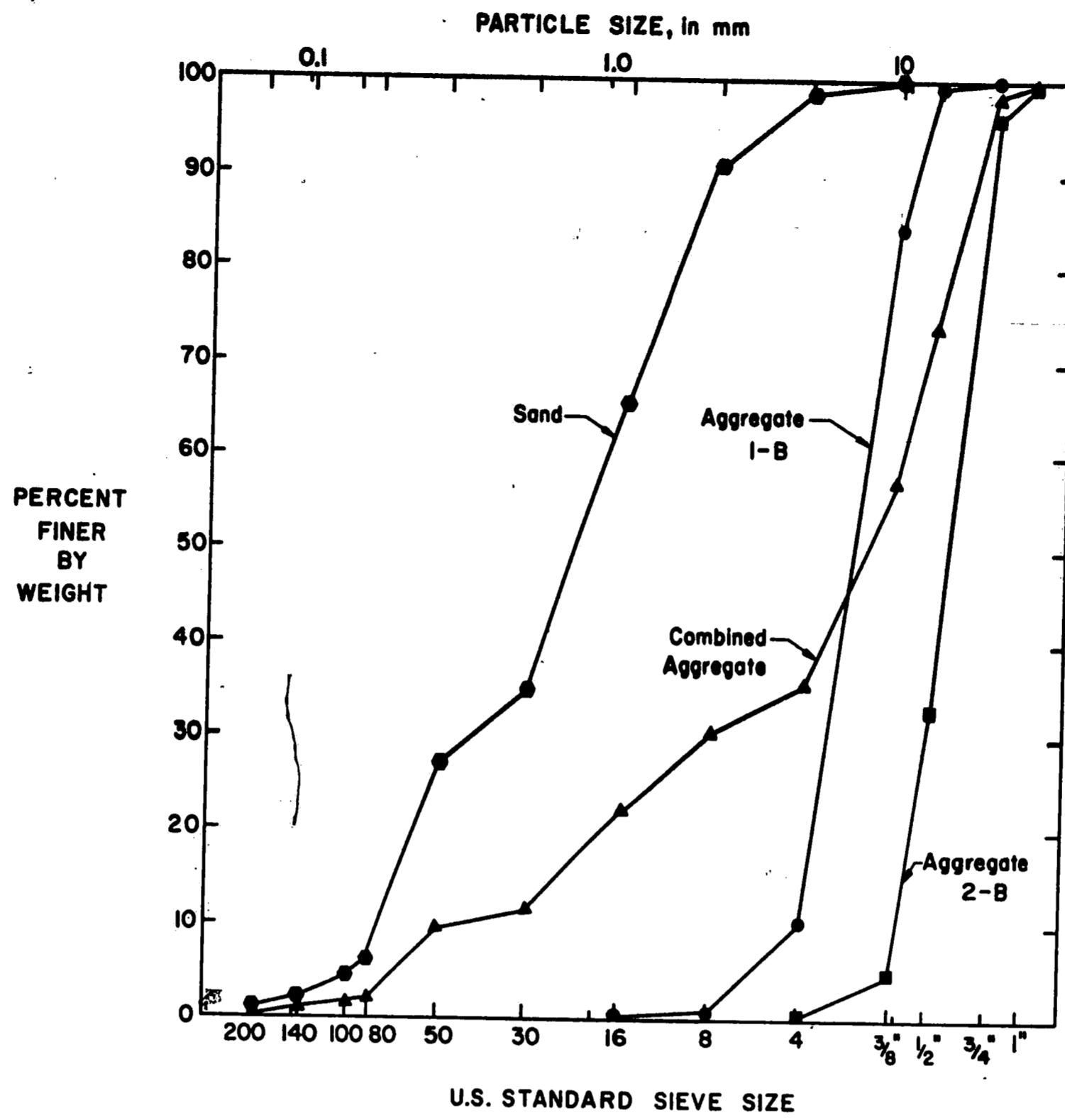


Fig. 3 Gradation of Fine and Coarse Aggregate

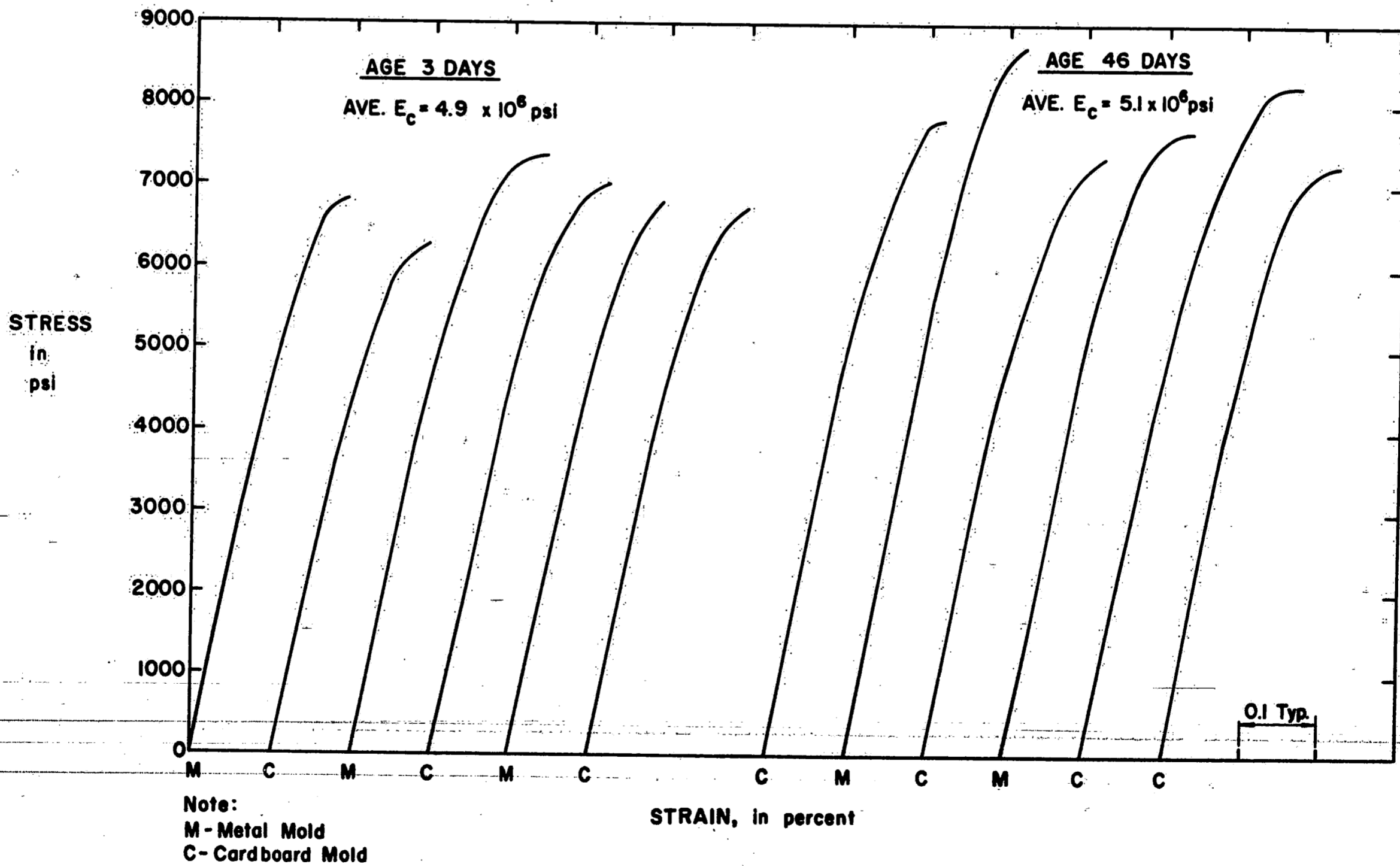


Fig. 4 Cylinder Tests for Beam G-1

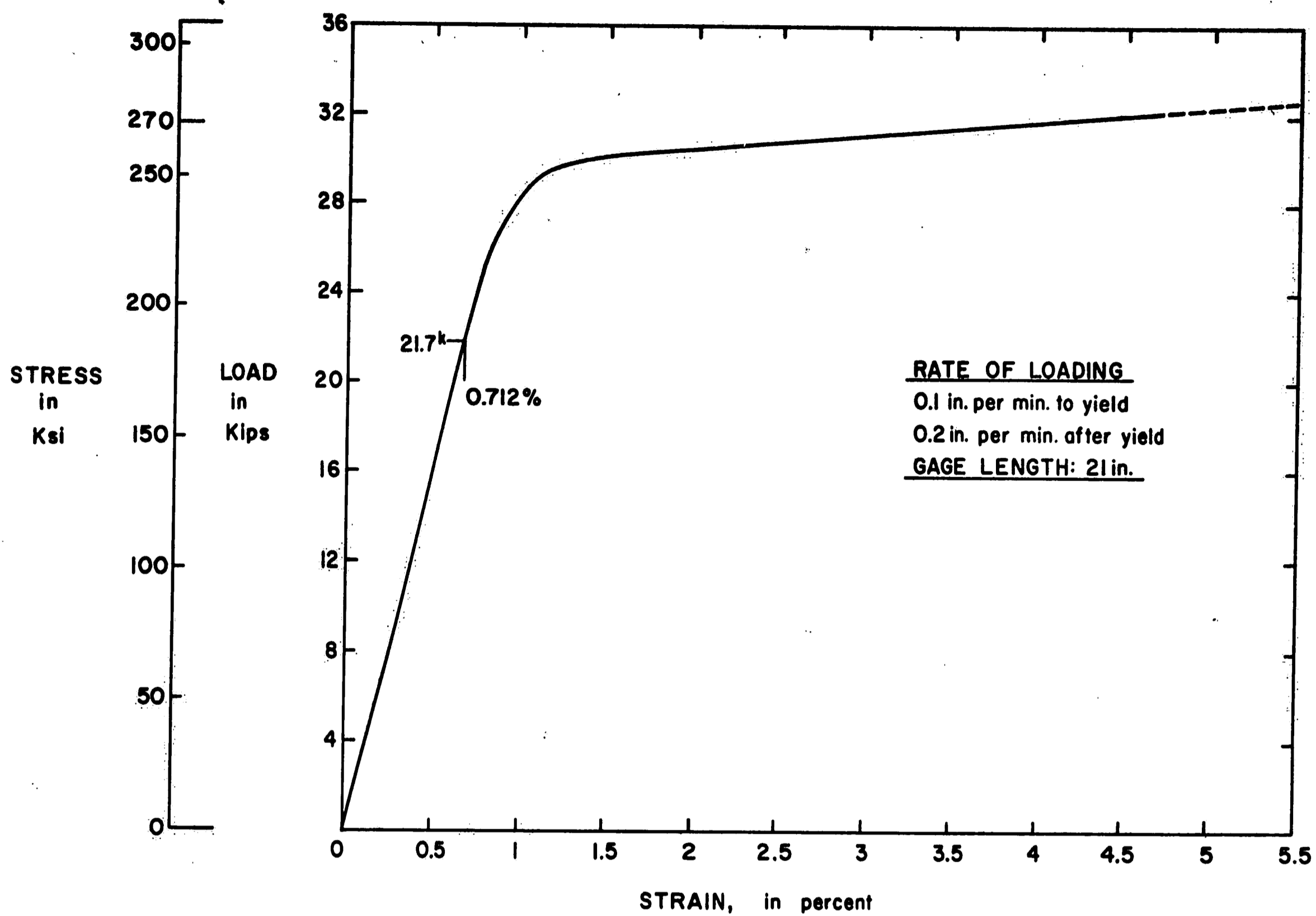


Fig. 5 Load-Strain Curve for Prestressing Strand

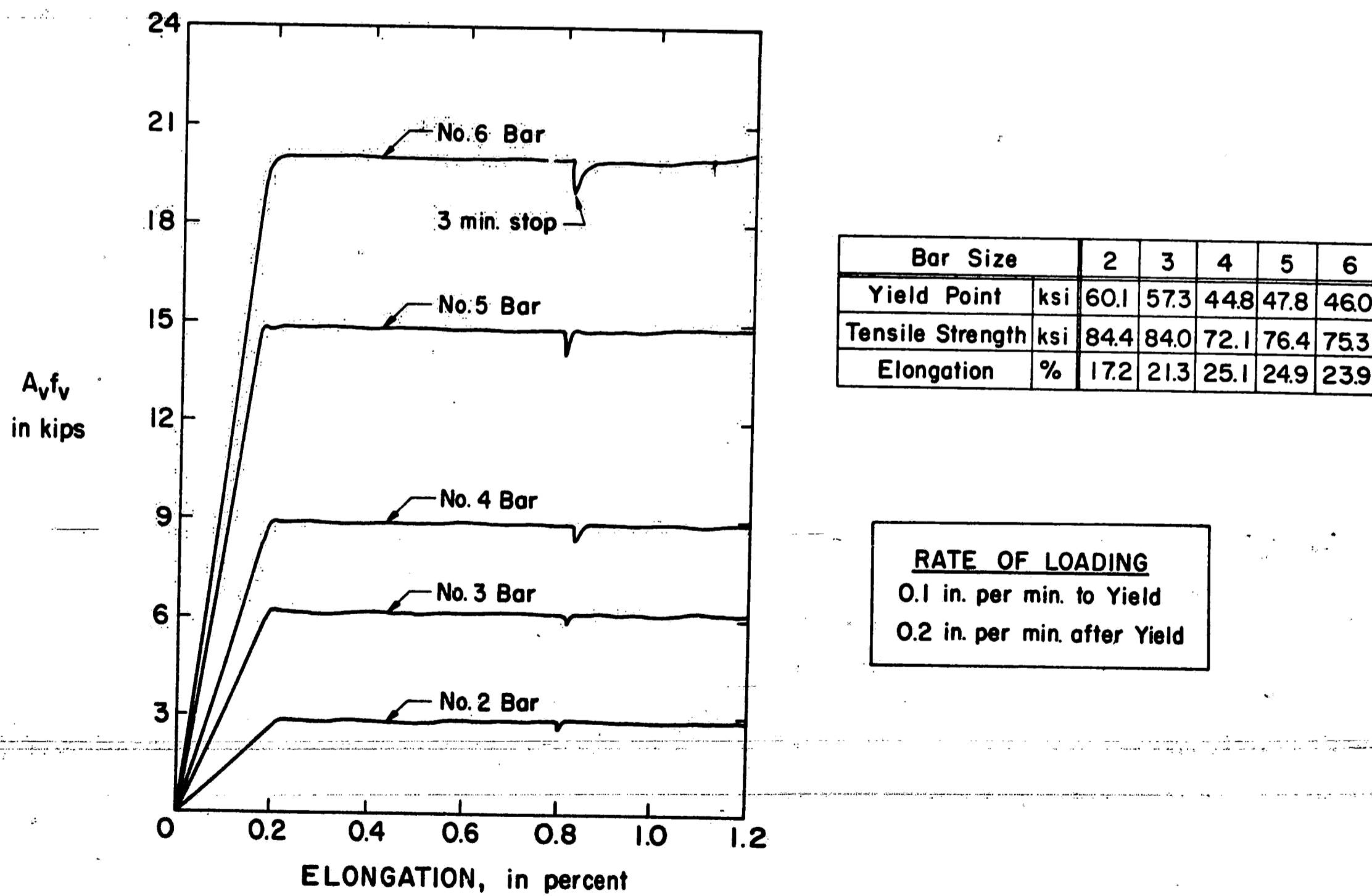
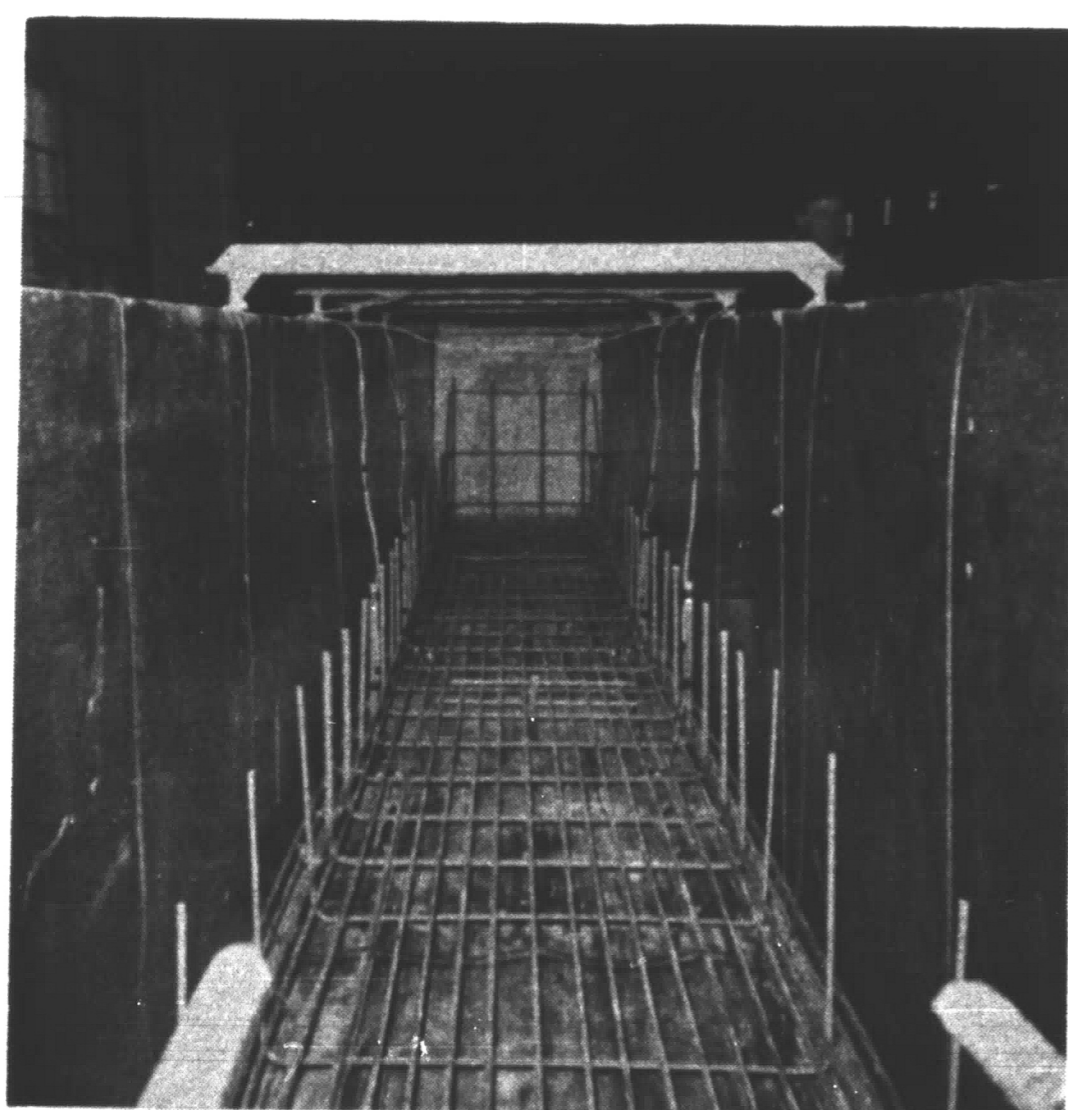


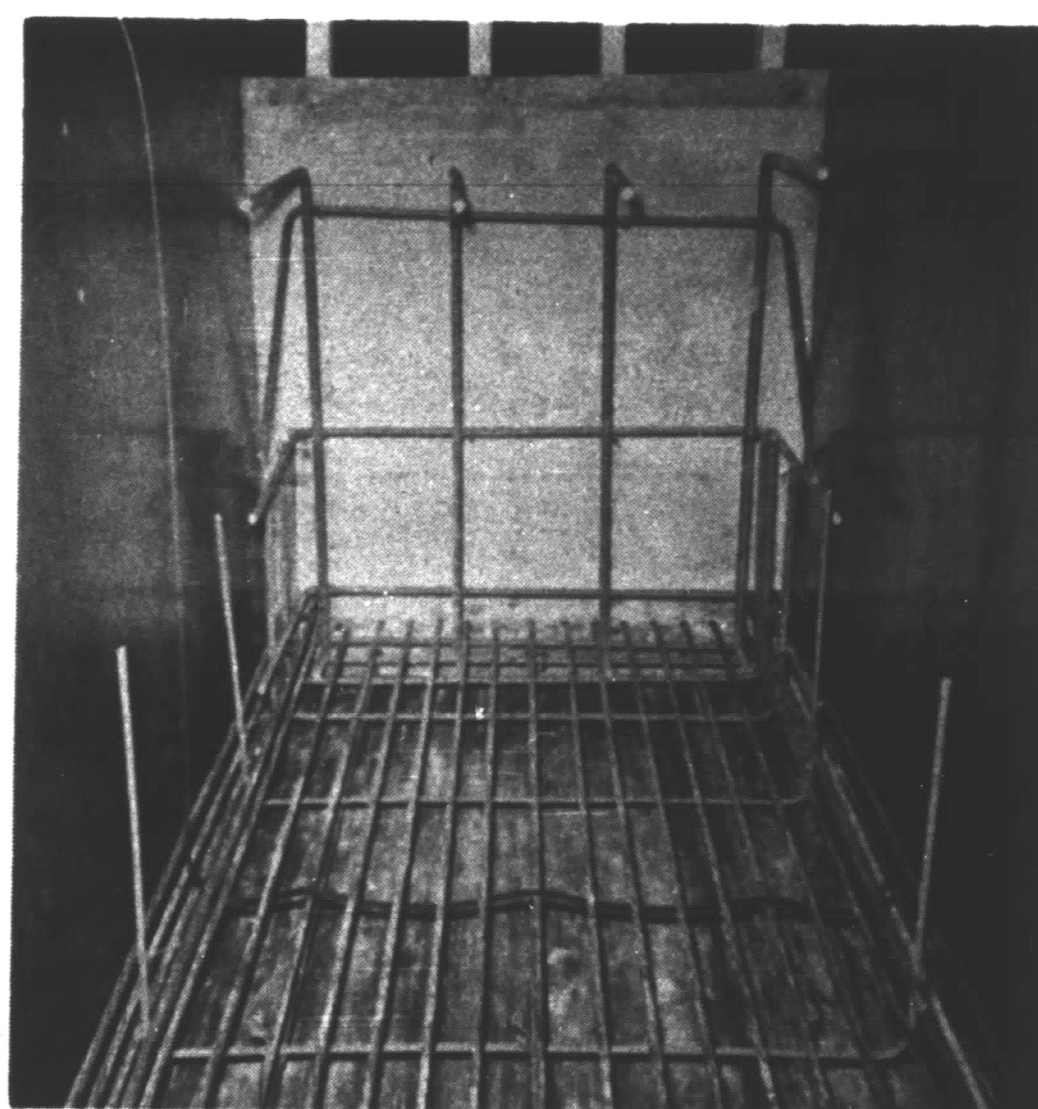
Fig. 6 Load-Strain Curve for Non-Prestressed Steel



Fig. 7 Stressing of Individual Strands

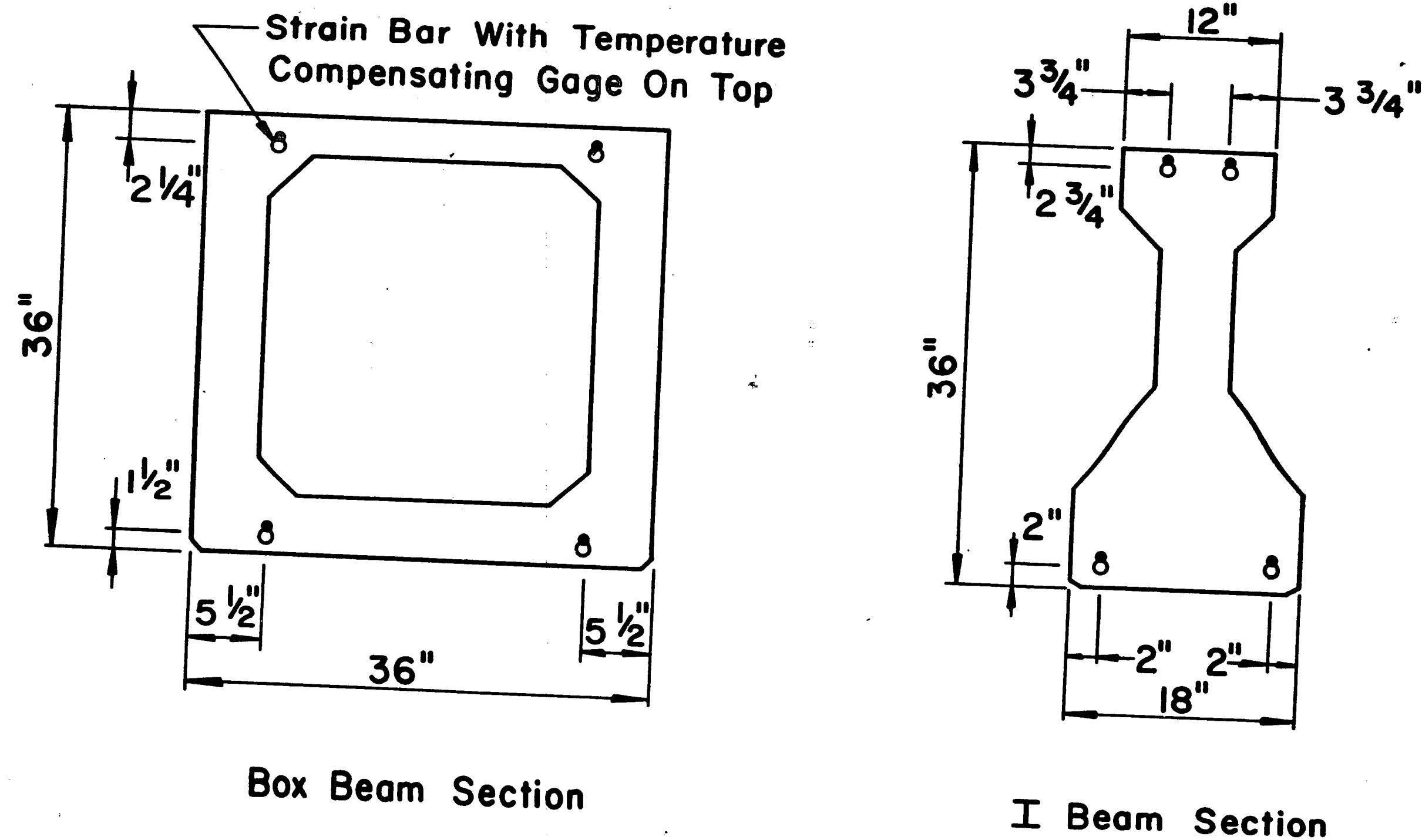


a. Lower Reinforcement and Strand



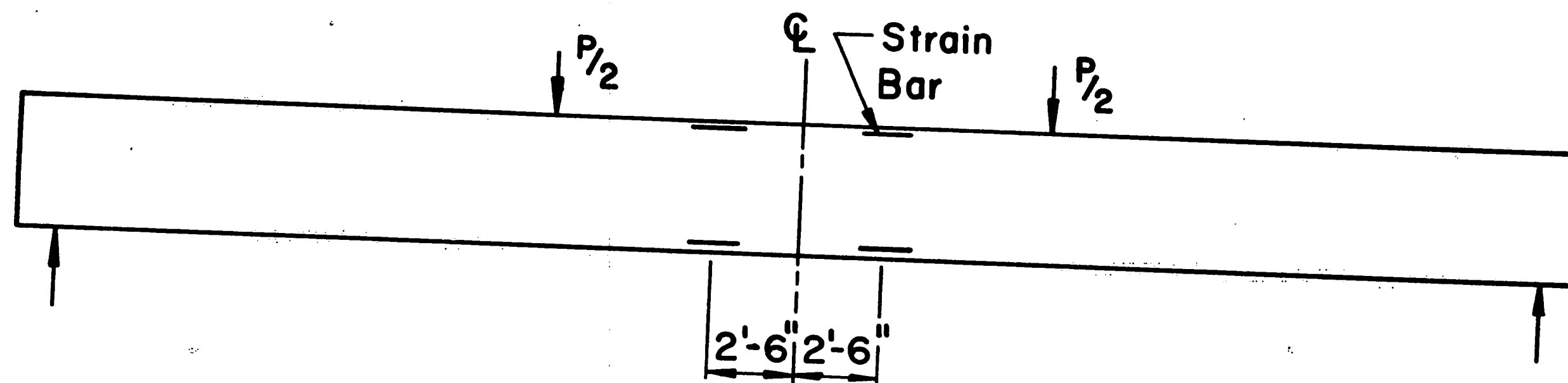
b. Detail of End Region

Fig. 8 Reinforcing Steel for Box Beams



Box Beam Section

I Beam Section



TEST BEAM ELEVATION

Fig. 9 Location of Internal Strain Bars

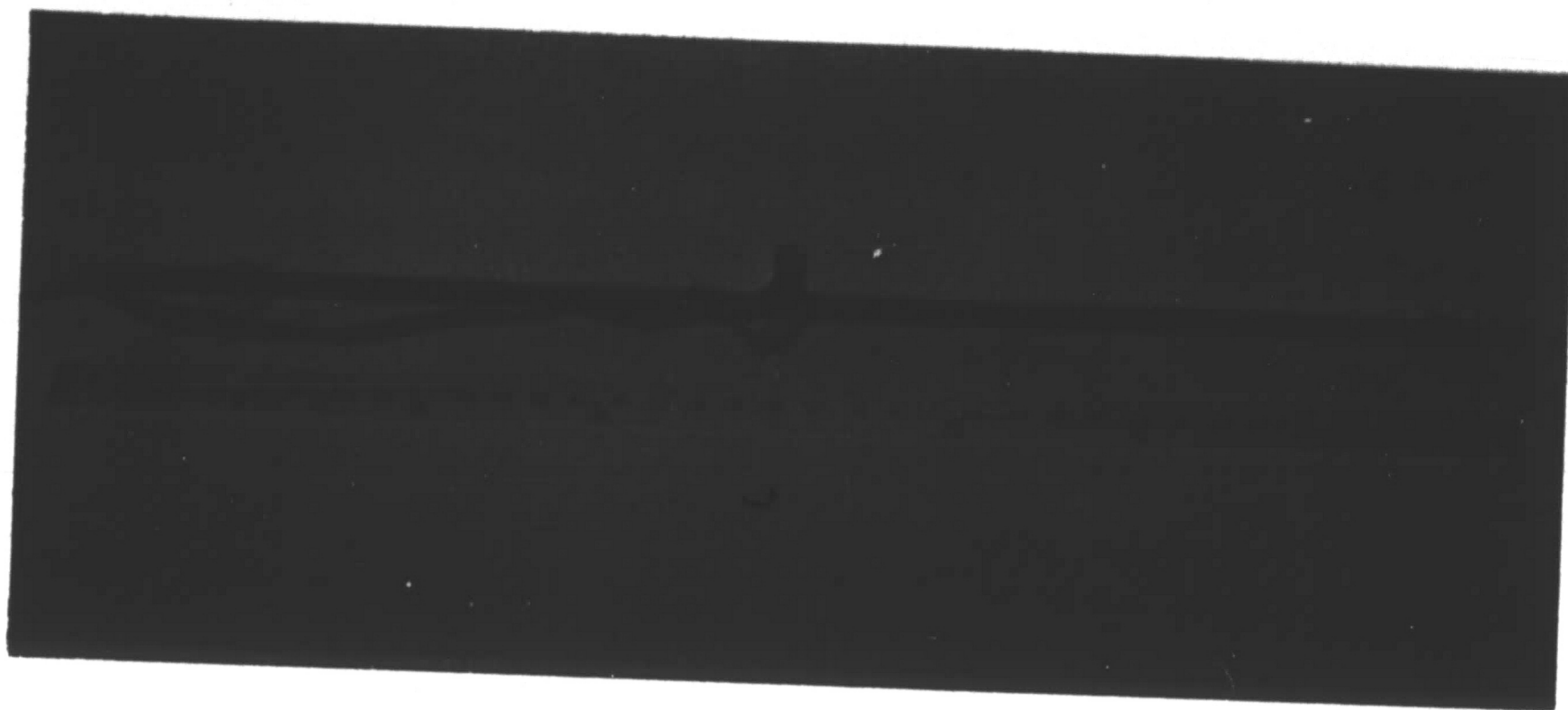


Fig. 10 Strain Bar Assembly

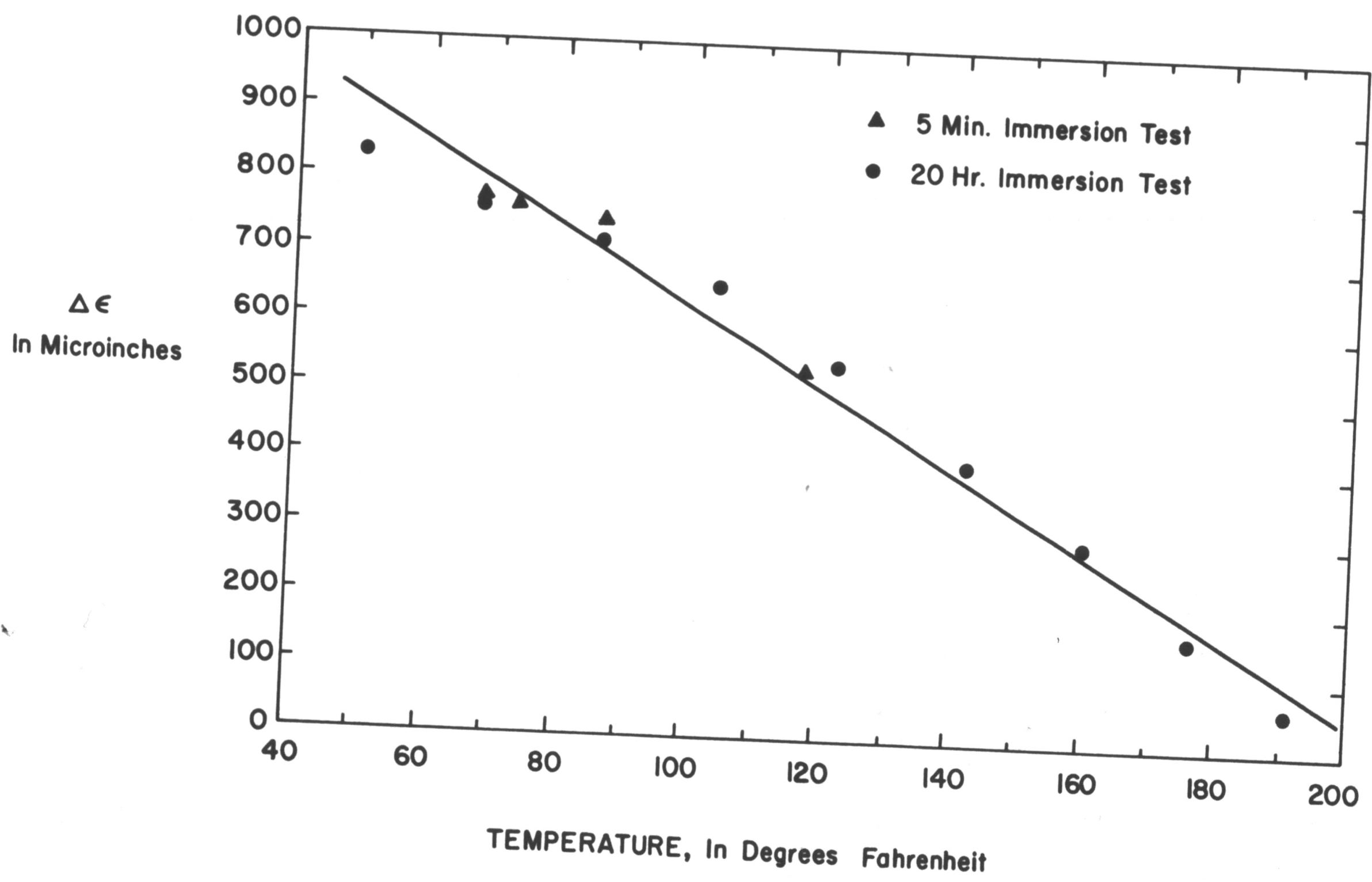


Fig. 11 Strain-Temperature Curve for Strain Bar Gages

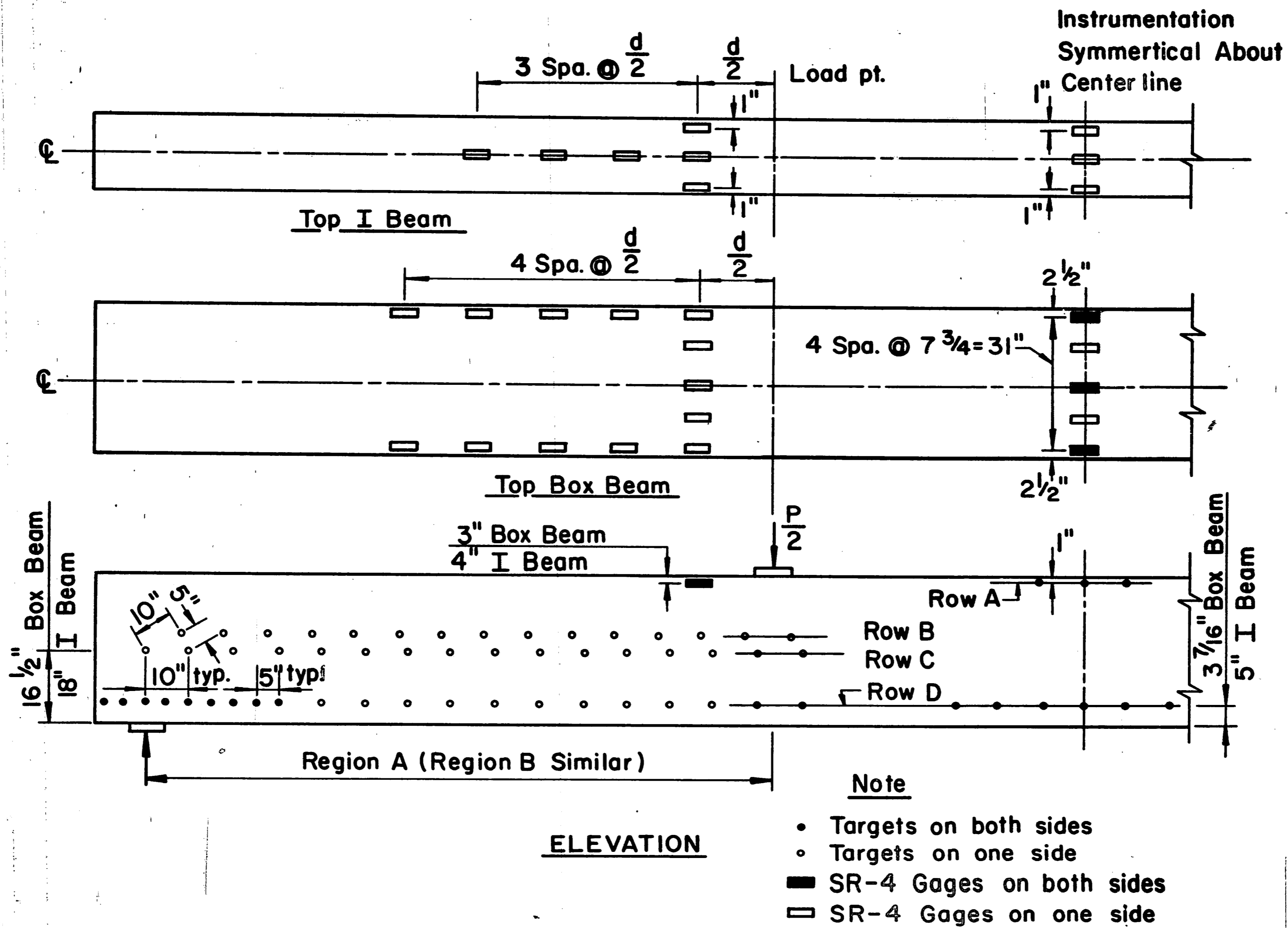
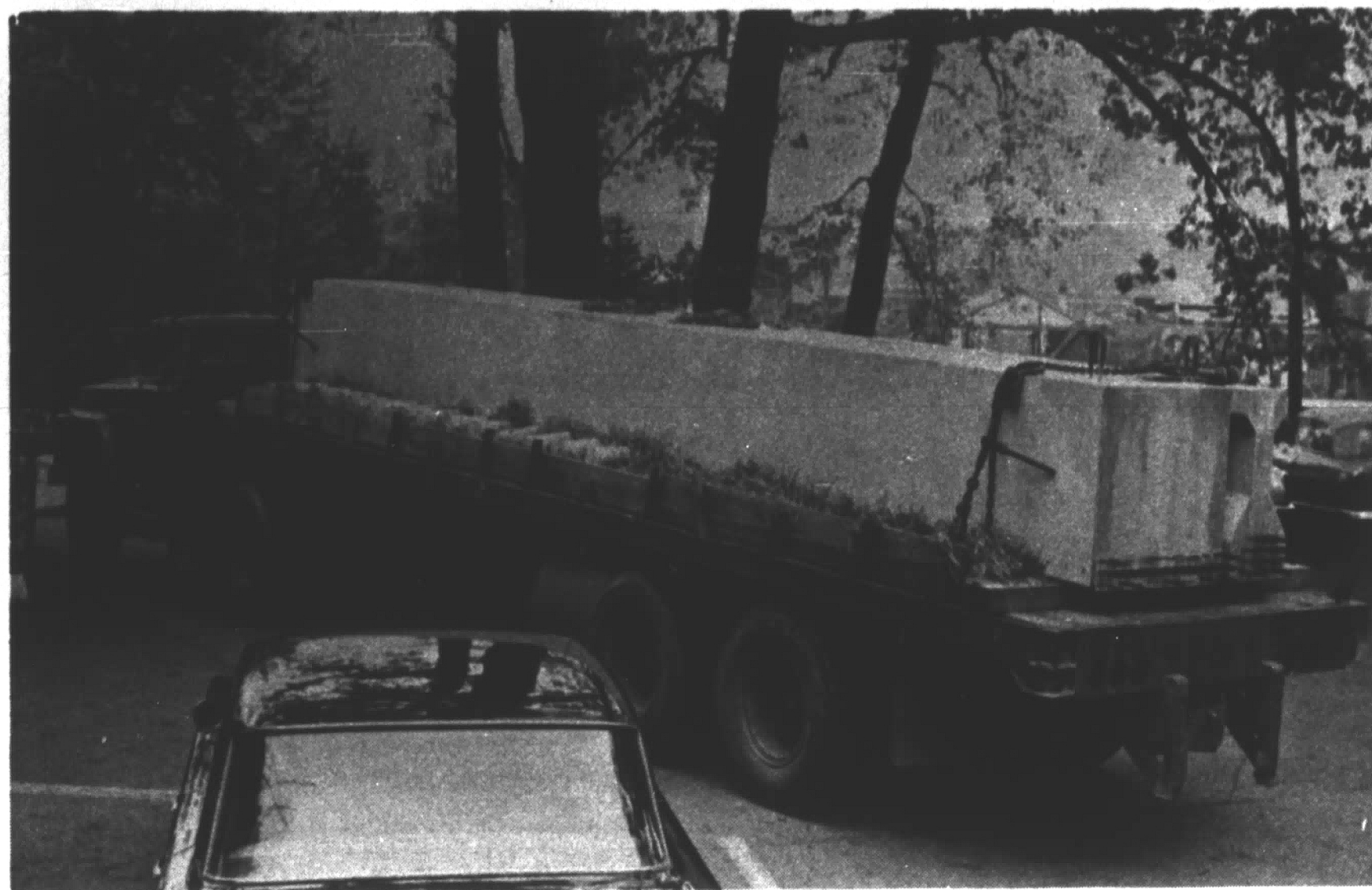


Fig. 12 Location of Whittemore Targets and Electrical Strain Gages



a. Beams G-1 and G-2

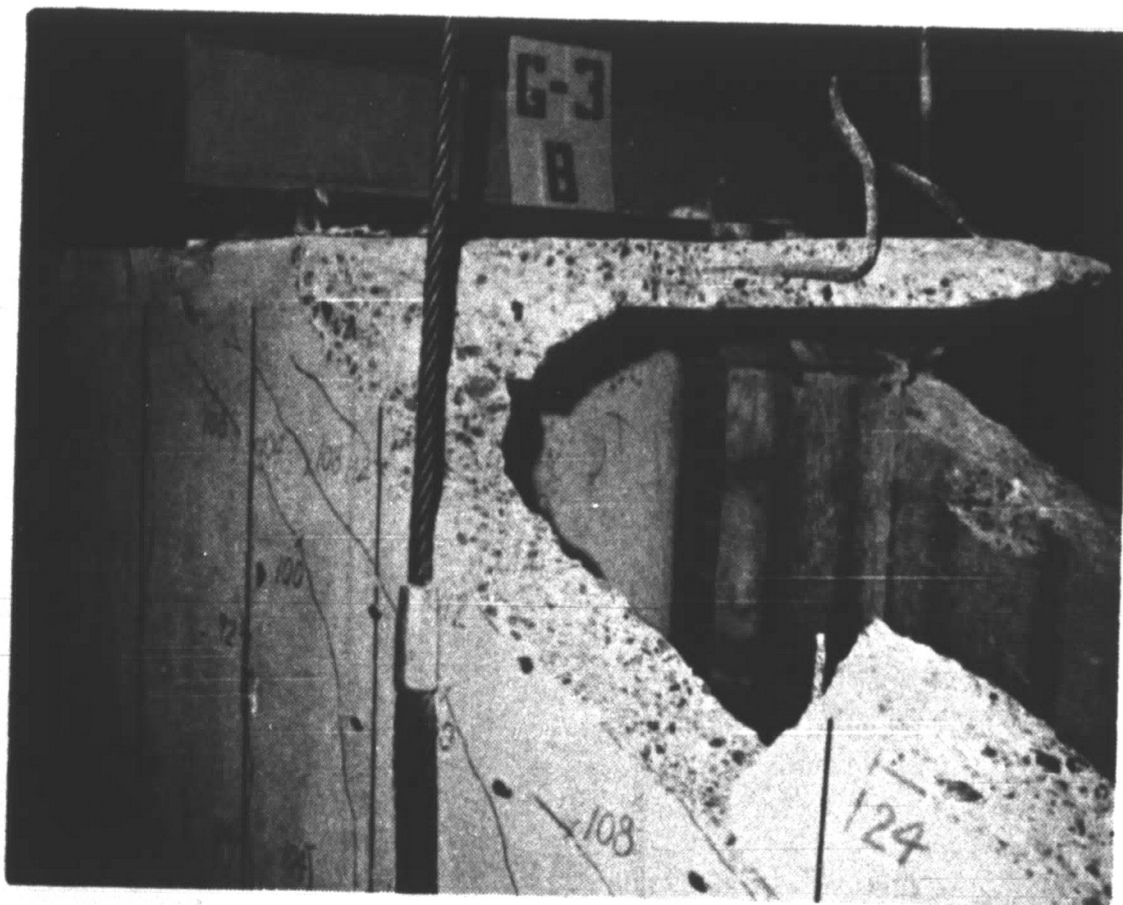


b. Beam G-4

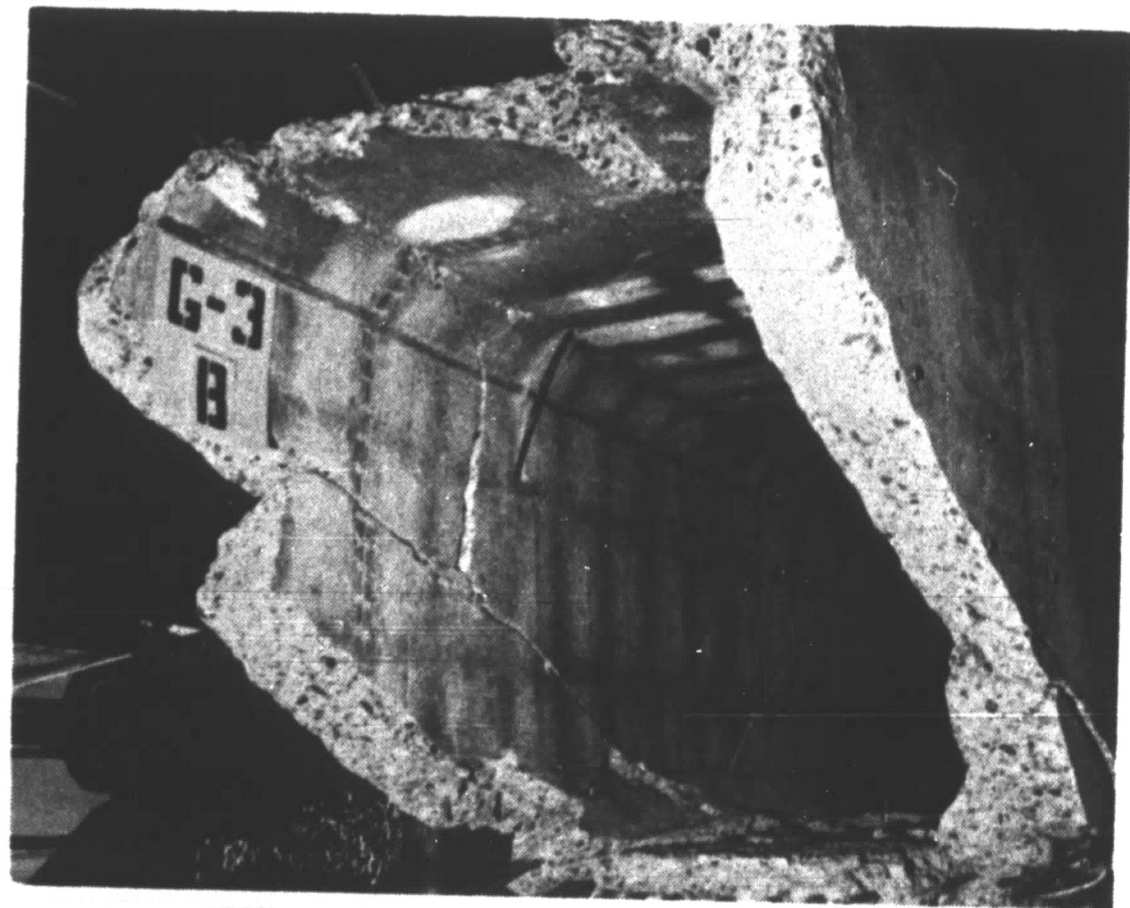
Fig. 13 Beams Arriving at Fritz Engineering Laboratory



a. Overhead View



b. Exterior Left Side View



c. Interior Left Side View

Fig. 14 Cross Section of Box Beam G-3

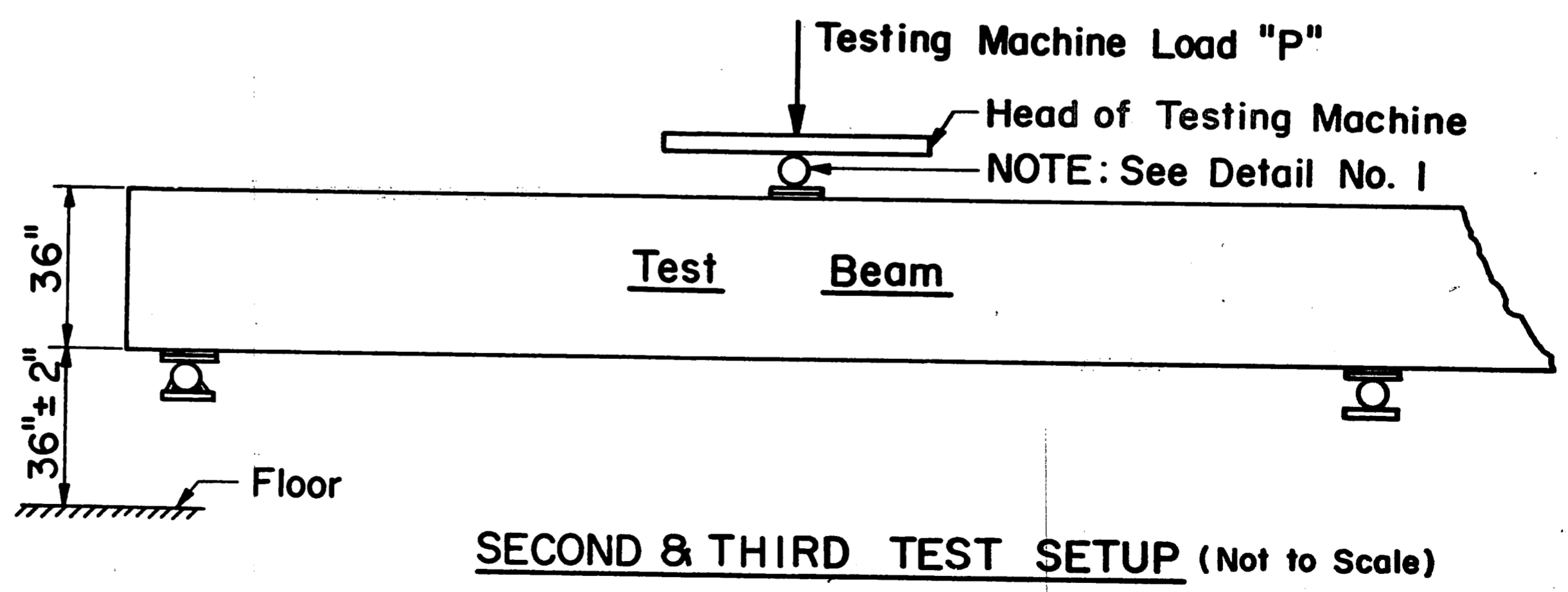
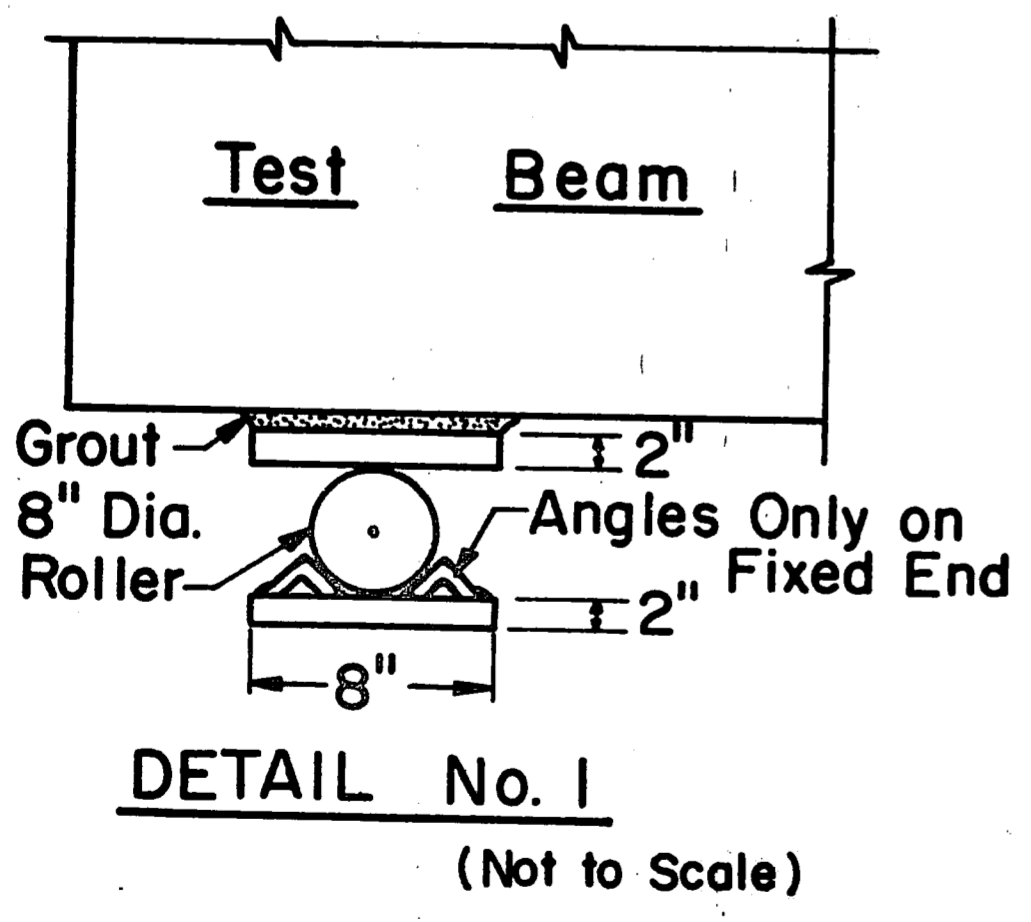
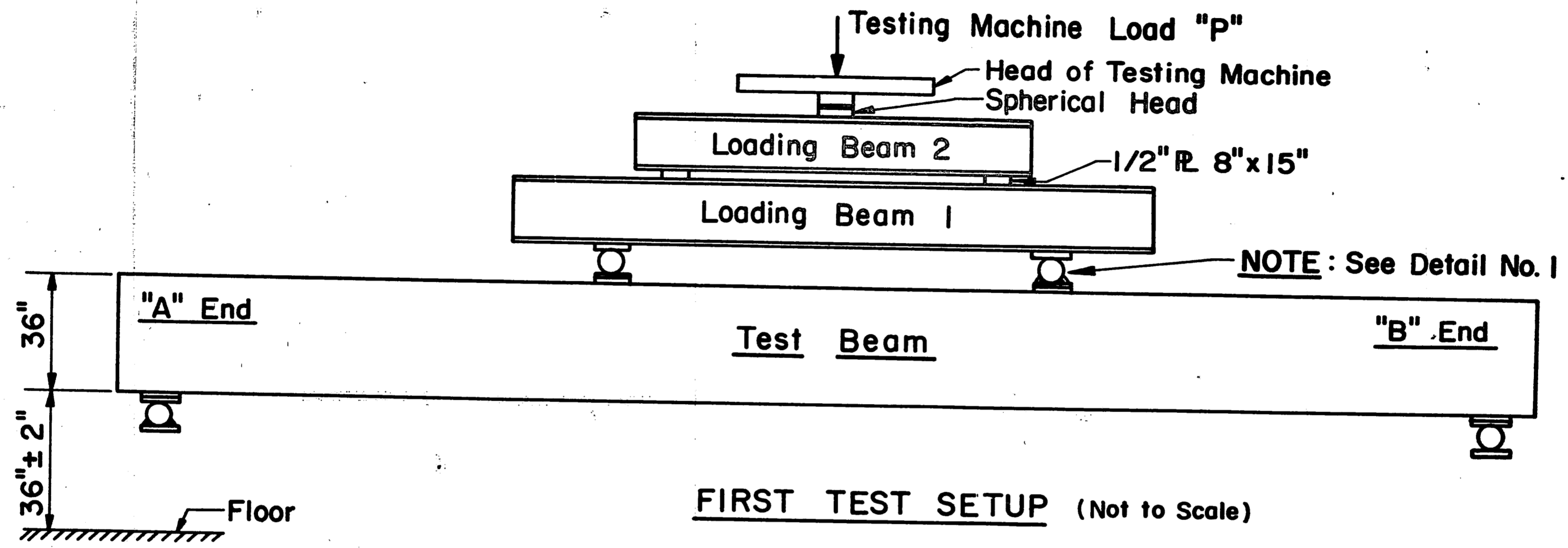
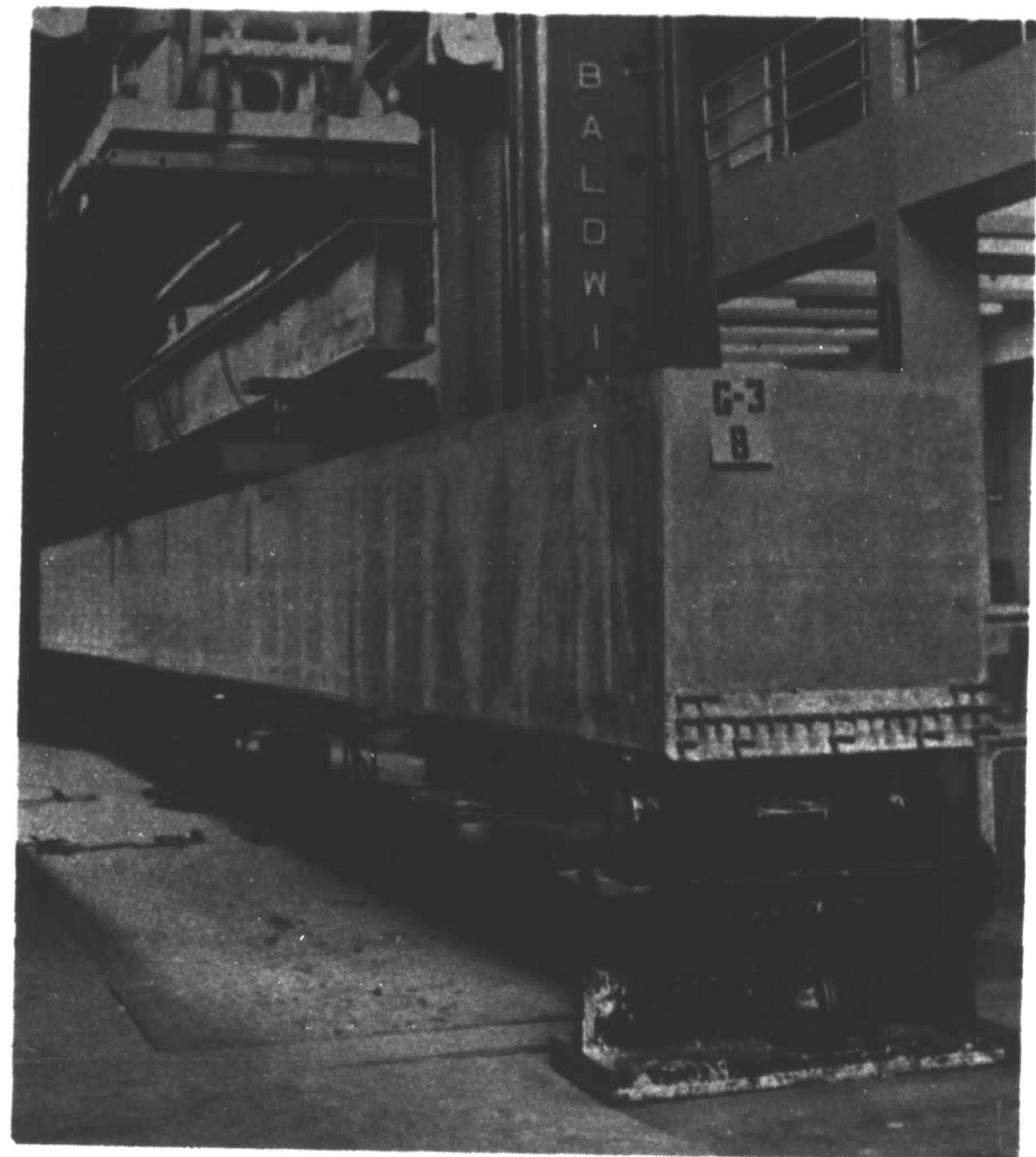


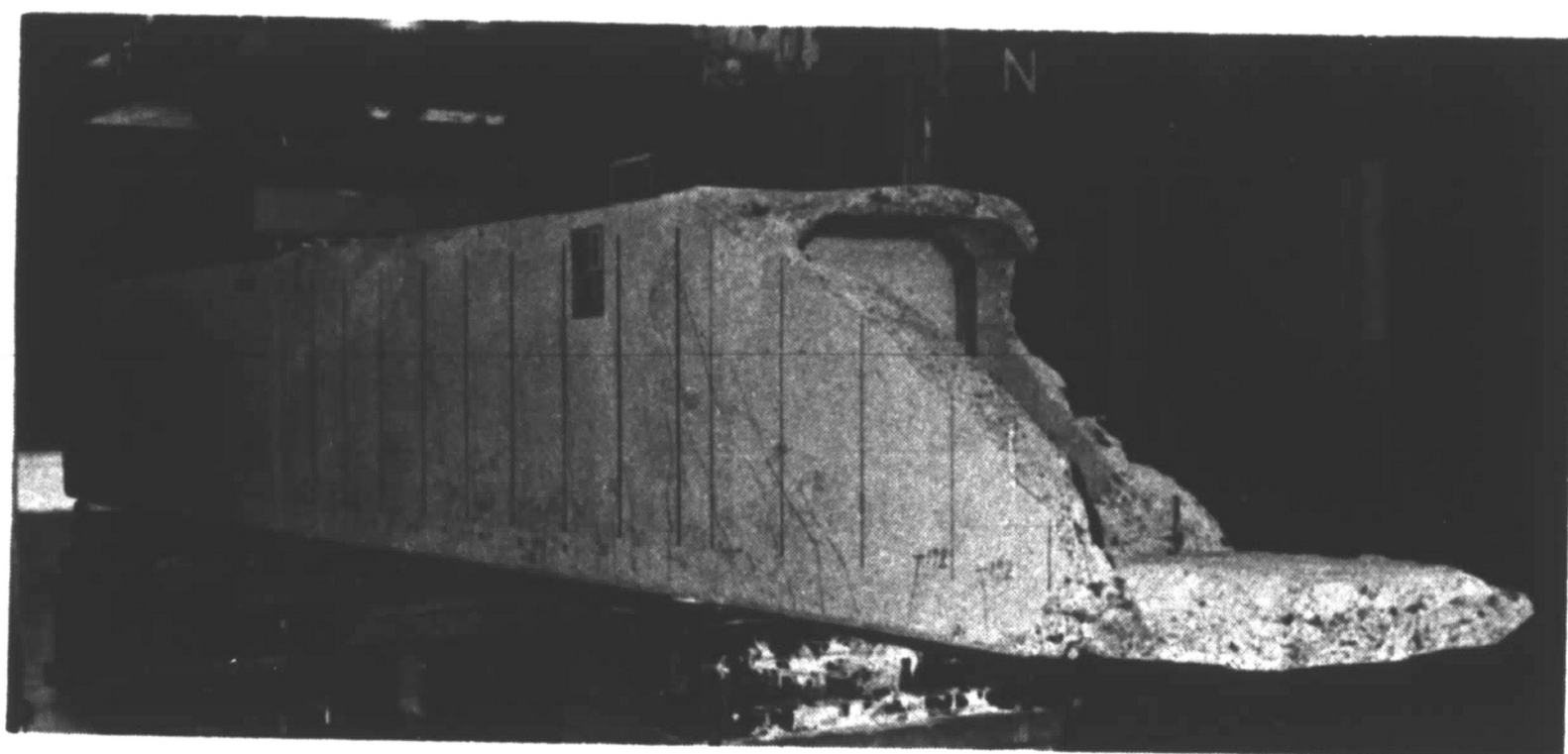
Fig. 15 Testing Arrangement



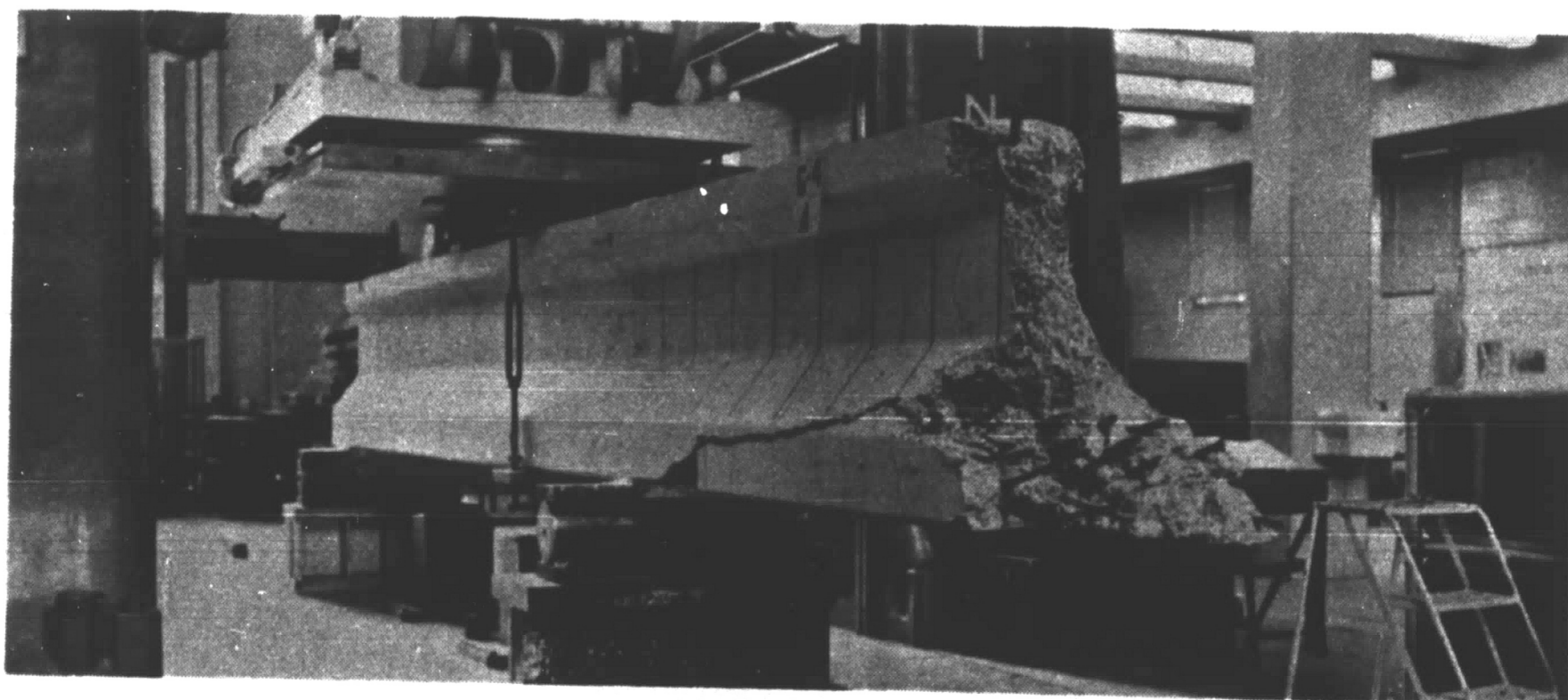
a. First Test on Long I-Beam, G-4



b. First Test on Long Box Beam, G-3

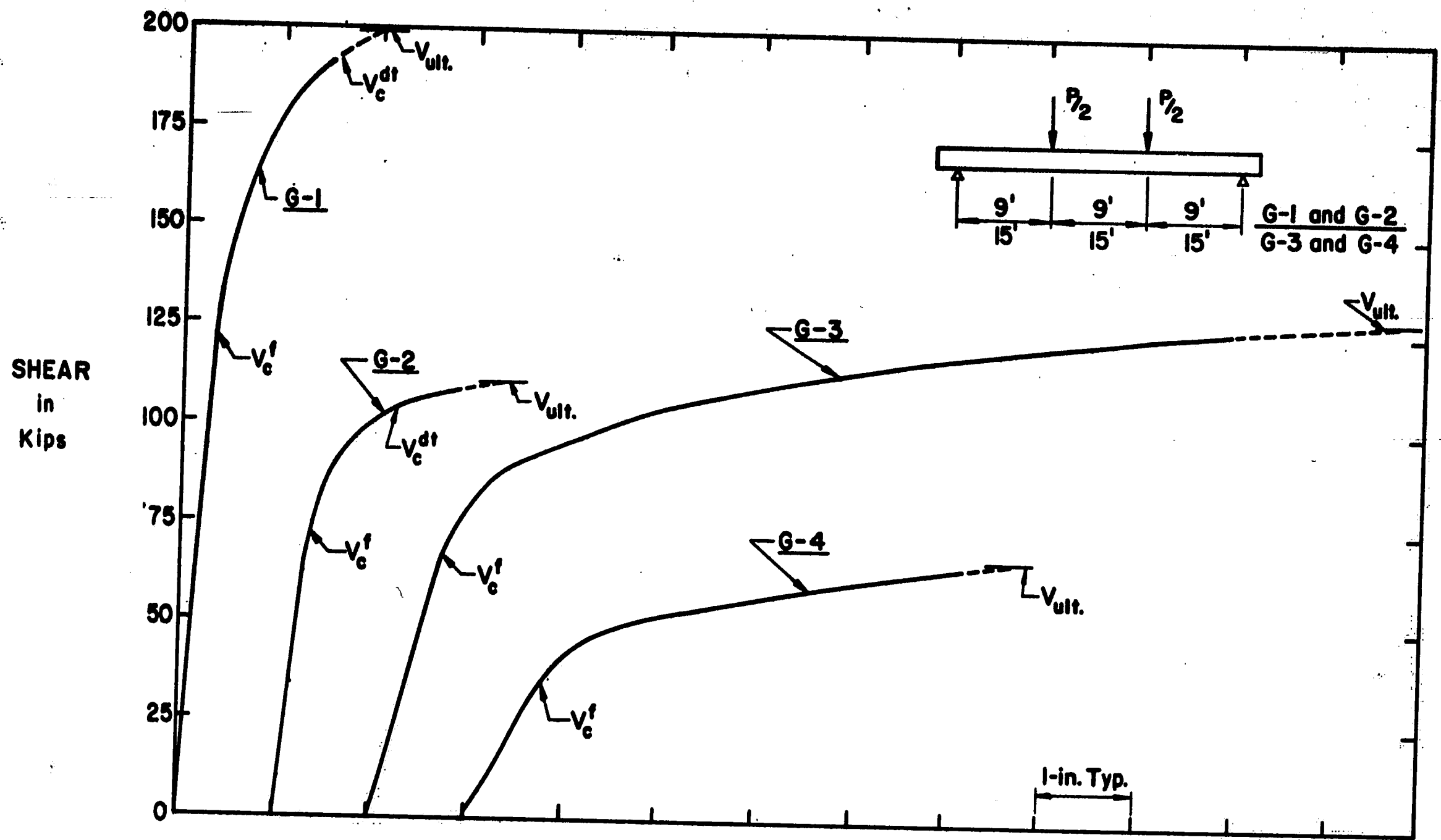


c. Second Test on Short Box Beam, G-1



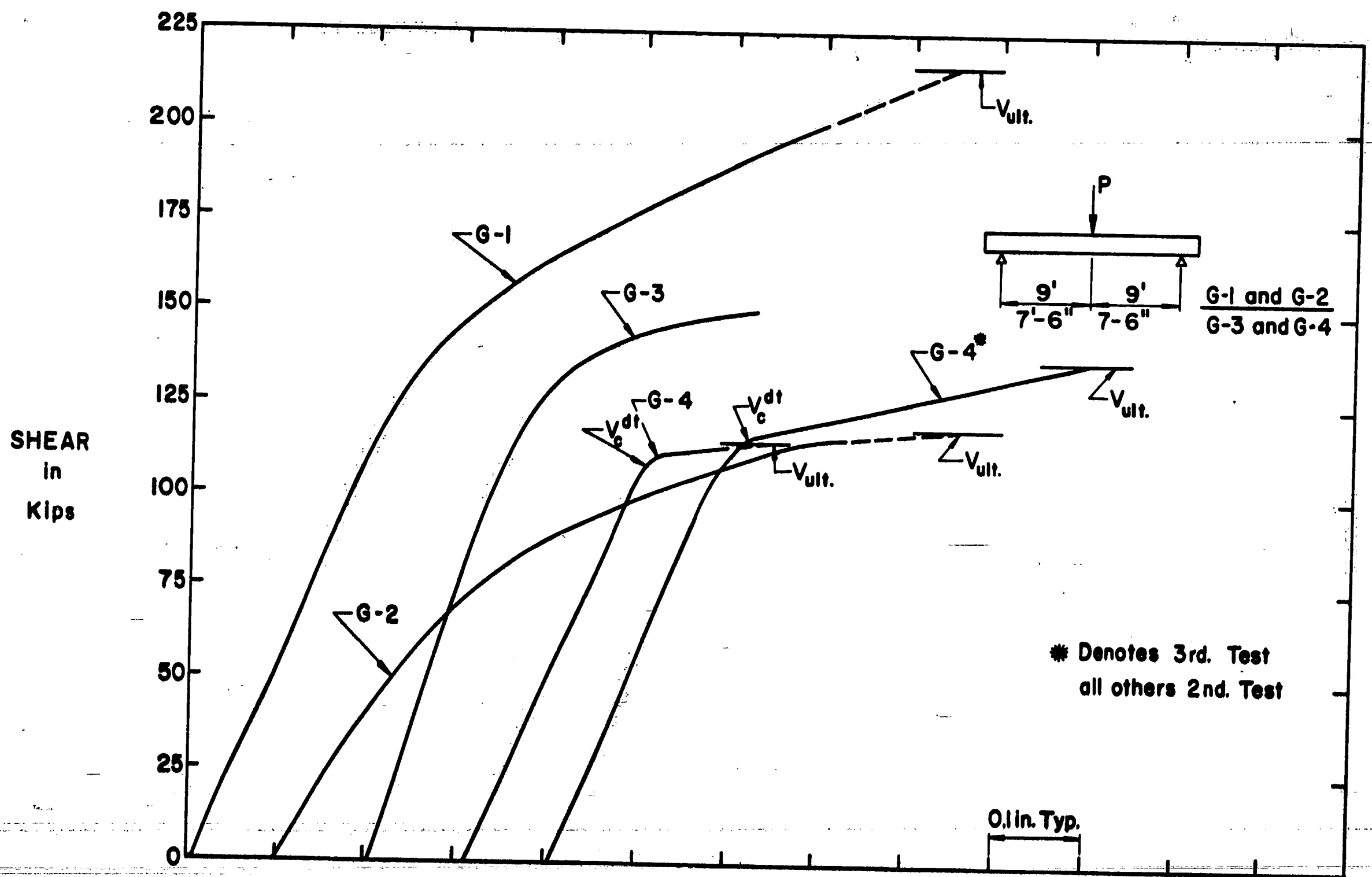
d. Third Test on Long I-Beam, G-4

Fig. 16 Test Setup



MID-SPAN DEFLECTION, 1st. TEST

a. First Test



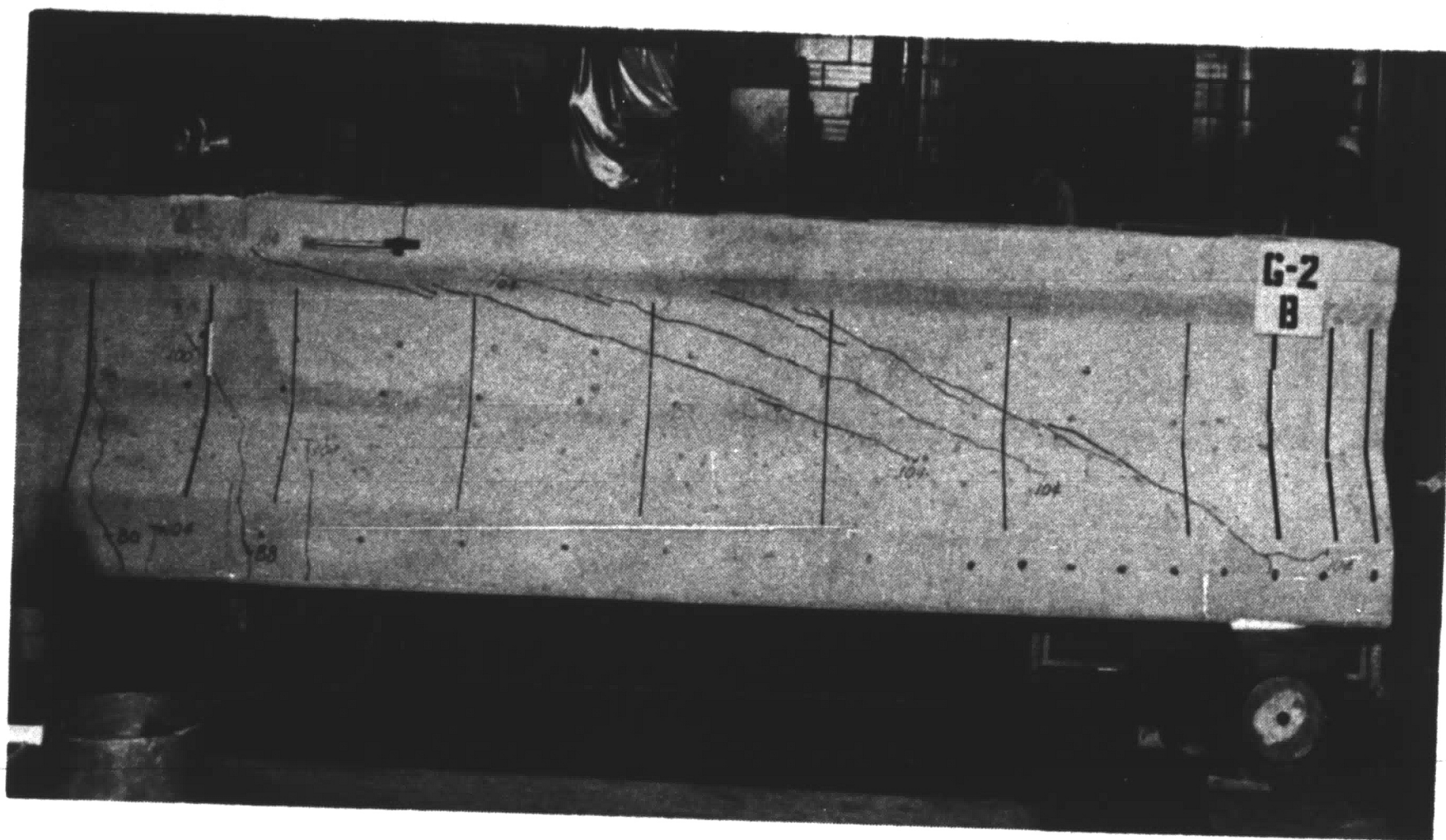
MID-SPAN DEFLECTION, 2nd. and 3rd Tests

b. Second and Third Tests

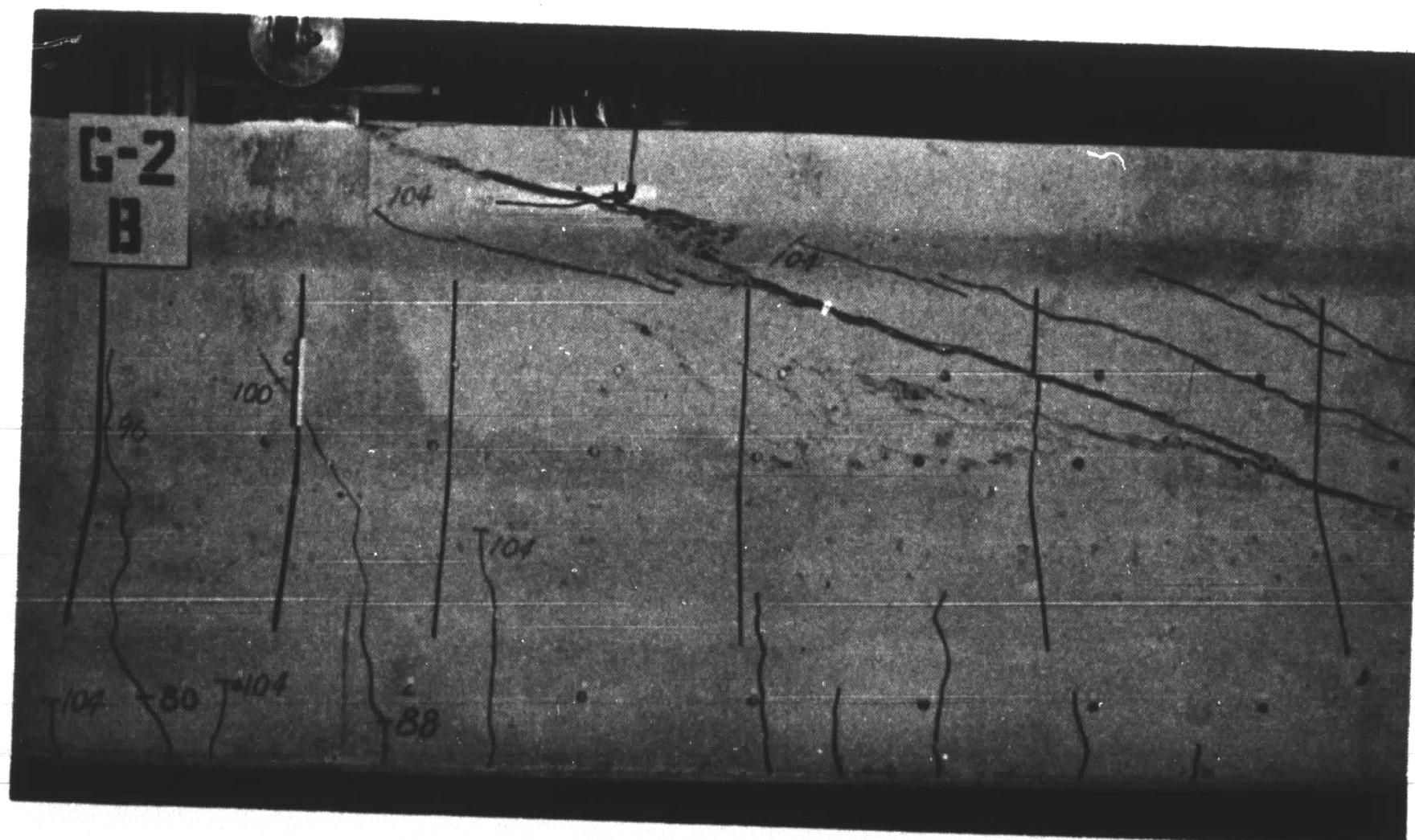
Fig. 17. Load-Deflection Curves



a. A Shear Span After Inclined Cracking

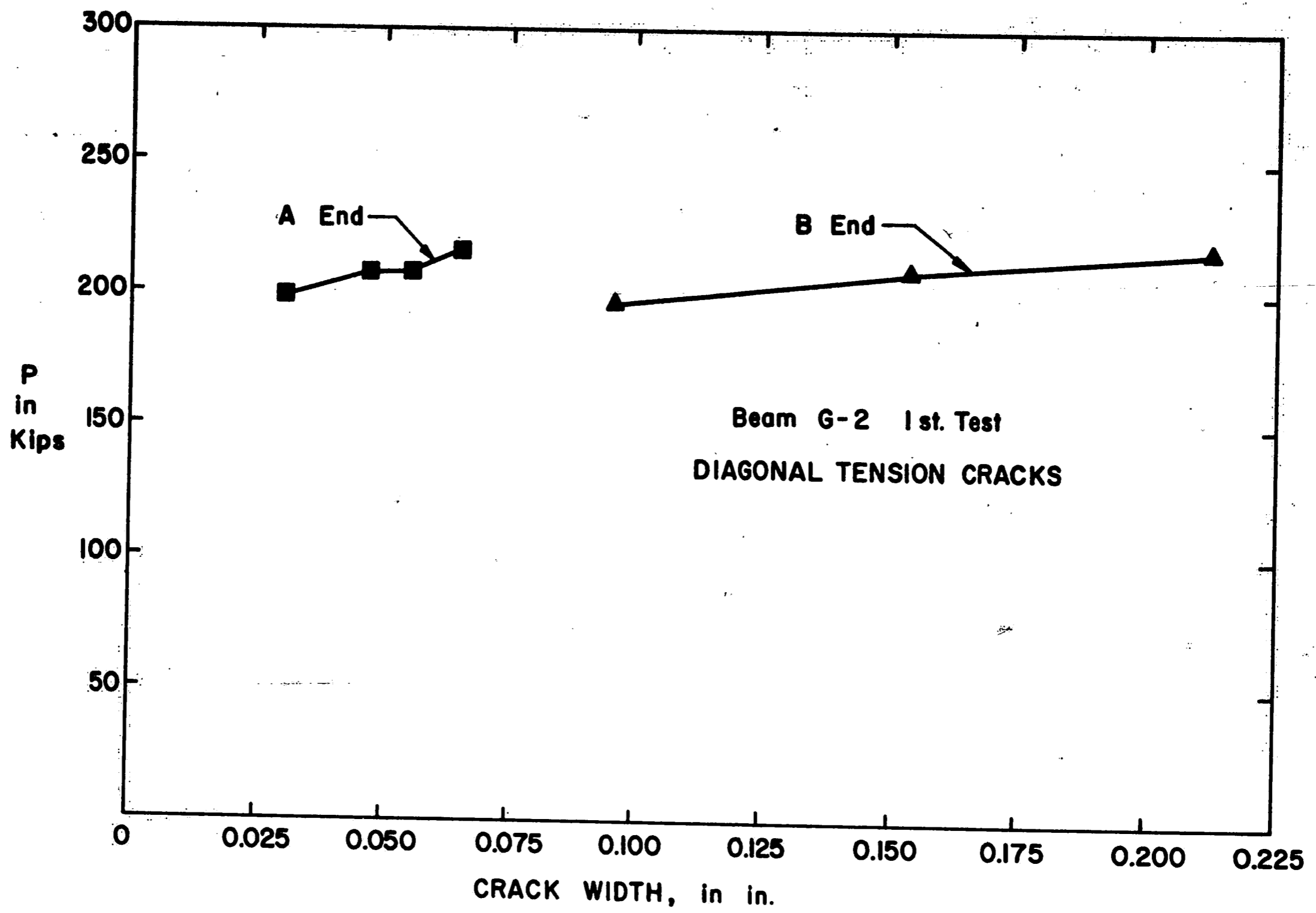


b. B Shear Span After Diagonal Tension Inclined Cracking

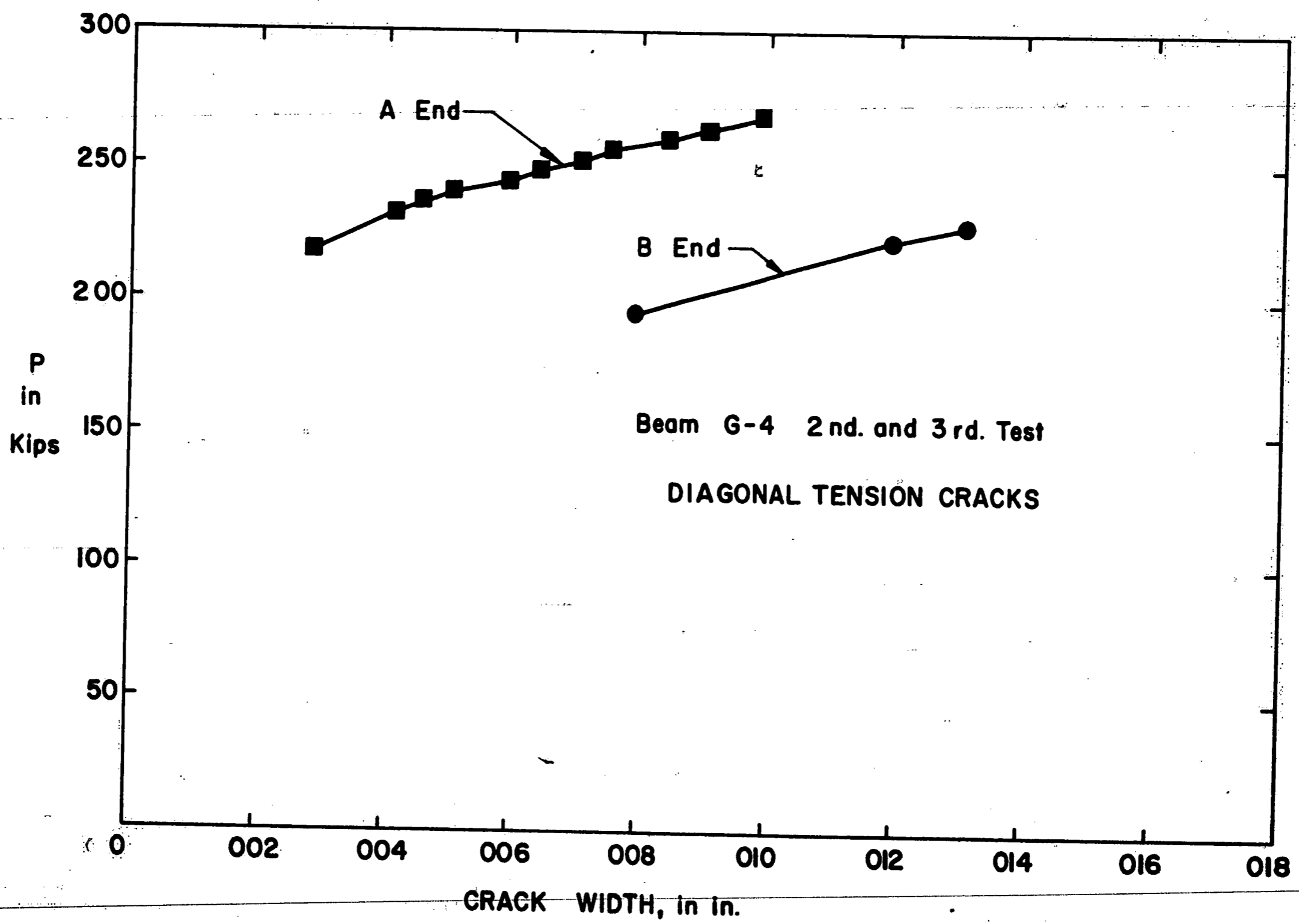


c. View of Failure Region

Fig. 18 First Test on Short I-Beam, G-2

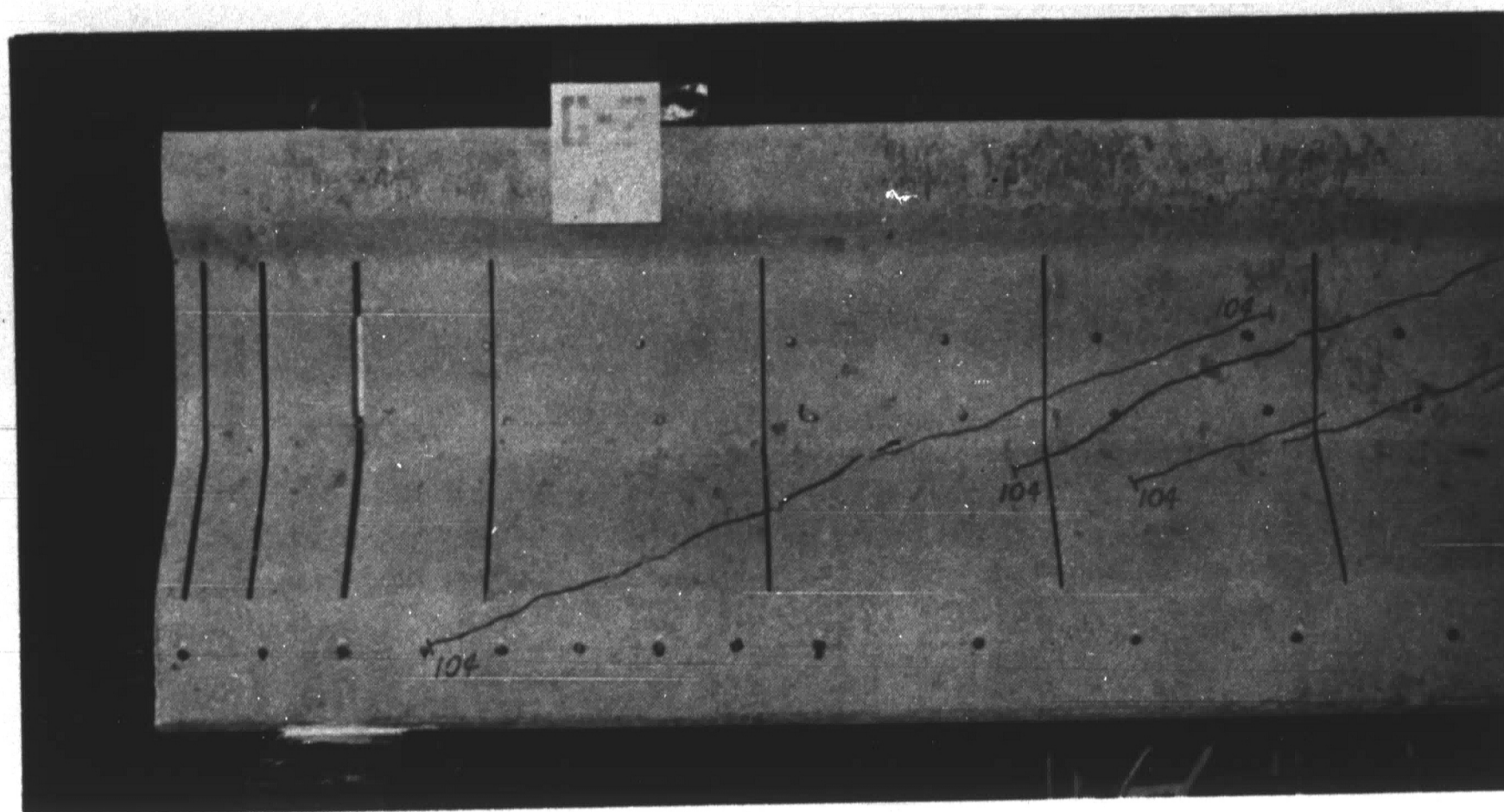


a. First Test on Short I-Beam, G-2

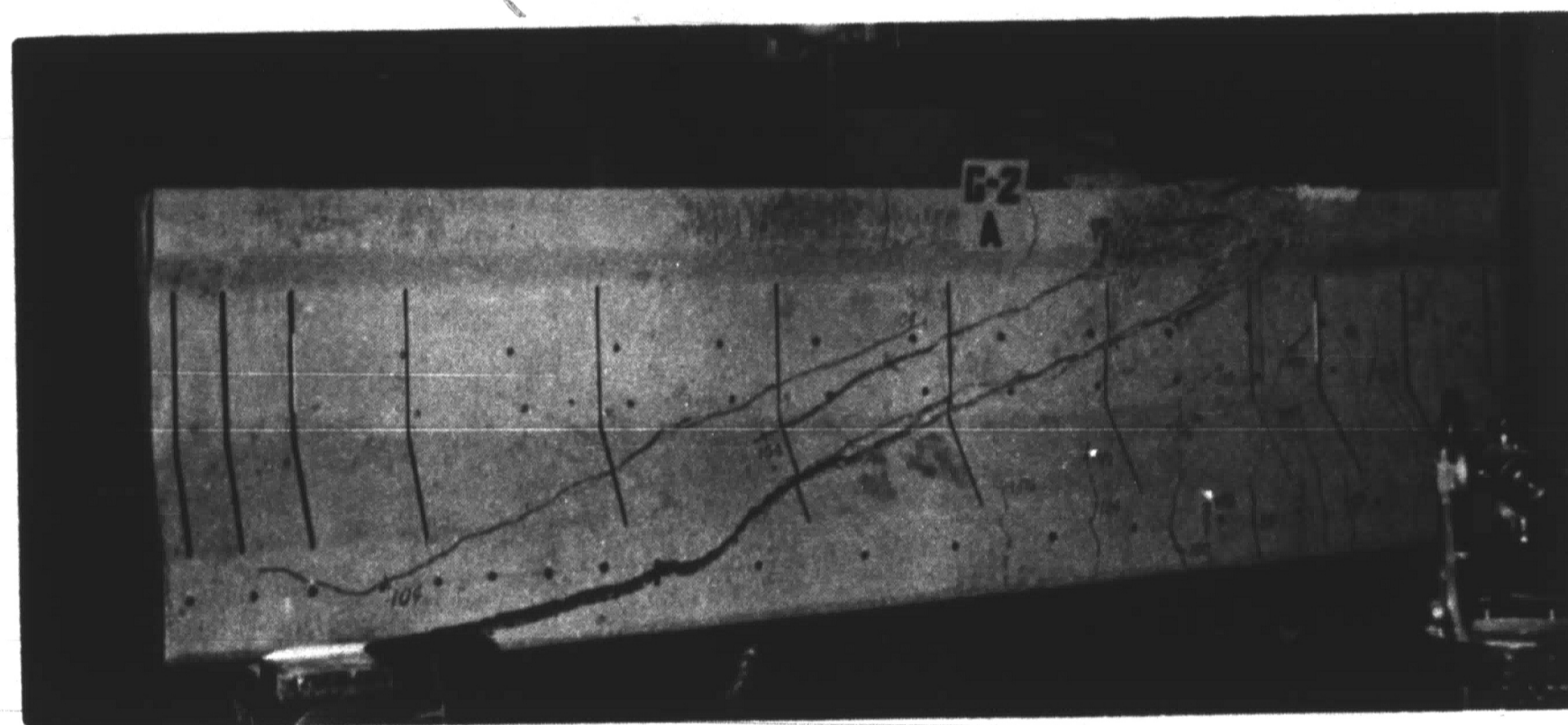


b. Second and Third Tests on Long I-Beam, G-4

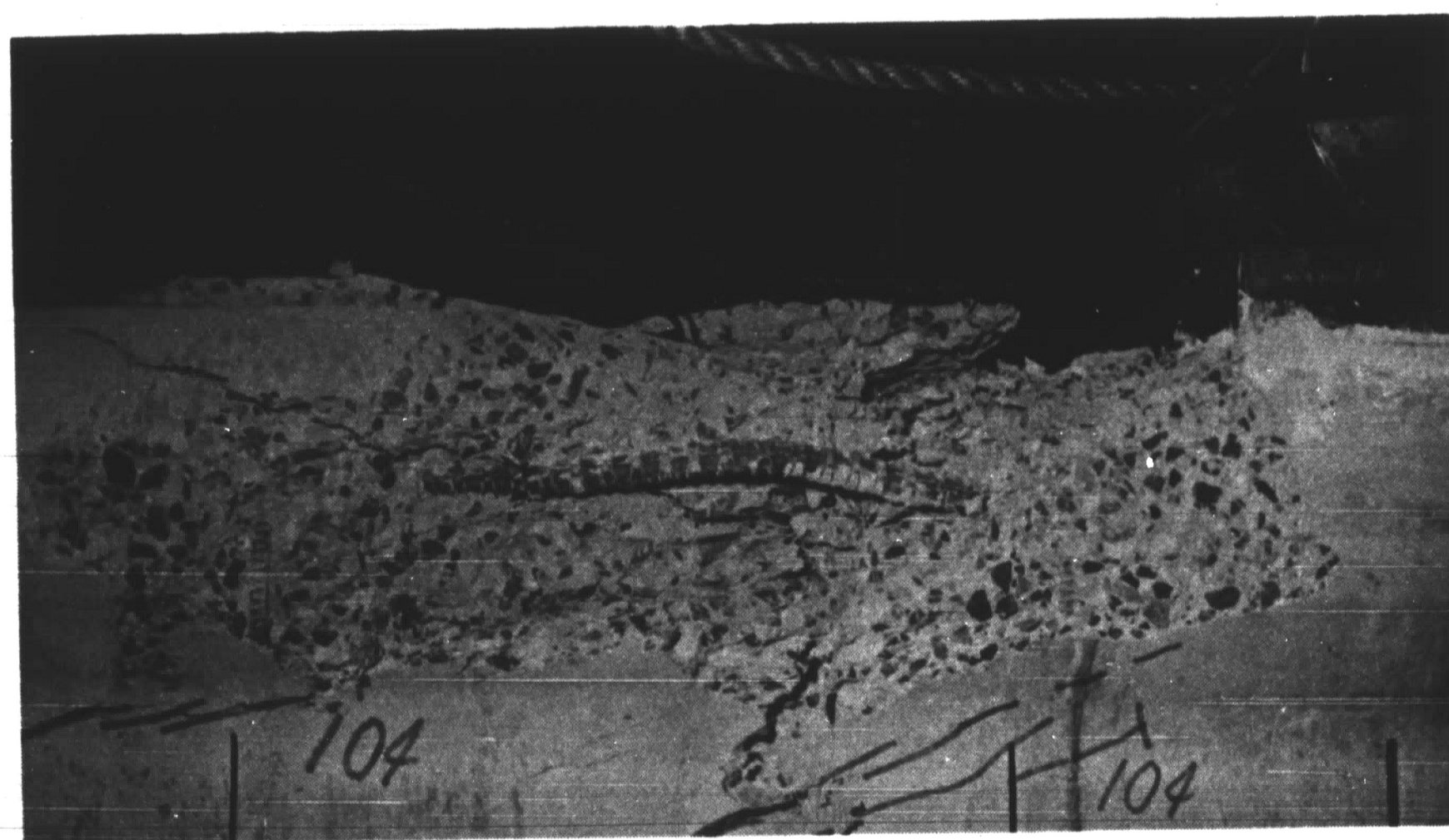
Fig. 19 Diagonal Tension Inclined Crack Width Growth



a. Condition of A Shear Span at Start of Test

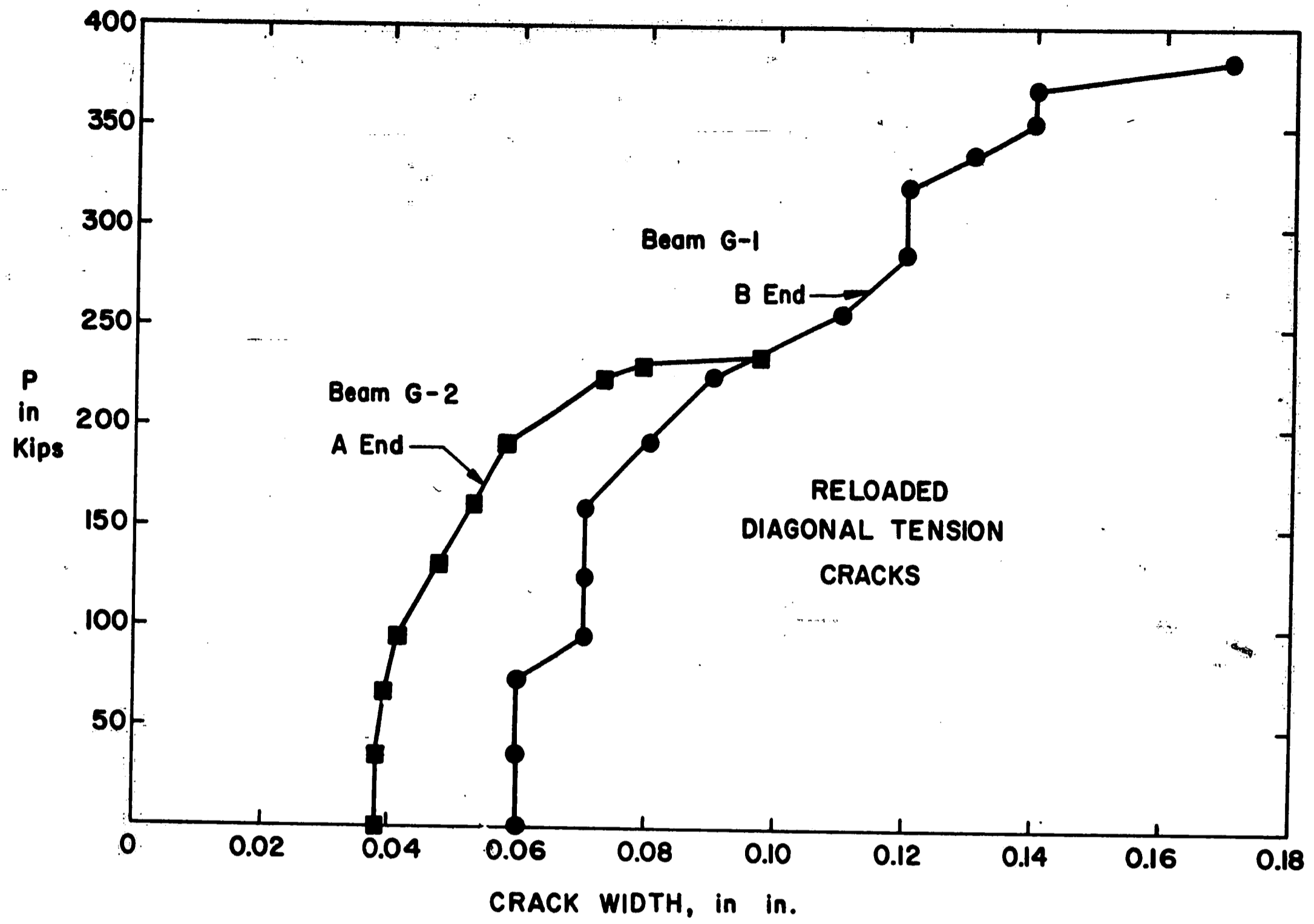


b. A Shear Span After Failure

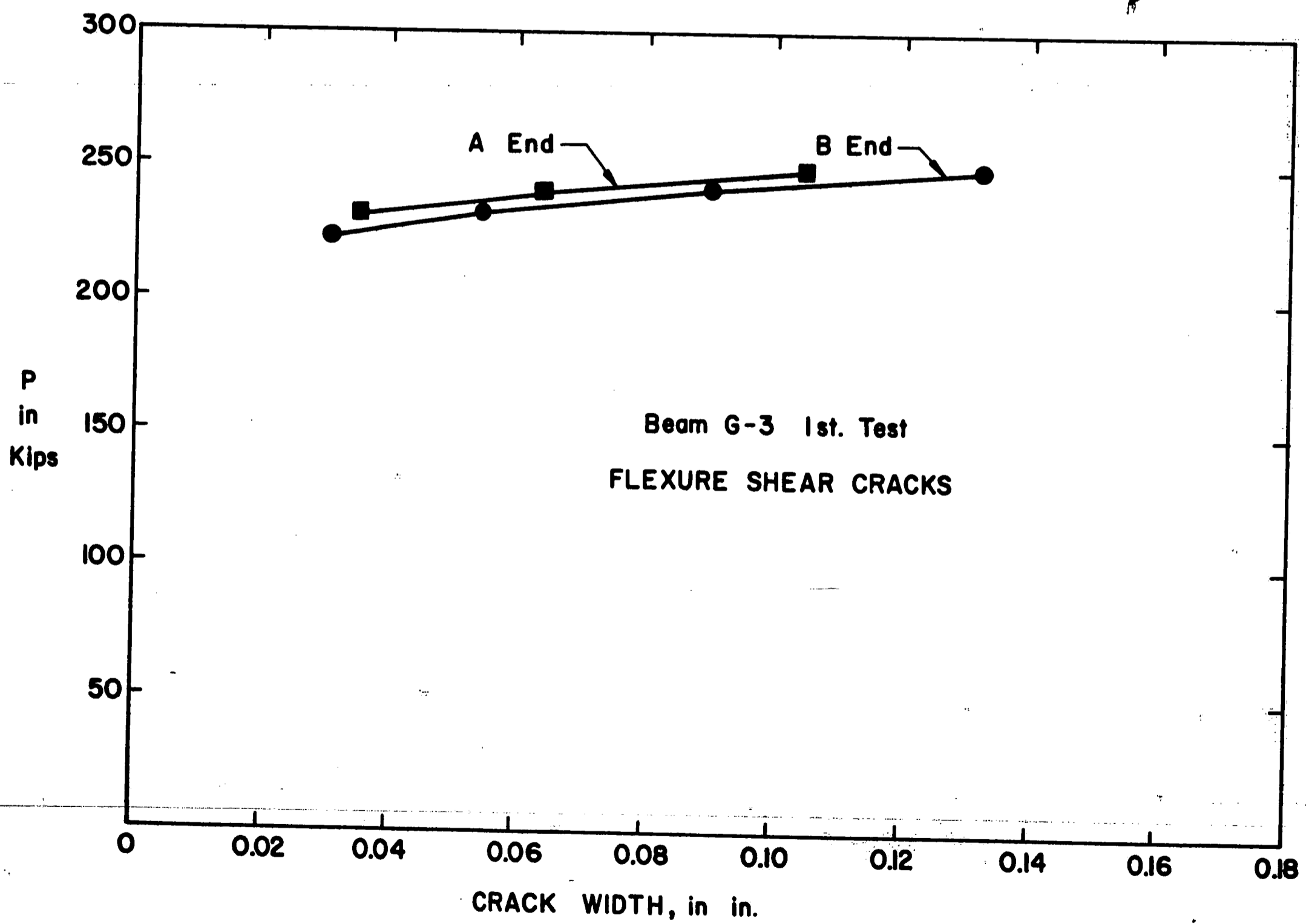


c. View of Failure Region

Fig. 20 Second Test on Short I-Beam, G-2

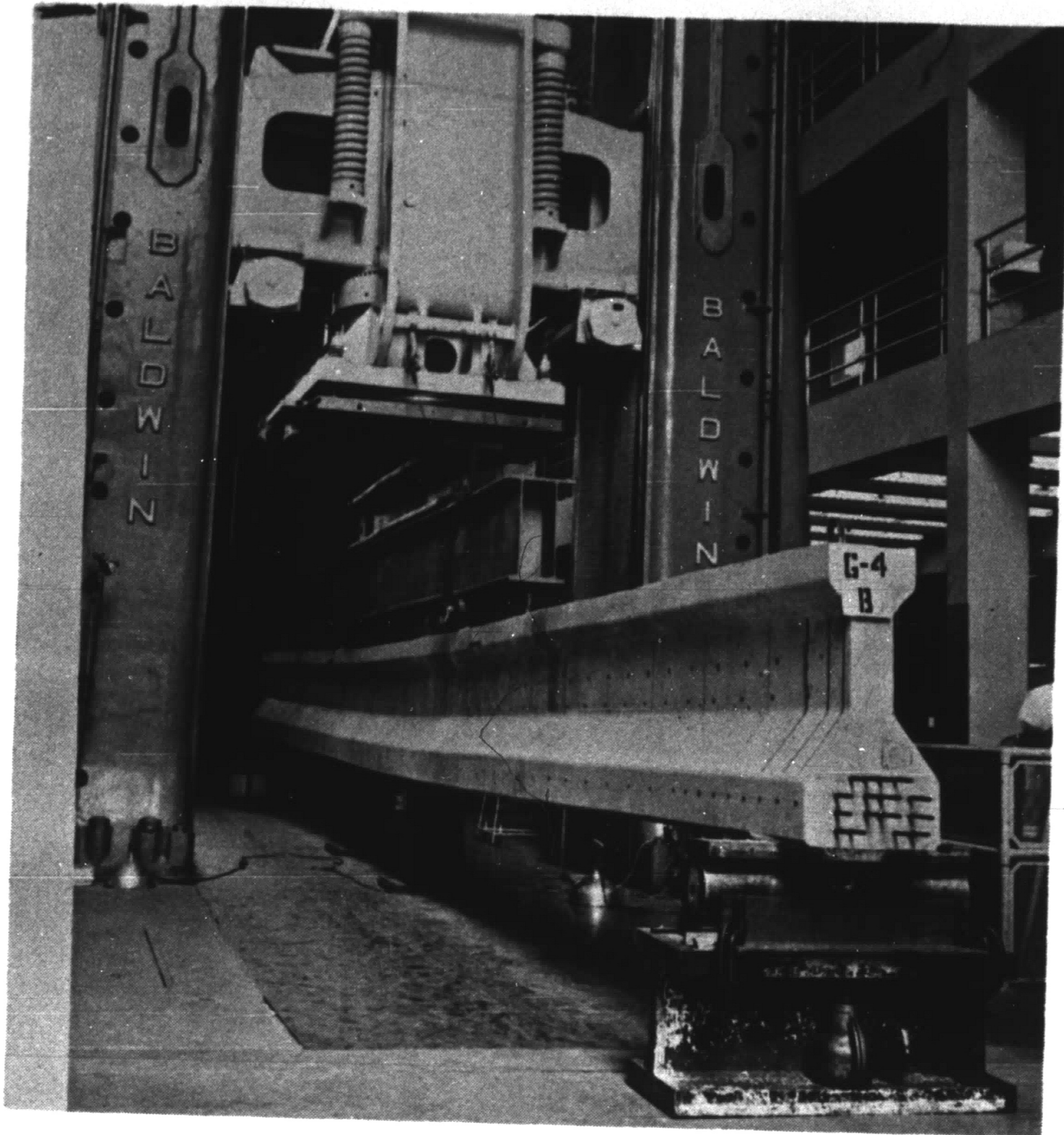


a. Reloading of a Cracked Beam to Failure
Second Test on Short I-Beam, G-2, and
Second Test on Short Box Beam, G-1



b. Flexure Shear Crack Width Growth at cg
First Test on Long Box Beam, G-3

Fig. 21. Inclined Crack Width Growth



a. During Loading Near Ultimate Capacity



b. View of Center Region of Beam After Flexural Failure

Fig. 22 First Test on Long I-Beam, G-4

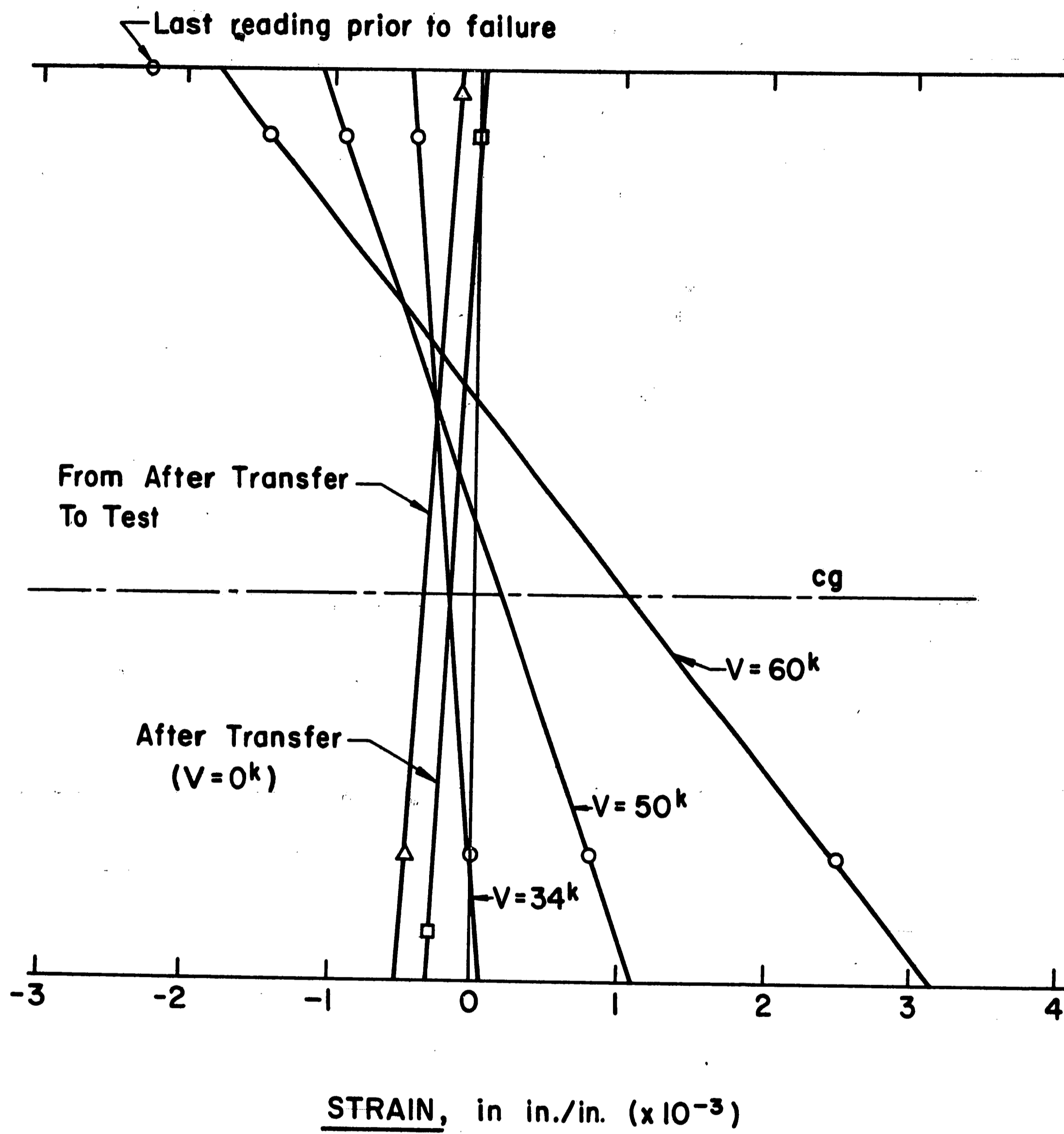
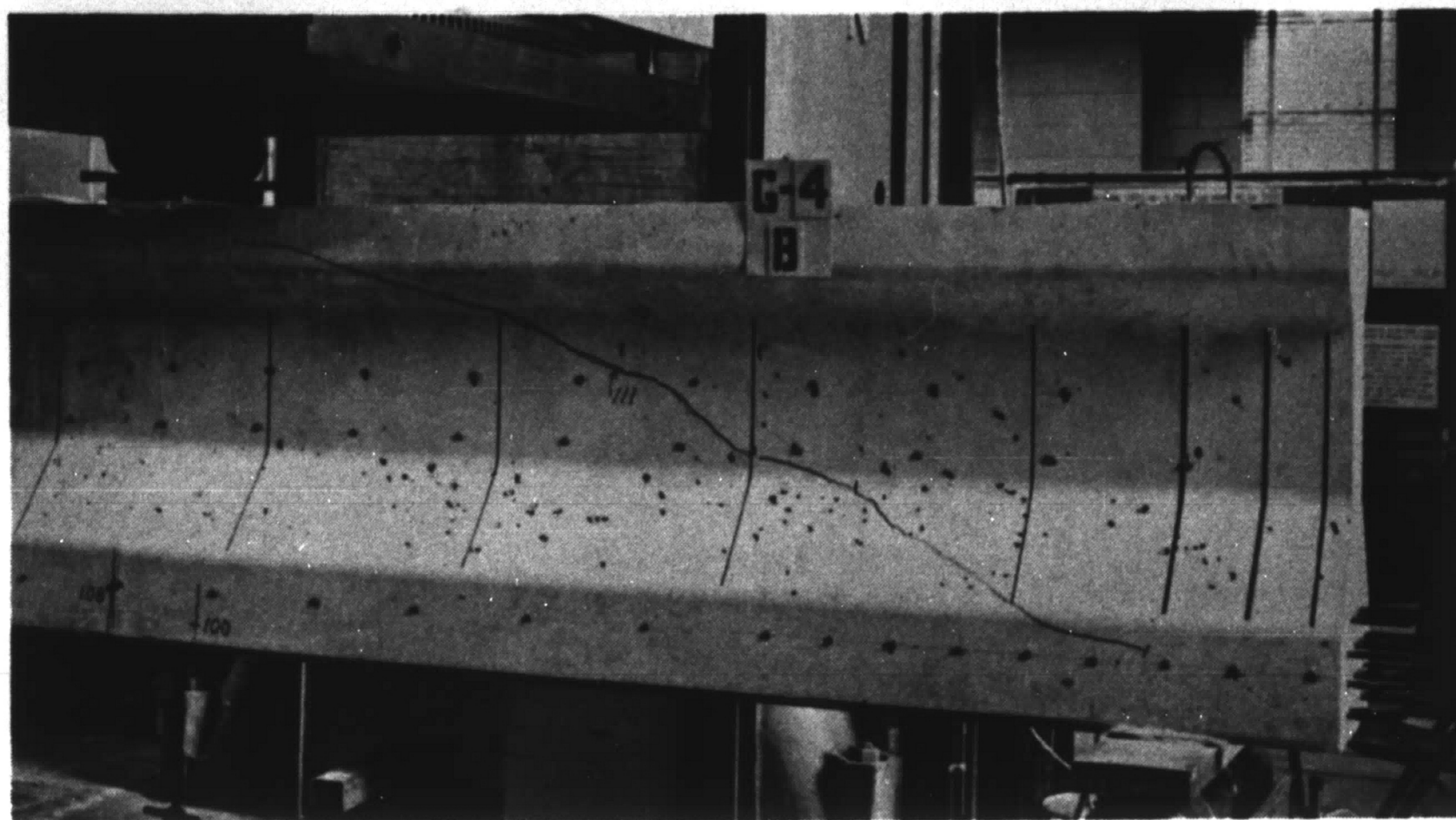
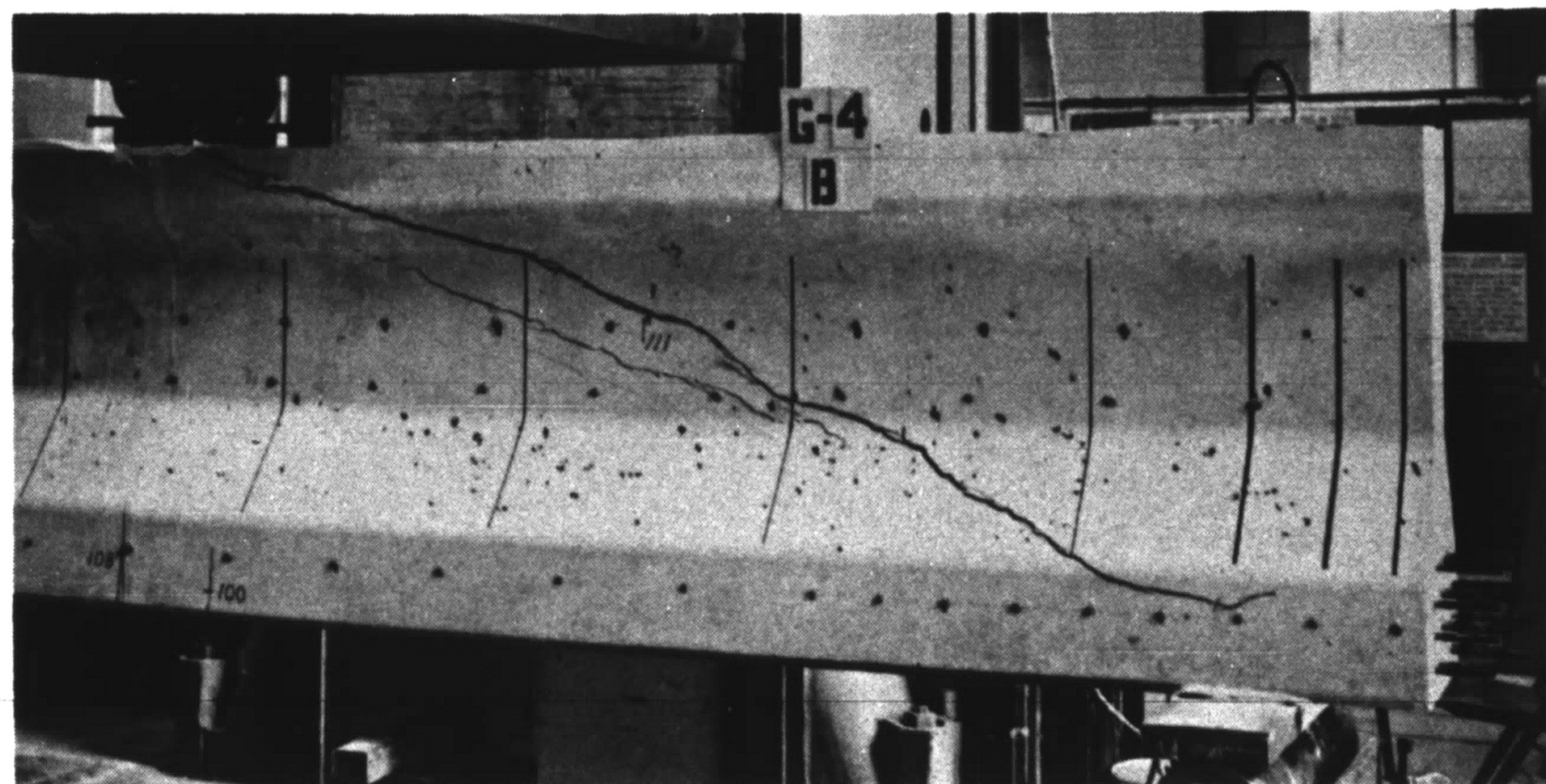


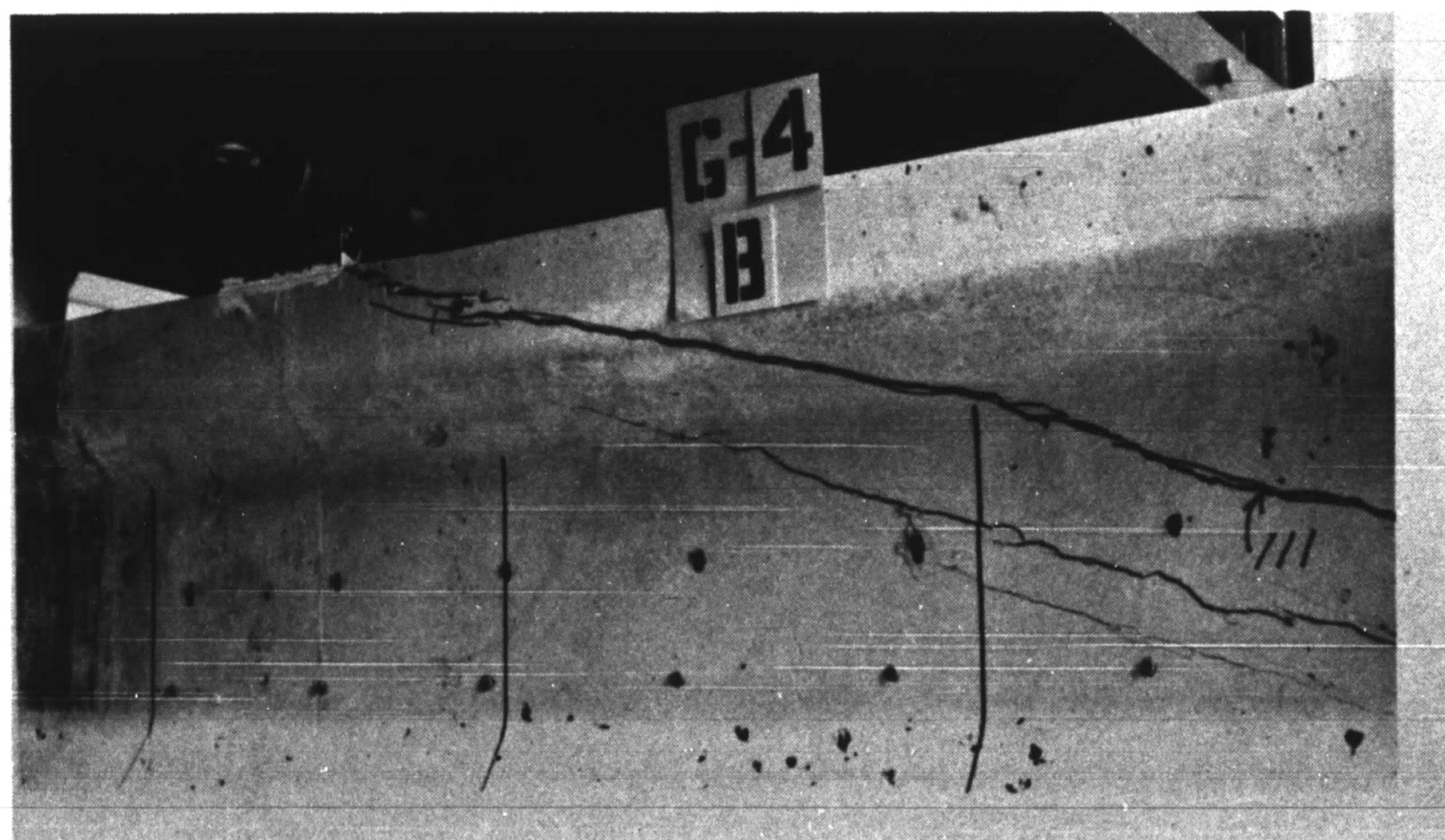
Fig. 23 First Test on Long I-Beam, G-4
Strain Distribution at Mid-Span



a. B Shear Span After Diagonal Tension Inclined Cracking

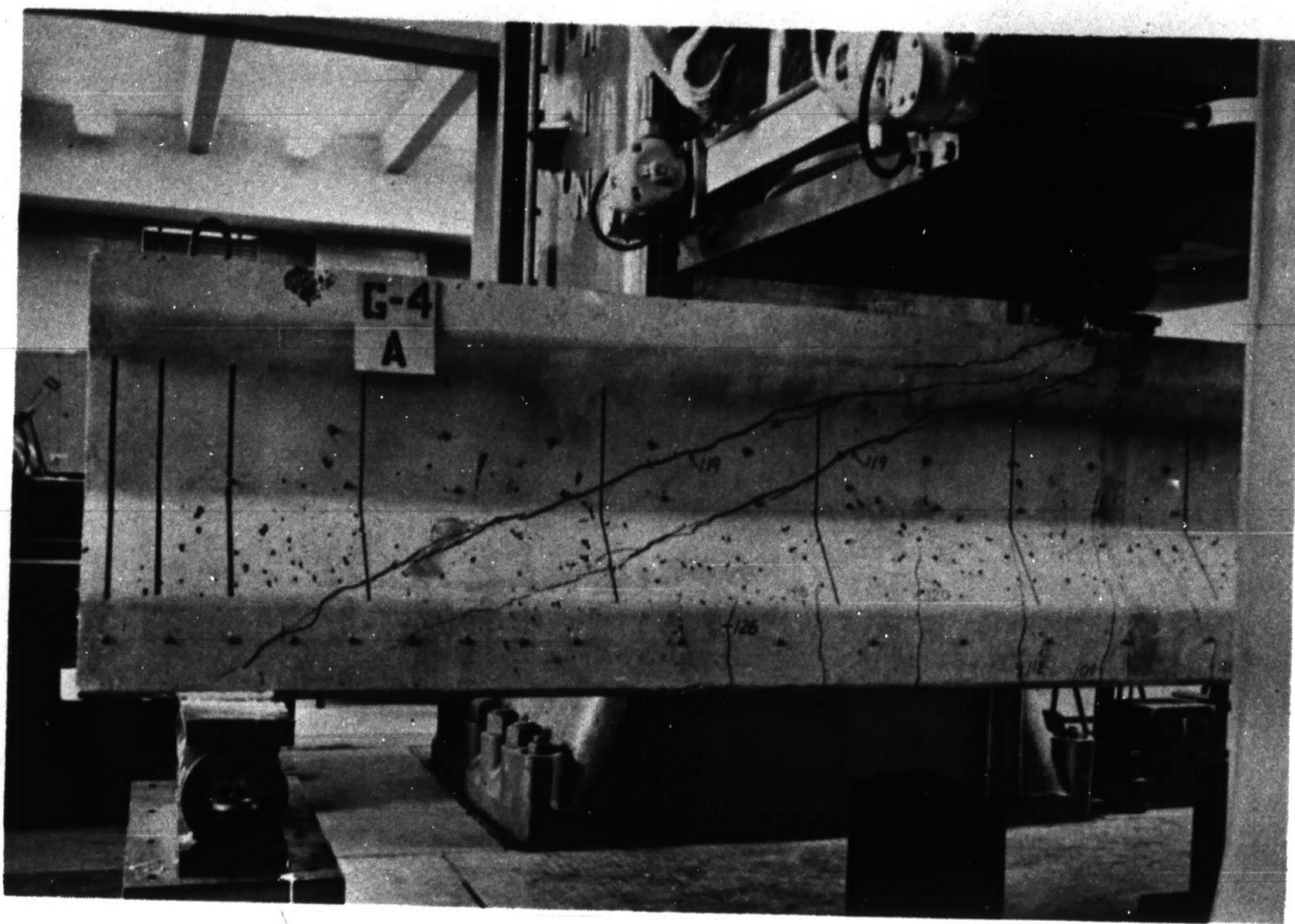


b. B Shear Span After Failure



c. View of Failure Region

Fig. 24 Second Test on Long I-Beam, G-4

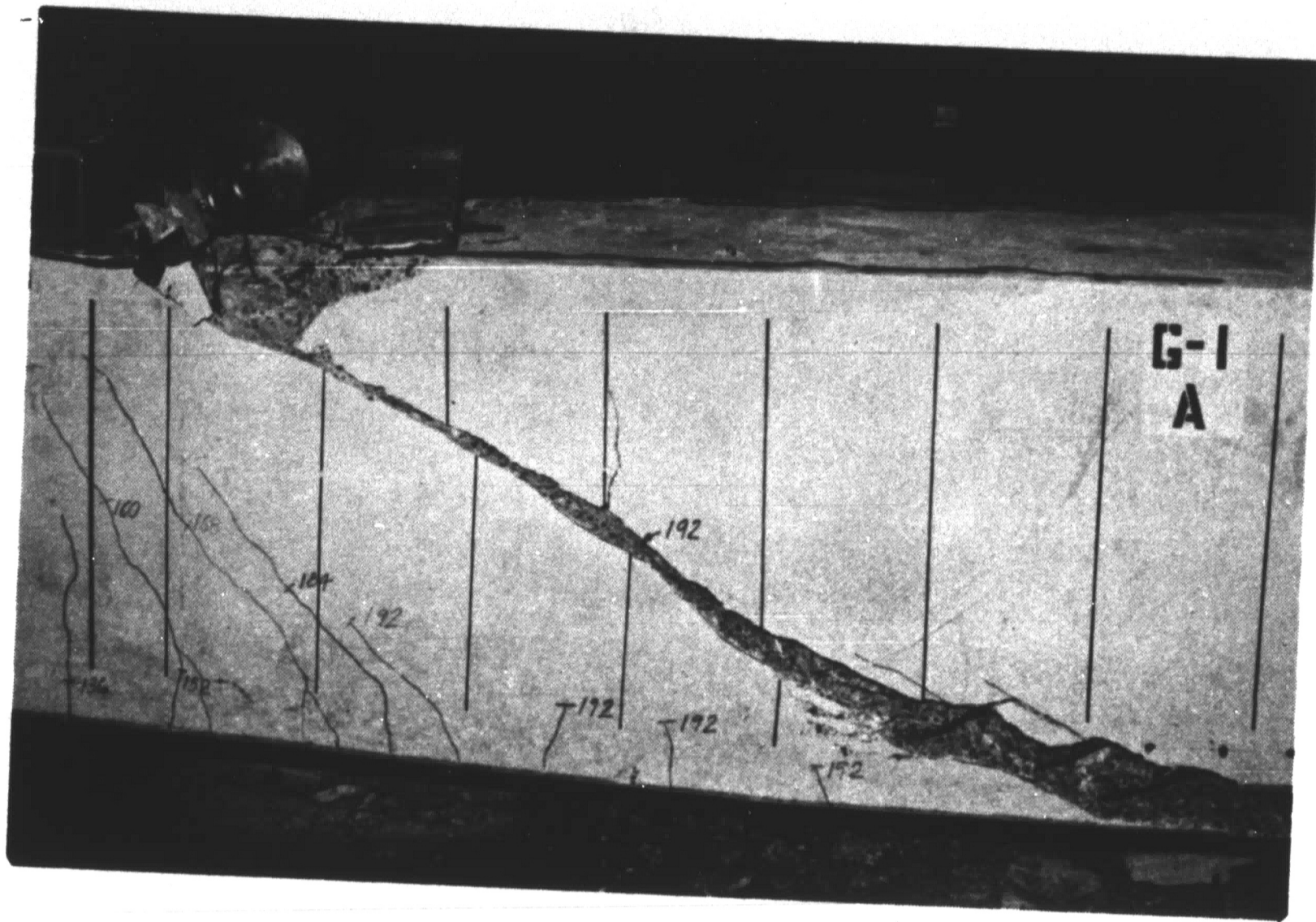


a. A Shear Span After Diagonal Tension Inclined Cracking



b. A Shear Span After Failure

Fig. 25 Third Test on Long I-Beam, G-4

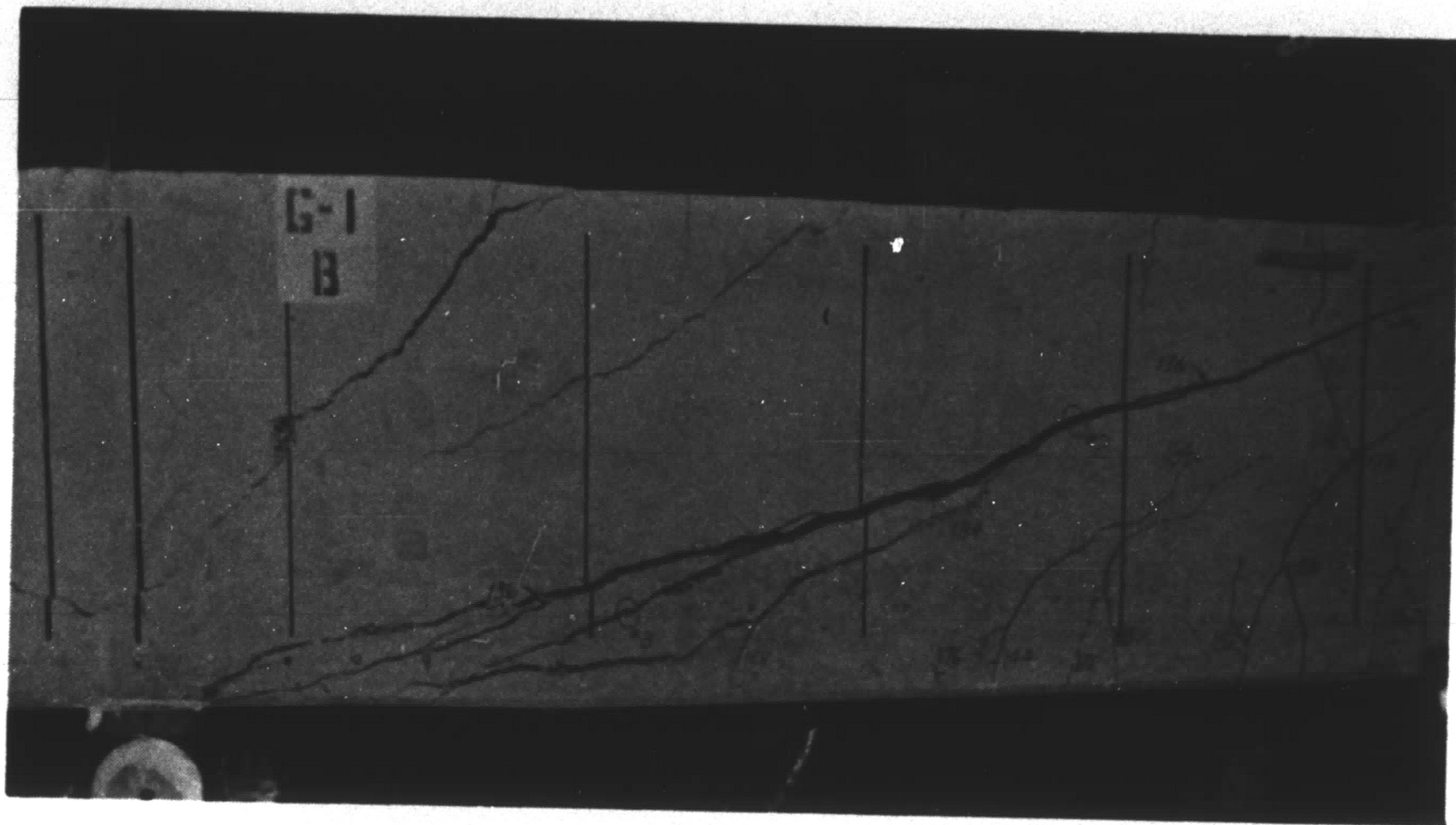


a. Right Side of A Shear Span After Diagonal Tension Inclined Cracking and Failure



b. Left Side of A Shear Span After Torsional Inclined Cracking and Failure

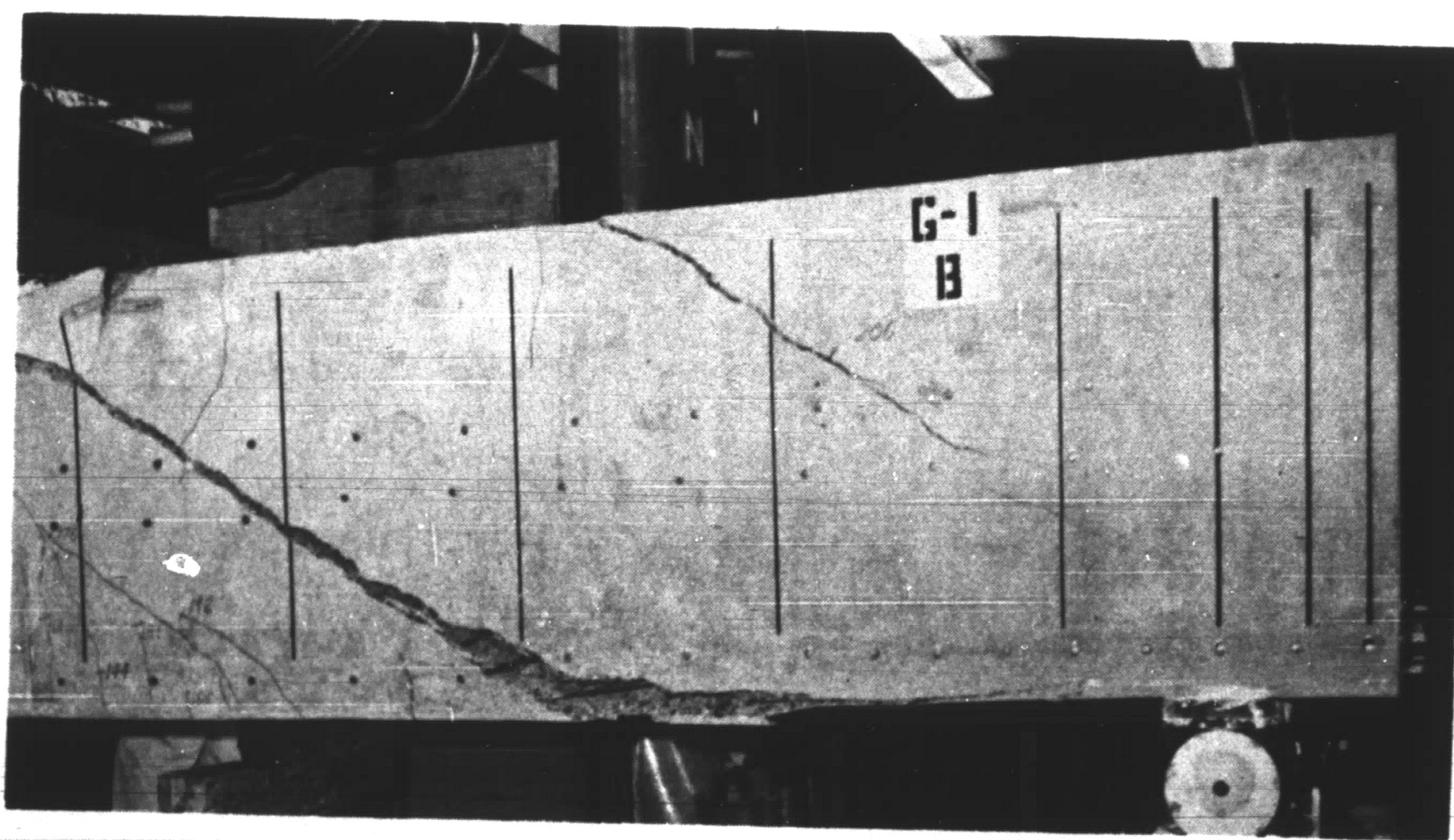
Fig. 26 First Test on Short Box Beam, G-1



a. Right Side of B Shear Span at Start of Test



b. Left Side of B Shear Span at Start of Test

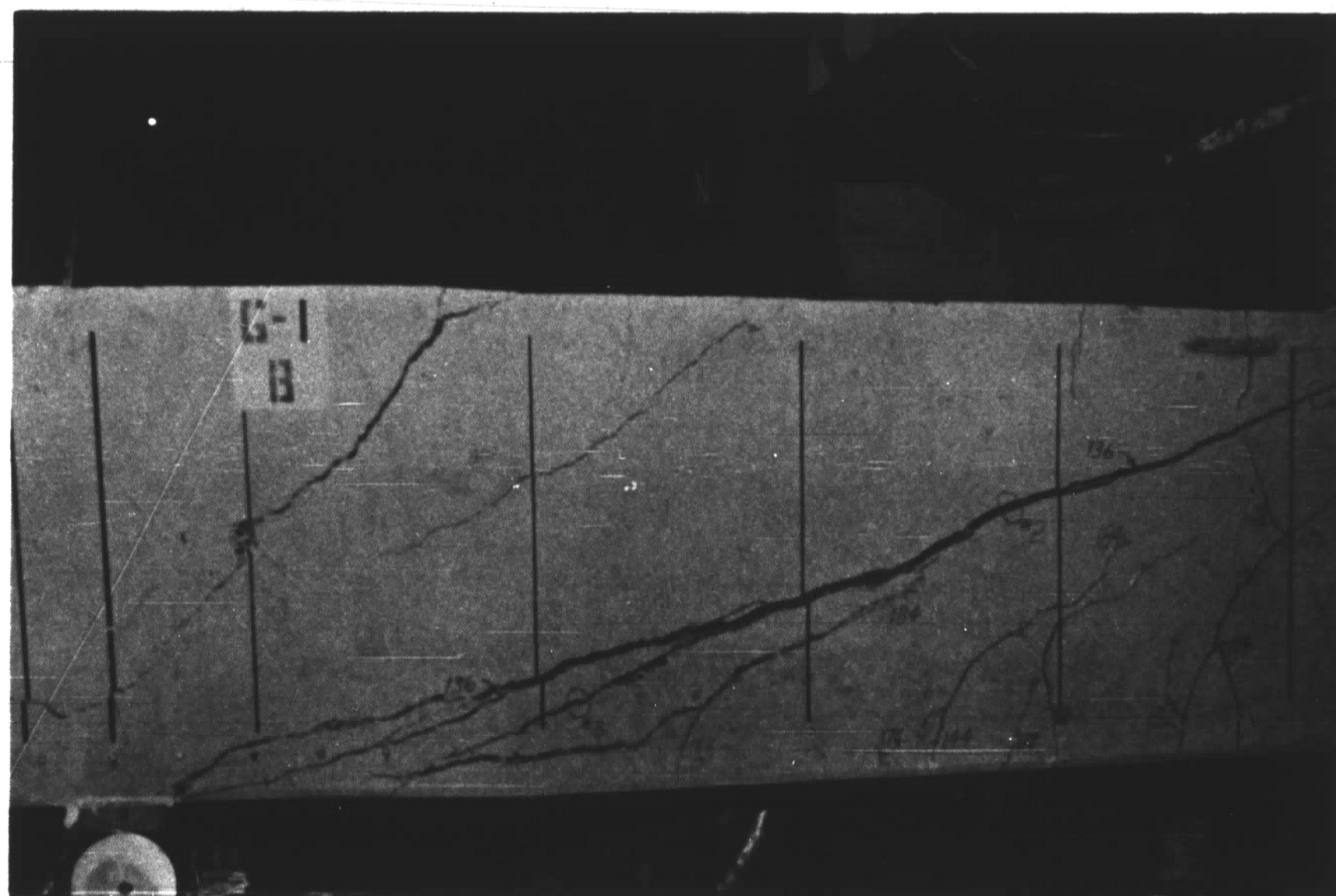


c. Left Side of B Shear Span After Torsional
Inclined Cracking and Failure

Fig. 27 Second Test on Short Box Beam, G-1



d. Left Side and Top Flange of B
Load Point After Failure



e. Right Side of B Shear Span After Failure

Fig. 27 Second Test on Short Box Beam, G-1

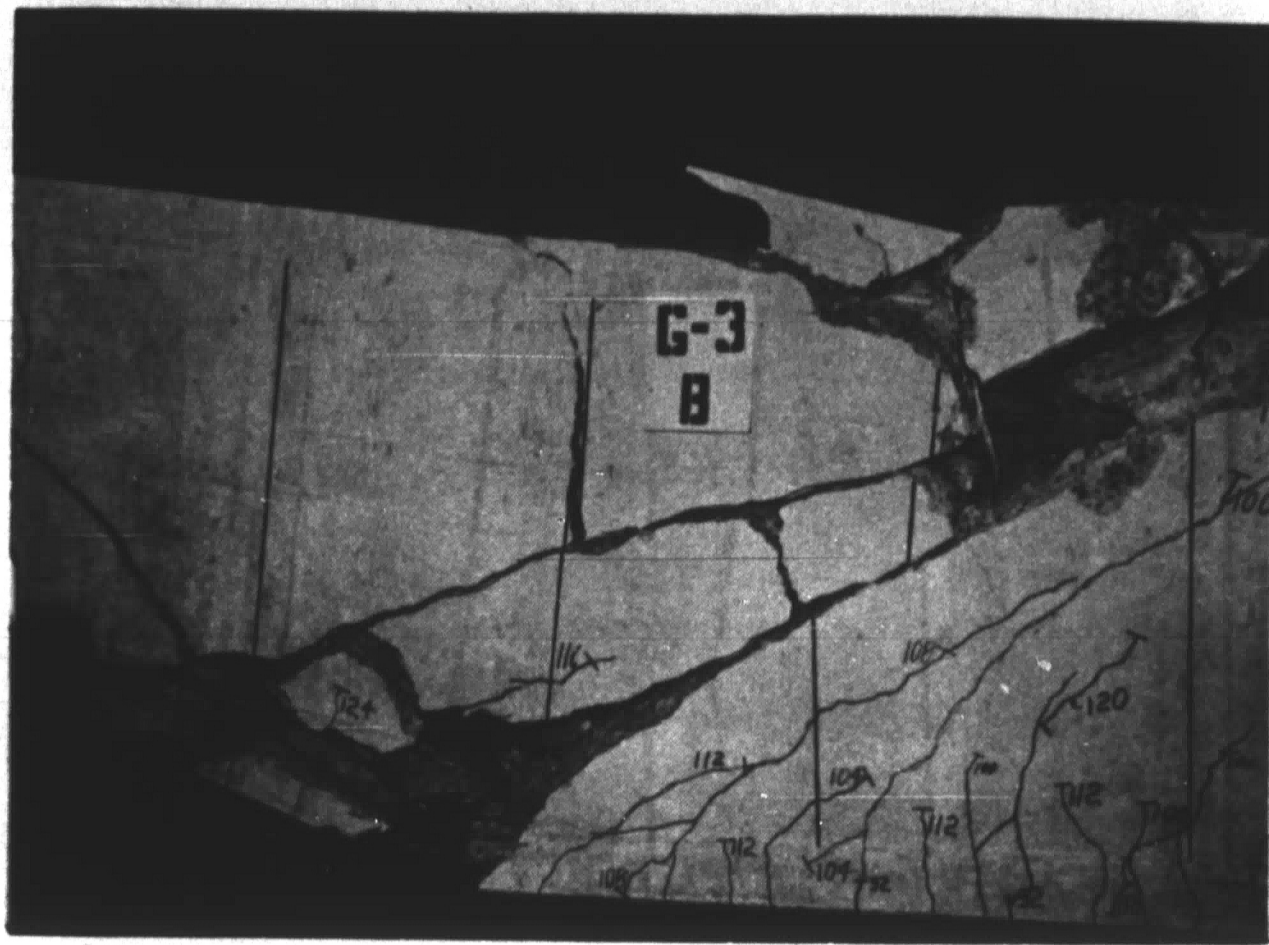


a. During Loading Near Ultimate Capacity

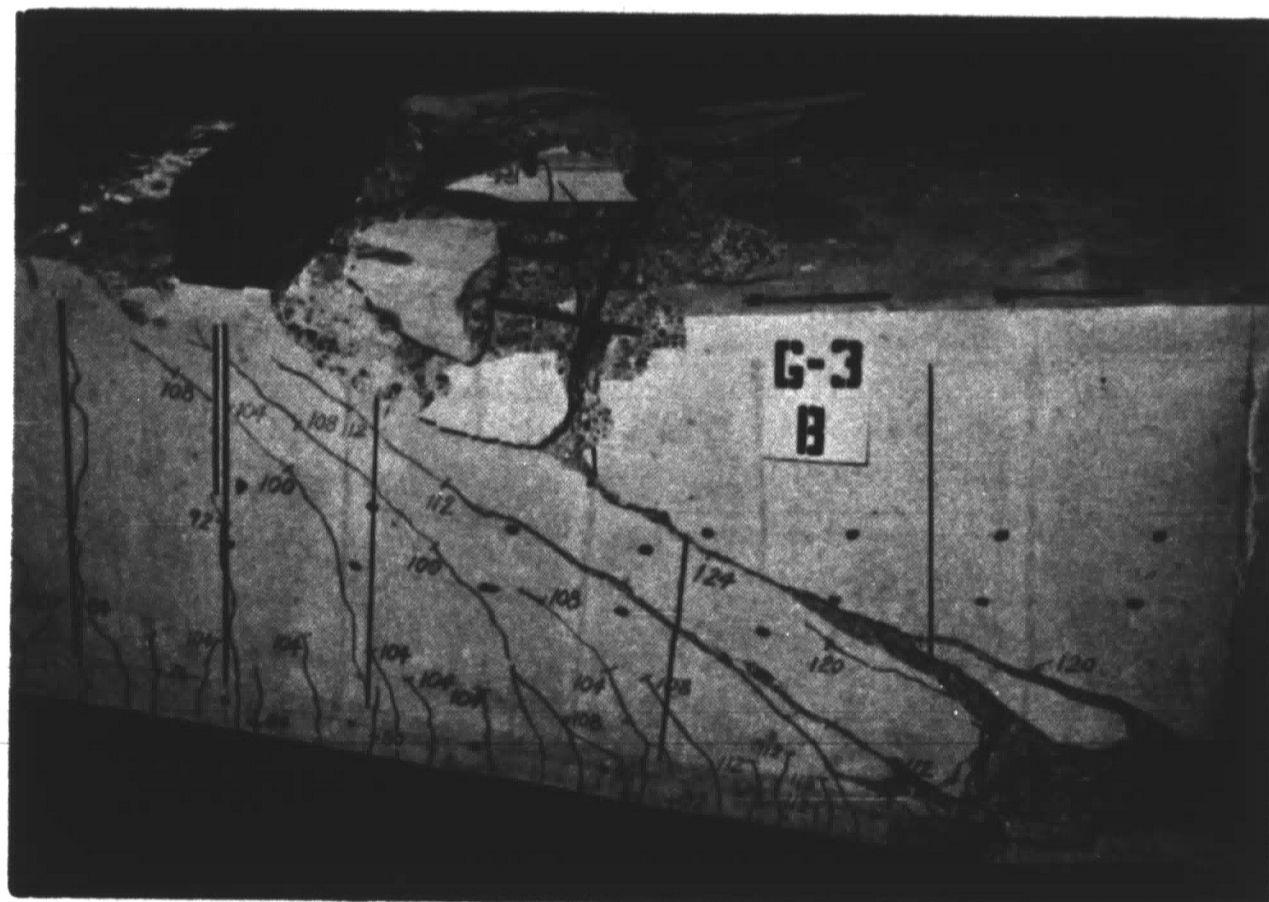


b. B Shear Span After Failure

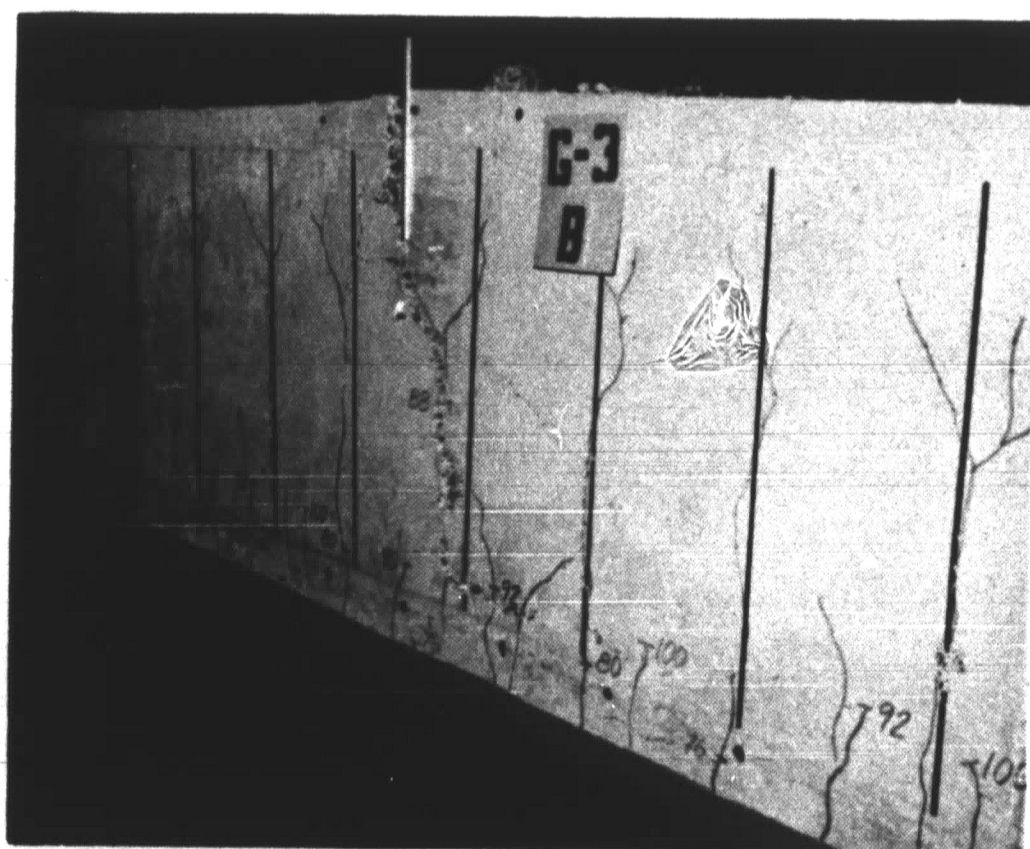
Fig. 28 First Test on Long Box Beam, G-3



a. Right Side of B Shear Span After Failure

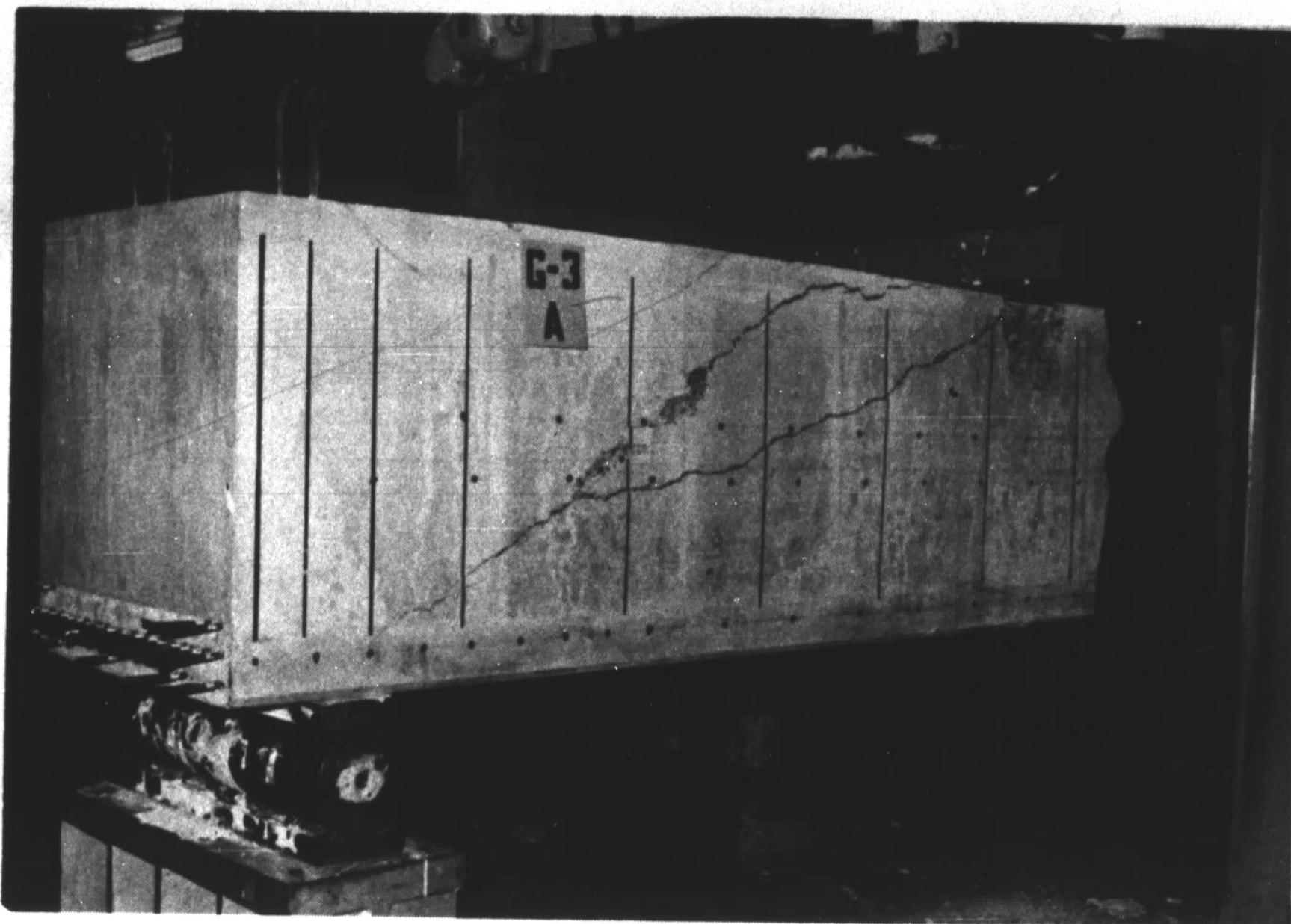


b. Left Side and Top of B Shear Span After Failure

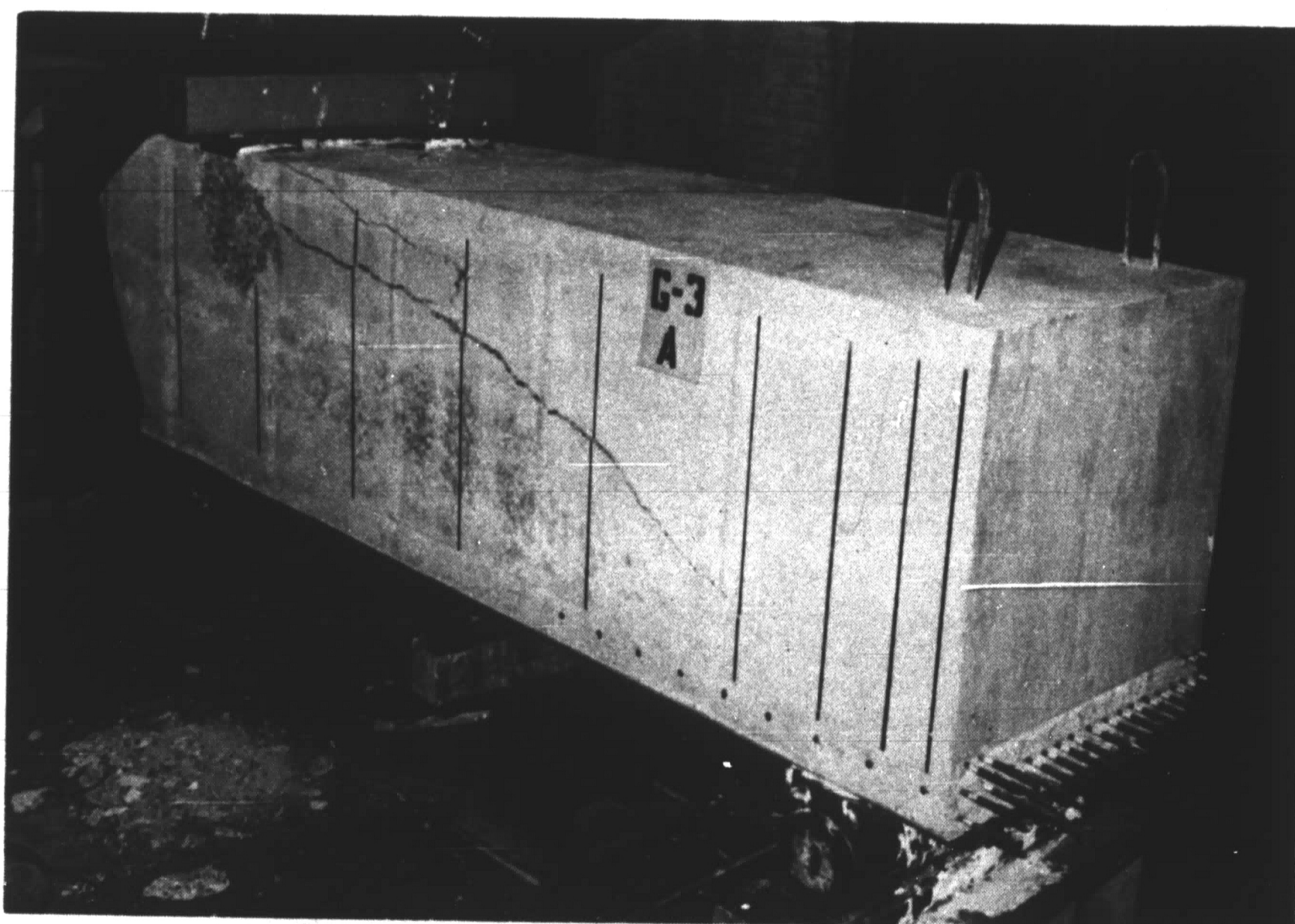


c. Left Side of C Region at Mid-Span After Failure

Fig. 29 First Test on Long Box Beam, G-3



a. Left Side of A Shear Span After Failure



b. Right Side of A Shear Span After Failure

Fig. 30 Second Test on Long Box Beam, G-3

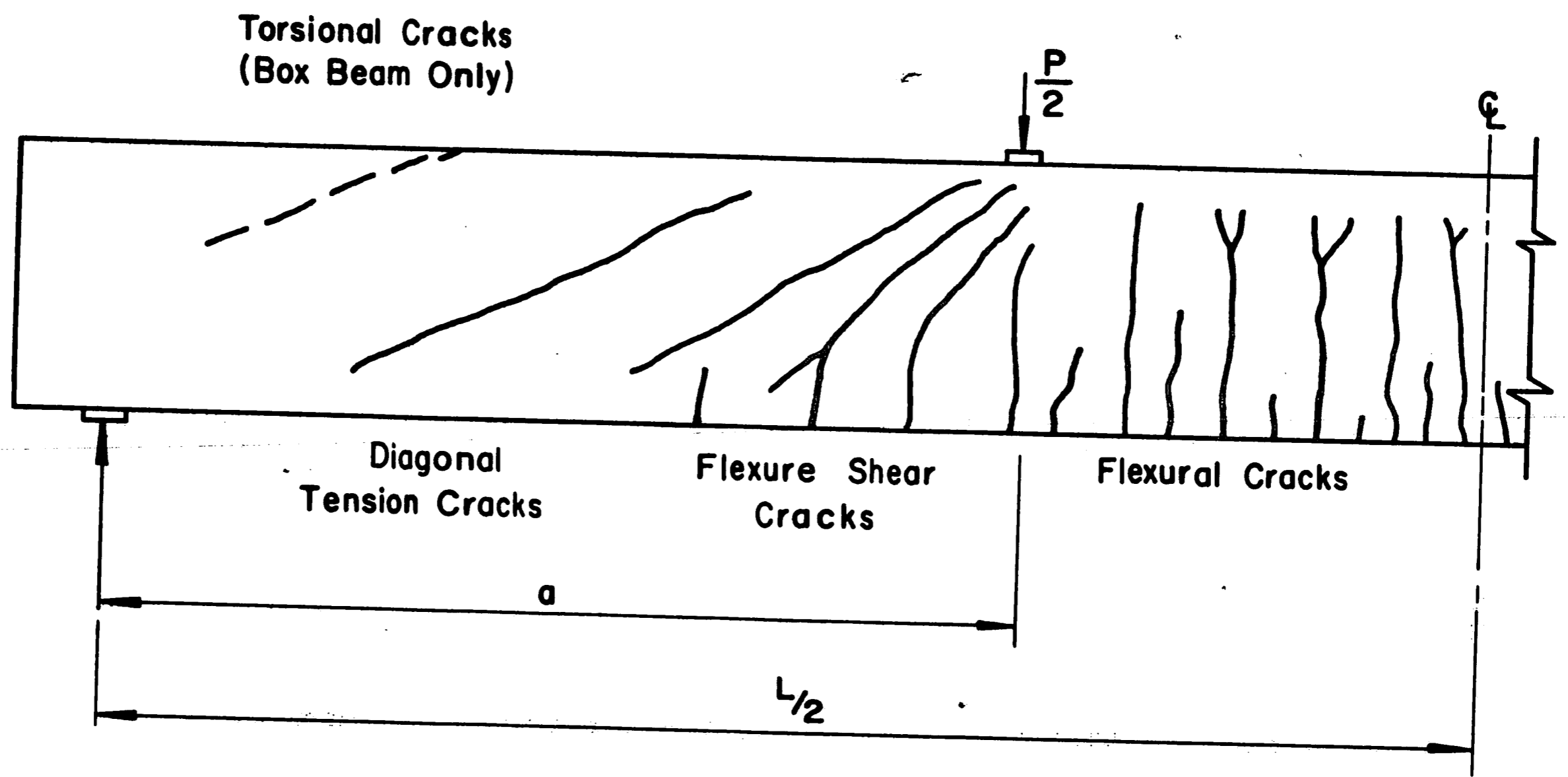


Fig. 31 Types of Inclined Cracking Observed During Testing

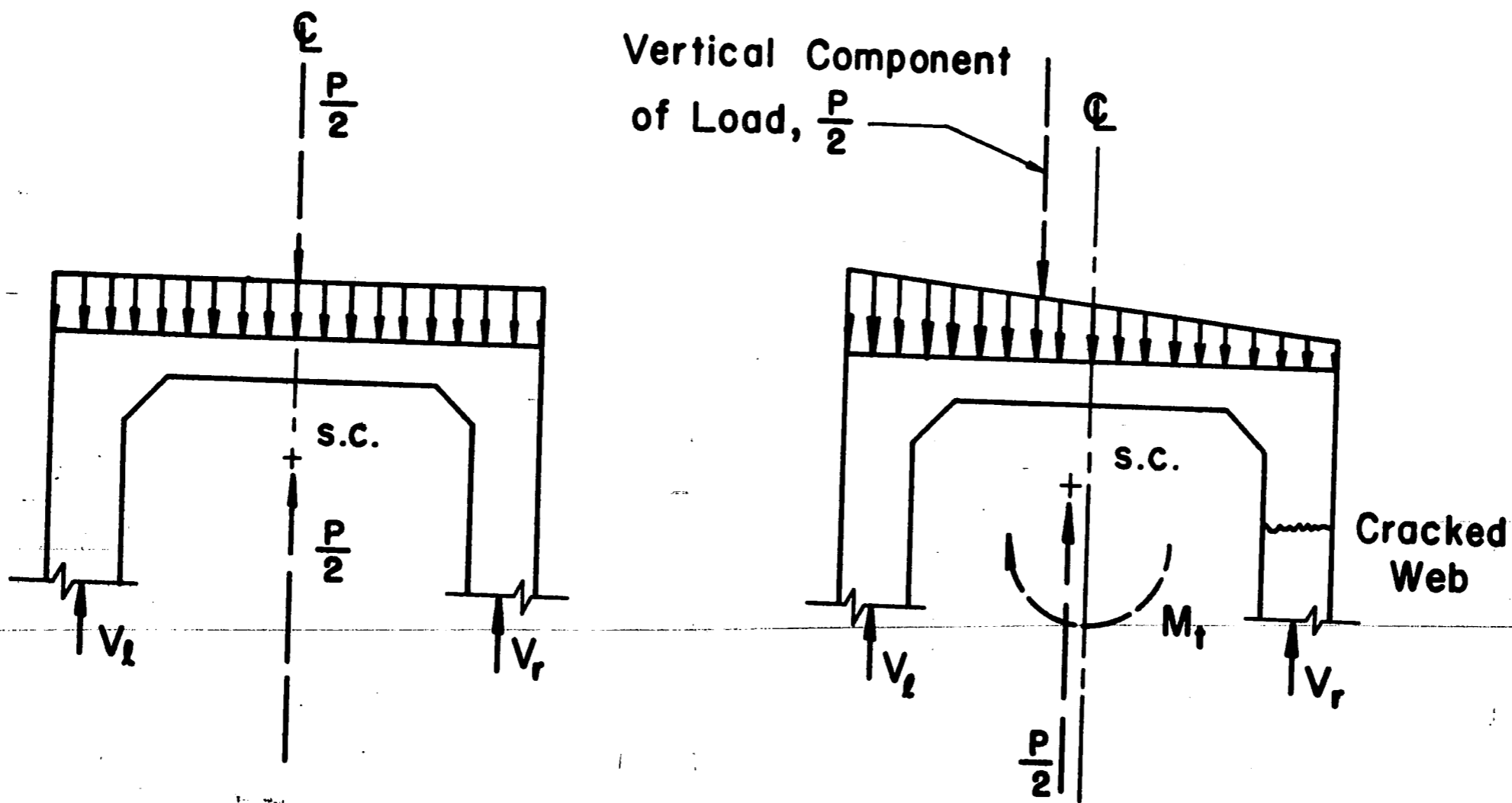
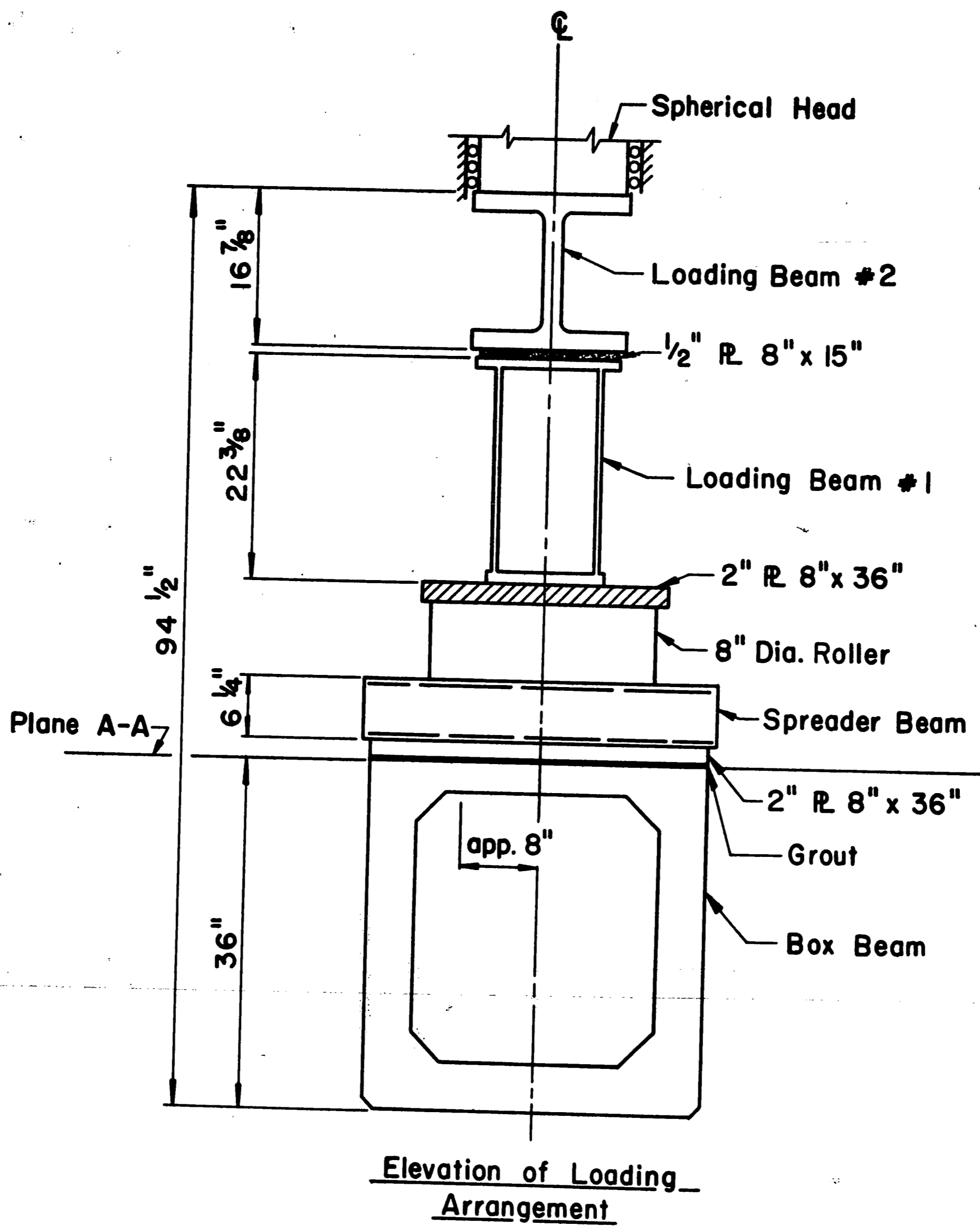
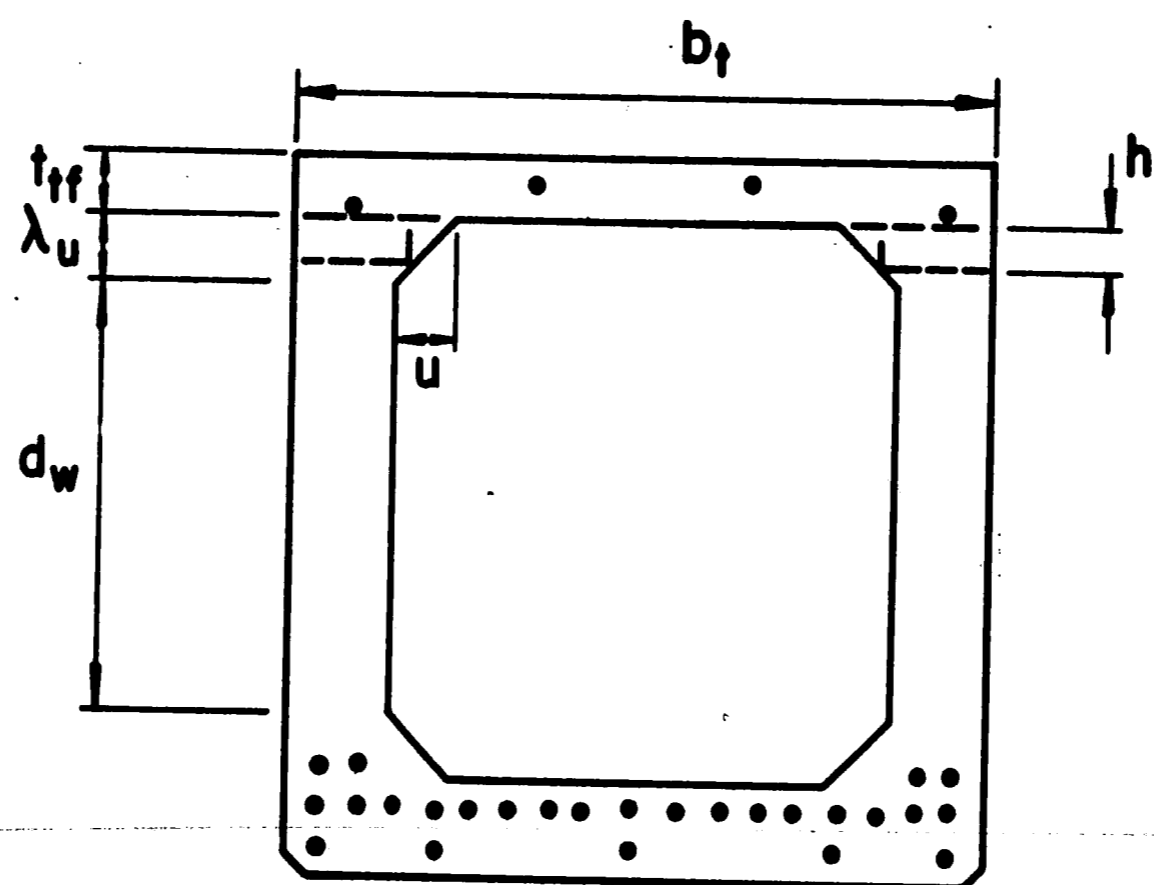
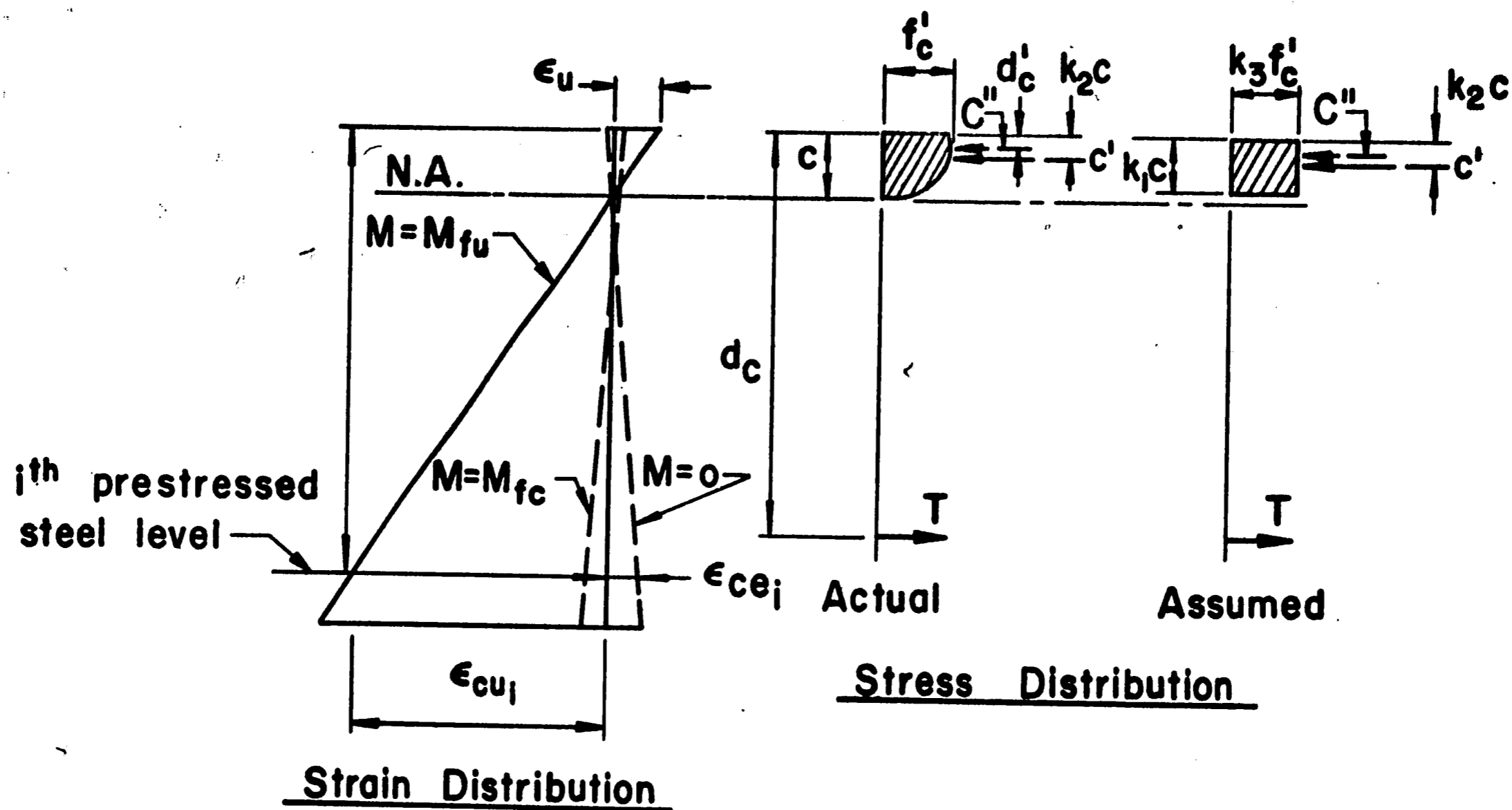
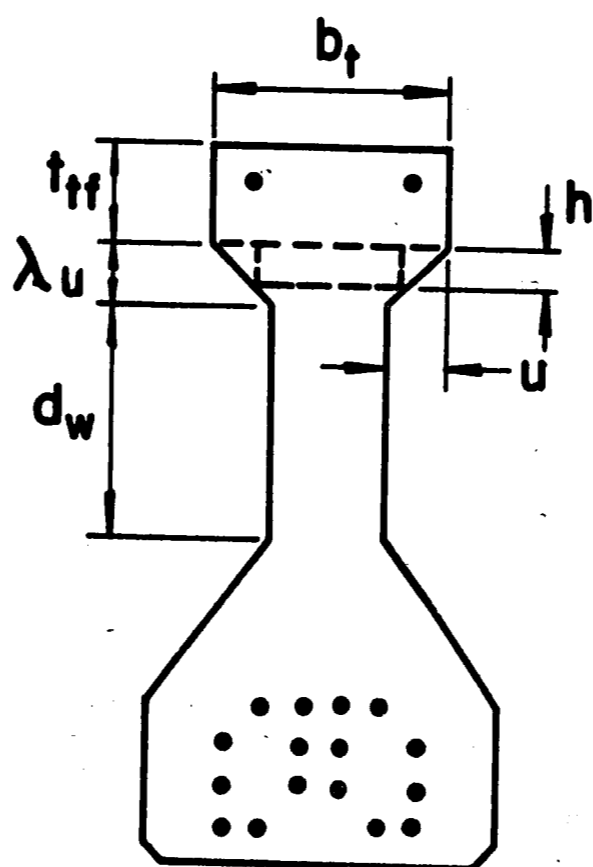


Fig. 32 Internal Torsional Effects of Box Beams which Sustained Inclined Cracks in One Web Only



Box Beam



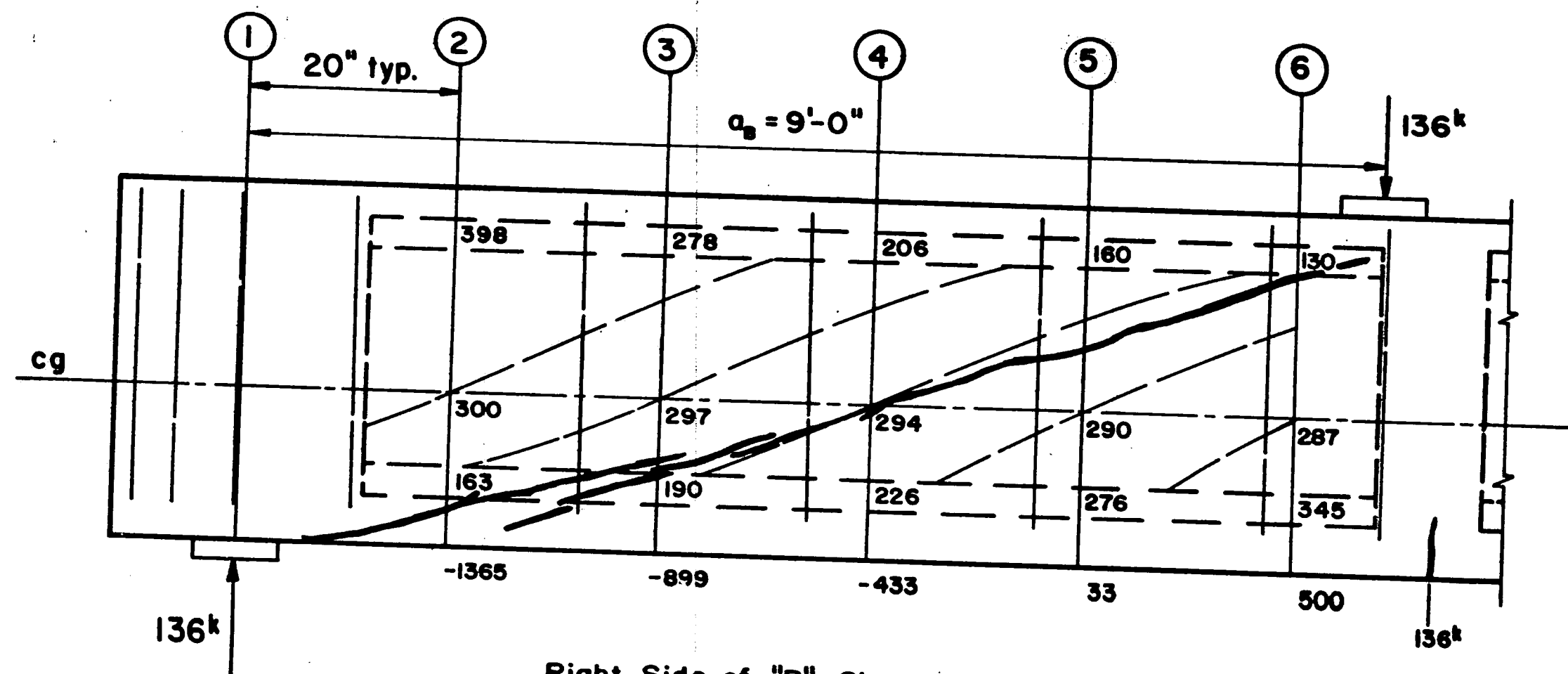
I Beam

Fig. 33 Assumed Strain and Stress Distribution at Flexural Failure

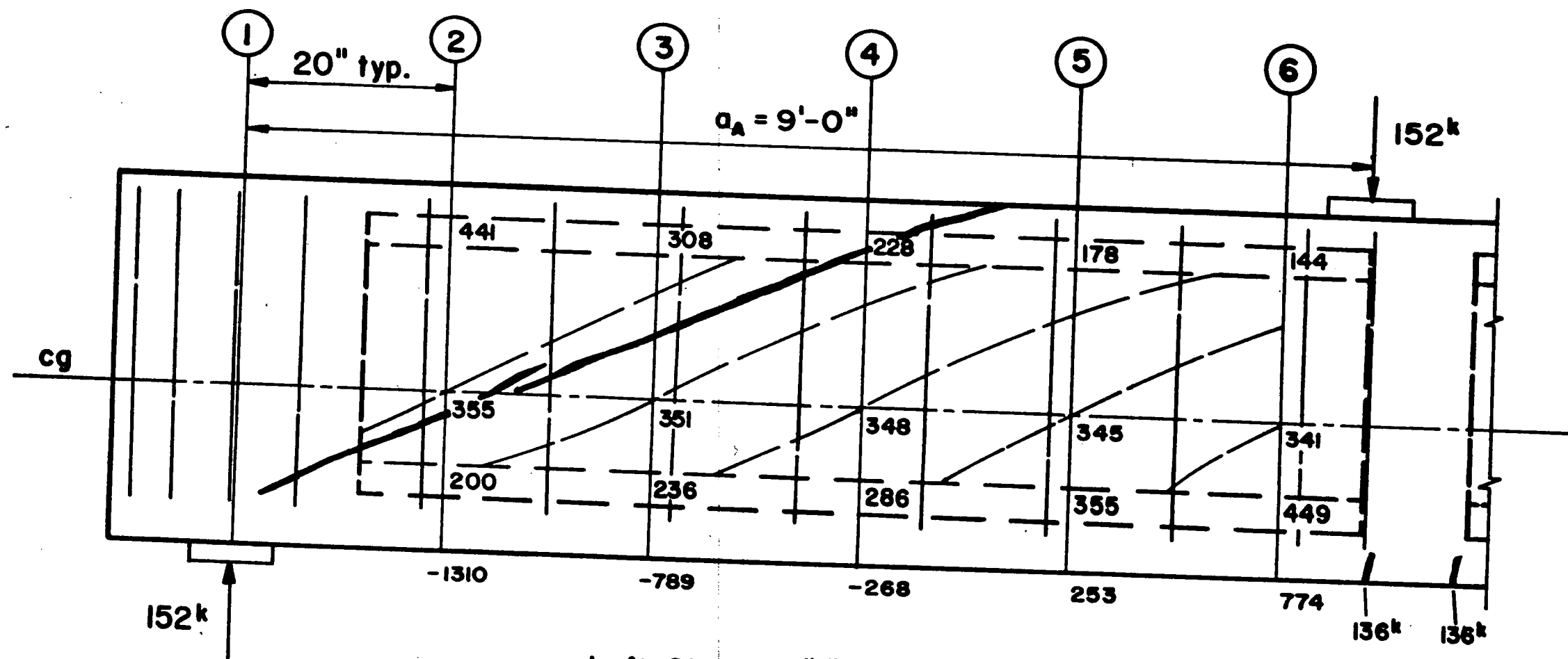
11. A P P E N D I X A

CRACK PATTERNS

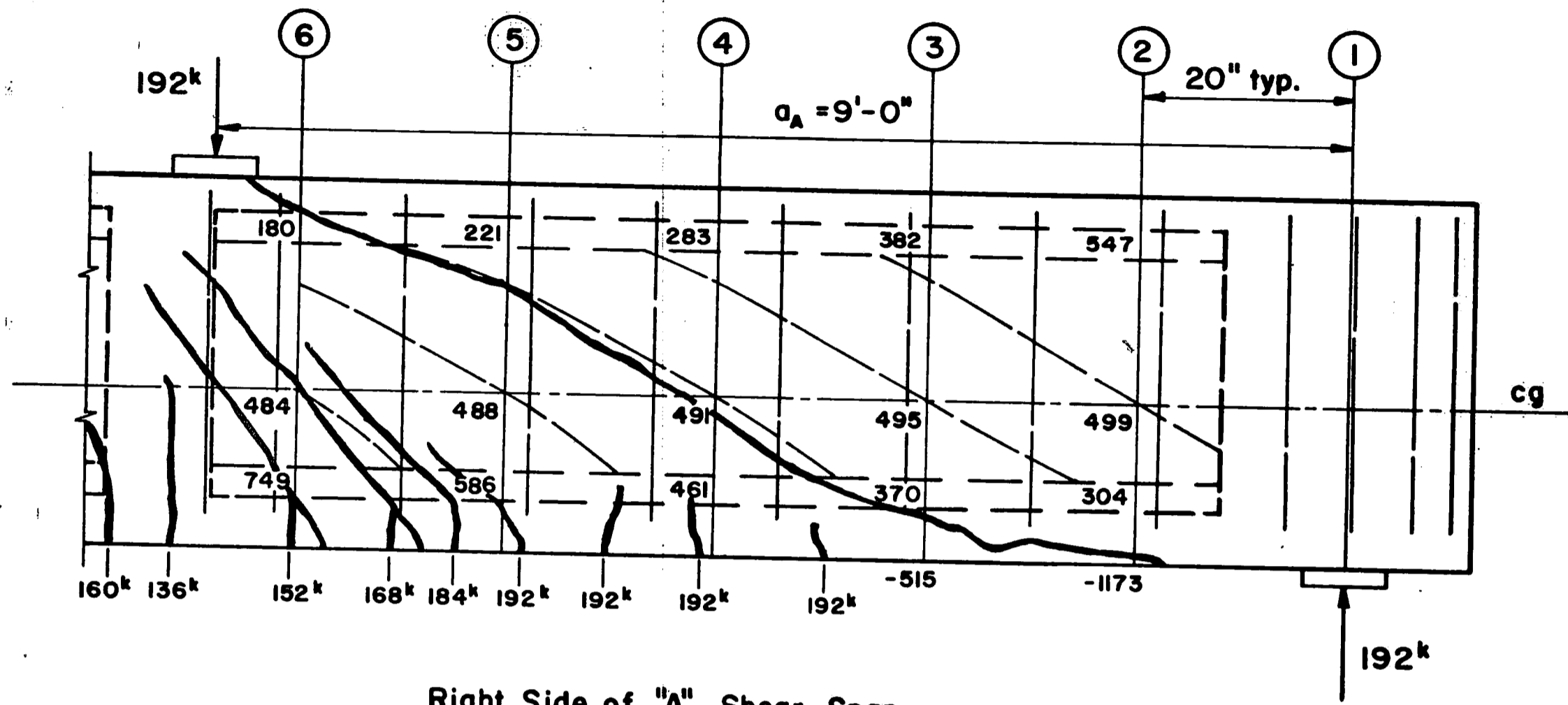
(See Section 6.3.2
for discussion)



Right Side of "B" Shear Span
Beam G-1 1st. Test



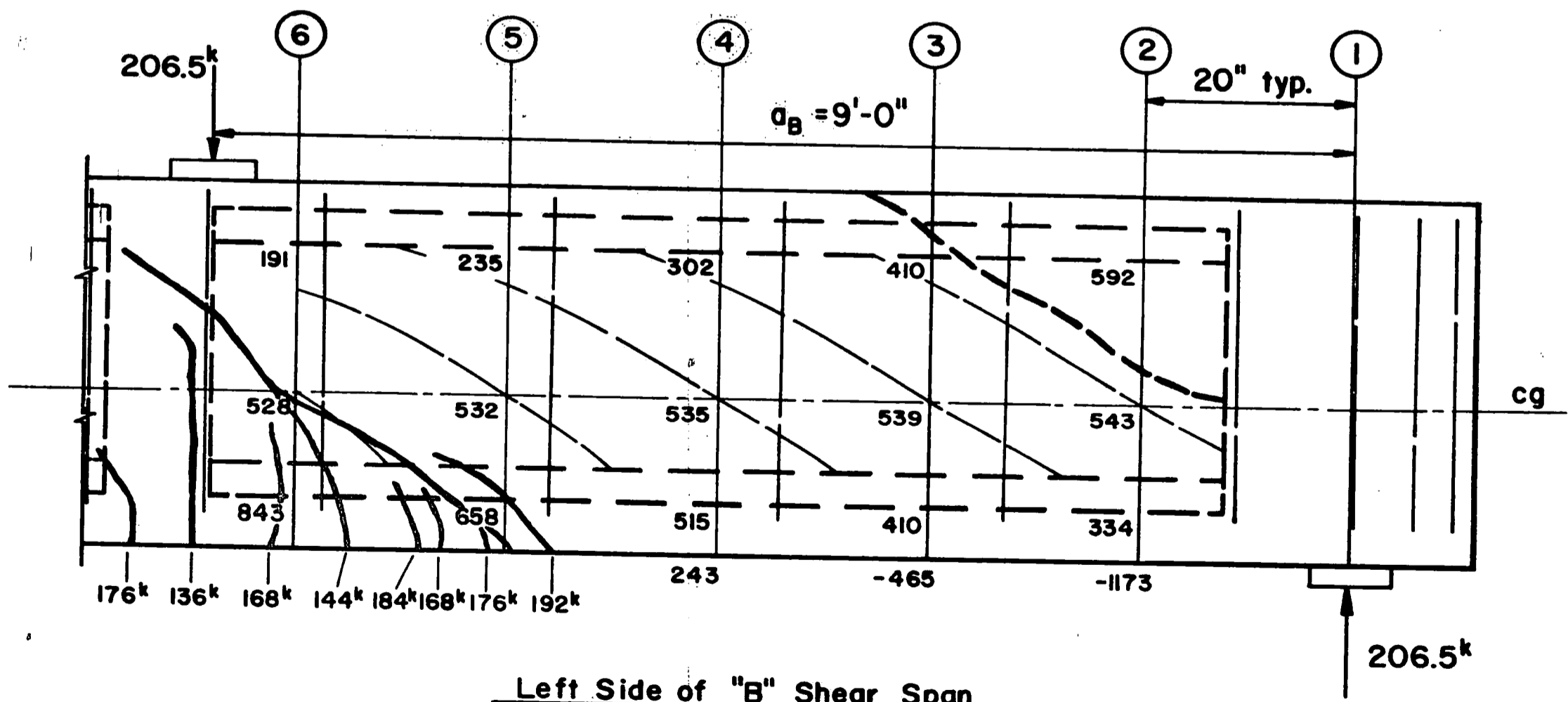
Left Side of "A" Shear Span
Beam G-1 1st. Test



Right Side of "A" Shear Span

Beam G-1

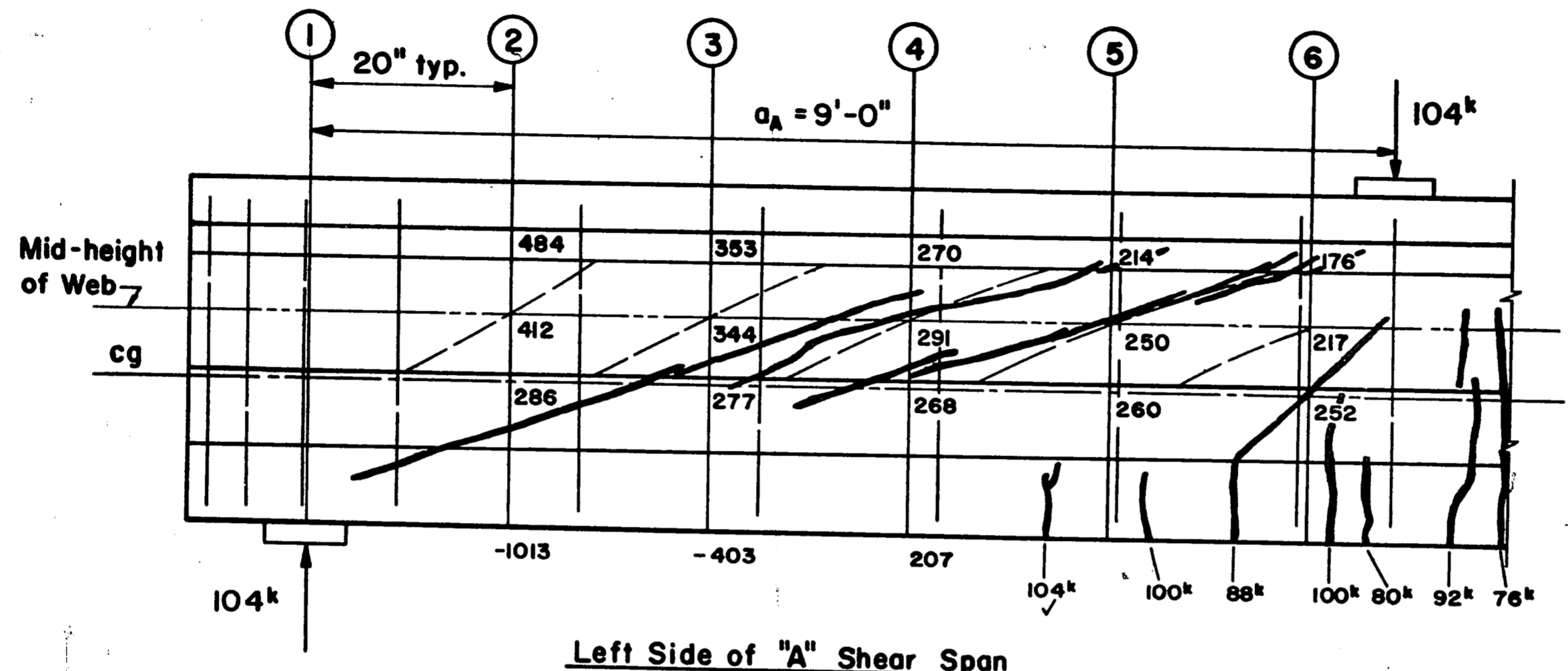
1st. Test



Left Side of "B" Shear Span

Beam G-1

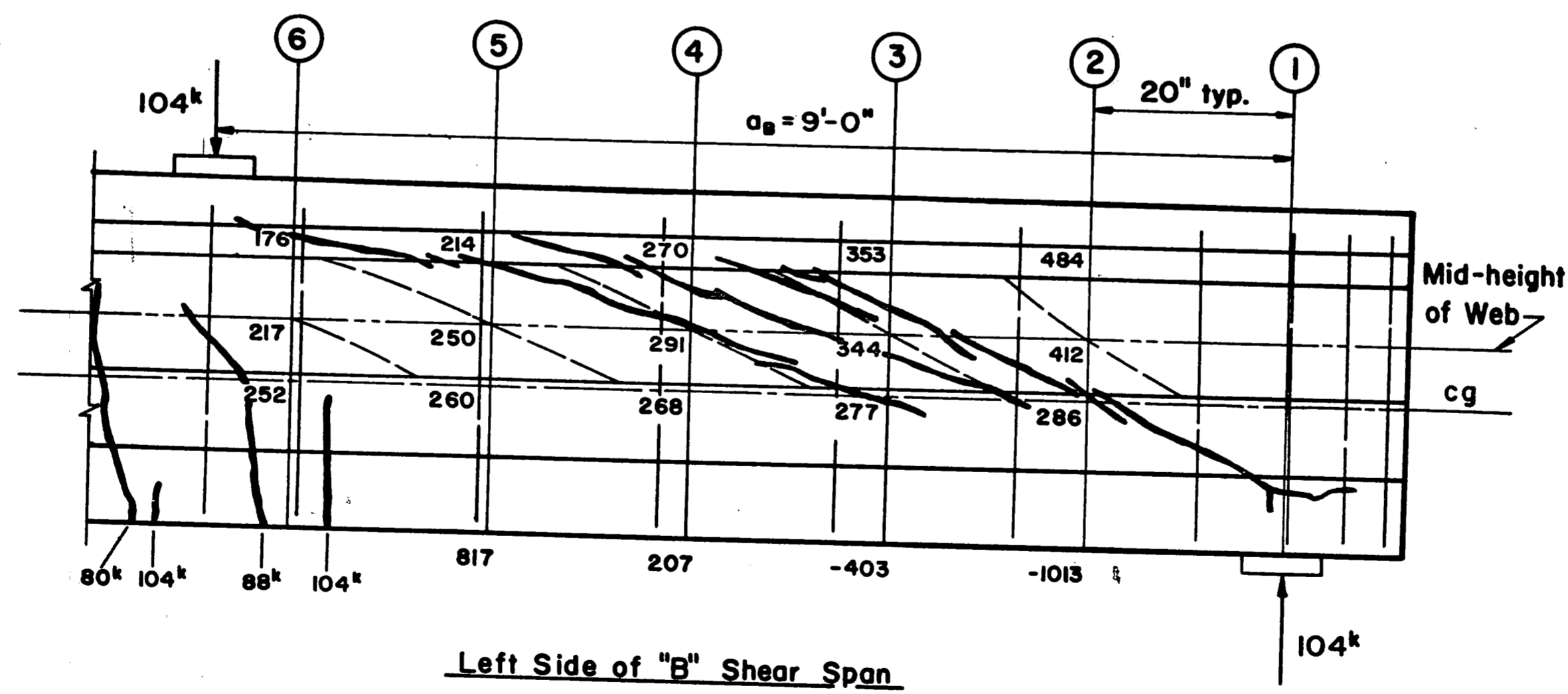
2nd. Test



Left Side of "A" Shear Span

Beam G-2

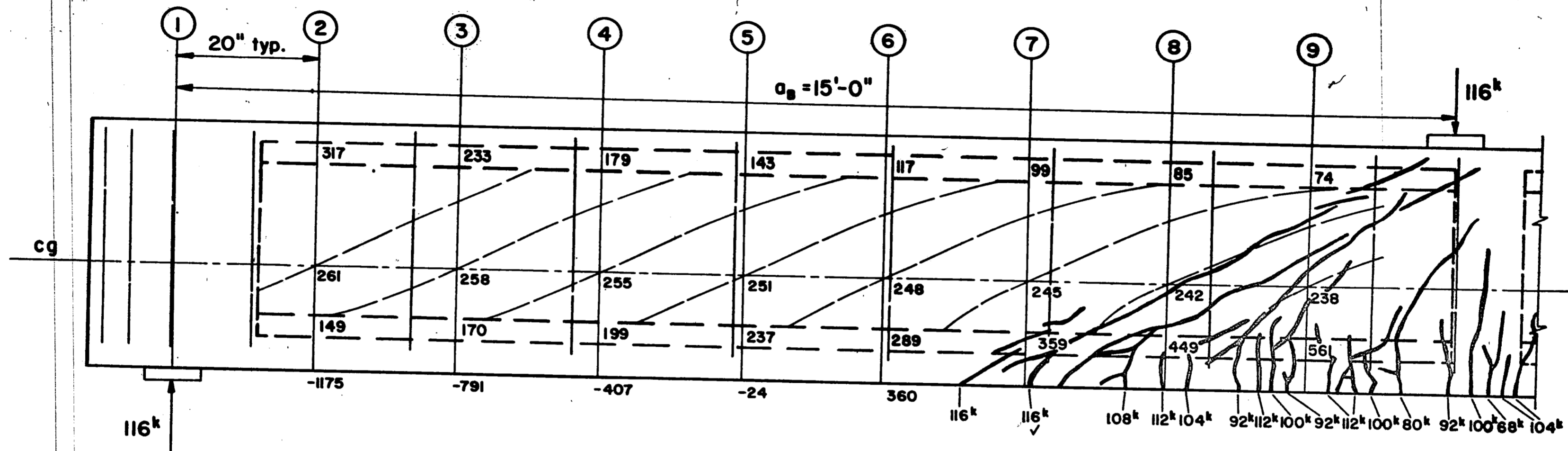
Ist. Test



Left Side of "B" Shear Span

Beam G-2

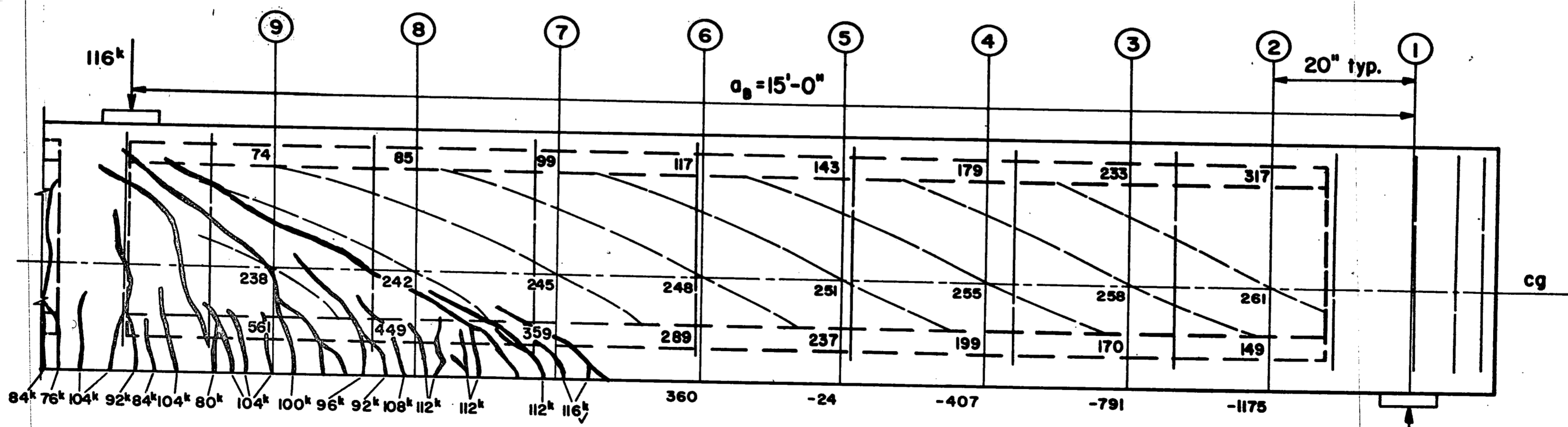
Ist. Test



Right Side of "B" Shear Span

Beam G-3

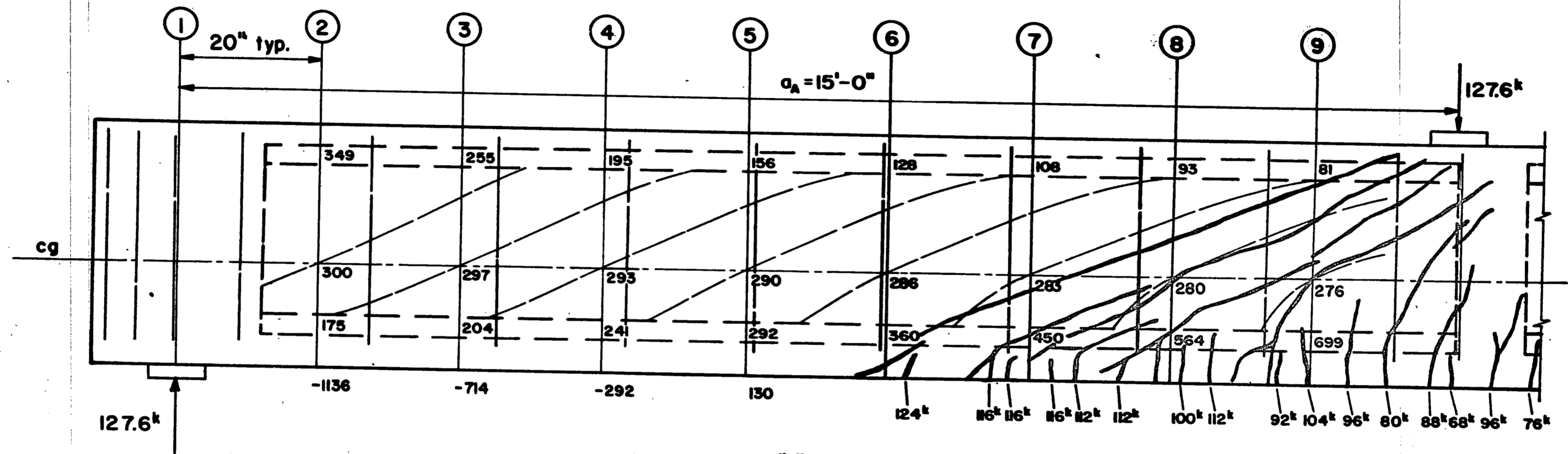
Ist. Test



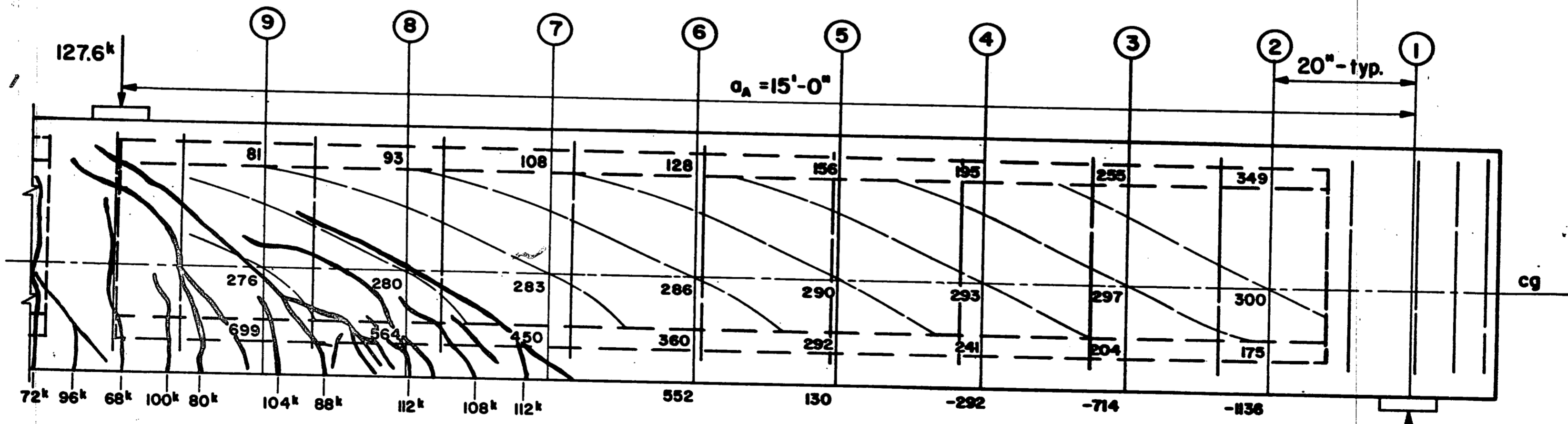
Left Side of "B" Shear Span

Beam G-3

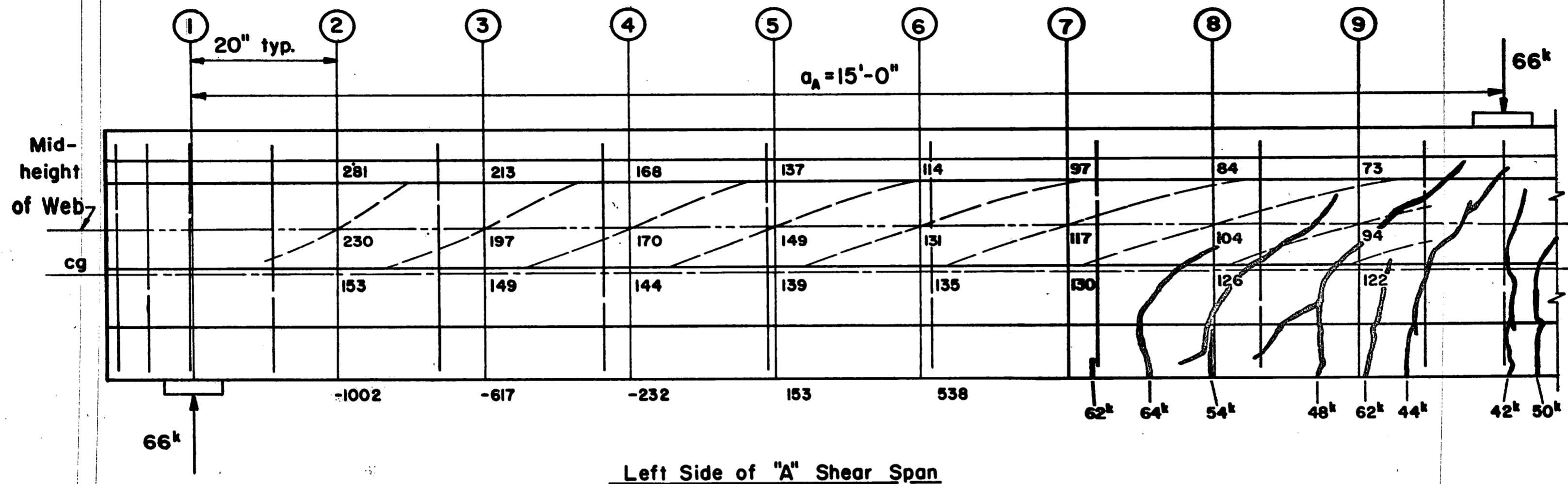
Ist. Test



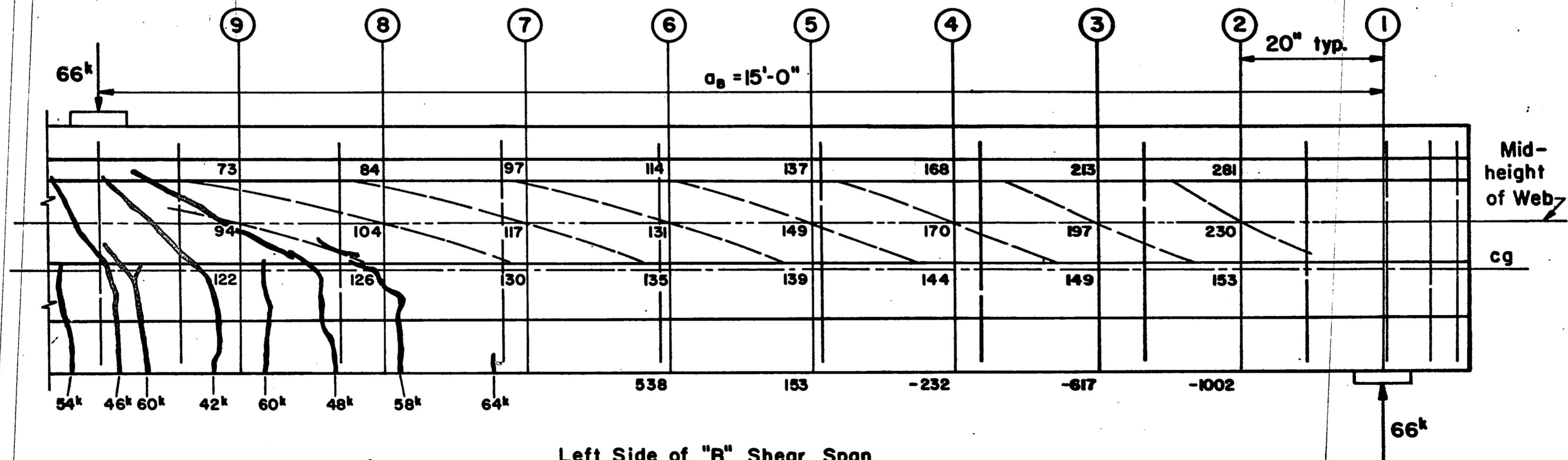
Left Side of "A" Shear Span
 Beam G-3 Ist. Test



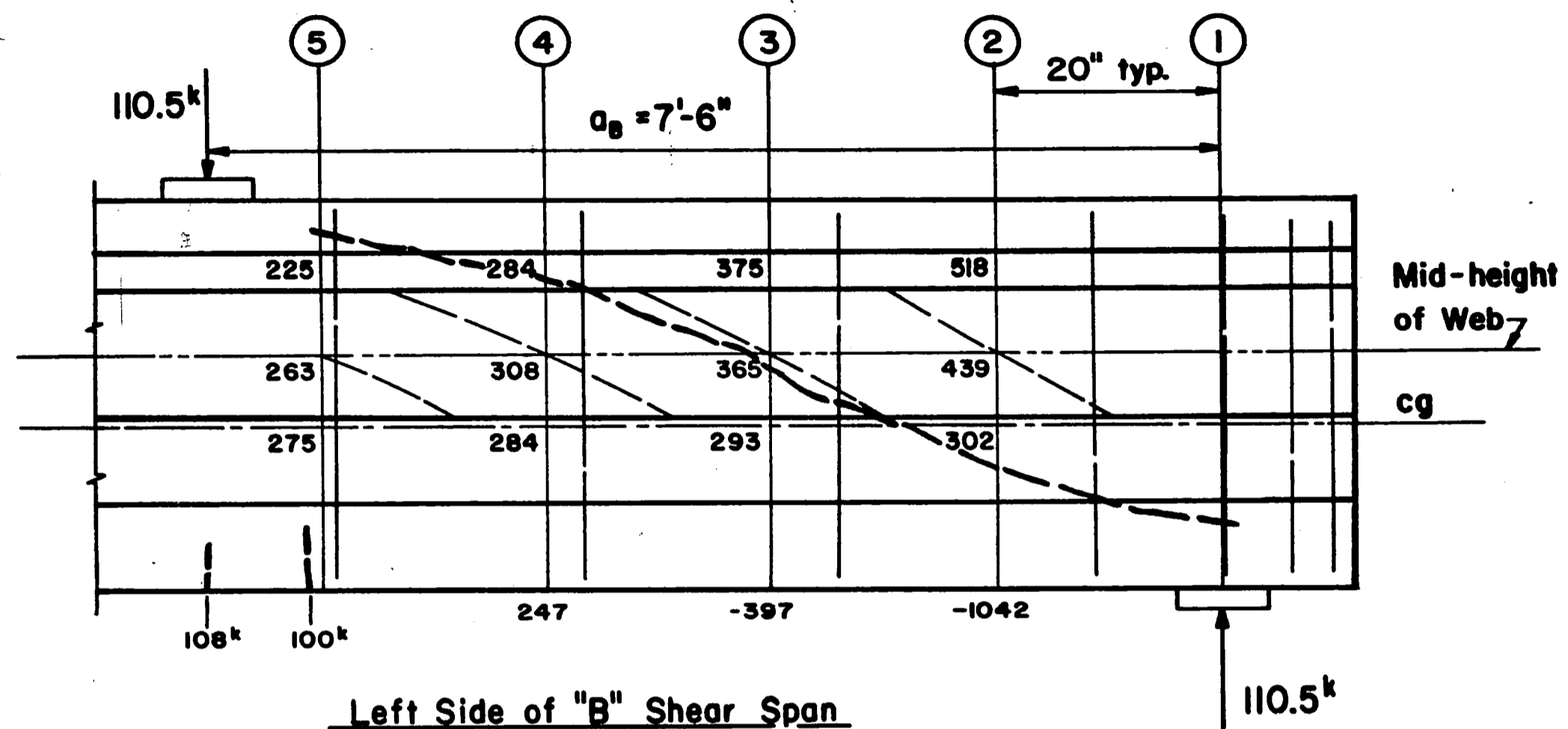
Right Side of "A" Shear Span
 Beam G-3 Ist. Test



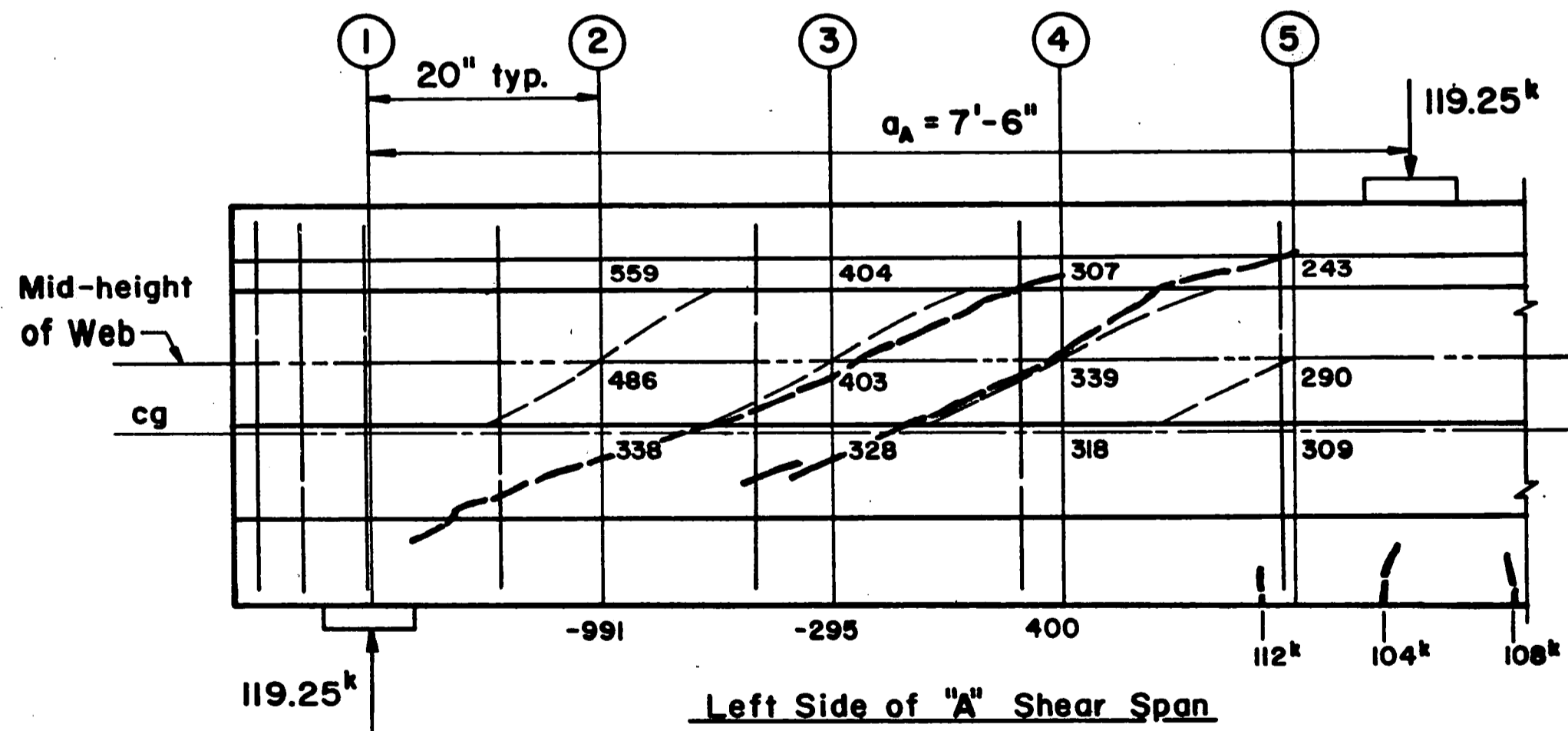
Left Side of "A" Shear Span
 Beam G-4 Ist. Test



Left Side of "B" Shear Span
 Beam G-4 Ist. Test

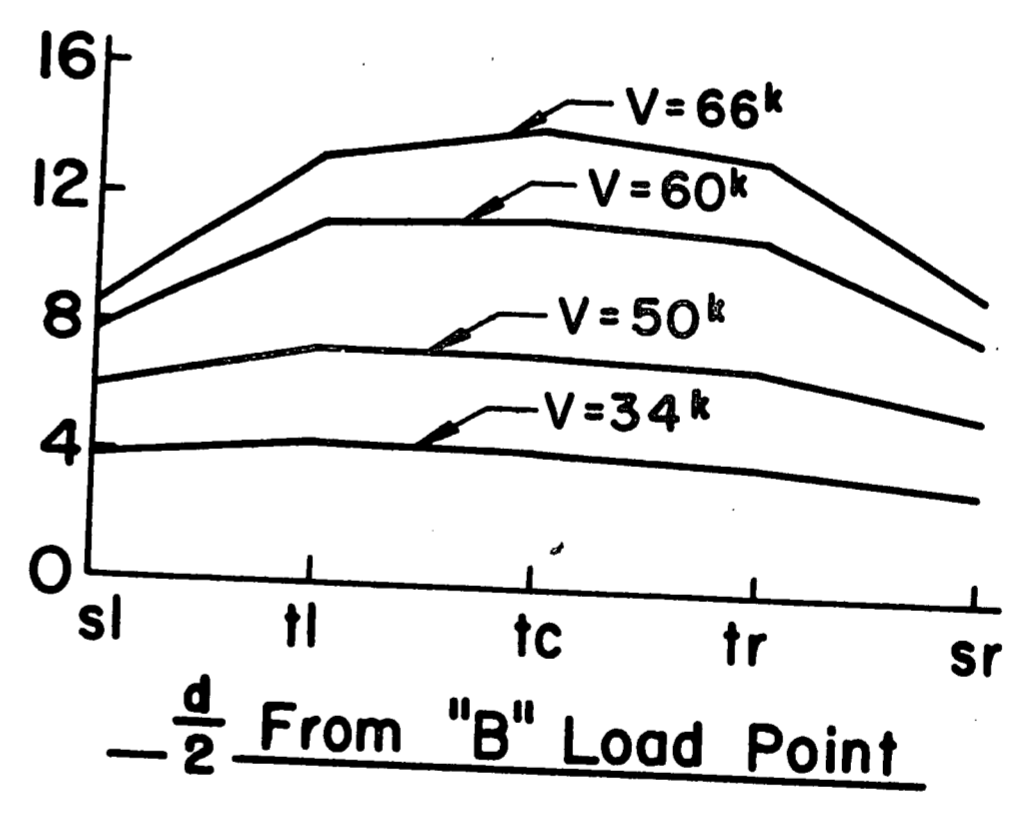
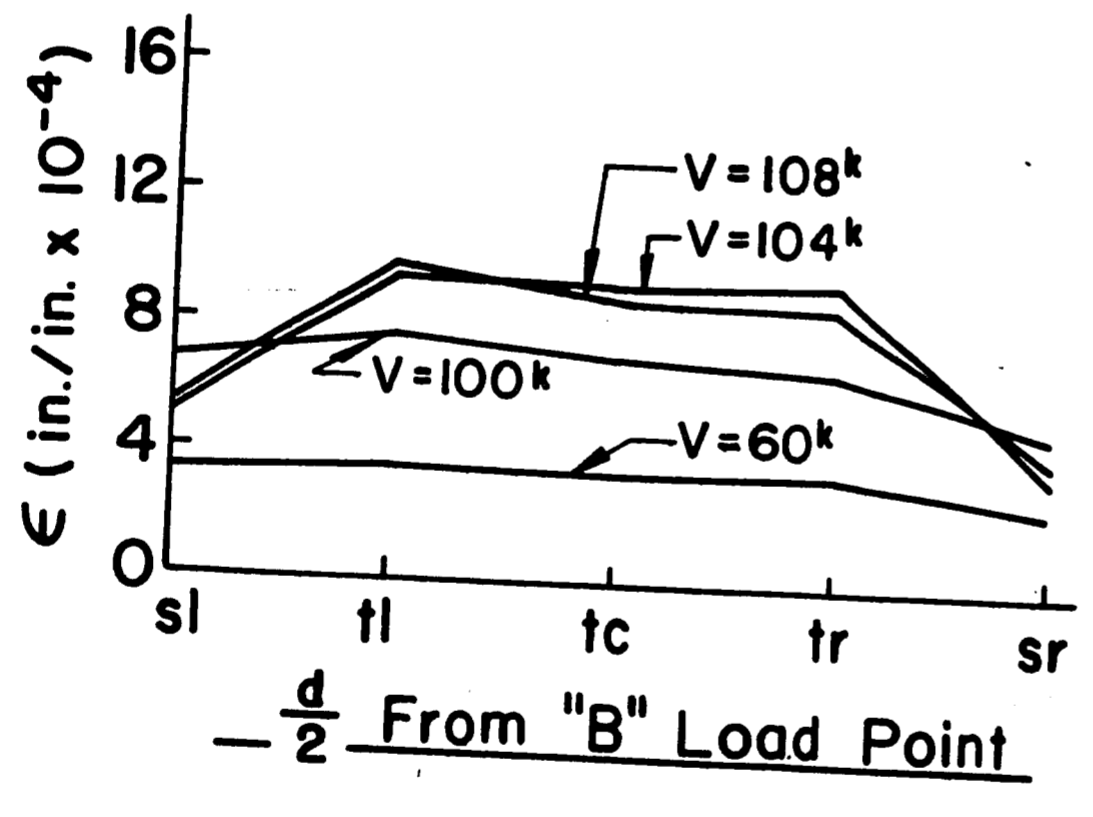
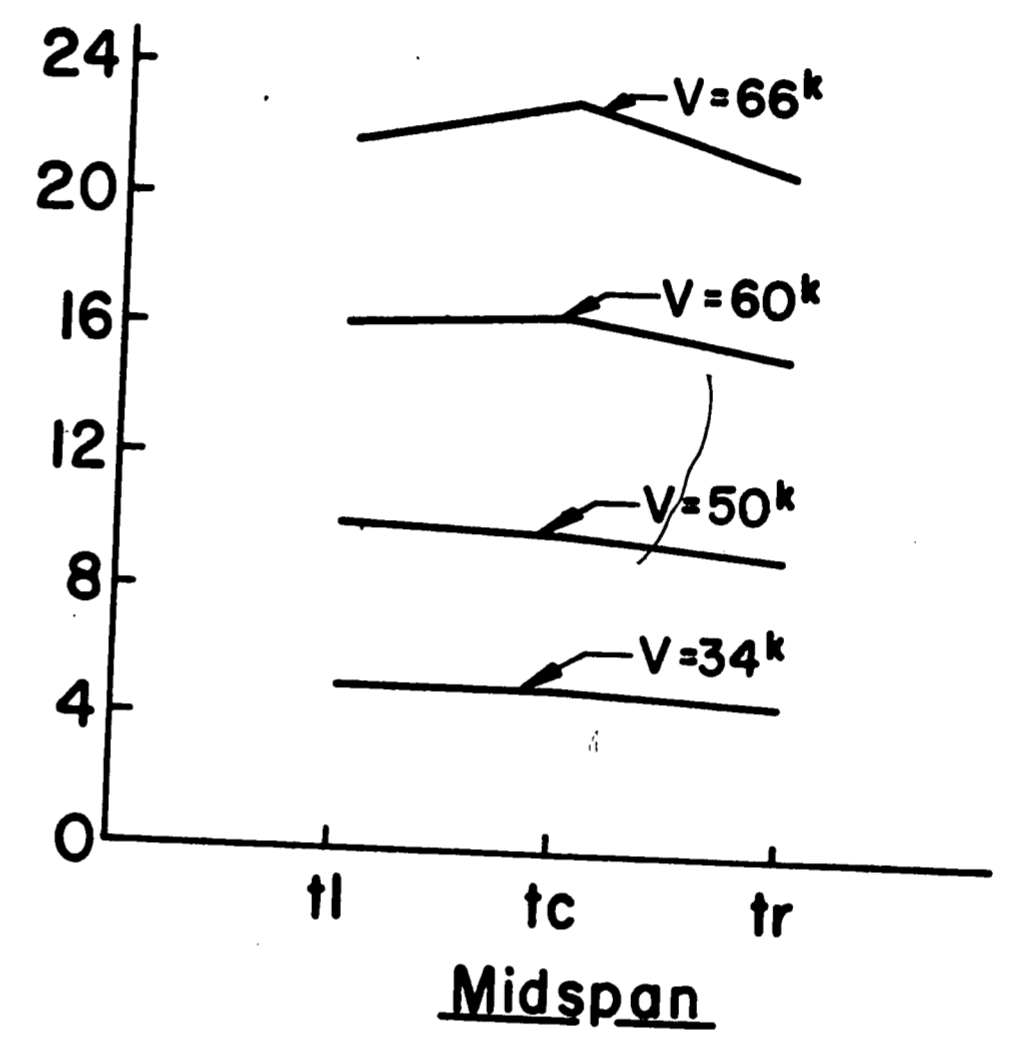
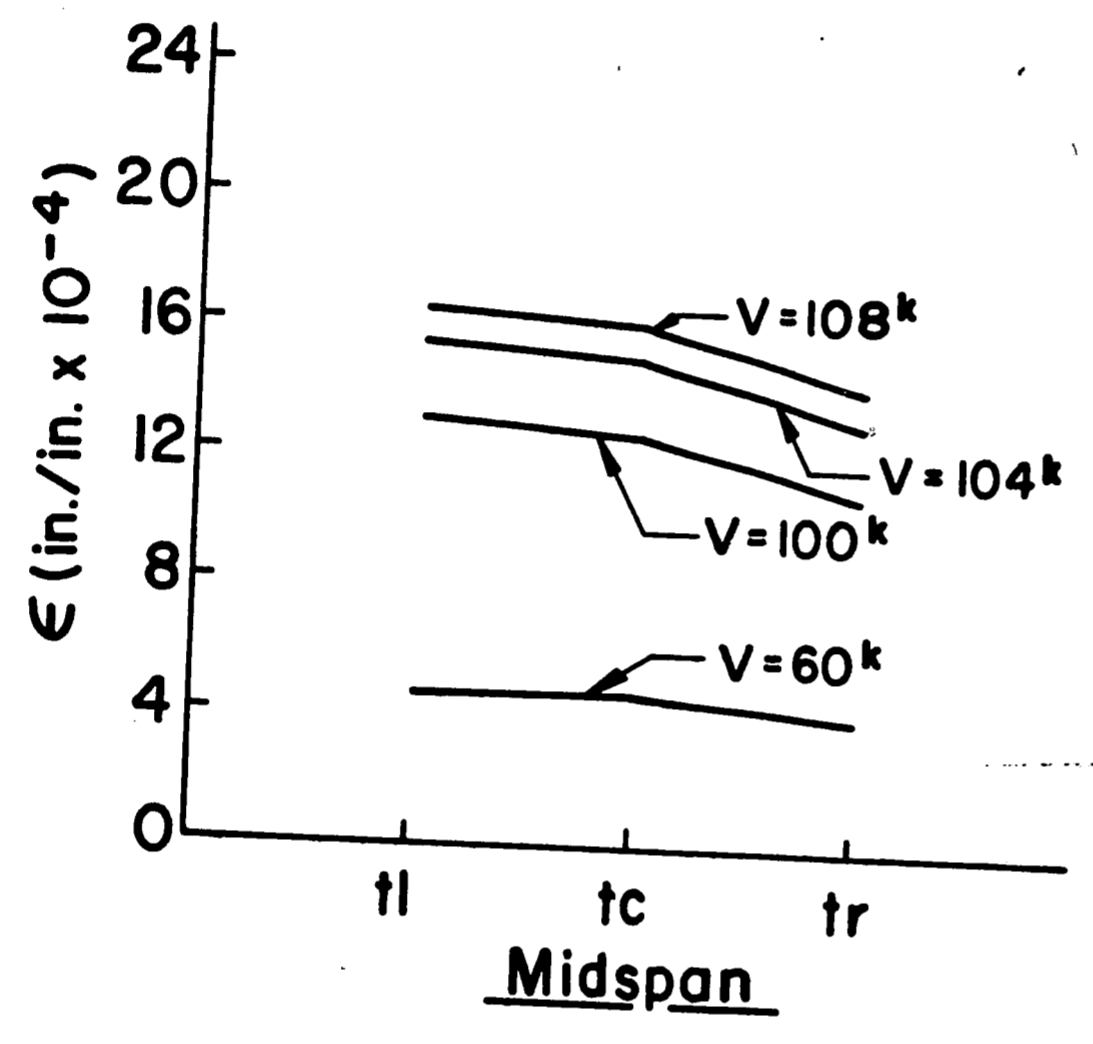
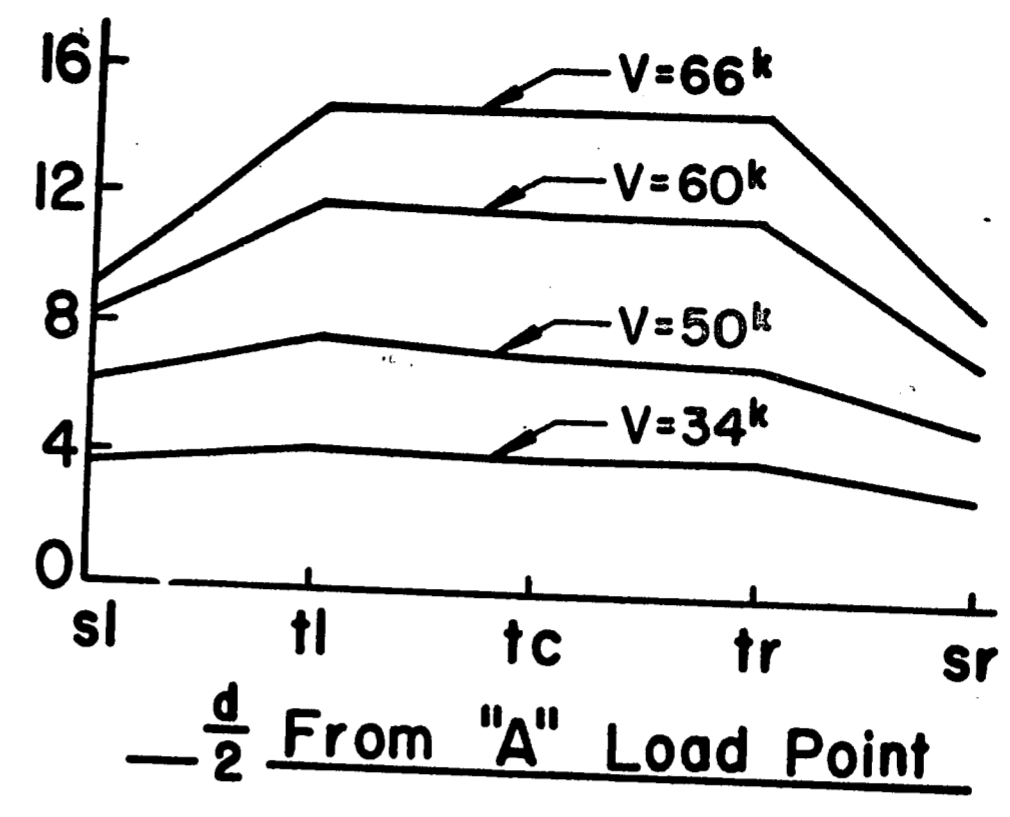
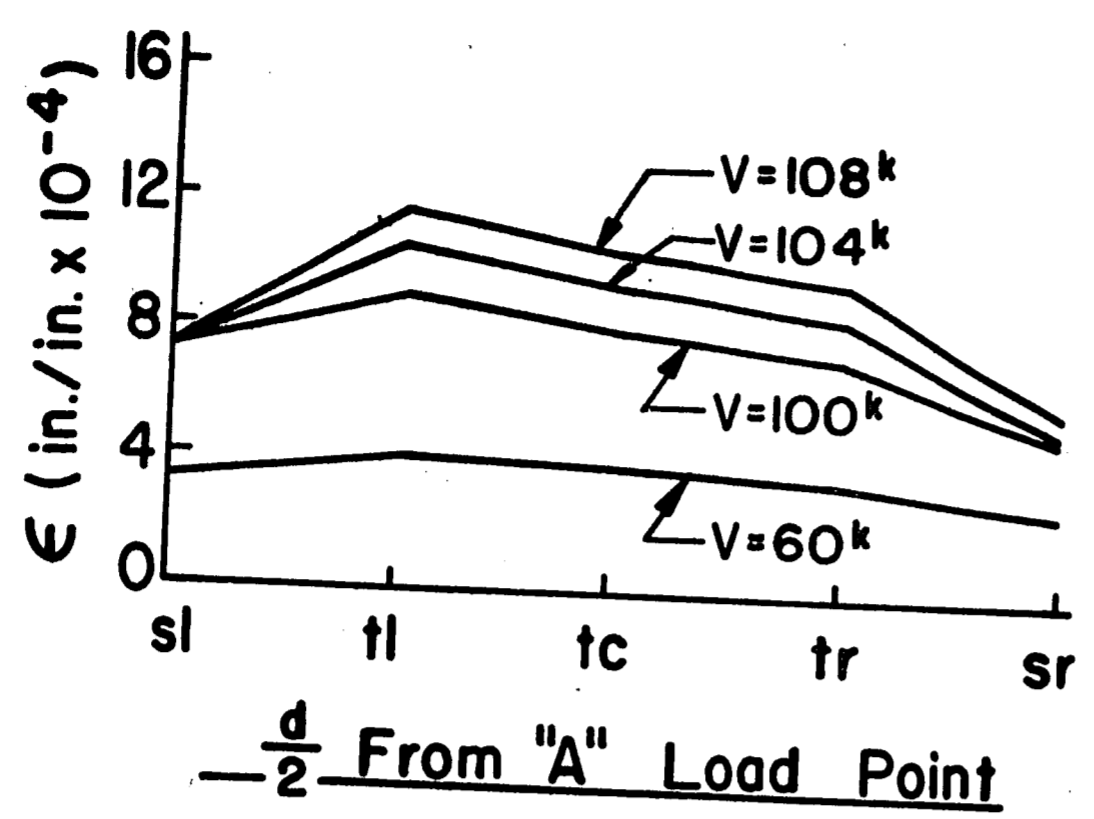


Left Side of "B" Shear Span
 Beam G-4 2nd. Test



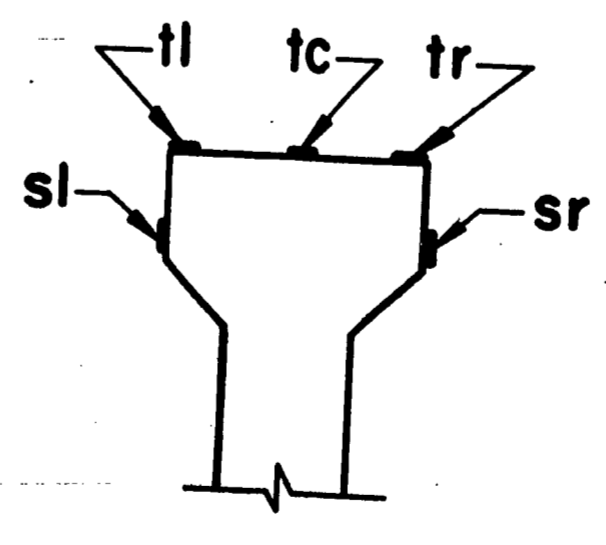
Left Side of "A" Shear Span
 Beam G-4 3rd. Test

12. APPENDIX B
STRAIN DISTRIBUTIONS

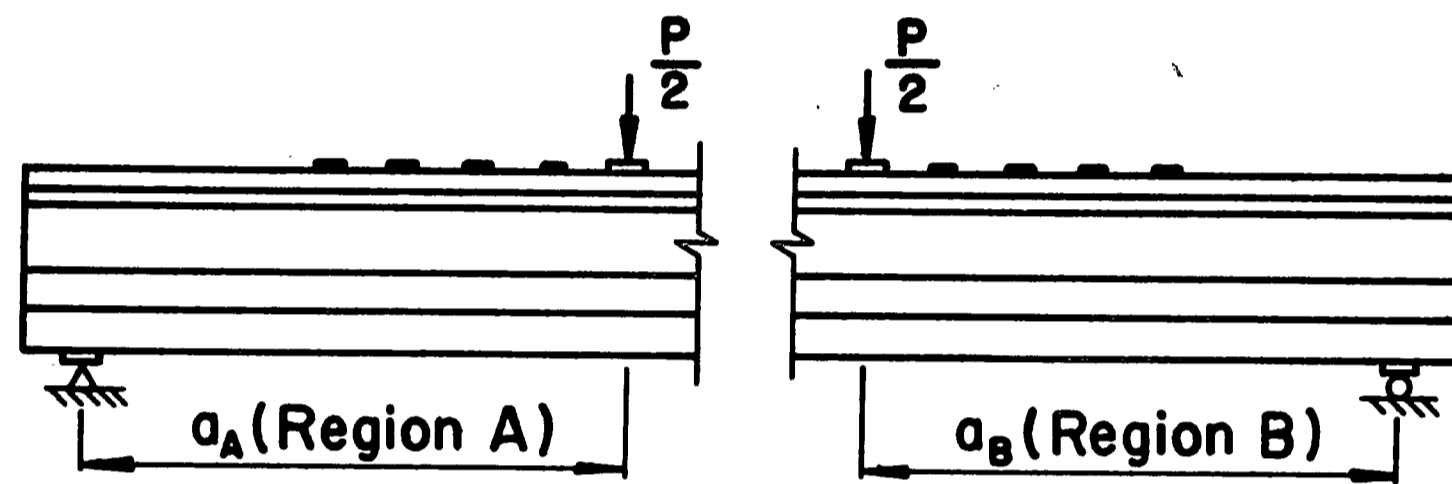
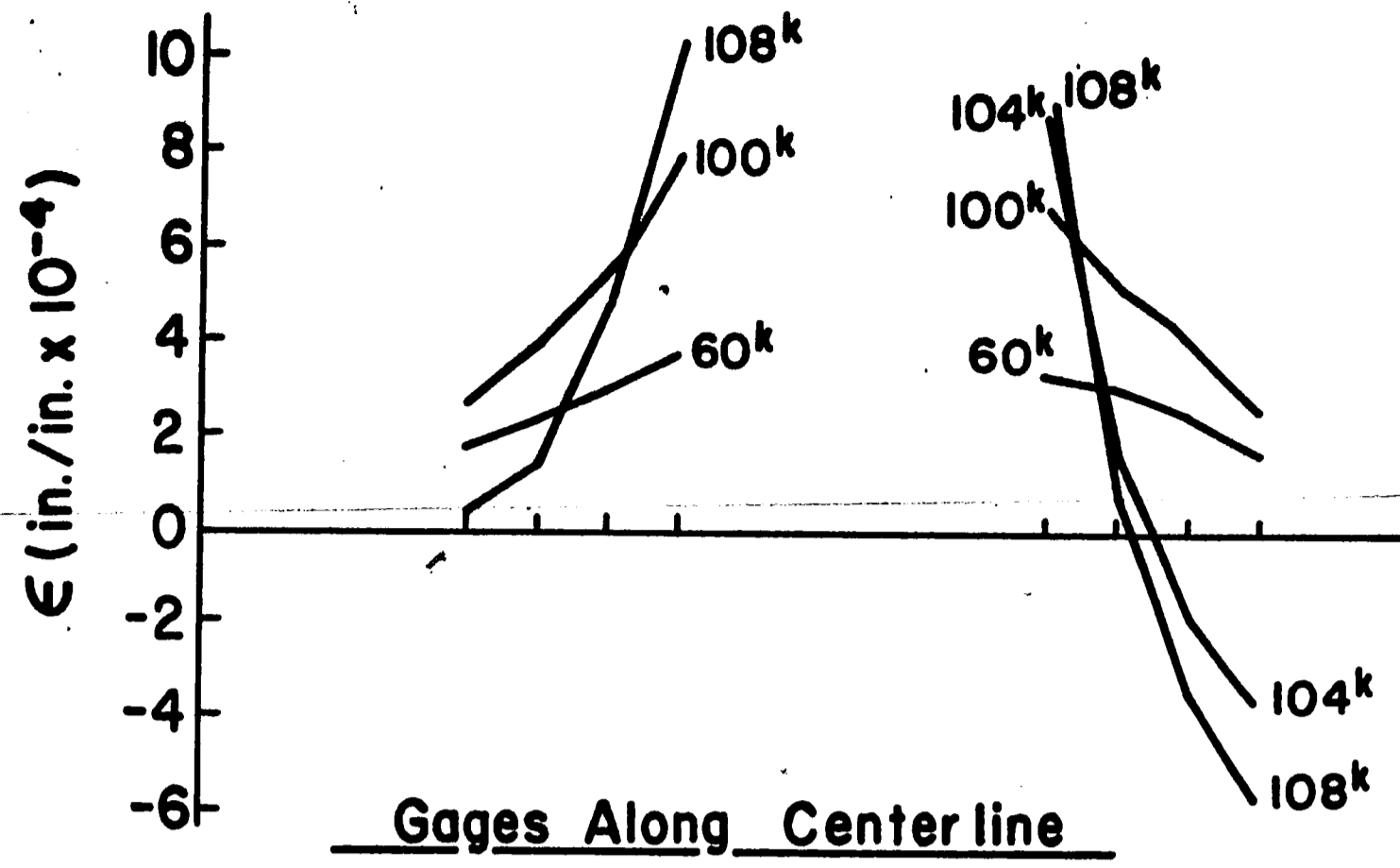


Beam G-2

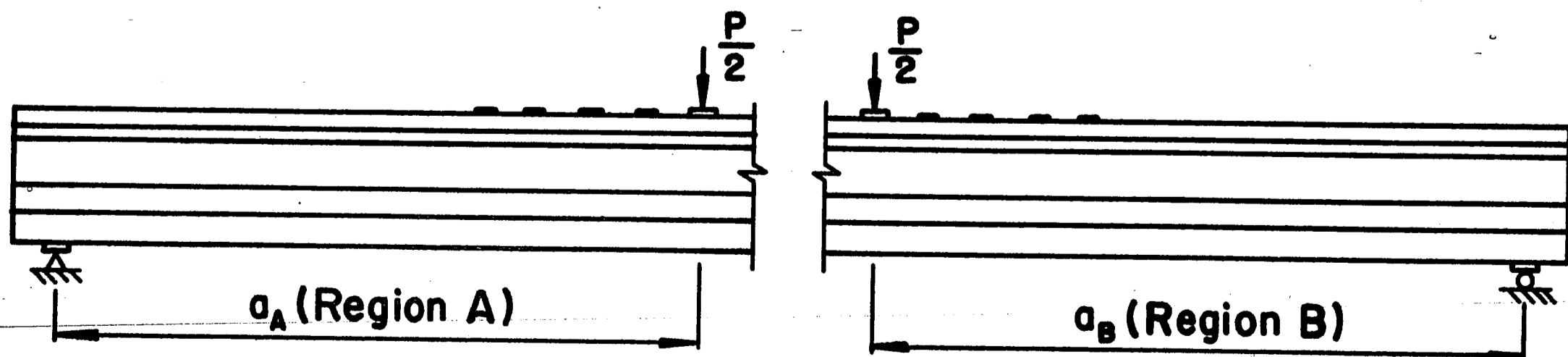
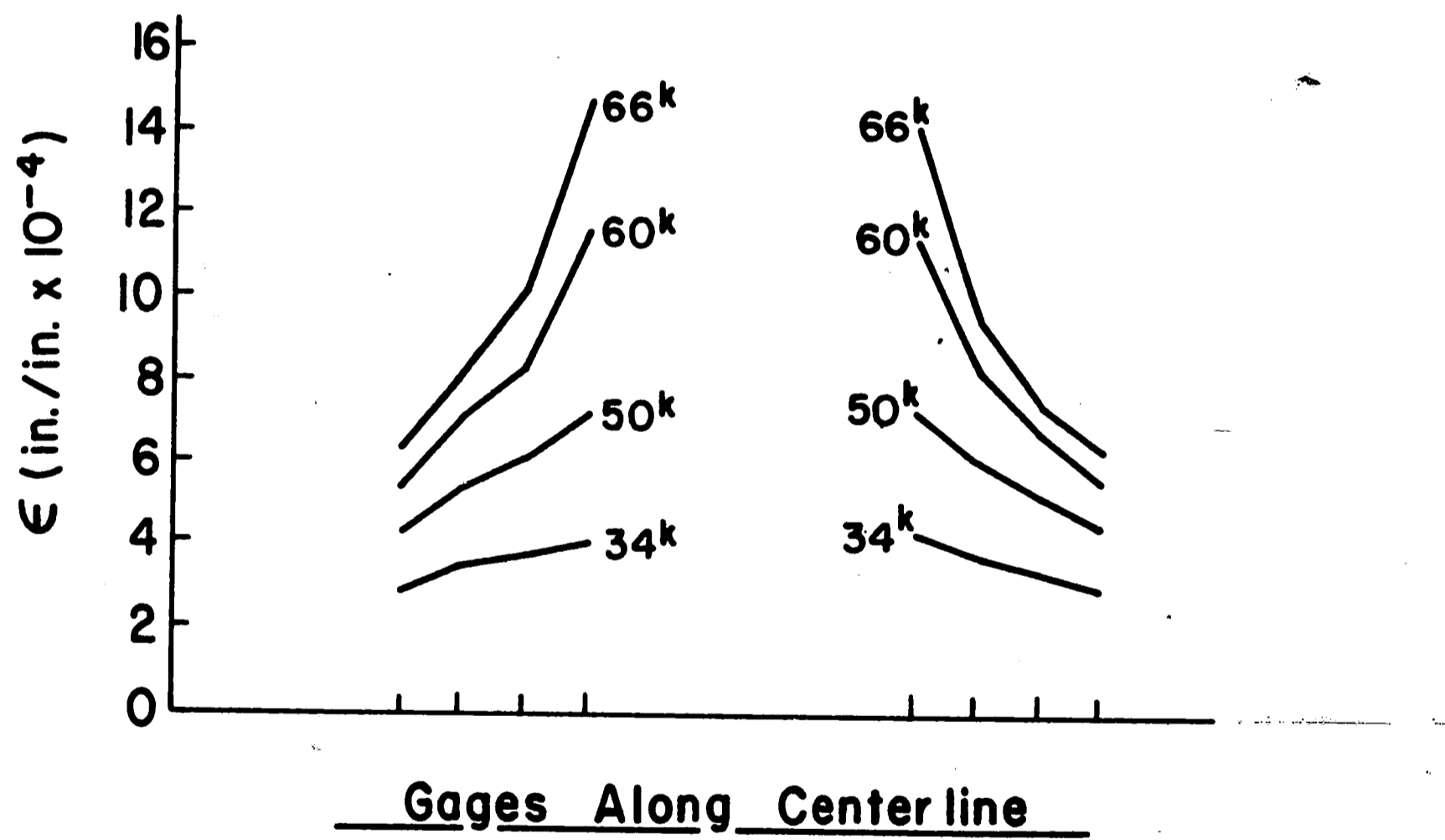
Beam G-4



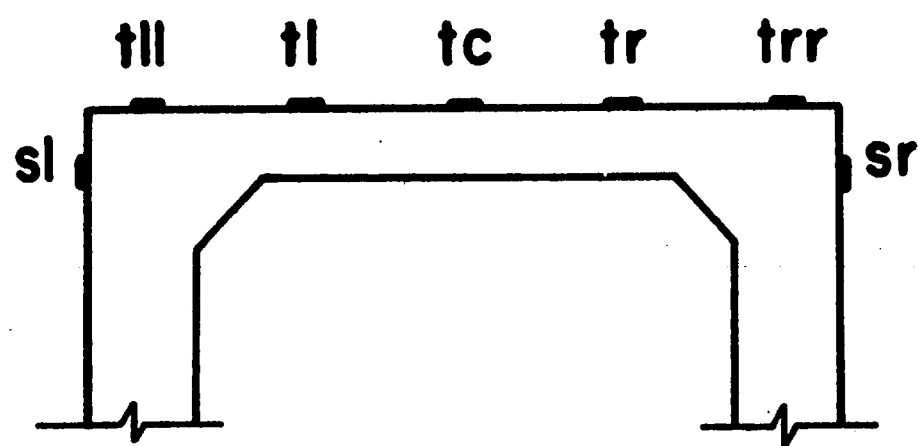
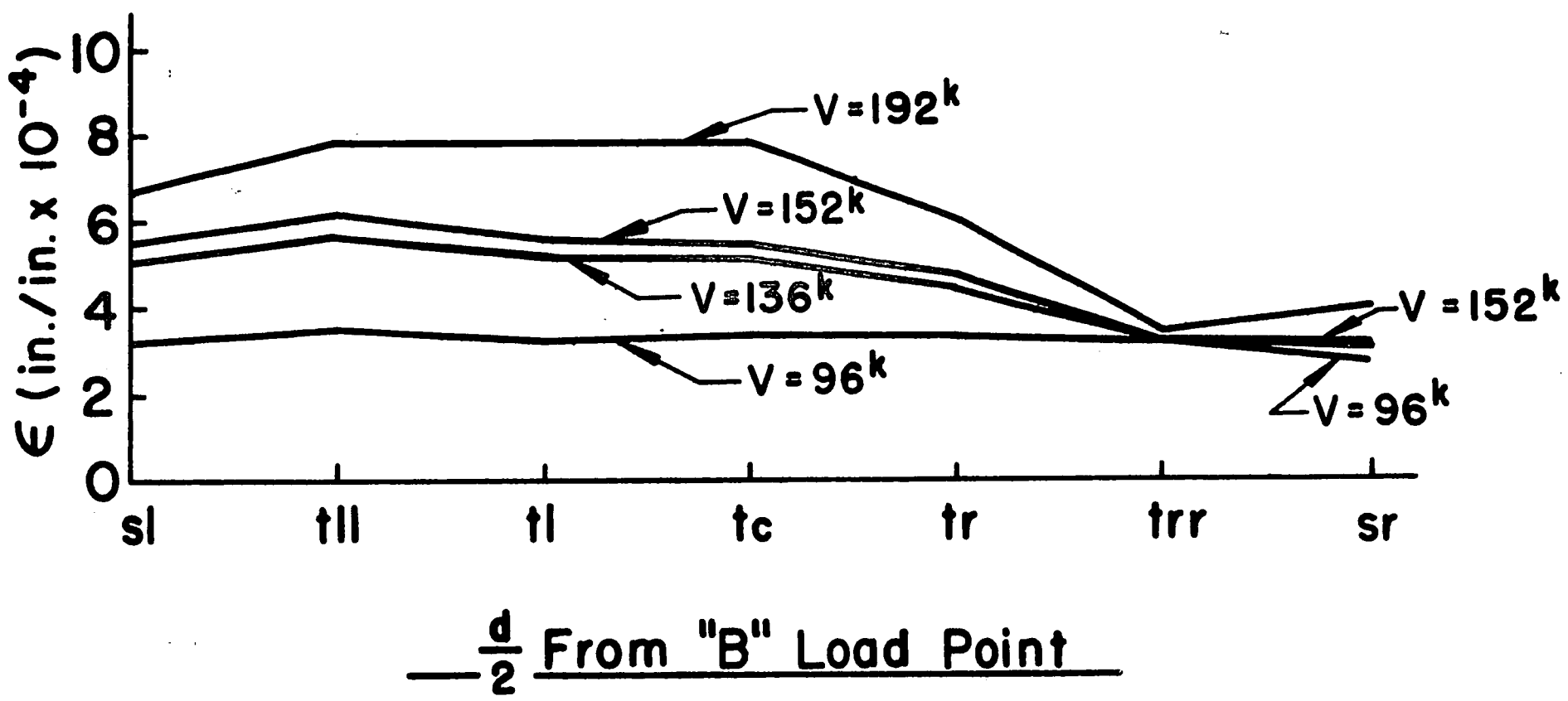
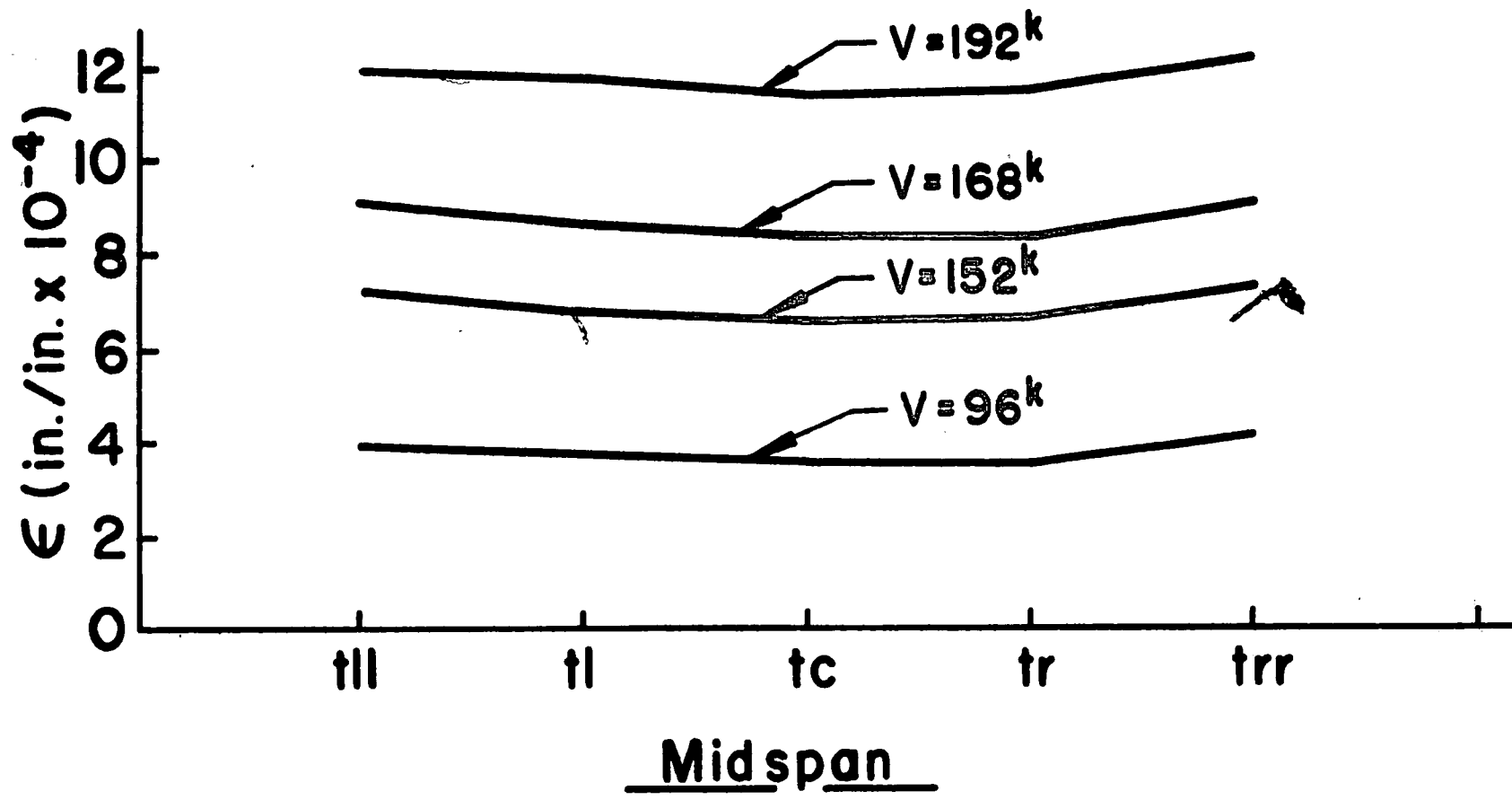
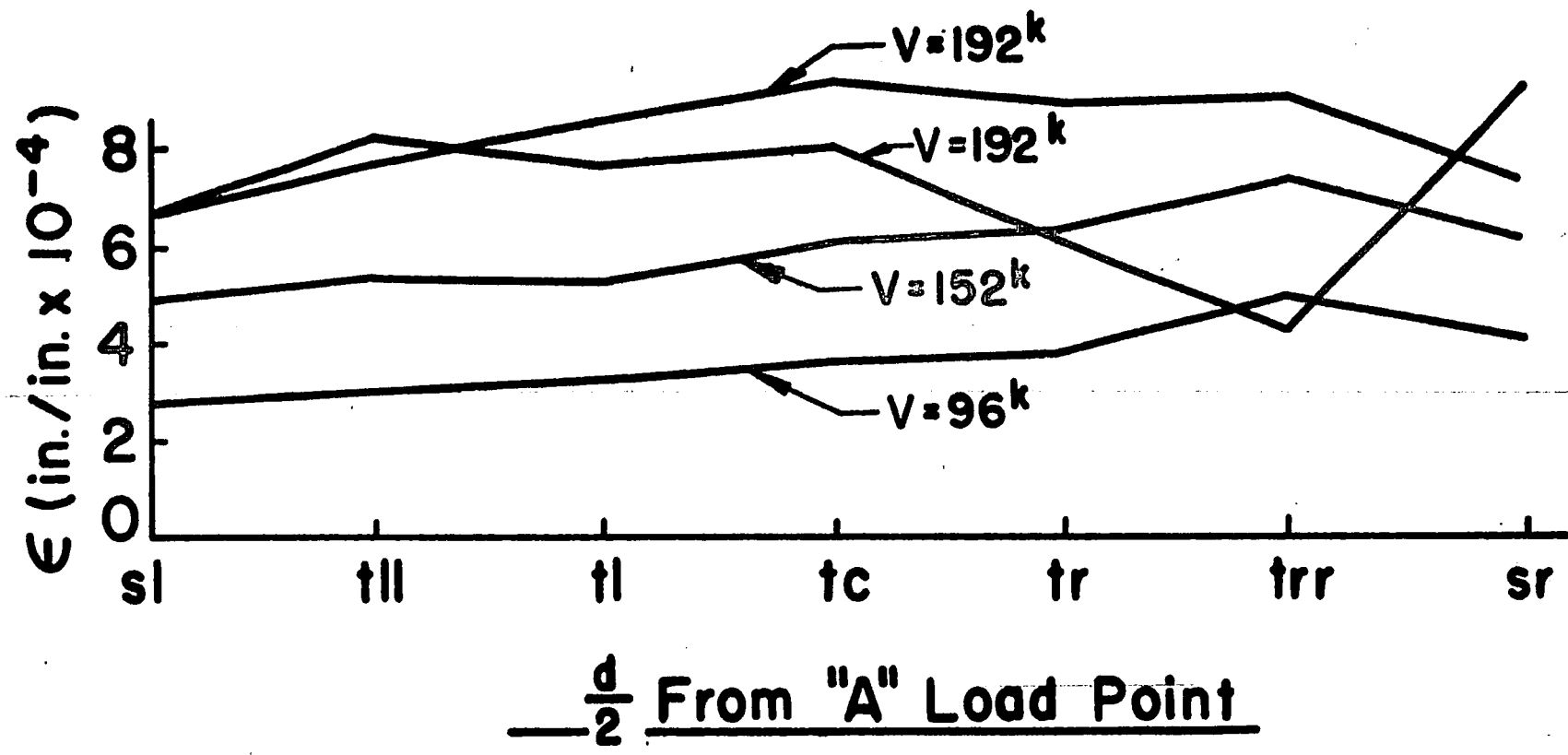
Location of Gages



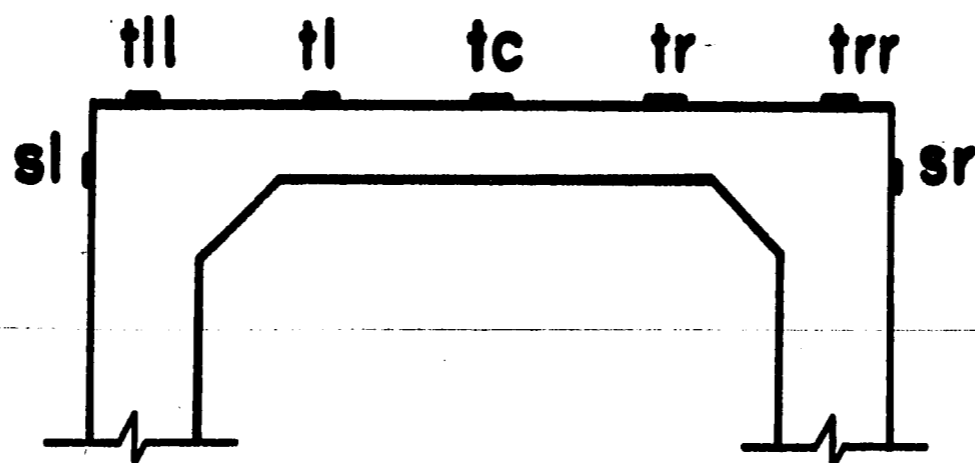
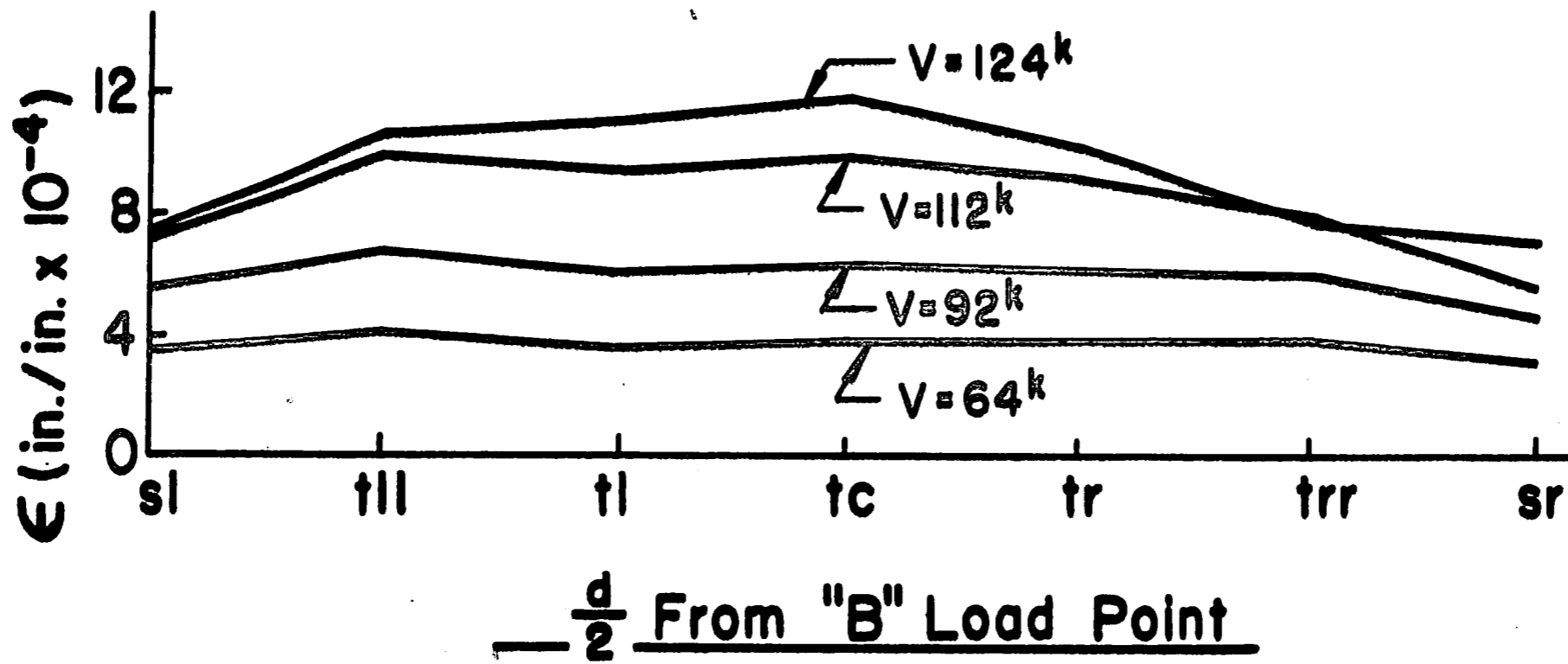
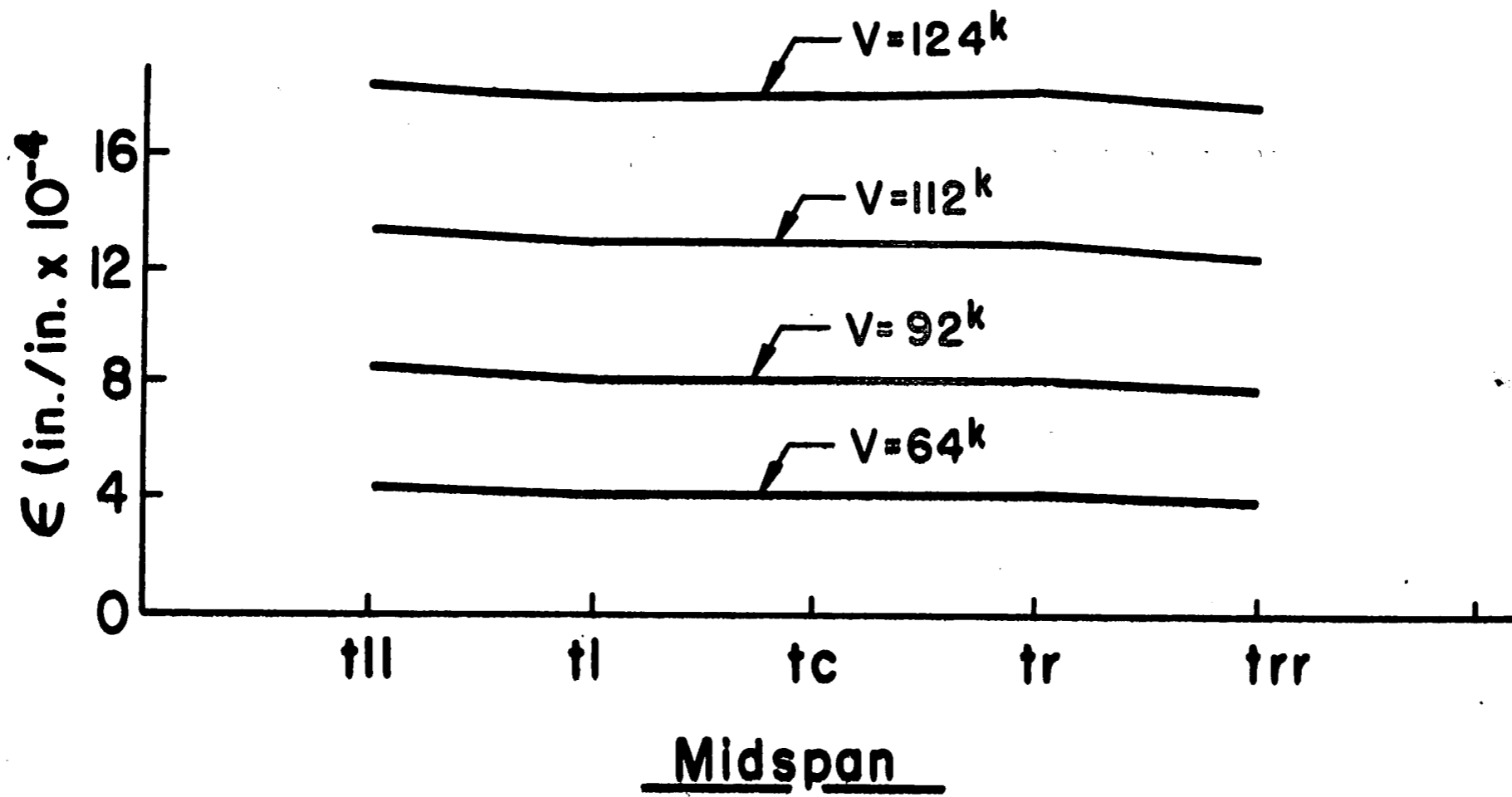
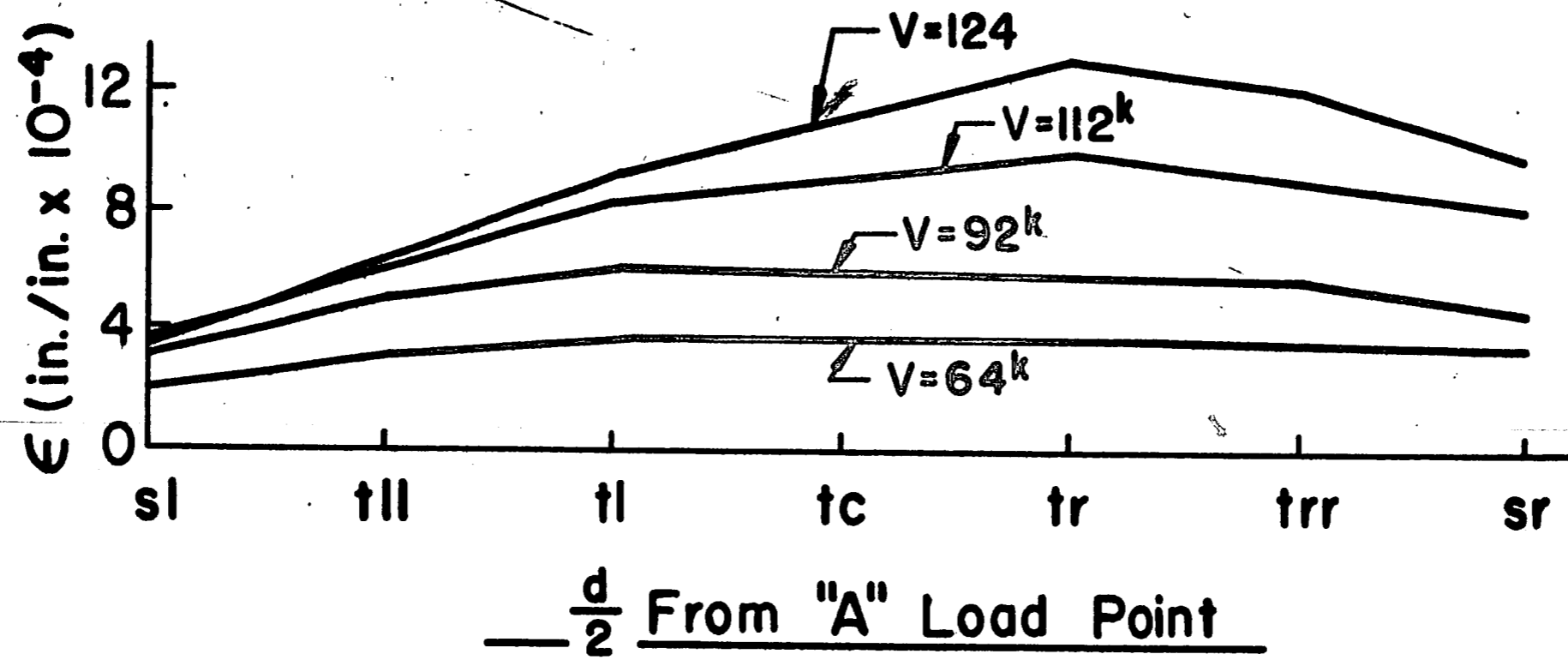
Beam G-2



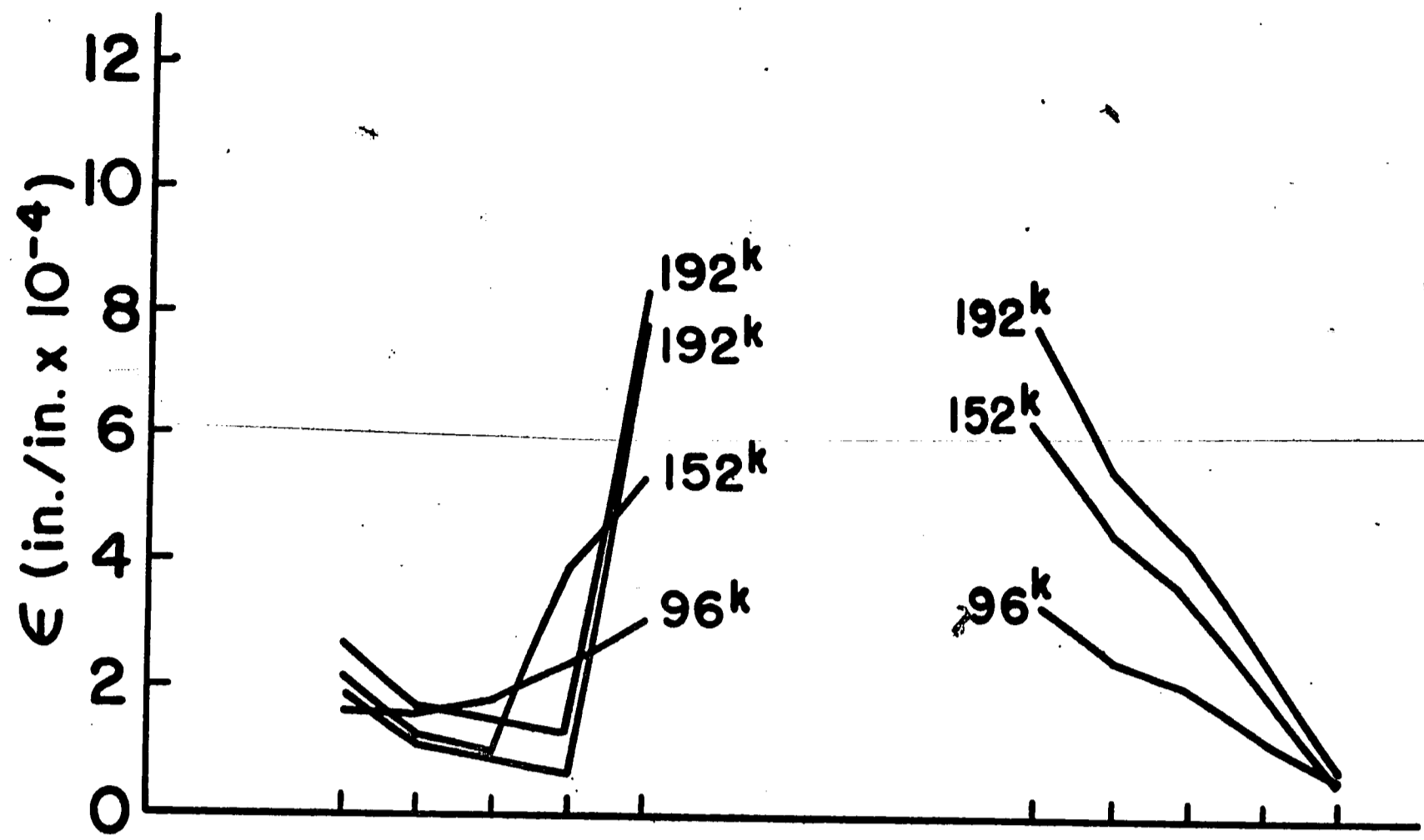
Beam G-4



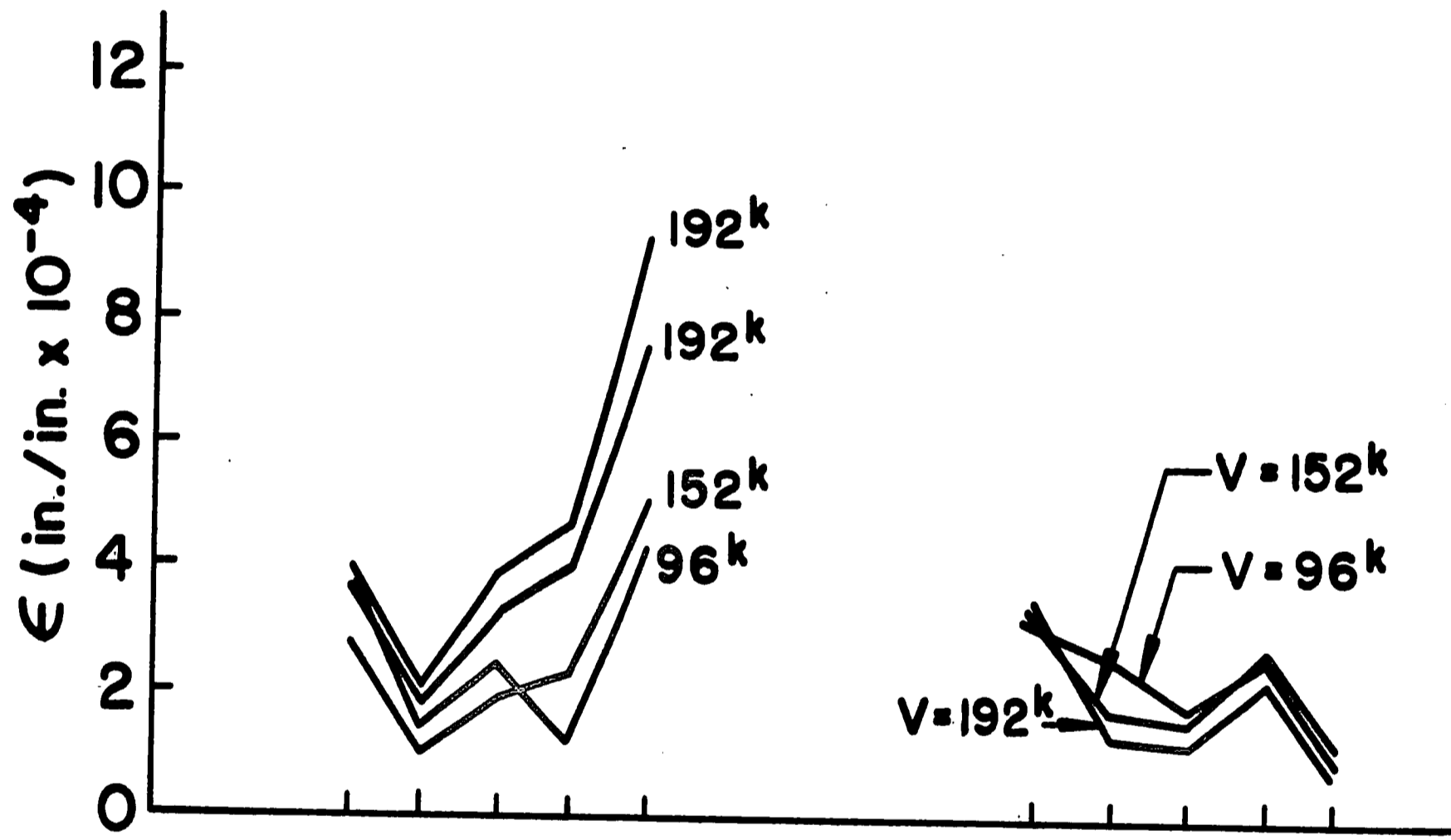
Beam G-1



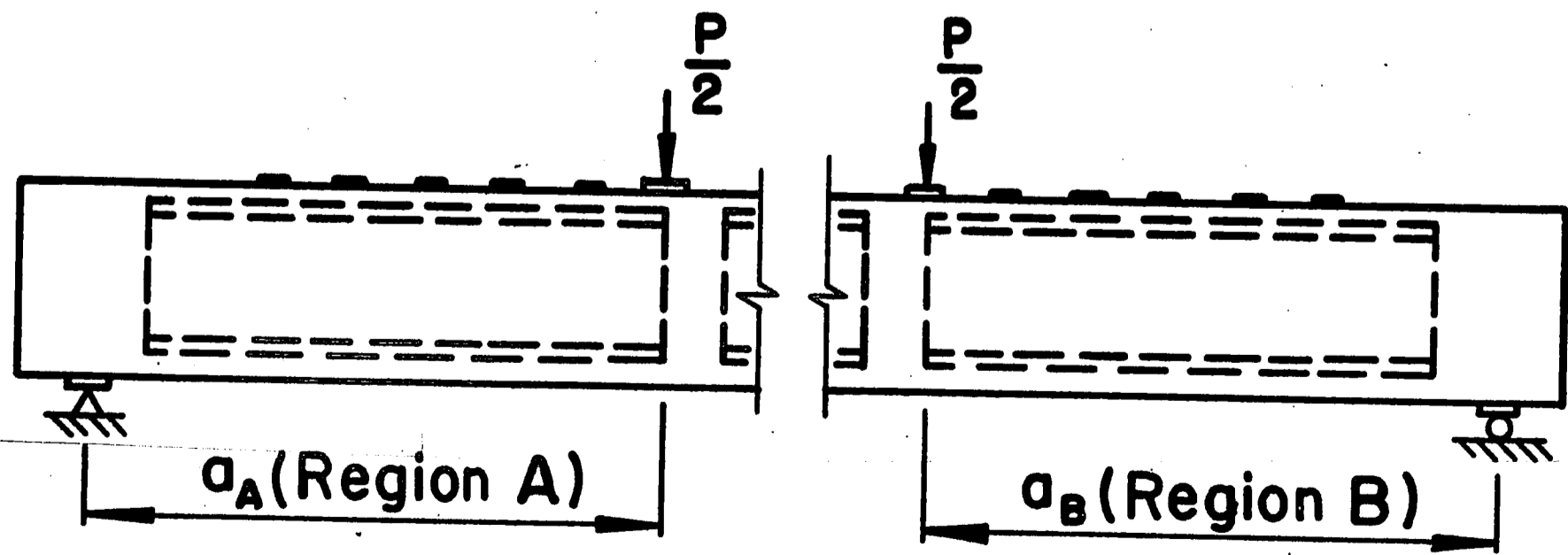
Beam G-3



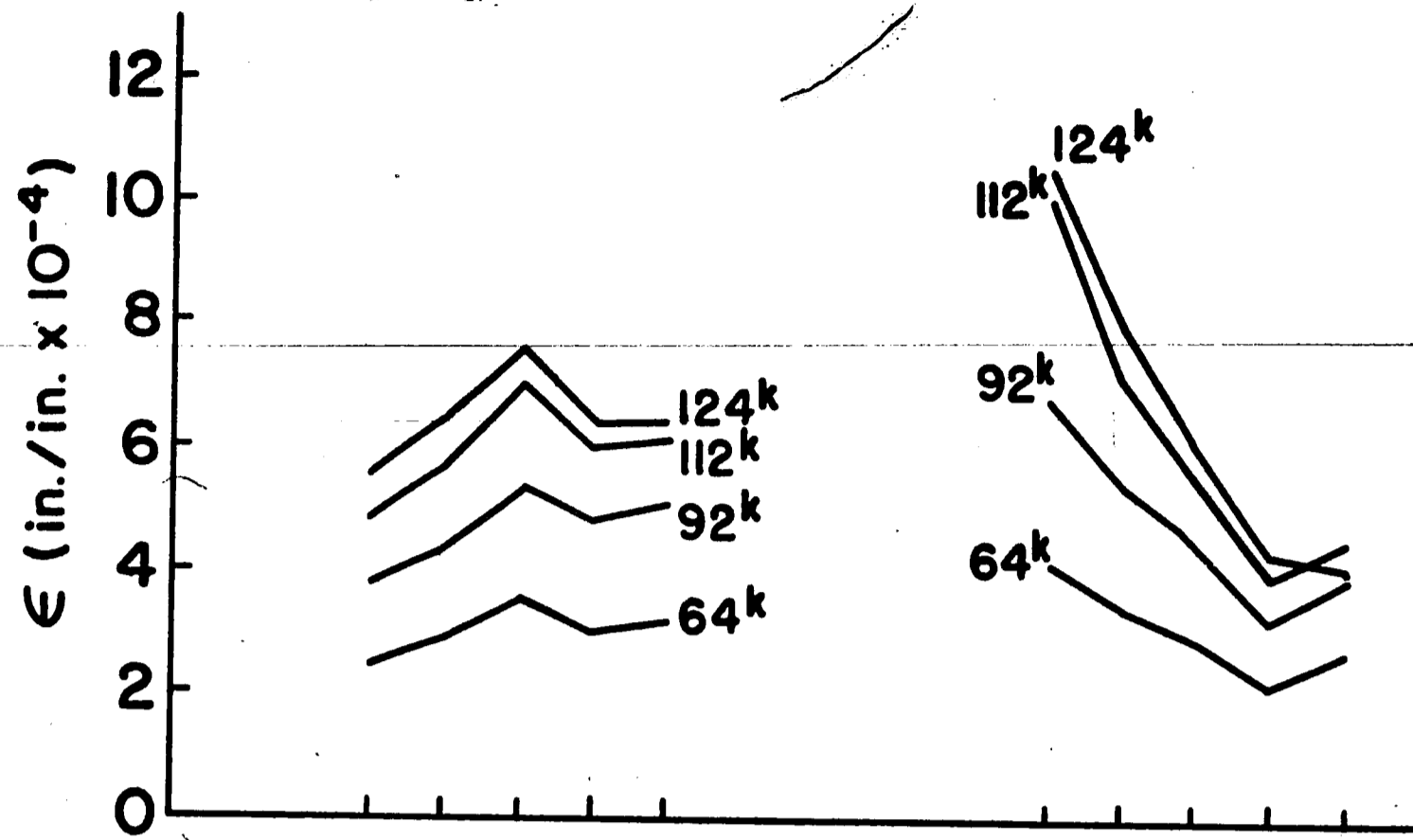
Gages Along Left Side of Top Flange



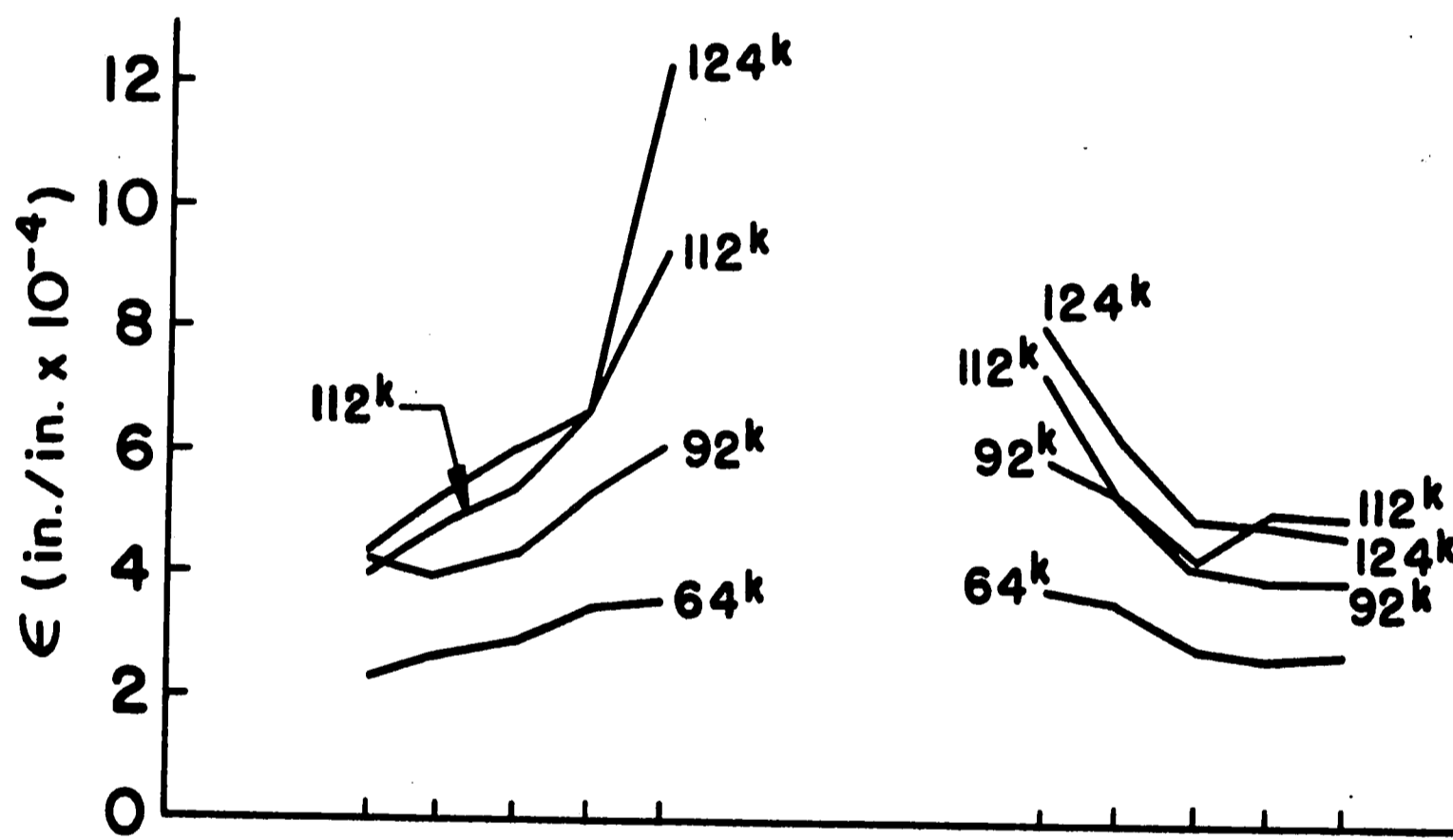
Gages Along Right Side of Top Flange



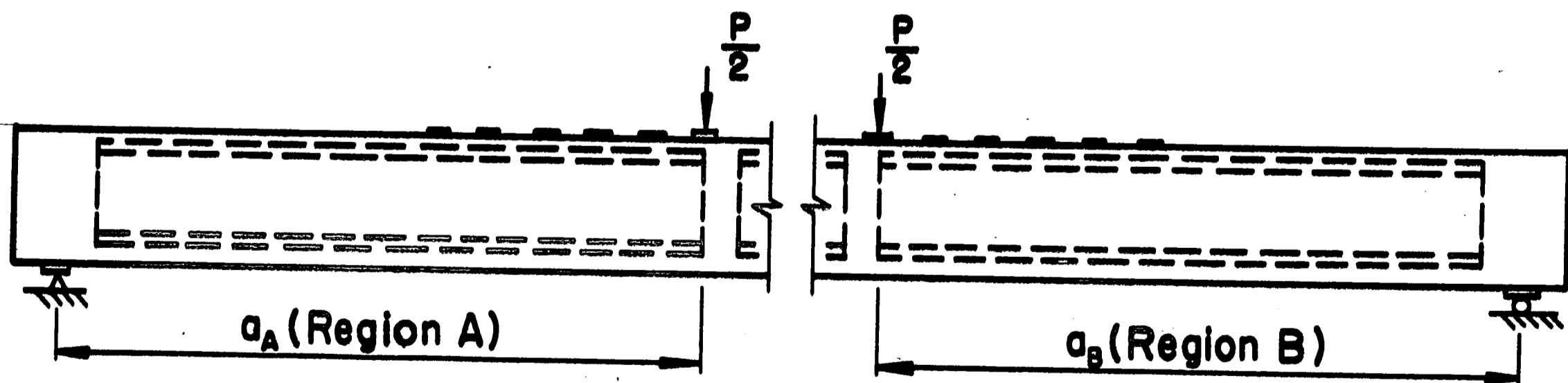
Beam G-1



Gages Along Left Side of Top Flange



Gages Along Right Side of Top Flange



Beam G-3

13. REFERENCES

1. Komendant, August E.
PRESTRESSED CONCRETE STRUCTURES
McGraw-Hill Book Co., 1952, pp. 185-193
2. Knudsen, K. E., Eney, W. J.
ENDURANCE OF A FULL-SCALE PRE-TENSIONED CONCRETE BEAM
Fritz Engineering Laboratory Report 223.5, Lehigh
University, April 1953
3. Smislova, A., Roesli, A., Brown, D. H. Jr., Eney, W. J.
ENDURANCE OF A FULL-SCALE POST-TENSIONED CONCRETE MEMBER
Fritz Engineering Laboratory Report No. 223.6, Lehigh
University, May 1954
4. Roesli, A., Ekberg, C. E. Jr., Smislova, A., Eney, W. J.
FIELD TESTS ON A PRESTRESSED CONCRETE MULTI-BEAM BRIDGE
Fritz Engineering Laboratory Report No. 223.9, Lehigh
University, 1956
5. Roesli, A.
THE LATERAL LOAD DISTRIBUTION IN MULTI-BEAM BRIDGES
Fritz Engineering Laboratory Report No. 223.10, Lehigh
University, July 1955
6. Dinsmore, G. A., Deutsch, P. L.
ANCHORAGE CHARACTERISTICS OF STRAND IN PRE-TENSIONED PRE-
STRESSED CONCRETE
Fritz Engineering Laboratory Report No. 223.16, Lehigh
University, July 1957
7. Ekberg, C. E., Jr., Walther, R. E., Slutter, R. G.
FATIGUE RESISTANCE OF PRESTRESSED CONCRETE BEAMS IN BENDING
Structural Division Journal, ASCE, July 1957
8. Ekberg, C. E. Jr.
REPORT ON 70 FT BEAM TEST FOR CONCRETE PRODUCTS COMPANY OF
AMERICA
Fritz Engineering Laboratory, Lehigh University, Sept. 1956
9. Ekberg, C. E. Jr.
DYNAMIC TESTS OF A 55 FT MEMBER FOR CONCRETE PRODUCTS OF
AMERICAN-MARIETTA COMPANY
Fritz Engineering Laboratory, Lehigh University, March 1956

10. Walther, R. E.
THE ULTIMATE STRENGTH OF PRESTRESSED AND CONVENTIONALLY REINFORCED CONCRETE UNDER THE COMBINED ACTION OF MOMENT AND SHEAR
Fritz Engineering Laboratory Report No. 223.17, Lehigh University, October 1957
11. Walther, R. E., Warner, R. F.
ULTIMATE STRENGTH TESTS OF PRESTRESSED AND CONVENTIONALLY REINFORCED CONCRETE BEAMS IN COMBINED BENDING AND SHEAR
Fritz Engineering Laboratory Report No. 223.18, Lehigh University, Sept. 1958
12. McClarnon, F. M., Wakabayashi, M., Ekberg, C. E. Jr.
FURTHER INVESTIGATION INTO THE SHEAR STRENGTH OF PRESTRESSED CONCRETE BEAMS WITHOUT WEB REINFORCEMENT
Fritz Engineering Laboratory Report No. 223.22, Lehigh University, January 1962
13. Hanson, J. M., Hulsbos, C. L.
OVERLOAD BEHAVIOR OF PRESTRESSED CONCRETE BEAMS WITH WEB REINFORCEMENT
Fritz Engineering Laboratory Report No. 223.25, Lehigh University, February 1963
14. Hanson, J. M.
ULTIMATE SHEAR STRENGTH OF PRESTRESSED CONCRETE BEAMS WITH WEB REINFORCEMENT
Fritz Engineering Laboratory Report No. 223.27B, Lehigh University, Sept. 1964
15. Hanson, J. M., Hulsbos, C. L.
ULTIMATE SHEAR STRENGTH OF PRESTRESSED CONCRETE WITH WEB REINFORCEMENT
Fritz Engineering Laboratory Report No. 223.27, Lehigh University, May 1965
16. Commonwealth of Pennsylvania, Department of Highways, Bridge Unit
STANDARDS FOR PRESTRESSED CONCRETE BRIDGES
September 1960
17. Cusens, A. R.
STRENGTH OF CONCRETE TEST CYLINDERS CAST IN WAXED PAPER MOLDS
Journal of the American Concrete Institute, Proceedings V. 61, No. 3, March 1964, pp. 287-292
18. Burmeister, Robert A.
TESTS OF PAPER MOLDS FOR CONCRETE CYLINDERS
Journal of the American Concrete Institute, Proceedings V. 47, No. 1, Sept. 1950, pp. 17-24

19. Warner, R. F., Hulsbos, C. L.
PROBABLE FATIGUE LIFE OF PRESTRESSED CONCRETE FLEXURAL MEMBERS
Fritz Engineering Laboratory Report No. 223.24A, Lehigh University, July 1962
20. Taylor, I. J., Liebig, J. O., Eney, W. J.
CONTINUOUSLY REINFORCED CONCRETE PAVEMENTS REPORT NO. 5
Fritz Engineering Laboratory Report No. 256.9, Lehigh University, February 1962
21. Lepper, H. A., Garber, D. L.
MARYLAND CONTINUOUSLY-REINFORCED CONCRETE PAVEMENT: FIRST YEAR STRAIN OBSERVATIONS
University of Maryland, Department of Civil Engineering, College Park, Maryland, December 1960
22. Mattock A. H., Kriz, L. S., Hognestad, E.
RECTANGULAR CONCRETE STRESS DISTRIBUTION IN ULTIMATE STRENGTH DESIGN
Journal of the American Concrete Institute, Proceedings, V. 57, No. 8, February 1961, pp. 875-928
23. The American Concrete Institute
ACI STANDARD BUILDING CODE REQUIREMENTS FOR REINFORCED CONCRETE
Published by the Institute, Detroit, Michigan, 1963
24. The American Association of State Highway Officials
STANDARD SPECIFICATIONS FOR HIGHWAY BRIDGES, EIGHTH EDITION
Published by the Association, Washington D.C., 1961

14. V I T A

The author was born in Philadelphia, Pennsylvania, on June 17, 1941, the second son of Edward F. Brecht and Florence Foster. He was married to Leona M. Holpp in June, 1963.

After graduating from Northeast High School in January 1959, the author enrolled in the cooperative education program at Drexel Institute of Technology. There he completed the requirements of the Department of Civil Engineering and received the degree of Bachelor of Science in Civil Engineering in June 1963. He was commissioned as an officer in the Corps of Engineers, United States Army Reserves, in June 1963. During his industrial periods under the cooperative education program, he was employed by the City of Philadelphia in the Water Department and by Texaco, Inc. at the Eagle Point Refinery, Westville, New Jersey. From June 1963 to September 1963, the author was employed as an instructor in the Department of Civil Engineering and Mechanics at Drexel Institute of Technology.

The author joined the staff at Fritz Engineering Laboratory, Lehigh University, in September 1963, as a research assistant in the Structural Concrete Division. He has been associated with research concerning the ultimate strength of prestressed concrete bridge members.